

Some Applications of Hard Thermal Loop Perturbation Theory in Quark Gluon Plasma

By
NAJMUL HAQUE
PHYS05200804003

Saha Institute of Nuclear Physics

*A thesis submitted to the
Board of Studies in Physical Sciences
In partial fulfillment of requirements*

For the Degree of
DOCTOR OF PHILOSOPHY

of
HOMI BHABHA NATIONAL INSTITUTE



July, 2014

Homi Bhabha National Institute

Recommendations of the Viva Voce Board

As members of the Viva Voce Board, we certify that we have read the dissertation prepared by **NAJMUL HAQUE** entitled **Some Applications of Hard Thermal Loop Perturbation Theory in Quark Gluon Plasma** and recommend that it maybe accepted as fulfilling the dissertation requirement for the Degree of Doctor of Philosophy.

_____ Date:
Chair - Prof. Asit Kumar De

_____ Date:
Guide/Convener - Prof. Munshi Golam Mustafa

_____ Date:
Member 1 - Prof. Avaroth Harindranath

_____ Date:
Member 2 - Prof. Pradip Kumar Roy

_____ Date:
External Examiner - Prof. Saumen Datta

Final approval and acceptance of this dissertation is contingent upon the candidate's submission of the final copies of the dissertation to HBNI.

I hereby certify that I have read this dissertation prepared under my direction and recommend that it may be accepted as fulfilling the dissertation requirement.

Date:

Place:

Guide: _____

Prof. Munshi Golam Mustafa

STATEMENT BY AUTHOR

This dissertation has been submitted in partial fulfillment of requirements for an advanced degree at Homi Bhabha National Institute (HBNI) and is deposited in the Library to be made available to borrowers under rules of the HBNI.

Brief quotations from this dissertation are allowable without special permission, provided that accurate acknowledgement of source is made. Requests for permission for extended quotation from or reproduction of this manuscript in whole or in part may be granted by the Competent Authority of HBNI when in his or her judgment the proposed use of the material is in the interests of scholarship. In all other instances, however, permission must be obtained from the author.

Najmul Haque

DECLARATION

I, hereby declare that the investigation presented in the thesis has been carried out by me. The work is original and has not been submitted earlier as a whole or in part for a degree / diploma at this or any other Institution / University.

Najmul Haque

List of Publications arising from the thesis

Journal

1. Three-loop HTLpt thermodynamics at finite temperature and chemical potential, *Najmul Haque, Aritra Bandyopadhyay, Jens O. Andersen, Munshi G. Mustafa, Michael Strickland and Nan Su*, **JHEP** **1405**, **027** (2014).
2. Three-loop HTLpt Pressure and Susceptibilities at Finite Temperature and Density, *Najmul Haque, Jens O. Andersen, Munshi G. Mustafa, Michael Strickland, Nan Su*, **Phys. Rev. D** **89**, **061701(R)** (2014) .
3. Quark Number Susceptibilities from Two-Loop Hard Thermal Loop Perturbation Theory, *Najmul Haque, Munshi G. Mustafa, Michael Strickland*, **JHEP** **1307**, **184** (2013).
4. Two-loop HTL pressure at finite temperature and chemical potential, *Najmul Haque, Munshi G. Mustafa, Michael Strickland*, **Phys. Rev. D** **87**, **105007** (2013).
5. Conserved Density Fluctuation and Temporal Correlation Function in HTL Perturbation Theory, *Najmul Haque, Munshi G. Mustafa, Markus H. Thoma*, **Phys. Rev. D** **84**, **054009** (2011).
6. Low Mass Dilepton Rate from the Deconfined Phase, *Carsten Greiner , Najmul Haque, Munshi G. Mustafa, Markus H. Thoma*, **Phys. Rev. C** **83b**, **014908** (2011).

Chapters in books and lectures notes

N. A.

Conferences

- Quark Number Susceptibility and Thermodynamics in HTL approximation
Najmul Haque, Munshi G. Mustafa,
Nucl. Phys. A 862-863, 271 (2011).

Others

- A Modified Hard Thermal Loop Perturbation Theory
Najmul Haque, Munshi G. Mustafa
arXiv: 1007.2076 [hep-ph].

Najmul Haque

DEDICATIONS

Dedicated to my daughter.

ACKNOWLEDGEMENTS

First of all, I would like to express my deep gratitude to my supervisor Munshi Golam Mustafa. He has introduced me to the Thermal Field Theory and guided me throughout the whole PhD tenure in academic as well as non-academic purpose. I am greatly grateful to my collaborator Michael Strickland who always has tried to give me a hand whenever needed. Gratitude also goes to my collaborators from my institute and outside the institute. Special acknowledgement goes to my colleague/collaborator Somdeb Chakraborty who has introduced me to the applications of AdS/CFT duality to Quark Gluon Plasma. I am also grateful to my other collaborators: Jens Andersen, Nan Su, Markus Thoma, Carsten Greiner, Shibaji Roy, Aritra Bandyopadhyay, Shankhadeep Chakraborty, Binoy Krishna Patra, Lata Thakur and Uttam Kakade.

I appreciate the fruitful and enlightening interactions with Palash B. Pal, Asit K. De, Purnendu Chakraborty, Swapan Majhi. Also special acknowledgement goes to our divisional head Asit K. De for non-academic supports during my stay in SINP.

The time at SINP could not be more lively and lovely without my dear colleagues and thanks to them : Raktim Abir, Ramanuj Banerjee, Pratyay Banerjee, Srijit Bhattacharjee, Anirban Biswas, Soumyajyoti Biswas, Pritibhajan Byakti, Baishali Chakraborty, Mainak Chakraborty, Sovan Chakraborty, Dipankar Das, Jayanta Das, Chowdhury Aminul Islam, Santanu Maiti, Arindam Mazumdar, Amaresh Metya, Manas Mondal, Santanu Mondal, Shyamal Mondal, Rana Nandi, Tapan Naskar, Lab Saha, Niladri Sarkar, Sreemoyee Sarkar, Satyajit Seth.

The financial supports from DAE are gratefully acknowledged.

Last but not least, I am indebted to the countless supports from my family over years specially from my wife and my daughter.

Contents

Synopsis	xvii
List of Figures	xxiii
1 Introduction	1
1.1 Statistical physics and quantum partition function	10
1.2 QCD at finite temperature	11
1.3 Perturbative pressure in QCD	17
1.4 Beta function and asymptotic freedom	20
1.5 Scope of the thesis	22
2 Hard Thermal Loop Perturbation Theory	23
2.1 Scalar field theory	24
2.2 Gauge theories	29
2.2.1 Polarization tensor	30
2.2.2 Gluon propagator	36
2.2.3 Fermionic propagator	39
2.2.4 Three point quark gluon vertex	46
2.2.5 Quark-gluon four-vertex	47
2.2.6 Three gluon vertex	47
2.2.7 Four-gluon Vertex	49
2.2.8 The HTL effective lagrangian in QCD	50
3 One loop HTL thermodynamics	55

3.1	Introduction	55
3.2	Generalities	57
3.2.1	Correlation Functions	57
3.2.2	Density Fluctuation and its Response	59
3.2.3	Thermodynamics functions and quark number susceptibility	60
3.2.4	QNS and Temporal Euclidean Correlation Function	60
3.3	Leading order QNS in HTLpt	62
3.3.1	Quasiparticle part (QP)	63
3.3.2	Landau Damping part (LD)	65
3.4	Results and Discussions:	68
3.5	Conclusion	71
4	Two-loop HTL Thermodynamics	73
4.1	Introduction	73
4.2	Ingredients for the NLO Thermodynamic potential in HTLpt	75
4.3	Scalarization of the fermionic diagrams	76
4.4	High temperature expansion	79
4.4.1	One-loop sum-integrals	79
4.4.2	Two-loop sum-integrals	81
4.4.3	Thermodynamic potential	83
4.5	The necessary Sum-Integrals	88
4.5.1	Simple one loop sum-integrals	89
4.5.2	HTL one loop sum-integrals	91
4.5.3	Simple two loop sum-integrals	92
4.5.4	HTL two loop sum-integrals	98
4.6	Integrals	99
4.6.1	Three dimensional integrals	99
4.6.2	Thermal Integrals	99
4.7	Pressure	103
4.7.1	LO Pressure	104

4.7.2	NLO HTLpt Pressure and Variational Mass Gap Equations . . .	104
4.8	Quark Number Susceptibility	109
4.8.1	LO HTLpt second-order QNS	111
4.8.2	LO HTLpt fourth-order QNS	111
4.8.3	NLO HTLpt second-order QNS	112
4.8.4	NLO HTLpt fourth-order QNS	114
4.9	Conclusions and Outlook	116
5	Three-loop HTLpt thermodynamics	119
5.1	Contributions to the HTLpt thermodynamic potential through NNLO	120
5.2	Expansion in mass parameters	125
5.2.1	One-loop sum-integrals	126
5.2.2	Two-loop sum-integrals	128
5.2.3	Three-loop sum-integrals	132
5.3	Sum-Integrals	137
5.3.1	One loop sum-integrals	138
5.3.2	Two loop sum-integrals	140
5.3.3	Three loop sum-integrals	140
5.4	Three-dimensional integrals	142
5.4.1	One-loop integrals	142
5.4.2	Two-loop integrals	143
5.5	NNLO HTLpt thermodynamic potential	143
5.5.1	NNLO result for equal chemical potentials	143
5.5.2	NNLO result – General case	147
5.6	Mass prescription	149
5.7	Thermodynamic functions	149
5.7.1	Scales	150
5.7.2	Pressure	150
5.7.3	Energy density	152
5.7.4	Entropy density	153

5.7.5	Trace anomaly	154
5.7.6	Speed of sound	155
5.8	Quark number susceptibilities	156
5.8.1	Baryon number susceptibilities	158
5.8.2	Single quark number susceptibilities	161
5.9	Conclusions and outlook	165
6	Dilepton Production Rate	167
6.1	Introduction	167
6.2	Dilepton Rate From Deconfined Phase	169
6.2.1	Born Rate	170
6.2.2	Rate using Hard Thermal Loop perturbation theory	170
6.2.3	Rate using Gluon Condensate	176
6.2.4	Rate from quark and rho-meson Interaction	179
6.2.5	Rate from Lattice Gauge Theory	183
6.3	Momentum Integrated Rate	187
6.4	Thoughts on the Quark-Hadron Duality Hypothesis	189
6.5	Conclusion	190
7	Summary and Outlook	193
A	Properties of the aleph functions	197
	Bibliography	199

Synopsis

In recent years substantial experimental and theoretical efforts have been undertaken to investigate the versatile physics issues involved in ultra-relativistic heavy-ion collisions, i.e., collisions of atomic nuclei in which center-of-mass energy per nucleon is much larger than the nucleon rest mass. The principal goal of this initiative is to explore the phase structure of the underlying theory of strong interactions - Quantum Chromodynamics (QCD) - by creating in the laboratory the new state of matter “Quark-Gluon Plasma (QGP)”. This new state of matter is predicted to exist under extreme conditions like at high temperatures and/or densities, when a phase transition takes place from a hadronic to a deconfined state of quarks and gluons. In nature such new states are believed to have existed and still may be encountered on large scales in at least two astrophysical aspects: i) in the evolution of early universe where a few tens of microseconds after the ‘big bang’ a transient stage of strongly interacting matter prevailed at temperatures 10^{12}K ($\sim 200\text{MeV}$) with a very small net baryon numbers; ii) in the interior of neutron stars where mass densities are likely to exceed 10^{15}gm/cm^3 about four times the central density of nuclei while the surface temperatures are as low as 10^5K or less. However, these astrophysical objects are by far remote in space and time so that their use for the study of QGP are quite difficult. This makes us to turn attention for a consistent study of QGP in the laboratory through high energy heavy-ion collisions.

The collider experiments currently dedicated to this search are the Relativistic

Heavy Ion Collider (RHIC) at Brookhaven National Laboratory (BNL) and the Large Hadron Collider (LHC) at the European Organization for Nuclear Research (CERN). Future experiments are planned at the Facility for Antiproton and Ion Research (FAIR) at the Gesellschaft für Schwerionenforschung (GSI) facility. These experiments at RHIC BNL and LHC CERN have provided us wealth of information [1–4] in understanding the properties of hot and dense matter and the theoretical predictions. On the other hand recent numerical lattice QCD (LQCD) has given us information on various thermodynamic properties of the matter *viz.*, critical temperature [5, 6], nature of phase transition, the equation of state [7–10], various susceptibilities [11], transport coefficients, spectral properties of pseudo-scalar and vector meson resonances etc. at finite temperature and density. Ultimately, one would again expect to validate this by characterizing the QGP in terms of its experimentally observed properties. The commissioning of RHIC and LHC, and various experiments performed therein have ushered in a new era. The analysis of the data has yielded a rich abundances of results that possibly indicate a glimpse of the predicted plasma phase of QCD. This calls for a better theoretical understanding of the particle properties in a hot and dense medium.

Quantum chromodynamics (QCD) exhibits a rich phase structure and the equation of state (EoS) which describes the matter can be characterized by different degrees of freedom depending upon the temperature and the chemical potential. The determination of the equation of state (EoS) of QCD matter is extremely important to QGP phenomenology. There are various effective models to describe the EoS of strongly interacting matter; however, one would prefer to utilize systematic first-principles QCD methods. The currently most reliable method for determining the EoS is lattice QCD. Finite temperature lattice QCD calculations are now quite sound; however, due to the sign problem, it is not straightforward to extend such calculations to finite baryon chemical potential. In practice, it is possible to obtain information about the behavior of the thermodynamic functions at small baryon

chemical potential by making a Taylor expansion of the partition function around zero chemical potential and extrapolating the result. This requires the calculation of various quark-number susceptibilities evaluated at zero chemical potential. Since extrapolations based on a finite number of Taylor coefficients can only be trusted within the radius of convergence of the expansion, it would be nice to have an alternative framework for calculating the finite temperature and chemical potential QCD thermodynamic potential and associated quantities. Perturbative QCD (pQCD) is an alternative framework which can be applied at high temperature and/or chemical potentials where the strong coupling ($g^2 = 4\pi\alpha_s$) is small in magnitude and non-perturbative effects are expected to be small. However, due to infrared singularities in the gauge sector, the perturbative expansion of the finite-temperature and density QCD partition function breaks down at order g^6 requiring non-perturbative input albeit through a single numerically computable number [12]. Up to order $g^6 \ln(1/g)$ it is possible to calculate the necessary coefficients using analytic (resummed) perturbation theory [13] at finite temperature and chemical potential.

The hard thermal loop perturbation theory (HTLpt) is a state-of-the-art resummed perturbation theory with a given mass prescription that reorganizes the usual perturbation theory at finite temperature/density quantum chromodynamics. In hard thermal loop (HTL) approximation the loop expansion and coupling expansion are not symmetrical as higher order diagrams contribute to the lower order one. As a result some of the quantities, such as equation of states, various susceptibilities, trace anomaly, speed of sound etc., calculated within a given loop order using the hard thermal loop approximation suffer incompleteness in the corresponding perturbative order. At each order in HTLpt the result is an infinite series in g , the strong coupling. Using the mass expansion one keeps terms through order g^5 (if one uses only LO mass prescription) all loop-orders of HTLpt in order to make the calculation tractable. At leading order (LO) one obtains only the correct perturbative coefficients for g^0 and g^3 terms when one expands in a strict power series in g .

At next-to-leading order (NLO) one obtains the correct g^0 , g^2 and g^3 coefficients whereas at next-to-next leading order (NNLO) one obtains the correct g^0 , g^2 , g^3 , g^4 and g^5 coefficients.

In the thesis I shall discuss a systematic computation of QCD pressure at finite temperature and finite chemical potential in one-loop [14], two-loop [15] and three-loop [16, 17] Hard Thermal Loop perturbation theory. The corresponding results will be compared with recent lattice QCD data.

Fluctuations of conserved quantities have been considered as important and relevant probes of Quark Gluon Plasma formation in relativistic heavy-ion collision. These fluctuations measure the response to system with an external field. In particular Quark Number Susceptibility(QNS) defines the response of conserved quark number density when we change the chemical potential of the system. Quark Number Susceptibility can be related to the charge fluctuations of the system and is therefore of direct experimental relevance. This thesis will also discuss a very systemic computation of Quark Number Susceptibilities in one-loop [14, 18, 19], two-loop [20] and three-loop [16, 17] Hard Thermal Loop perturbation theory. Also in three-loop HTLpt case, in general, off diagonal susceptibilities are non-zero, so I shall also extend NNLO HTLpt to calculate various order diagonal and off-diagonal susceptibilities. For NNLO calculation we will use the two-loop perturbative mass prescription for debye mass, the effective order of g becomes higher than g^5 . The results of various order HTLpt are gauge invariant and in particular, NNLO results are complete in g^5 . This result is completely analytic that does not require any free fit parameter beside renormalization scale. I shall also extend three-loop HTLpt to calculate other thermodynamical quantities, which are relevant to deconfined state of matter, *viz.* energy density, trace anomaly, speed of sound, entropy density etc. The various quantities agree very well with lattice QCD results within error bars down to 200 MeV.

In addition to calculations of the thermodynamic quantities, hard-thermal-loop perturbation theory can be used to calculate various physical quantities which are relevant to the deconfined state of matter. The dilepton rate is a good probe to study the deconfined state of matter as the mean free path for real or virtual photons are large and accordingly thermal dileptons have been theoretically proposed as a signal of QGP a long time ago [21]. So, this thesis will also analyze the dilepton rates from HTLpt with various non-perturbative results obtained using Gluon condensate in the quark propagator, ρ meson-quark interaction in an effective model and lattice QCD in [22]. The results will also be contrasted with in-medium Hadron gas rate. Based on this, a more realistic way of the quark-hadron duality hypothesis can be advocated than it was done in the literature.

List of Figures

1.1	Nuclear matter at extreme conditions.	1
1.2	Schematic view of QCD phase diagram.	3
1.3	Contour for bosonic frequency sum.	14
1.4	Contour for fermionic frequency sum.	16
1.5	pQCD pressure as a function of the temperature. Successive perturbative approximations are shown through order $\alpha_s^3 \ln \alpha_s$ for vanishing μ (left) and for non-vanishing μ (right).	19
1.6	QCD running coupling as a function of energy scale	21
2.1	One and two-loop scalar self-energy	25
2.2	Bubble diagrams contributing to the scalar self-energy	26
2.3	Three-loop scalar self-energy diagram	27
2.4	One-loop photon self-energy	30
2.5	Feynman diagrams for gluon self energy.	36
2.6	Dispersion laws for photon/gluon.	39
2.7	One loop quark self energy.	40

2.8	Dispersion laws for fermionic excitations.	44
2.9	One loop correction to the three-point quark gluon vertex.	46
2.10	One-loop correction to three gluon vertex.	48
3.1	The 2-flavor scaled QNS with that of free one as a function of T/T_C . The solid lines are for LO in HTLpt whereas the dashed lines are for LO (proportional to g^2) in pQCD. The symbols represent the various lattice data.	68
3.2	(Color online) <i>Left panel:</i> The ratio of 2-flavour HTL to free quark QNS and also that of LO perturbative one as a function of m_q/T . <i>Right panel:</i> R as a function of m_q/T	69
3.3	The scaled temporal correlation function with T^3 for $N_f = 1$ (left panel) and $N_f = 3$ (right panel) at $T = 1.45T_C$ for $Q = 2\pi T$ (red) and $4\pi T$ (blue) as a function of scaled Euclidean time. The symbols represent the recent lattice data.	70
3.4	Same as Fig. (3.3) but at $T = 1.2T_C$ and the corresponding lattice data are preliminary [311] with lattice size $148^3 \times 40$	71
3.5	Same as Fig. (3.3) but at $T = 2.98T_C$ and the corresponding lattice data are preliminary [311] with lattice size $148^3 \times 16$	72
4.1	Diagrams containing fermionic lines relevant for NLO thermodynam- ics potential in HTLpt with finite chemical potential. Shaded circles indicate HTL n -point functions.	75
4.2	The NLO HTLpt pressure scaled with ideal gas pressure plotted along with four-loop pQCD pressure for two different values of chemical potential with $N_f = 3$ and 2-loop running coupling constant α_s	107

4.3	Same as Fig. 4.2 but for 3-loop α_s	107
4.4	<i>Left panel:</i> ΔP for $N_f = 3$ is plotted as a function of T for two-loop HTLpt result along with those of four-loop pQCD and lattice QCD data using 2-loop running coupling constant α_s . <i>Right panel:</i> Same as left panel but using 3-loop running coupling.	108
4.5	<i>Left panel:</i> χ_2 scaled by the free field value for LO (grey band) and NLO (sea green band) in 2-loop HTLpt, 4-loop pQCD (sky blue band) along-with various LQCD data using 2-loop α_s . <i>Right panel:</i> Same as left panel but using 3-loop α_s	113
4.6	χ_4 scaled by the free field value for LO and NLO HTLpt, 4-loop pQCD, and LQCD are plotted as a function of the temperature . . .	116
5.1	One and two loop Feynman diagrams that will contribute to the thermodynamic potential.	121
5.2	Three loop HTL Feynman diagrams that will contribute to the thermodynamic potential.	123
5.3	The shorthand notations used in Fig. (5.2).	124
5.4	Comparison of the $N_f = 2 + 1$, $\mu_B = 0$ (left) and $\mu_B = 400$ MeV (right) NNLO HTLpt pressure using one-loop running coupling constant with lattice data.	151
5.5	Comparison of the $N_f = 2 + 1$, $\mu_B = 0$ (left) and $\mu_B = 400$ MeV (right) NNLO HTLpt pressure using three-loop running coupling constant with lattice data.	152

5.6	Comparison of the Stefan-Boltzmann limit (dashed lines) and NNLO HTLpt (solid lines) results for the scaled pressure difference with lattice data.	153
5.7	Comparison of the $N_f = 2 + 1$, $\mu_B = 0$ (left) and $\mu_B = 400$ MeV (right) NNLO HTLpt energy density with lattice data.	154
5.8	Comparison of the $N_f = 2 + 1$, $\mu_B = 0$ (left) and $\mu_B = 400$ MeV (right) NNLO HTLpt entropy density with lattice data.	155
5.9	Comparison of the $N_f = 2 + 1$, $\mu_B = 0$ (left) and $\mu_B = 400$ MeV (right) NNLO HTLpt trace anomaly with lattice data.	156
5.10	Comparison of the $N_f = 2 + 1$, $\mu_B = 0$ (left) and $\mu_B = 400$ MeV (right) NNLO HTLpt speed of sound squared with lattice data.	157
5.11	The scaled second order baryon number susceptibility compared with various lattice data using one loop running (left) and three-loop running (right).	159
5.12	The scaled fourth order baryon number susceptibility compared with various lattice data using one loop running (left) and three-loop running (right).	160
5.13	Comparison of the $N_f = 2 + 1$ NNLO HTLpt ratio of the fourth to second order baryon susceptibility with lattice data.	160
5.14	The $N_f = 2+1$ NNLO HTLpt scaled sixth-order baryon susceptibility as a function of temperature.	161
5.15	Comparison of the $N_f = 2 + 1$ NNLO HTLpt ratio of the fourth order diagonal single quark number susceptibility (left) and the only non-vanishing fourth order off-diagonal quark number susceptibility (right) with lattice data.	162

5.16	Comparison of the $N_f = 2 + 1$ NNLO HTLpt ratio of the fourth to second order single quark susceptibility with lattice data.	163
5.17	The $N_f = 2 + 1$ NNLO HTLpt scaled sixth-order diagonal single quark susceptibility as a function of temperature.	164
5.18	The $N_f = 2 + 1$ NNLO HTLpt scaled sixth-order off-diagonal single quark susceptibilities as a function of temperature.	165
6.1	One-loop dilepton rate from HTLpt for small invariant masses at zero momentum alongwith born-rate versus the scaled invariant photon mass	171
6.2	Complete 2-loop dilepton rate for small invariant masses $M \sim gT$ at zero momentum and Born-rate (dashed line) versus the scaled invariant photon mass	174
6.3	α_s -correction to the dilepton rate and Born-rate (dashed line) versus the invariant photon mass scaled with the thermal quark mass	175
6.4	Van Hove singularities in the dilepton rate in the presence of gluon condensate as a function of invariant mass scaled with T_c	178
6.5	<i>Left panel:</i> ρ -meson spectral function as a function of the invariant mass for a set of values T . <i>Right panel:</i> The dilepton rate from ρ -meson in a QGP as a function of M . The dashed lines are corresponding Born-rates.	181
6.6	<i>Left panel:</i> Imaginary part of ρ -meson propagator (spectral function) as a function of M for a set of values of μ . <i>Right panel:</i> The dilepton rate from ρ -meson in a QGP as a function of M . We chose $G_\rho = 6$. The dash-dotted lines are corresponding Born-rates.	182

6.7	The zero momentum vector spectral function within lattice gauge theory	184
6.8	Comparison of various dilepton rates in QGP and hadron gas.	185
6.9	Momentum integrated dilepton rate	188

CHAPTER 1

Introduction

It is now well-known that colored quarks and gluons are confined within color singlet hadronic bound states by strong interactions [23]. The theory which describes the behavior of quarks and gluons is known as Quantum Chromodynamics (QCD). Much of the support for QCD derives from its ability to produce the almost noninteracting behavior of quarks at short distances [23]. This feature of the theory, known as asymptotic freedom, explains the approximate scaling observed in the deep inelastic scattering of leptons off hadrons and leads to many quantitative predictions of scaling deviations at high energy. The success of these predictions, as well as many other confirmations of the predictions of perturbative QCD at short distances has greatly increased the confidence in the theory.

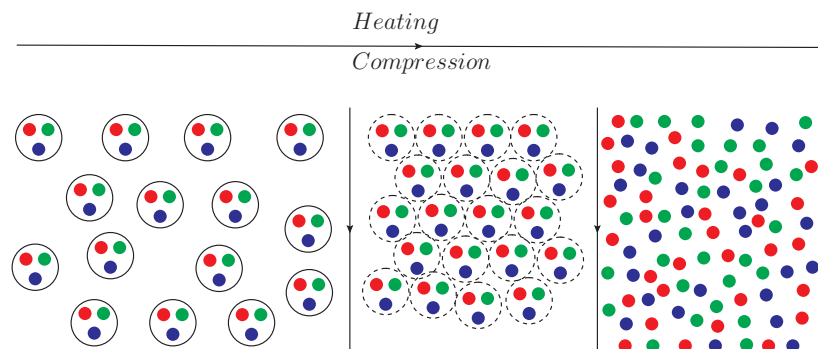


Figure 1.1: Nuclear matter at extreme conditions.

So it is worth to apply the knowledge of QCD to explore the properties of hadronic matter in extreme environments, such as at high temperature and/or at high baryonic density. As nuclear matter is heated and compressed hadrons occupy more and more of the available space within nucleus as schematically depicted in Fig. (1.1). Eventually they start to overlap and quarks and gluons confined initially begin to percolate between hadrons thus being liberated. Under this conditions quarks and gluons are no longer remain confined within hadrons and a new state of matter known as Quark Gluon Plasma (QGP) is produced. There are three places where one might look for this deconfined state of matter, *viz.*

- i) in the evolution of early universe where a few tens of microseconds after the ‘big bang’ a transient stage of strongly interacting matter prevailed at temperatures $10^{12}\text{K}(\sim 200\text{MeV})$ with a very small net baryon numbers;
- ii) in the interior of neutron stars where mass densities are likely to exceed 10^{15}gm/cm^3 which is about four times the central density of nuclei while the surface temperatures are as low as 10^5K or less;
- iii) in the collision of heavy ions at very high energy per nucleon, in which states of high density and temperature might be produced.

The above mentioned three situations have been schematically depicted in QCD phase diagram in Fig. (1.2). Nevertheless, the ‘big bang’ is far remote in time and the astrophysical objects are far remote in space and their use for the study of QGP are quite difficult. This makes us to turn attention for a consistent study of QGP in the laboratory through high energy heavy-ion collisions.

In heavy-ion-collisions experiments, two heavy nuclei are accelerated to ultra-relativistic speeds and directed towards each other. During the collision, kinetic energy of the Lorentz contracted nuclei are deposited at the collision region that produce a very hot and dense “fireball”. This fireball expands hydrodynamically under its own

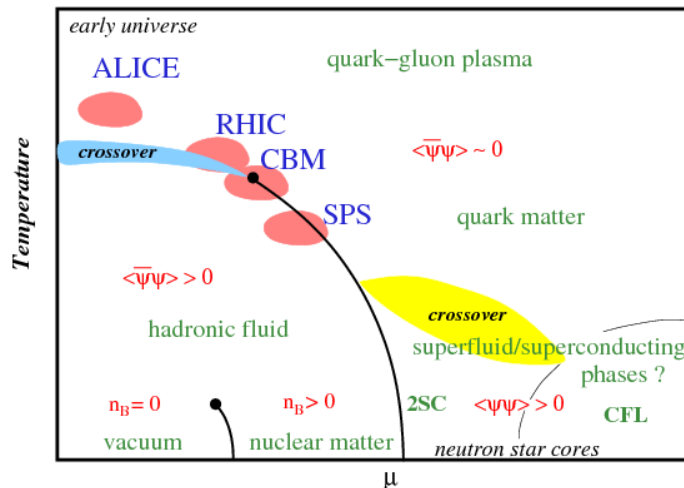


Figure 1.2: Schematic view of QCD phase diagram.

pressure, and cools while expanding. This expansion continues till all of the hot and dense fireball is converted into the hadronic phase. Upon completion of phase conversion, the hadronic matter continues to expand until the mean free path of the hadrons becomes larger than the dimensions of the system and they lose thermal contact. This is called freeze-out. At the freeze-out temperature, the hadrons cease to interact with each other and they stream freely away to be detected in the experiments.

In recent years substantial experimental efforts have been undertaken to investigate the versatile physics issues involved in ultra-relativistic heavy-ion collisions, i.e., collisions of atomic nuclei in which center-of-mass energy per nucleon is much larger than the nucleon rest mass. The principal goal of this initiative is to explore the phase structure of QCD by creating QGP in the laboratory; in other words, how QCD works in extreme conditions. Heavy-ion experiments have been performed at Alternating Gradient Synrotron in Brookhaven National Laboratory (BNL), USA with $E_{\text{lab}} \sim 14$ GeV/nucleon continued at Super Proton Synrotron (SPS) in the European Organization for Nuclear Research (CERN) with $E_{\text{lab}} \sim 200$ GeV/nucleon. At present the relativistic heavy-ion collision experiments in Relativistic Heavy Ion Collider (RHIC) at BNL with $E_{\text{cm}} \sim 200$ GeV/nucleon (and with

beam energy scan down to 7.7 GeV/nucleon) and Large Hadron Collider (LHC) at CERN [24, 25] with $E_{\text{cm}} \sim 2.76$ and 5.5 TeV/nucleon are operational. Further, at the forthcoming fixed target experiment at the Facility for Antiproton and Ion Research (FAIR) [26] in Gesellschaft für Schwerionenforschung (GSI), Germany as well as heavy-ion-collisions experiment at Nuclotron-based Ion Collider fAcility (NICA) in Joint Institute for Nuclear Research(JINR), Russia also plan to scan energy ranges from 10-45 GeV/nucleon and 4-11 GeV/nucleon respectively. These past experiments in CERN-SPS [27], ongoing experiments in BNL-RHIC [1-4, 28-32] and CERN-LHC [33-38] have provided us wealth of information in understanding the properties of hot and dense matter and the theoretical predictions.

Theoretical study of hot and dense nuclear matter which produced in early universe just after big bang or expected to exist in astrophysical objects like neutron star or produced in heavy-ion experiments are very important. QCD exhibits a rich phase structure and the equation of state (EoS) which describes that the matter can be characterized by different degrees of freedom depending upon the temperature and the chemical potential. The determination of the EoS of QCD matter is extremely important to QGP phenomenology. There are various effective models to describe the EoS and various order conserved density fluctuations of strongly interacting matter, *e.g.*, the Nambu-Jona-Lasinio (NJL) [39-42], Polyakov-loop extended Nambu-Jona-Lasinio (PNJL) [43-57], Renormalization Group approach [58, 59], quasi-particle models [60-68], Polyakov-loop extended quark meson (PQM) model [69-71], AdS/CFT correspondence and holographic QCD [72-75] have been used to calculate various thermodynamic functions and various order quark number susceptibilities.

However, one would prefer to utilize systematic first-principles QCD methods. The currently most reliable method for determining the EoS, various order quark number susceptibilities and other relevant quantities for deconfined matter is lattice

QCD [8–11, 76–126]. At this point in time lattice calculations can be performed at arbitrary temperature, however, due to the sign problem, it is not straightforward to extend such calculations to finite baryon chemical potential. In practice, it is possible to obtain information about the behavior of the thermodynamic functions at small baryon chemical potential [127] by making a Taylor expansion of the partition function around $\mu_B = 0$ and extrapolating the result. This requires the calculation of various quark-number susceptibilities evaluated at zero chemical potential. Since extrapolations based on a finite number of Taylor coefficients can only be trusted at small chemical potential, it would be nice to have an alternative framework for calculating the finite temperature and chemical potential QCD thermodynamic potential and associated quantities. This is important in light of the ongoing beam energy scan at the Relativistic Heavy Ion Collider (RHIC) and the forthcoming experiments at the Facility for Antiproton and Ion Research (FAIR). As an alternative to lattice QCD calculations, one natural option is to compute the thermodynamic potential using perturbation theory.

Perturbative QCD (pQCD) can be applied at high temperature and/or chemical potentials where the strong coupling ($g^2 = 4\pi\alpha_s$) is small in magnitude and non-perturbative effects are expected to be small; however, one does not know a priori how large the temperature should be for this method to result in a good approximation to reality. The calculation of thermodynamic functions at finite temperature and/or finite chemical potential using perturbative approach has a long history. In 1977 free energy for electron [128] and also for quark [129] have been computed at zero temperature and finite chemical potential up to order g^4 where the coefficient of g^4 term was obtained numerically. Later this calculation was reproduced in [13] analytically. In 1978, QCD free energy at finite temperature and zero chemical potential was calculated in [130, 131] up to order g^2 . In 1979, QCD free energy at finite temperature and finite chemical potential was extended in [132] up to order g^3 . In 1983, QCD free energy up to order $g^4 \log g$ at finite temperature and finite chemical

potential was calculated in [133]. In early 1990s the free energy at finite temperature but at zero chemical potential was calculated to order g^4 for massless scalar ϕ^4 theory [134–136], quantum electrodynamics (QED) [135–137] and QCD [135, 136], respectively. The corresponding calculations to order g^5 were obtained soon afterwards [138–144]. Later this calculation has been extended to calculate the QCD free energy at finite temperature but at zero chemical potential up to order g^6 in Ref. [12] where the coefficient of $g^6 \log g$ term was computed analytically but the coefficient of the g^6 term was fitted from lattice QCD data. In 2003, the free energy at finite chemical potential [13, 145] and hence quark number susceptibility [146] has been extended in up to order $g^6 \log g$. The results of QCD pressure at finite temperature and chemical potential up to order $g^6 \log g$ from Ref. [13] will be discussed in Sec. (1.3). For massless scalar theories the perturbative free energy is now known to order g^6 [147] and order $g^8 \log g$ [148].

Unfortunately, for all the above-mentioned theories the resulting weak-coupling approximations, truncated order-by-order in the coupling constant, are poorly convergent unless the coupling constant is tiny. Therefore, a straightforward perturbative expansion in powers of α_s for QCD does not seem to be of any quantitative use even at temperatures many orders of magnitude higher than those achievable in heavy-ion collisions. Also, due to infrared singularities in the gauge sector, the perturbative expansion of the finite-temperature and density QCD partition function breaks down at order g^6 requiring non-perturbative input albeit through a single numerically computable number [149].

The poor convergence of finite-temperature perturbative expansions of thermodynamic functions stems from the fact that at high temperature the classical solution is not described by massless gluonic states. Instead one must include plasma effects such as the screening of electric fields and Landau damping via a self-consistent resummation [150]. The inclusion of plasma effects can be achieved by reorganizing

perturbation theory.

There are several ways of systematically reorganizing the finite-temperature perturbative expansion [60–63,151–162]. In this thesis I will focus on the hard-thermal-loop (HTL) perturbation theory method [14–20,163–179]. The HTL perturbation theory is inspired by variational perturbation theory [180–185]. HTL perturbation theory is a gauge-invariant extension of screened perturbation theory (SPT) [186–189], which is a perturbative reorganization for finite-temperature massless scalar field theory. In the SPT approach, one introduces a single variational parameter which has a simple interpretation as a thermal mass. In SPT a mass term is added to and subtracted from the scalar Lagrangian, with the added piece kept as part of the free Lagrangian and the subtracted piece associated with the interactions. The mass parameter is then required to satisfy a variational equation which is obtained by a principle of minimal sensitivity. This naturally led to the idea that one could apply a similar technique to gauge theories by adding and subtracting a mass in the Lagrangian. However, in gauge theories, one cannot simply add and subtract a local mass term since this would violate gauge invariance. As a result, a gauge-invariant generalization of SPT called hard-thermal-loop (HTL) perturbation theory was developed [150] by Braaten and Pisarski in 1990 by distinguishing soft ($p \sim gT$) and hard ($p \sim T$) momenta scale. HTL perturbation theory is a reorganization of usual perturbation theory at finite temperature where higher order diagrams contribute to the lower order one. In HTL perturbation theory one needs to add and subtract HTL improvement term which modifies the propagators and vertices self-consistently so that the reorganization is manifestly gauge invariant [155].

In the thesis I shall discuss a systematic computation of QCD thermodynamics in leading order as well as beyond leading order at finite temperature and finite chemical potential using HTL perturbation theory. Conserved density fluctuations and quark number susceptibility will be discussed in leading order withing HTL perturba-

tion theory. In next-to-leading order QCD pressure and various order quark number susceptibilities will be discussed. In next-to-next-leading order, the computation of all the thermodynamical quantities *viz.* pressure, various order quark number susceptibilities, energy density, entropy density, speed of sound, trace anomaly etc. will be discussed. The corresponding HTL perturbation theory results in all order will be compared with recent lattice QCD data.

Besides the thermodynamic calculations, this thesis will also be focused to analyzed the dilepton rate from hot and dense nuclear matter. As the electromagnetic probes, such as real photon and dileptons, are a particular example of ‘circumstantial evidence’, and accordingly thermal dileptons have been theoretically proposed long time ago [21]. At SPS energies [190–193] there was an indication for an enhancement of the dilepton production at low invariant mass ($0.2 \leq M(\text{GeV}) \leq 0.8$) compared to all known sources of electromagnetic decay of the hadronic particles and the contribution of a radiating simple hadronic fireball (for comprehensive reviews see Refs. [194–196]). One of the possible explanations of this is the modification of the in-medium properties of the vector meson (*viz.*, ρ -meson) by rescattering in a hadronic phase along with only the lowest order perturbative rate, *i.e.*, $q\bar{q}$ annihilation from a QGP [194–213]. Also at RHIC energies [28] a substantial amount of excess of electron pairs was reported in the low invariant mass region. Models taking into account in-medium properties of hadrons with various ingredients (see for details [214, 215]) can not explain the data from RHIC in the range $0.15 \leq M(\text{GeV}) \leq 0.5$, whereas they fit the SPS data more satisfactorily, indicating that a possible non-hadronic source becomes important at RHIC.

On the other hand, the higher order perturbative calculations [216] are also not very reliable at temperatures within the reach of the heavy-ion collisions. Moreover, perturbative calculations of the dilepton rate seem not to converge even in small coupling (g) limit. Nevertheless, the lowest order perturbative $q\bar{q}$ annihilation is the

only dilepton rate from the QGP phase that is extensively used in the literatures. However, at large invariant mass this contribution should be dominant but not at low invariant mass, where nonperturbative effects should play an important role. Unfortunately, the lattice data [217] due to its limitations also could not shed any light on the low mass dileptons. However, the lattice calculations [7, 109–112, 218, 219] provide evidence for the existence of nonperturbative effects associated with the bulk properties of the deconfined phase, in and around the deconfinement temperature, T_c . Also, indications have been found that the QGP at RHIC energies behaves more as a strongly coupled liquid than a weakly coupled gas [220]. Thus, a nonperturbative analysis of the dilepton rate from the deconfined phase is essential.

The dilepton emission at low invariant mass from the deconfined phase is still an unsettled issue in heavy-ion collisions at SPS and RHIC energies and, in particular, would be an important question for LHC energies and for compact baryonic matter formation in future FAIR energies, and also for the quark-hadron duality [194, 195, 221] that entails a reminiscence to a simple perturbative lowest order quark-antiquark annihilation rate [222]. In this thesis we reconsider the dilepton production rates within the perturbative QCD, and non-perturbative models based on lattice inputs and phenomenological $\rho - q$ interaction in the deconfined phase. The analysis suggests that the nonperturbative dilepton rates are indeed important at the low invariant mass regime.

Below we give a brief introduction to statistical physics, QCD at finite temperature and density, pQCD pressure up to $g^6 \log g$ and asymptotic nature of QCD which will be necessary to study various quantities in the following chapters.

1.1 Statistical physics and quantum partition function

For a relativistic system which can freely exchange energy and particles with its surroundings, the most important function in thermodynamics is the grand canonical partition function

$$Z = \sum_{\text{states}} e^{-\beta(\mathcal{E}_i - \mu N)} = \sum_{\text{states}} \langle \mathcal{E}_i | e^{-\beta(\mathcal{H} - \mu N)} | \mathcal{E}_i \rangle = \text{Tr} e^{-\beta(\mathcal{H} - \mu N)}. \quad (1.1)$$

Here \mathcal{E}_i is the energy of the state $|\mathcal{E}_i\rangle$, N is the number of particles and \mathcal{H} is the Hamiltonian of the system. The inverse temperature of the system is denoted by $\beta = 1/T$, and μ is the chemical potential of the particles in the system. All of the thermodynamic properties can be determined from (1.1). For example, the pressure, entropy density, particle density and energy density are given by

$$\mathcal{P} = \frac{\partial(T \log Z)}{\partial V}, \quad (1.2)$$

$$\mathcal{S} = \frac{1}{V} \frac{\partial(T \log Z)}{\partial T} = \frac{\partial \mathcal{P}}{\partial T}, \quad (1.3)$$

$$n_i = \frac{1}{V} \frac{\partial(T \log Z)}{\partial \mu_i} = \frac{\partial \mathcal{P}}{\partial \mu_i}, \quad (1.4)$$

$$\mathcal{E} = -\mathcal{P} + T\mathcal{S} + \sum_{i=1}^{N_f} \mu_i n_i, \quad (1.5)$$

where V is the volume of the system and N_f is the number of flavors of the system. Typically, the width L of a system is much larger than the inverse temperature, (i.e. $L \gg 2\pi/T$), such that one can use the infinite volume limit to describe the thermodynamics of a finite volume to good approximation. In all calculations performed in this thesis, this infinite volume limit is taken. Then it turns out that $\log Z$ becomes

proportional to V , such that the pressure becomes

$$\mathcal{P} = \frac{T \log Z}{V}. \quad (1.6)$$

The extension to field theory is straightforward. If \mathcal{H} is the Hamiltonian of a quantum field theory in d -dimensional space and hence $(d + 1)$ -dimensional space-time, then the partition function (1.1) is

$$Z = \text{Tr} e^{-\mathcal{H}/T} = \int \mathcal{D}\varphi e^{-\int_0^{1/T} d\tau \int d^d x \mathcal{L}(\varphi)}, \quad (1.7)$$

with \mathcal{L} the Lagrangian density of the theory and *periodic* boundary conditions

$$\varphi(0, \mathbf{x}) = \varphi(1/T, \mathbf{x}). \quad (1.8)$$

for bosonic fields φ . For fermionic fields, it turns out that to implement Pauli statistics one must impose *anti-periodic* boundary conditions

$$\varphi(0, \mathbf{x}) = -\varphi(1/T, \mathbf{x}). \quad (1.9)$$

1.2 QCD at finite temperature

Quantum Chromodynamics is a gauge theory for the strong interaction describing the interactions between quarks and gluons. The QCD Lagrangian density in Minkowski space can be written as

$$\begin{aligned} \mathcal{L}_{\text{QCD}} = & -\frac{1}{2} \text{Tr} [F_{\mu\nu} F^{\mu\nu}] + \sum_i \bar{\psi}_i [i\gamma^\mu D_\mu - \gamma_0 \mu_i - m_i] \psi_i \\ & + \mathcal{L}_{\text{gf}} + \mathcal{L}_{\text{ghost}} + \Delta \mathcal{L}_{\text{QCD}}. \end{aligned} \quad (1.10)$$

where $\Delta\mathcal{L}_{\text{QCD}}$ contains counterterms necessary to cancel the ultraviolet divergences in perturbative calculations. The gluon field strength is $F_{\mu\nu} = \partial_\mu A_\nu - \partial_\nu A_\mu - ig[A_\mu, A_\nu]$. The gluon field is $A_\mu = A_\mu^a t^a$, with generators t^a of the fundamental representation of SU(3) normalized so that $\text{Tr } t^a t^b = \delta^{ab}/2$. In the quark sector there is an explicit sum over the N_f quark flavors with masses m_i and $D_\mu = \partial_\mu - igA_\mu$ is the covariant derivative in the fundamental representation. The Lagrangian (1.10) is mathematically simple and beautiful, however in order to carry out a physical calculation with it perturbatively, a gauge fixing is needed to remove unphysical degrees of freedom. The ghost term $\mathcal{L}_{\text{ghost}}$ depends on the choice of the gauge-fixing term \mathcal{L}_{gf} . One popular choice for the gauge-fixing term that depends on an arbitrary gauge parameter ξ is the general covariant gauge:

$$\mathcal{L}_{\text{gf}} = -\frac{1}{\xi} \text{Tr} [(\partial^\mu A_\mu)^2] . \quad (1.11)$$

The corresponding ghost term in the general covariant gauge reads

$$\mathcal{L}_{\text{ghost}} = -\bar{\eta}^a \partial^2 \eta^a + g f^{abc} \bar{\eta}^a \partial^\mu (A_\mu^b \eta^c) , \quad (1.12)$$

where η and $\bar{\eta}$ are anti-commuting ghosts and anti-ghosts respectively and f^{abc} is structure constant of SU(3).

The finite temperature QCD partition function is obtained by a Wick rotation of the theory from Minkowski space to Euclidean space. It is achieved by the substitution $t = i\tau$ with t being the Minkowski time and τ being the Euclidean one. The resulting Euclidean partition function is

$$Z = \int \mathcal{D}A_\mu \mathcal{D}\bar{\psi} \mathcal{D}\psi \mathcal{D}\bar{\eta} \mathcal{D}\eta \exp \left[- \int_0^{1/T} d\tau \int d^3x \mathcal{L}_{\text{QCD}}^E \right] , \quad (1.13)$$

with $\mathcal{L}_{\text{QCD}}^E$ the Wick-rotated Lagrangian density. Feynman rules are exactly the same as in zero-temperature field theory except that the imaginary time τ is now

compact with extent $1/T$. To go from τ to frequency space, one should perform a Fourier series decomposition rather than a Fourier transform. The only difference with zero-temperature Feynman rules will then be that loop frequency integrals are replaced by loop frequency sums:

$$\int \frac{d^4 P}{(2\pi)^4} \rightarrow T \sum_{\omega_n} \int \frac{d^3 p}{(2\pi)^3} \quad (1.14)$$

with the sum over discrete imaginary-time frequencies known as Matsubara frequencies

$$\omega_n = 2n\pi T \quad \text{bosons ,} \quad (1.15)$$

$$\omega_n = (2n + 1)\pi T - i\mu \quad \text{fermions .} \quad (1.16)$$

to implement the periodic or anti-periodic boundary conditions in Eq. (1.8) and Eq. (1.9) respectively.

We define the dimensionally regularized bosonic and fermionic sum-integrals as

$$\oint_P \equiv \left(\frac{e^{\gamma_E} \Lambda^2}{4\pi} \right)^\epsilon T \sum_{P_0=2n\pi T} \int \frac{d^{3-2\epsilon} p}{(2\pi)^{3-2\epsilon}} , \quad (1.17)$$

$$\oint_{\{P\}} \equiv \left(\frac{e^{\gamma_E} \Lambda^2}{4\pi} \right)^\epsilon T \sum_{P_0=(2n+1)\pi T - i\mu} \int \frac{d^{3-2\epsilon} p}{(2\pi)^{3-2\epsilon}} , \quad (1.18)$$

where $3 - 2\epsilon$ is the dimension of space, $\gamma_E \approx 0.577216$ the Euler-Mascheroni constant commonly known as Euler gamma, Λ is an arbitrary momentum scale, $P = (P_0, p)$ is the bosonic loop momentum, and $\{P\}$ is the fermionic loop momentum. The factor $(e^{\gamma_E}/4\pi)^\epsilon$ is introduced so that, after minimal subtraction of the poles in ϵ due to ultraviolet divergences, Λ coincides with the renormalization scale of the $\overline{\text{MS}}$ renormalization scheme. Note that we are denoting four momentum in Euclidean space as $P = (P_0, p)$ and in Minkowski space as $P = (p_0, p)$.

Sometimes we use shorthand notation for $d = 3 - 2\epsilon$ dimensional integration as

$$\int_{\mathbf{p}} \equiv \int \frac{d^{3-2\epsilon}p}{(2\pi)^{3-2\epsilon}}. \quad (1.19)$$

So one needs to evaluate the frequency sum(1.14) for bosonic case as

$$T \sum_{p_0} f(p_0 = i\omega_n = 2n\pi iT) = \frac{T}{2\pi i} \oint_C dp_0 \frac{\beta}{2} f(p_0) \coth \frac{\beta p_0}{2}, \quad (1.20)$$

where the contour C is as shown Fig. (1.3a): The function $\frac{\beta}{2} \coth \frac{\beta p_0}{2}$ has poles

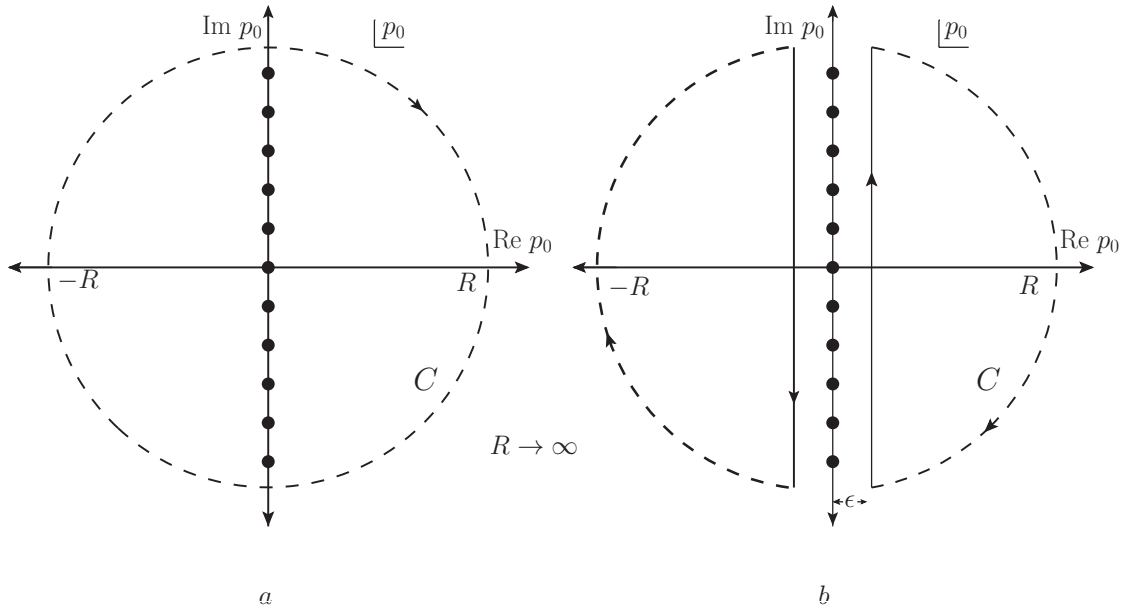


Figure 1.3: Contour for bosonic frequency sum.

at $p_0 = 2\pi niT$ and is everywhere else bounded and analytic. The contour can be deformed as Fig. (1.3b).

So the frequency sum in Eq. (1.20) can be rewritten as

$$\begin{aligned}
 T \sum_{p_0} f(p_0 = i\omega_n = 2n\pi iT) &= \frac{1}{2\pi i} \int_{-i\infty+\epsilon}^{i\infty+\epsilon} dp_0 f(p_0) \frac{1}{2} \coth \frac{\beta p_0}{2} \\
 &+ \frac{1}{2\pi i} \int_{i\infty-\epsilon}^{-i\infty-\epsilon} dp_0 f(p_0) \frac{1}{2} \coth \frac{\beta p_0}{2} \\
 &= \frac{1}{2\pi i} \int_{-i\infty+\epsilon}^{i\infty+\epsilon} dp_0 f(p_0) \left[\frac{1}{2} + \frac{1}{e^{\beta p_0} + 1} \right] \\
 &- \frac{1}{2\pi i} \int_{-i\infty-\epsilon}^{i\infty-\epsilon} dp_0 f(p_0) \left[\frac{1}{2} + \frac{1}{e^{\beta p_0} + 1} \right] \quad (1.21)
 \end{aligned}$$

Below we demonstrate one examples of frequency sum for bosonic momentum:

$$\begin{aligned}
 \sum_{p_0=2n\pi iT} \frac{1}{P^2} &= \sum_{p_0=2n\pi iT} \frac{1}{p_0^2 - p^2} = \sum_{p_0=2n\pi iT} \frac{1}{2p} \left[\frac{1}{p_0 - p} - \frac{1}{p_0 + p} \right] \\
 &= \frac{1}{2p} \left[- \left(\frac{1}{2} + \frac{1}{e^{\beta p} - 1} \right) + \left(\frac{1}{2} + \frac{1}{e^{-\beta p} - 1} \right) \right] \\
 &= -\frac{1}{p} \left[\frac{1}{2} + n_B(p) \right], \quad (1.22)
 \end{aligned}$$

where $n_B(p) = 1/(\exp(\beta p) - 1)$ is Bose-Einstein distribution function. When one calculates $(d+1)$ dimensional sum-integrals, the first term of the frequency sum (1.22) vanishes due to dimensional regularization and gets the finite results for this particular sum-integration.

One can also evaluate the frequency sum(1.14) for fermionic case in the similar manner as

$$T \sum_{p_0} f(p_0 = i\omega_n = (2n + 1)\pi iT + \mu) = \frac{T}{2\pi i} \oint_{C'} dp_0 \frac{\beta}{2} f(p_0) \tanh \frac{\beta(p_0 - \mu)}{2} \quad (1.23)$$

where the contour C' is as shown in the Fig. (1.4). The function $\frac{\beta}{2} \tanh \frac{\beta(p_0 - \mu)}{2}$ has poles at $p_0 = (2n + 1)\pi iT + \mu$ and is everywhere else bounded and analytic. The

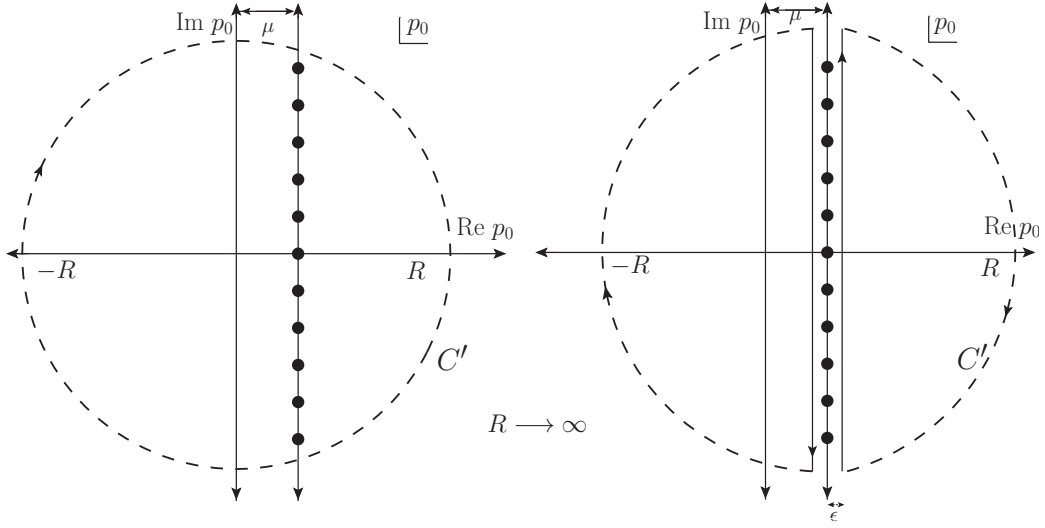


Figure 1.4: Contour for fermionic frequency sum.

contour C' can be deformed in the similar manner as in the bosonic case to avoid the pole on the contour. Then the frequency sum in Eq. (1.23) can be rewritten as

$$\begin{aligned}
 T \sum_{p_0} f(p_0 = i\omega_n = (2n + 1)\pi iT + \mu) &= \frac{1}{2\pi i} \int_{-i\infty + \mu + \epsilon}^{i\infty + \mu + \epsilon} dp_0 f(p_0) \frac{1}{2} \tanh \frac{\beta p_0}{2} \\
 &+ \frac{1}{2\pi i} \int_{i\infty + \mu - \epsilon}^{-i\infty + \mu - \epsilon} dp_0 f(p_0) \frac{1}{2} \tanh \frac{\beta(p_0 - \mu)}{2} \\
 &= \frac{1}{2\pi i} \int_{-i\infty + \mu + \epsilon}^{i\infty + \mu + \epsilon} dp_0 f(p_0) \left[\frac{1}{2} + \frac{1}{e^{\beta(p_0 - \mu)} + 1} \right] \\
 &- \frac{1}{2\pi i} \int_{-i\infty + \mu - \epsilon}^{i\infty + \mu - \epsilon} dp_0 f(p_0) \left[\frac{1}{2} + \frac{1}{e^{\beta(p_0 - \mu)} + 1} \right]. \quad (1.24)
 \end{aligned}$$

Below we demonstrate one examples of frequency sum for fermionic momentum:

$$\begin{aligned}
 \sum_{p_0=2n\pi iT} \frac{1}{P^2} &= \sum_{p_0=2n\pi iT} \frac{1}{p_0^2 - p^2} = \sum_{p_0=2n\pi iT} \frac{1}{2p} \left[\frac{1}{p_0 - p} - \frac{1}{p_0 + p} \right] \\
 &= \frac{1}{2p} \left[- \left(\frac{1}{2} - \frac{1}{e^{\beta(p-\mu)} + 1} \right) + \left(\frac{1}{2} - \frac{1}{e^{-\beta(p+\mu)} + 1} \right) \right] \\
 &= -\frac{1}{2p} [1 - n_F(p)], \quad (1.25)
 \end{aligned}$$

where $n_F(p) = [e^{\beta(p-\mu)} + 1]^{-1} + [e^{\beta(p+\mu)} + 1]^{-1} = [n_F^-(p) + n_F^+(p)]$.

After performing the frequency sum, one is left with dimensionally regularized spatial momentum integration, which will be discussed in the subsequently chapter. However, all other frequency sums can be evaluated in similar way as discussed above.

1.3 Perturbative pressure in QCD up to order $g^6 \log g$

In perturbation theory one can explicitly separate the contributions coming from the soft sector (momenta on the order of gT where $g^2 = 4\pi\alpha_s$) and the hard sector (momenta on the order of T) using effective field theory/dimensional reduction methods [12, 139, 144, 153, 223–225]. After doing this one finds that the hard-sector contributions, which form a power series in even powers of g , converge reasonably well; however, the soft sector perturbative series, which contains odd powers of g , is poorly convergent. Below we present the result of QCD free energy $\mathcal{F}(T, \mu)$ for N_f flavor in perturbative series up to order up to order $g^6 \log g$ *i.e.*, $\alpha_s^3 \ln(\alpha_s)$.

$$\begin{aligned} \mathcal{F} = & -\frac{8\pi^2}{45} T^4 \left[\mathcal{F}_0 + \mathcal{F}_2 \frac{\alpha_s}{\pi} + \mathcal{F}_3 \left(\frac{\alpha_s}{\pi} \right)^{3/2} + \mathcal{F}_4 \left(\frac{\alpha_s}{\pi} \right)^2 \right. \\ & \left. + \mathcal{F}_5 \left(\frac{\alpha_s}{\pi} \right)^{5/2} + \mathcal{F}_6 \left(\frac{\alpha_s}{\pi} \right)^3 + \dots \right], \end{aligned} \quad (1.26)$$

where we have specialized to the case $N_c = 3$ and

$$\mathcal{F}_0 = 1 + \frac{21}{32} N_f \left(1 + \frac{120}{7} \hat{\mu}^2 + \frac{240}{7} \hat{\mu}^4 \right), \quad (1.27)$$

$$\mathcal{F}_2 = -\frac{15}{4} \left[1 + \frac{5N_f}{12} \left(1 + \frac{72}{5} \hat{\mu}^2 + \frac{144}{5} \hat{\mu}^4 \right) \right], \quad (1.28)$$

$$\mathcal{F}_3 = 30 \left[1 + \frac{1}{6} (1 + 12\hat{\mu}^2) N_f \right]^{3/2} \quad (1.29)$$

$$\begin{aligned} \mathcal{F}_4 = & 237.223 + (15.963 + 124.773 \hat{\mu}^2 - 319.849 \hat{\mu}^4) N_f \\ & - (0.415 + 15.926 \hat{\mu}^2 + 106.719 \hat{\mu}^4) N_f^2 \\ & + \frac{135}{2} \left[1 + \frac{1}{6} (1 + 12\hat{\mu}^2) N_f \right] \log \left[\frac{\alpha_s}{\pi} (1 + \frac{1}{6} (1 + 12\hat{\mu}^2) N_f) \right] \\ & - \frac{165}{8} \left[1 + \frac{5}{12} \left(1 + \frac{72}{5} \hat{\mu}^2 + \frac{144}{5} \hat{\mu}^4 \right) N_f \right] \left(1 - \frac{2}{33} N_f \right) \log \hat{\Lambda}, \quad (1.30) \end{aligned}$$

$$\begin{aligned} \mathcal{F}_5 = & - \left(1 + \frac{1 + 12\hat{\mu}^2}{6} N_f \right)^{1/2} \left[799.149 + (21.963 - 136.33 \hat{\mu}^2 + 482.171 \hat{\mu}^4) N_f \right. \\ & \left. + (1.926 + 2.0749 \hat{\mu}^2 - 172.07 \hat{\mu}^4) N_f^2 \right] \\ & + \frac{495}{2} \left(1 + \frac{1 + 12\hat{\mu}^2}{6} N_f \right) \left(1 - \frac{2}{33} N_f \right) \log \hat{\Lambda}, \quad (1.31) \end{aligned}$$

$$\begin{aligned} \mathcal{F}_6 = & - \left[659.175 + (65.888 - 341.489 \hat{\mu}^2 + 1446.514 \hat{\mu}^4) N_f \right. \\ & + (7.653 + 16.225 \hat{\mu}^2 - 516.210 \hat{\mu}^4) N_f^2 - \frac{1485}{2} \left(1 + \frac{1 + 12\hat{\mu}^2}{6} N_f \right) \\ & \times \left(1 - \frac{2}{33} N_f \right) \log \hat{\Lambda} \left. \right] \log \left[\frac{\alpha_s}{\pi} \left(1 + \frac{1 + 12\hat{\mu}^2}{6} N_f \right) 4\pi^2 \right] \\ & - 475.587 \log \left[\frac{\alpha_s}{\pi} 4\pi^2 C_A \right], \quad (1.32) \end{aligned}$$

where here and throughout all hatted quantities are scaled by $2\pi T$, e.g. $\hat{\mu} = \mu/(2\pi T)$, Λ is the modified minimum subtraction ($\overline{\text{MS}}$) renormalization scale, and $\alpha_s = \alpha_s(\hat{\Lambda})$ is the running coupling. At finite T the central value of the renormalization scale is usually chosen to be $2\pi T$. However, at finite T and μ we use the central scale $\Lambda = 2\pi\sqrt{T^2 + (\mu/\pi)^2}$ [13, 68, 146, 226–228]. In Fig. (1.5) we plot the ratio of

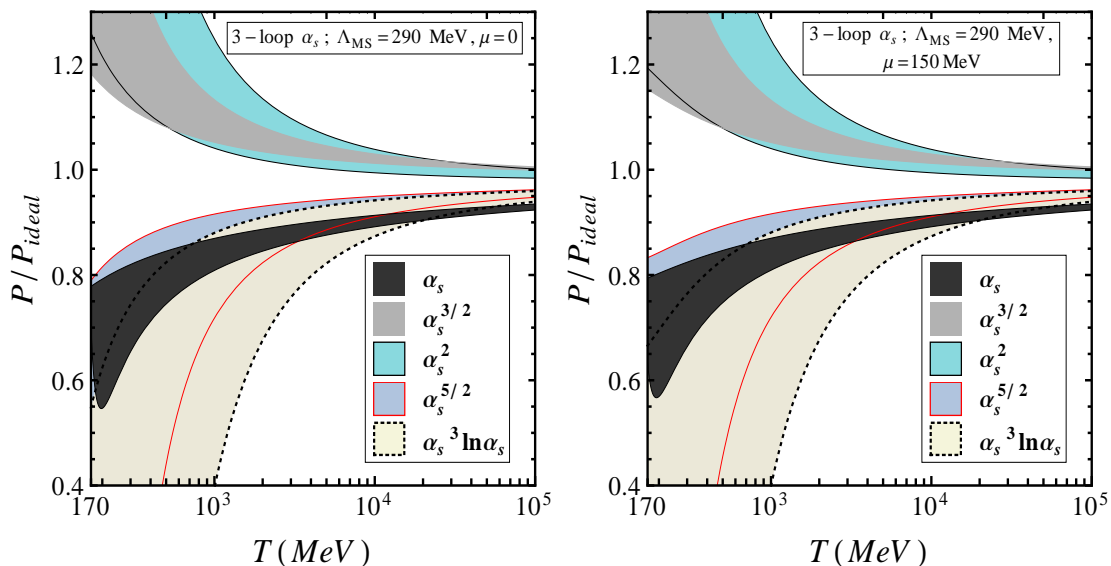


Figure 1.5: The $N_f = 3$ pQCD pressure specified in Eq. (1.26) as a function of the temperature. Successive perturbative approximations are shown through order $\alpha_s^3 \ln \alpha_s$ for vanishing μ (left) and for non-vanishing μ (right). The shaded bands indicate the variation of the pressure as the $\overline{\text{MS}}$ renormalization scale is varied around a central value of $\Lambda = 2\pi\sqrt{T^2 + \mu^2/\pi^2}$ [13, 68, 146, 226–228] by a factor of two. We use $\Lambda_{\overline{\text{MS}}} = 290$ MeV based on recent lattice calculations [229] of the three-loop running of α_s .

the pressure to an ideal gas of quarks and gluons. The figure clearly demonstrates the poor convergence of the naive perturbative series and the increasing sensitivity of the result to the renormalization scale as successive orders in the weak coupling expansion are included.

The poor convergence in soft sector which contains the odd power of g in perturbative series suggests that in order to improve the convergence of the resulting perturbative approximation one should treat the soft sector non-perturbatively, or at least resum soft corrections to the pressure. There have been works in the framework of dimensional reduction which effectively perform such soft-sector resummations by not truncating the soft-scale contributions in a power series in g , see *e.g.* [12, 223, 225]. This method seems to improve the convergence of the perturbation series and provides motivation to find additional analytic methods to accomplish soft-sector resummations.

1.4 Beta function and asymptotic freedom

The beta function $\beta(\alpha_s)$ of a quantum field theory encodes the dependence of a coupling parameter α_s on the energy scale Λ of a given physical process. The coupling satisfy the following relation [230, 231]:

$$\Lambda^2 \frac{\partial \alpha_s}{\partial \Lambda^2} = \beta(\alpha_s) = -\alpha_s^2 (b_0 + b_1 \alpha_s + b_2 \alpha_s^2 + b_3 \alpha_s^3 + \dots) \quad (1.33)$$

where b_0, b_1, b_2 and b_3 are referred to as beta-function coefficient in one, two, three and four loop respectively with

$$\begin{aligned} b_0 &= \frac{11c_A - 2N_f}{12\pi} \\ b_1 &= \frac{17c_A^2 - N_f(5c_A + 3c_F)}{24\pi^2} \\ b_2 &= \frac{1}{128\pi^3} \left[\frac{2857}{27}c_A^2 + N_f \left(2c_F^2 - \frac{205}{9}c_Ac_F - \frac{1415}{27}c_A^2 \right) \right. \\ &\quad \left. + N_f^2 \left(\frac{22}{9}c_F + \frac{79}{27}c_A \right) \right] \end{aligned} \quad (1.34)$$

where $c_A = N_c$ is number of colors, $c_F = (N_c^2 - 1)/2N_c$.

This dependence on the energy scale is known as the running of the coupling parameter, and theory of this kind of scale-dependence in quantum field theory is described by the renormalization group which refers to a mathematical apparatus that allows one to investigate the changes of a physical system as one views it at different distance scales.

To lowest order in the coupling constant a beta function is either positive indicating the growth of charge at short distance or negative indicating the decrease of charge at short distance. Until 1973, only examples of the former were known ¹. The

¹t Hooft reported a similar discovery at the Marseille conference on renormalization of Yang-Mills fields and applications to particle physics in 1972 without publishing it.

discovery that only non-Abelian gauge theories allow for a negative beta function is usually credited to Gross and Wilczek [23], and to Politzer [232]. The solution to (1.33) for QCD in one loop level reads

$$\alpha_s(\Lambda) = \frac{g(\Lambda)^2}{4\pi} = \frac{2\pi}{\left(11 - \frac{2}{3}N_f\right) \log(\Lambda/\Lambda_{\text{QCD}})}, \quad (1.35)$$

which clearly shows *asymptotic freedom* [23, 232], i.e. $\alpha_s \rightarrow 0$ as $\Lambda \rightarrow \infty$. The parameter Λ_{QCD} is a scale above which the theory works as “chosen” by the world in which we live.

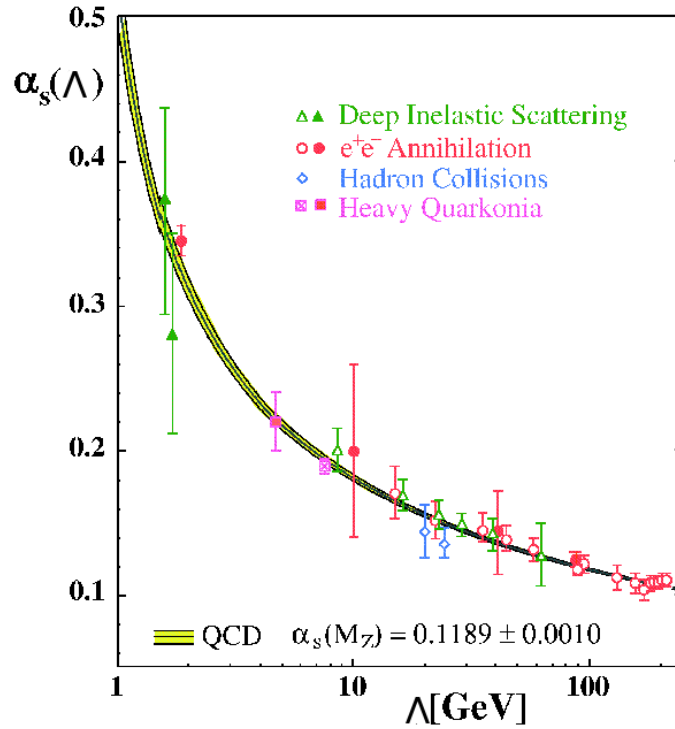


Figure 1.6: QCD running coupling as a function of energy scale. This figure is adapted from Ref. [233].

In three loop level, the solution to (1.33) is

$$\alpha_s(\Lambda) = \frac{1}{b_0 t} \left[1 - \frac{b_1 \ln t}{b_0^2 t} + \frac{b_1^2 (\ln^2 t - \ln t - 1) + b_0 b_2}{b_0^4 t} - \frac{b_1^3 (\ln^3 t - \frac{5}{2} \ln^2 t - 2 \ln t + \frac{1}{2}) + 3b_0 b_1 b_2 \ln t - \frac{1}{2} b_0^2 b_3}{b_0^6 t^3} + \dots \right] \quad (1.36)$$

with $t = \ln \frac{\Lambda^2}{\Lambda_{MS}^2}$. It is well known that QCD exhibits confinement at large distances or low energies which terminates the validity of perturbation theory due to the infrared growth of the coupling. However it is precisely the asymptotic freedom that ensures the possibility of a perturbative treatment for the ultraviolet sector of the theory which sets the stage to study the high temperature phase of non-Abelian theory in this thesis.

1.5 Scope of the thesis

The thesis is organized as follows: In Chapter 2, we discuss the limitations of bare perturbation theory and a brief introduction to HTL perturbation theory. In Chapter 3 we discuss conserved density fluctuation and temporal correlation function in hard thermal loop perturbation theory. In Chapter 4 we discuss thermodynamic functions *viz* pressure and quark number susceptibilities using HTL perturbation theory in two loop level. The Chapter 5 is devoted to the study of all possible three-loop thermodynamic functions at finite temperature and finite chemical potential using HTL perturbation theory for QCD. Low mass dilepton rate from deconfined state of matter will be discussed in Chapter 6. We summarize in Chapter 7 together with a brief outlook of HTL perturbation theory.

CHAPTER 2

Hard Thermal Loop Perturbation Theory

In this chapter, and in the rest of the thesis, we consider thermal field theories at high temperature, which means temperature much higher than all zero-temperature masses or any mass scales generated at zero temperature.

We can apply finite temperature field theory to calculate various thermodynamic quantities perturbatively. But naive perturbation theory have some serious problems. One of the problem is in the computation of gluon damping rate. If one uses naive perturbation theory to calculate gluon damping rate, one gets gauge dependent results and it is also negative in some gauges. This was sometimes interpreted as signal of plasma instability. Yet one knows from general field theoretical arguments that the positions of the pole of the gluon propagator, whose imaginary part gives the gluon damping rate, is gauge-independent.

Another problem in naive perturbation theory is infrared divergence. It has been known for many years that for naive perturbative expansion of finite temperature, partition function breaks down due to infrared divergences. To cure those problem of naive perturbation theory, a consistent perturbative expansion requires the resummation of an infinite subset of diagrams from all orders of perturbation theory. Hard thermal loop (HTL) perturbation theory is one of such resummation. In HTL

perturbation theory, we define two scales of momenta *viz.* hard and soft. When the momentum $p \sim T$, it is called hard scale and when momenta $p \sim gT$, this is called soft scale with g coupling constant of the theory. We discuss the HTL perturbation theory in case of scalar as well as gauge theory in the next section in details.

2.1 Scalar field theory

In this section we discuss about the simplest interacting scalar field theory, namely a single massless scalar field with a ϕ^4 interaction. The Lagrangian for such scalar field in Euclidean space can be written as

$$\mathcal{L} = \frac{1}{2}(\partial_\mu\phi)^2 + \frac{1}{24}g^2\phi^4. \quad (2.1)$$

The Lagrangian density in Eq. (2.1) can be divided into a free part and an interacting part as

$$\mathcal{L}_{\text{free}} = \frac{1}{2}(\partial_\mu\phi)^2, \quad (2.2)$$

$$\mathcal{L}_{\text{int}} = \frac{1}{24}g^2\phi^4. \quad (2.3)$$

Radiative corrections are then calculated in a loop expansion which is equivalent to a power series in g^2 . We shall see that the perturbative expansion breaks down at finite temperature and the weak-coupling expansion becomes an expansion in g rather than g^2 .

We will first calculate the self-energy by evaluating the relevant diagrams. The Feynman diagrams that contribute to the self-energy up to two loops are shown in Fig. (2.1).

The one-loop diagram is independent of the external momentum and the resulting



Figure 2.1: One- and two-loop scalar self-energy graphs.

integral expression is

$$\begin{aligned}
 \Pi^{(1)} &= \frac{1}{2}g^2 \sum_P \frac{1}{P^2}, \\
 &= \frac{1}{24}g^2 T^2, \\
 &\equiv m^2,
 \end{aligned} \tag{2.4}$$

where the superscript indicates the number of loops. The notation $P = (P_0, \mathbf{p})$ represents the Euclidean four-momentum. The Euclidean energy P_0 has discrete values: $P_0 = 2n\pi T$ for bosons and $P_0 = (2n + 1)\pi T$ for fermions, where n is an integer. Eq. (2.4) represents the leading order thermal mass of scalar field with ϕ^4 interaction. The sum-integral over P is defined in Eq. (1.18), represents a summation over Matsubara frequencies and integration of spatial momenta in $d = 3 - 2\epsilon$ dimensions¹. The above sum-integral has ultraviolet power divergences that are set to zero in dimensional regularization. We are then left with the finite result (2.4), which shows that thermal fluctuations generate a mass for the scalar field of order gT . This thermal mass is analogous to the Debye mass which is well-known from the non-relativistic QED plasma.

We next focus on the two-loop diagrams and first consider the double-bubble in Fig. (2.2b).

This diagram is also independent of the external momentum and gives the following

¹For an introduction to thermal field theory and the imaginary time formalism see Refs. [234] and [235].

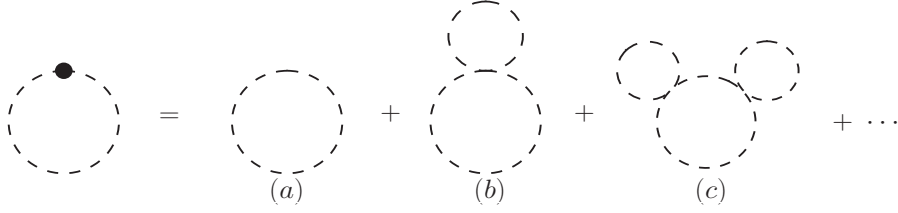


Figure 2.2: Bubble diagrams contributing to the scalar self-energy.

sum-integral

$$\Pi^{(2b)} = -\frac{1}{4}g^4 \sum_{PQ} \frac{1}{P^2} \frac{1}{Q^4}. \quad (2.5)$$

This integral is infrared divergent. The problem stems from the middle loop with two propagators. In order to isolate the source of the divergence, we look at the contribution from the zeroth Matsubara mode to the Q integration

$$-\frac{1}{4}g^4 \sum_P \frac{1}{P^2} T \int_{\mathbf{q}} \frac{1}{q^4}. \quad (2.6)$$

The integral over q in Eq. (2.6) behaves like $1/q$ and linearly infrared divergent as $q \rightarrow 0$. This infrared divergence indicates that naive perturbation theory breaks down at finite temperature. However, in practice this infrared divergence is screened by a thermally generated mass and we must somehow take this into account. The thermal mass can be incorporated by using an effective propagator:

$$\Delta(P) = \frac{1}{P^2 + m^2}, \quad (2.7)$$

where m can be obtained from Eq. (2.4) as $m = gT/\sqrt{24} \ll T$.

If the momenta of the propagator is of order T or *hard*, clearly the thermal mass is a perturbation and can be omitted. However, if the momenta of the propagator is of order gT or *soft*, the thermal mass is as large as the bare inverse propagator and cannot be omitted. The mass term in the propagator (2.7) provides an infrared

cutoff of order gT . The contribution from (2.6) would then be

$$-\frac{1}{4}g^4 \sum_P \frac{1}{P^2} T \int_{\mathbf{q}} \frac{1}{(q^2 + m^2)^2} = -\frac{1}{4}g^4 \left(\frac{T^2}{12}\right) \left(\frac{T}{\pi m}\right) + \mathcal{O}(g^4 m T) . \quad (2.8)$$

Since $m \sim gT$, this shows that the double-bubble contributes at order $g^3 T^2$ to the self-energy and not at order $g^4 T^2$ as one might have expected. Similarly, one can show that the diagrams with any number of bubbles like Fig. (2.2c) are all of order g^3 . Clearly, naive perturbation theory breaks down since the order- g^3 correction to the thermal mass receives contributions from all loop orders. On the other hand, the three-loop diagram shown in Fig. (2.3), is of order $g^4 T^2$ and thus sub-leading. Therefore, we only need to resum a subset of all possible Feynman graphs in order to obtain a consistent expansion in g .

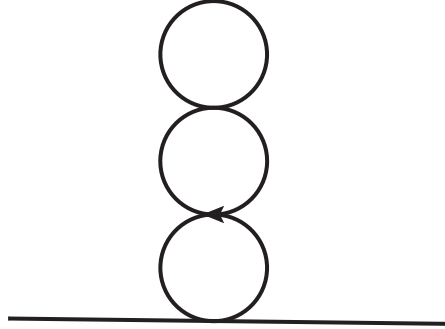


Figure 2.3: Subleading three-loop self-energy diagram.

If we use the effective propagator to recalculate the one-loop self-energy, we obtain

$$\begin{aligned} \Pi^{(1)}(P) &= \frac{1}{2}g^2 \sum_P \frac{1}{P^2 + m^2} \\ &= \frac{1}{2}g^2 \left[T \int_{\mathbf{p}} \frac{1}{p^2 + m^2} + \sum'_P \frac{1}{P^2} + \mathcal{O}(m^2) \right] \\ &= \frac{g^2}{24} T^2 \left[1 - \frac{g\sqrt{6}}{4\pi} + \mathcal{O}(g^2) \right] . \end{aligned} \quad (2.9)$$

where here, and in the following, the prime on the sum-integral indicates that we have excluded the $n = 0$ mode from the sum over the Matsubara frequencies. The order g^3 corresponds to the summation of the bubble diagrams in Fig. (2.2), which can be verified by expanding the effective propagator in Eqn. (2.7) around $m = 0$. Thus by taking the thermal mass into account, one is resumming an infinite set of diagrams from all orders of perturbation theory.

The one loop scalar self-energy in Eq (2.4) is the first example of a *hard thermal loop* (HTL). In HTL perturbation theory, loop corrections are $g^2 T^2/P^2$ times the corresponding tree-level amplitude, where P is a momentum that characterizes the external lines. From this definition, it is clear that, whenever the external momentum P is hard *i.e.* $P \sim T$, the loop correction is suppressed by g^2 and is thus a perturbative correction. However, when the external momentum P is soft *i.e.* $P(\sim gT)$, the HTL correction is same order of tree-level amplitude and is therefore as important as the tree-level contribution to the amplitude. These loop corrections are called “hard” because the relevant integrals are dominated by momenta of order T . Also note that the hard thermal loop in the two-point function is finite since it is exclusively due to thermal fluctuations. Quantum fluctuations do not enter. Both properties are shared by all hard thermal loops.

n- point functions in scalar theory

In the previous section we have discussed about two-point function in scalar field theory. If one calculate higher order n - point functions in scalar theory, one can show that the one-loop correction to the four-point function at high temperature behaves as [236]

$$\Gamma^{(4)} \propto g^4 \log(T/p) , \quad (2.10)$$

where p is the external spatial momentum. Thus the loop correction to the four-point function increases logarithmically with temperature (T). It is therefore always down by $g^2 \log(1/g)$ as the external momentum p is soft in HTL approximation, and one can conclude that it is sufficient to use a bare vertex. More generally, one can show that the only hard thermal loop in scalar field theory is the tadpole diagram in Fig. (2.1) and resummation is taken care of by including the thermal mass in the propagator. In gauge theories, the situation is much more complicated than the scalar theory as we shall discuss in the next section.

2.2 Gauge theories

In the previous section, we discussed about HTL resummation for scalar theory with ϕ^4 interaction. For scalar theories, the resummation simply amounts to include the thermal mass in the propagator. The higher order functions such as four point vertex depends logarithmically on the temperature, corrections to the bare vertex are always down by powers of $g^2 \log g$. In gauge theories, the situation is much more complicated. The equivalent HTL self-energies are no longer local, but depend in a nontrivial way on the external momentum. In addition, it is also necessary to use effective vertices that also depend on the external momentum. It turns out that all hard thermal loops are gauge-fixing independent [150, 156, 237–240]. This was shown explicitly in covariant gauges, Coulomb gauges, and axial gauges. All the n -point functions also satisfy tree-level like Ward identities. Furthermore, there exists a gauge invariant effective Lagrangian in gauge theory, found independently by Braaten and Pisarski [155] and by Taylor and Wong [239], that generates all of the hard thermal loop n -point functions. From a renormalization group point of view this is an effective Lagrangian for the soft scale gT that is obtained by integrating out the hard scale T .

2.2.1 Polarization tensor

In this section we discuss in some detail the hard thermal loop for the vacuum polarization tensor $\Pi^{\mu\nu}$ for photon. Later we extend it for gluon also. The hard thermal loop in the photon propagator was first calculated by Silin more than forty years ago [241]. The Feynman diagram for the one-loop self-energy photon is shown

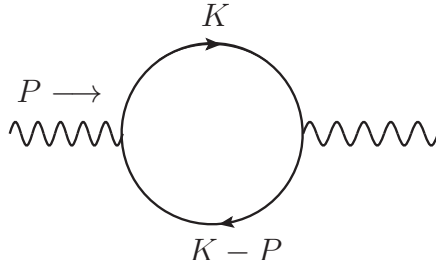


Figure 2.4: One-loop photon self-energy diagram.

in Fig. (2.4) and results can be expressed in Euclidean space as

$$\Pi^{\mu\nu}(P) = e^2 \int_{\{K\}} \text{Tr} \left[\frac{K\gamma^\mu(K-P)\gamma^\nu}{K^2(K-P)^2} \right], \quad (2.11)$$

where $P = (P_0, p)$ is momentum of the external photon and Tr denotes the trace over Dirac matrices. After taking the trace over Dirac matrices, the self-energy in $d = 3$ spatial dimension can be written as

$$\begin{aligned} \Pi^{\mu\nu}(P) = & 8e^2 \int_{\{K\}} \frac{K^\mu K^\nu}{K^2(K-P)^2} - 4\delta^{\mu\nu} e^2 \int_{\{K\}} \frac{1}{K^2} \\ & + 2\delta^{\mu\nu} P^2 e^2 \int_{\{K\}} \frac{1}{K^2(K-P)^2} - 4e^2 \int_{\{K\}} \frac{K^\mu P^\nu + K^\nu P^\mu}{K^2(K-P)^2}. \end{aligned} \quad (2.12)$$

As we are interested in the high-temperature limit, we may assume that $K \gg P$ because the leading contribution in T to the loop integral is given by the region

$K \sim T$. With this assumption, the self-energy in Eq. (2.12) simplifies to

$$\Pi^{\mu\nu}(P) = 8e^2 \sum_{\{K\}} \frac{K^\mu K^\nu}{K^2(K-P)^2} - 4\delta^{\mu\nu} e^2 \sum_{\{K\}} \frac{1}{K^2}. \quad (2.13)$$

We first consider the spatial components of $\Pi^{\mu\nu}(P)$. The sum over Matsubara frequencies can be evaluated using

$$\begin{aligned} T \sum_{\{K_0\}} \frac{1}{K^2(P-K)^2} &= \frac{1}{4k|\mathbf{p}-\mathbf{k}|} \left\{ \right. \\ &\quad \left. \left(1 - n_F(k) - n_F(|\mathbf{p}-\mathbf{k}|)\right) \left[\frac{-1}{iP_0 - k - |\mathbf{p}-\mathbf{k}|} + \frac{1}{iP_0 + k + |\mathbf{p}-\mathbf{k}|} \right] \right. \\ &\quad \left. + \left(n_F(k) - n_F(|\mathbf{p}-\mathbf{k}|) \right) \left[\frac{-1}{iP_0 - k + |\mathbf{p}-\mathbf{k}|} + \frac{1}{iP_0 + k - |\mathbf{p}-\mathbf{k}|} \right] \right\}, \end{aligned} \quad (2.14)$$

which is derived from a contour integral in the complex energy plane. The second term in Eq. (2.13) is rather simple. We obtain

$$\begin{aligned} \Pi^{ij}(P) &= -2e^2 \delta^{ij} \int_{\mathbf{k}} \frac{1}{k} (1 - 2n_F(k)) + 2e^2 \int_{\mathbf{k}} \frac{k^i k^j}{k|\mathbf{k}-\mathbf{p}|} \\ &\quad \times \left\{ \left(1 - n_F(k) - n_F(|\mathbf{k}-\mathbf{p}|)\right) \left[\frac{-1}{iP_0 - k - |\mathbf{k}-\mathbf{p}|} + \frac{1}{iP_0 + k + |\mathbf{k}-\mathbf{p}|} \right] \right. \\ &\quad \left. + \left(n_F(k) - n_F(|\mathbf{k}-\mathbf{p}|) \right) \left[\frac{-1}{iP_0 - k + |\mathbf{k}-\mathbf{p}|} + \frac{1}{iP_0 + k - |\mathbf{k}-\mathbf{p}|} \right] \right\}, \end{aligned} \quad (2.15)$$

where $n_F(x) = 1/(\exp(\beta x) + 1)$ represents the Fermi-Dirac distribution function. The zero-temperature part of Eq. (2.15) is logarithmically divergent in the ultraviolet region. This term depends on the external momentum and is canceled by standard zero-temperature wave-function renormalization. We next consider the terms that depend on temperature. In the case that the loop momentum is soft, the Fermi-Dirac distribution functions can be approximated by a constant. The contribution from the integral over the magnitude of k is then of order g^3 and subleading. When the loop momentum is hard, one can expand the terms in the integrand in powers

of the external momentum. We can then make the following approximations

$$n_F(|\mathbf{k} - \mathbf{p}|) \approx n_F(k) - \frac{dn_F(k)}{dk} \mathbf{p} \cdot \hat{\mathbf{k}}, \quad (2.16)$$

$$|\mathbf{k} - \mathbf{p}| \approx k - \mathbf{p} \cdot \hat{\mathbf{k}}, \quad (2.17)$$

where $\hat{\mathbf{k}} = \mathbf{k}/k$ is a unit vector. Thus the angular integration decouples from the integral over the magnitude k . This implies

$$\begin{aligned} \Pi^{ij}(P) &= -\frac{2e^2}{\pi^2} \int_0^\infty dk k^2 \frac{dn_F(k)}{dk} \int \frac{d\Omega}{4\pi} \frac{-iP_0}{-iP_0 + \mathbf{p} \cdot \hat{\mathbf{k}}} \hat{k}^i \hat{k}^j, \\ &= \frac{e^2 T^2}{3} \int \frac{d\Omega}{4\pi} \frac{-iP_0}{-iP_0 + \mathbf{p} \cdot \hat{\mathbf{k}}} \hat{k}^i \hat{k}^j. \end{aligned} \quad (2.18)$$

The results in Eq. (2.18) can be analytically continued to the Minkowski space by replacing $iP_0 \rightarrow p_0$ as

$$\Pi^{ij}(P) = \frac{e^2 T^2}{3} \int \frac{d\Omega}{4\pi} \frac{p_0}{p_0 - \mathbf{p} \cdot \hat{\mathbf{k}}} \hat{k}^i \hat{k}^j. \quad (2.19)$$

Note that the momentum in Minkowski space is denoted with $P = (p_0, p = |\mathbf{p}|)$ whereas momentum in Euclidean space is denoted with $P = (P_0, p = |\mathbf{p}|)$. The other components of the self-energy tensor $\Pi^{\mu\nu}(P)$ are derived in the same manner or obtained using the transversality of polarization tensor:

$$P_\mu \Pi^{\mu\nu}(P) = 0. \quad (2.20)$$

One find the other components of the self energy tensor from [235, 242] as

$$\Pi^{00}(P) = \frac{e^2 T^2}{3} \left(\int \frac{d\Omega}{4\pi} \frac{p_0}{p_0 - \mathbf{p} \cdot \hat{\mathbf{k}}} + 1 \right), \quad (2.21)$$

$$\Pi^{0j}(P) = \frac{e^2 T^2}{3} \int \frac{d\Omega}{4\pi} \frac{-p_0}{p_0 - \mathbf{p} \cdot \hat{\mathbf{k}}} \hat{k}^j. \quad (2.22)$$

In d dimensions, we can compactly write the self-energy tensor as

$$\Pi^{\mu\nu}(P) = m_D^2 [\mathcal{T}^{\mu\nu}(P, -P) - n^\mu n^\nu] , \quad (2.23)$$

where n specifies the thermal rest frame is canonically given by $n = (1, \mathbf{0})$. We have defined

$$m_D^2 = -4(d-1)e^2 \sum_{\{K\}} \frac{1}{K^2} = \frac{e^2 T^2}{3} , \quad (2.24)$$

and the tensor $\mathcal{T}^{\mu\nu}(P, Q)$, which is defined only for momenta that satisfy $P+Q=0$, is

$$\mathcal{T}^{\mu\nu}(P, -P) = \left\langle Y^\mu Y^\nu \frac{P \cdot n}{P \cdot Y} \right\rangle_{\hat{\mathbf{y}}} . \quad (2.25)$$

The angular brackets indicate averaging over the spatial directions of the light-like vector $Y = (1, \hat{\mathbf{y}})$. The tensor $\mathcal{T}^{\mu\nu}$ is symmetric in μ and ν and satisfies the ‘‘Ward identity’’

$$P_\mu \mathcal{T}^{\mu\nu}(P, -P) = P \cdot n n^\nu . \quad (2.26)$$

The self-energy tensor $\Pi^{\mu\nu}$ is therefore also symmetric in μ and ν and satisfies

$$P_\mu \Pi^{\mu\nu}(P) = 0 , \quad (2.27)$$

$$g_{\mu\nu} \Pi^{\mu\nu}(P) = -m_D^2 . \quad (2.28)$$

The gluon self-energy tensor can be expressed in terms of two scalar functions, the transverse and longitudinal self-energies Π_T and Π_L as

$$\Pi^{\mu\nu}(P) = -\Pi_T(P) T_P^{\mu\nu} + \frac{P^2}{p^2} \Pi_L(P) L_P^{\mu\nu} , \quad (2.29)$$

where the tensor $T_P^{\mu\nu}$ and $L_P^{\mu\nu}$ are

$$T_P^{\mu\nu} = g^{\mu\nu} - \frac{P^\mu P^\nu}{P^2} - \frac{n_P^\mu n_P^\nu}{n_P^2}, \quad (2.30)$$

$$L_P^{\mu\nu} = \frac{n_P^\mu n_P^\nu}{n_P^2} \quad (2.31)$$

The four-vector n_P^μ is

$$n_P^\mu = n^\mu - \frac{n \cdot P}{P^2} P^\mu \quad (2.32)$$

and satisfies $P \cdot n_P = 0$ and $n_P^2 = 1 - (n \cdot P)^2 / P^2$. (2.28) reduces to the identity

$$(d-1)\Pi_T(P) + \frac{1}{n_P^2}\Pi_L(P) = m_D^2. \quad (2.33)$$

We can express both self-energy functions in terms of the function \mathcal{T}^{00} , which is defined in Eq. (2.25), as:

$$\Pi_T(P) = \frac{m_D^2}{(d-1)n_P^2} [\mathcal{T}^{00}(P, -P) - 1 + n_P^2], \quad (2.34)$$

$$\Pi_L(P) = m_D^2 [1 - \mathcal{T}^{00}(P, -P)], \quad (2.35)$$

In the tensor $\mathcal{T}^{\mu\nu}(P, -P)$ defined in (2.25), the angular brackets indicate the angular average over the unit vector $\hat{\mathbf{y}}$. In almost all previous work, the angular average in (2.25) has been taken in $d = 3$ dimensions. For consistency of higher order corrections, it is essential to take the angular average in $d = 3 - 2\epsilon$ dimensions and analytically continue to $d = 3$ only after all poles in ϵ have been canceled. Expressing the angular average as an integral over the cosine of an angle, the expression for the 00 component of the tensor is

$$\mathcal{T}^{00}(p, -p) = \frac{w(\epsilon)}{2} \int_{-1}^1 dc (1 - c^2)^{-\epsilon} \frac{p_0}{p_0 - |\mathbf{p}|c}, \quad (2.36)$$

where the weight function $w(\epsilon)$ is

$$w(\epsilon) = \frac{\Gamma(2-2\epsilon)}{\Gamma^2(1-\epsilon)} 2^{2\epsilon} = \frac{\Gamma(\frac{3}{2}-\epsilon)}{\Gamma(\frac{3}{2})\Gamma(1-\epsilon)}. \quad (2.37)$$

The integral in (2.36) must be defined so that it is analytic at $p_0 = \infty$. It then has a branch cut running from $p_0 = -|\mathbf{p}|$ to $p_0 = +|\mathbf{p}|$. If we take the limit $\epsilon \rightarrow 0$, it reduces to

$$\mathcal{T}^{00}(P, -P) = \frac{p_0}{2|\mathbf{p}|} \log \frac{p_0 + |\mathbf{p}|}{p_0 - |\mathbf{p}|}, \quad (2.38)$$

which is the expression that appears in the usual HTL self-energy functions.

In three dimensions, the self-energies $\Pi_T(P)$ and $\Pi_L(P)$ reduce to

$$\Pi_T(P) = \frac{m_D^2 p_0^2}{2 p^2} \left[1 - \frac{P^2}{2p_0 p} \log \frac{p_0 + p}{p_0 - p} \right], \quad (2.39)$$

$$\Pi_L(P) = m_D^2 \left[1 - \frac{p_0}{2p} \log \frac{p_0 + p}{p_0 - p} \right]. \quad (2.40)$$

So far the HTL approximation for photon self energy tensor has been discussed.

Now we will discuss below the HTL approximation for gluon self energy tensor.

The hard thermal loop in the gluon self-energy was first calculated by Klimov and Weldon [243–245]. In QCD, if one calculate gluon self energy, the Feynman diagrams that will contribute to one loop gluon self energy are shown in fig. (2.5).

If one calculate all the four diagrams, one get gluon self energy tensor in the same form as photon self energy (2.23), but the Debye mass m_D should be replaced by

$$m_D^2 = g^2 \left[(d-1)^2 c_A \not\sum_K \frac{1}{K^2} - 4(d-1) s_F \not\sum_{\{K\}} \frac{1}{K^2} \right], \quad (2.41)$$

where, with the standard normalization, the QCD Casimir numbers are $c_A = N_c$

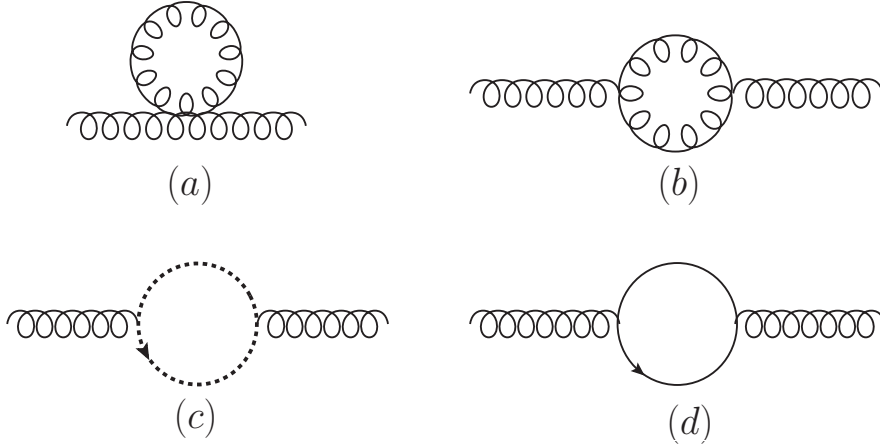


Figure 2.5: Feynman diagrams for gluon self energy.

and $s_F = N_f/2$. N_c and N_f denotes number of colors and number of flavors. In case of three spatial dimension *i.e.* for $d = 3$, the Debye mass for gluon becomes

$$m_D^2 = \frac{g^2 T^2}{3} [c_A + s_F (1 + 12\hat{\mu}^2)] . \quad (2.42)$$

2.2.2 Gluon propagator

The Feynman rule for the gluon propagator in Minkowski space is

$$i\delta^{ab}\Delta_{\mu\nu}(P) , \quad (2.43)$$

where the gluon propagator tensor $\Delta_{\mu\nu}$ depends on the choice of gauge fixing. We consider two possibilities that introduce an arbitrary gauge parameter ξ : general covariant gauge and general Coulomb gauge. In both cases, the inverse propagator reduces in the limit $\xi \rightarrow \infty$ to

$$\Delta_\infty^{-1}(P)^{\mu\nu} = -P^2 g^{\mu\nu} + P^\mu P^\nu - \Pi^{\mu\nu}(P) . \quad (2.44)$$

This can also be written

$$\Delta_{\infty}^{-1}(P)^{\mu\nu} = -\frac{1}{\Delta_T(P)}T_P^{\mu\nu} + \frac{1}{n_P^2\Delta_L(P)}L_P^{\mu\nu}, \quad (2.45)$$

where the transverse tensor $T_P^{\mu\nu}$ and longitudinal tensor $L_P^{\mu\nu}$ are defined in Eq. (2.31). $\Delta_T(P)$ and $\Delta_L(P)$ are the transverse and longitudinal propagators related to $\Pi_L(P)$ $\Pi_T(P)$ as

$$\Delta_T(P) = \frac{-1}{P^2 + \Pi_T(P)}, \quad (2.46)$$

$$\Delta_L(P) = \frac{1}{p^2 + \Pi_L(P)}. \quad (2.47)$$

The inverse propagator for general ξ is

$$\Delta^{-1}(P)^{\mu\nu} = \Delta_{\infty}^{-1}(P)^{\mu\nu} - \frac{1}{\xi}P^{\mu}P^{\nu} \quad \text{covariant}, \quad (2.48)$$

$$= \Delta_{\infty}^{-1}(P)^{\mu\nu} - \frac{1}{\xi}(P^{\mu} - P \cdot n n^{\mu})(P^{\nu} - P \cdot n n^{\nu}) \quad \text{Coulomb}. \quad (2.49)$$

The propagators obtained by inverting the tensors in (2.49) and (2.48) are

$$\Delta^{\mu\nu}(P) = -\Delta_T(P)T_P^{\mu\nu} + \Delta_L(P)n_P^{\mu}n_P^{\nu} - \xi\frac{P^{\mu}P^{\nu}}{P^4} \quad \text{covariant}, \quad (2.50)$$

$$= -\Delta_T(P)T_P^{\mu\nu} + \Delta_L(P)n^{\mu}n^{\nu} - \xi\frac{P^{\mu}P^{\nu}}{(n_P^2P^2)^2} \quad \text{Coulomb}. \quad (2.51)$$

It is convenient to define the following combination of propagators:

$$\Delta_X(P) = \Delta_L(P) + \frac{1}{n_P^2}\Delta_T(P). \quad (2.52)$$

Using (2.33), (2.46), and (2.47), it can be expressed in the alternative form

$$\Delta_X(P) = [m_D^2 - d\Pi_T(P)]\Delta_L(P)\Delta_T(P), \quad (2.53)$$

which shows that it vanishes in the limit $m_D \rightarrow 0$. In the covariant gauge, the propagator tensor can be written

$$\begin{aligned} \Delta^{\mu\nu}(P) = & [-\Delta_T(P)g^{\mu\nu} + \Delta_X(P)n^\mu n^\nu] - \frac{n \cdot P}{p^2} \Delta_X(P) (P^\mu n^\nu + n^\mu P^\nu) \\ & + \left[\Delta_T(P) + \frac{(n \cdot P)^2}{P^2} \Delta_X(P) - \frac{\xi}{P^2} \right] P^\mu P^\nu P^2. \end{aligned} \quad (2.54)$$

This decomposition of the propagator into three terms has proved to be particularly convenient for explicit calculations. For example, the first term satisfies the identity

$$[-\Delta_T(P)g_{\mu\nu} + \Delta_X(P)n_\mu n_\nu] \Delta_\infty^{-1}(P)^{\nu\lambda} = g_\mu^\lambda - \frac{P_\mu P^\lambda}{P^2} + \frac{n \cdot P}{n_P^2 P^2} \frac{\Delta_X(P)}{\Delta_L(P)} P_\mu n_P^\lambda. \quad (2.55)$$

The zeros of the denominators of the Eq. (2.50) or (2.51) gives the dispersion laws for transverse and longitudinal gluon, *i.e.*

$$\Delta_T(p_0 = \omega_T, p) = 0, \quad \Delta_L(p_0 = \omega_L, p) = 0. \quad (2.56)$$

The dispersion laws are illustrated in Fig. (2.6).

It is possible to find approximate analytic solution of $\omega_{L,T}$ for small and large values of momentum.

For small value of momentum ($p \ll m_D$),

$$\omega_T \approx \frac{m_D}{\sqrt{3}} \left(1 + \frac{9}{5} \frac{p^2}{m_D^2} - \frac{81}{35} \frac{p^4}{m_D^4} + \frac{792}{125} \frac{p^6}{m_D^6} \right), \quad (2.57)$$

$$\omega_L \approx \frac{m_D}{\sqrt{3}} \left(1 + \frac{9}{10} \frac{p^2}{m_D^2} - \frac{27}{280} \frac{p^4}{m_D^4} + \frac{9}{2000} \frac{p^6}{m_D^6} \right) \quad (2.58)$$

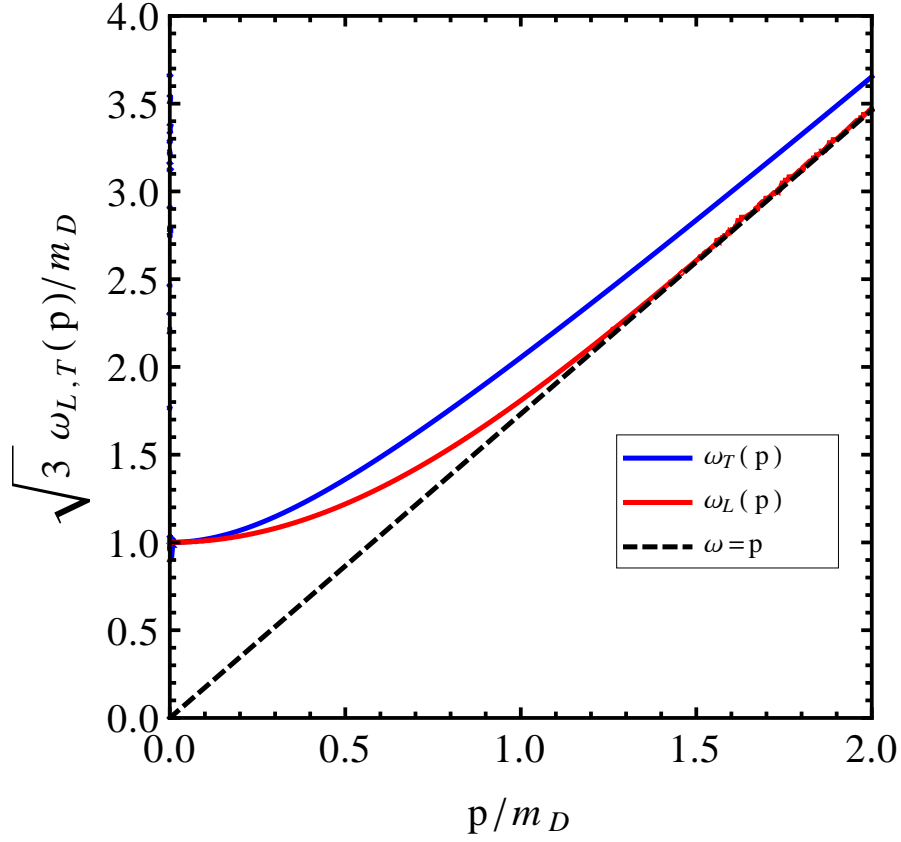


Figure 2.6: Dispersion laws for photon/gluon.

For large value of momentum ($p \gg m_D$),

$$\omega_T \approx p + \frac{m_D^2}{4p} + \frac{m_D^4}{32p^3} \left[3 - 2 \ln \frac{8p^2}{m_D^2} \right] + \frac{m_D^6}{128p^5} \left[2 \ln^2 \frac{8p^2}{m_D^2} - 10 \ln \frac{8p^2}{m_D^2} + 7 \right], \quad (2.59)$$

$$\omega_L \approx p + 2p \exp \left(-\frac{2(p^2 + m_D^2)}{m_D^2} \right). \quad (2.60)$$

2.2.3 Fermionic propagator

We want to examine the electron (quark) propagator within HTL approximation.

We must thus evaluate the Feynman diagram in Fig.(2.7).

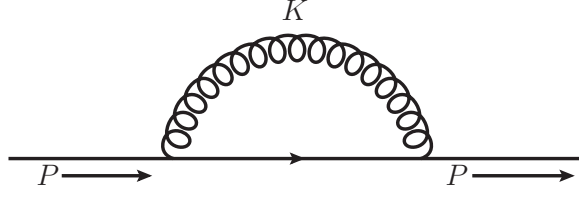


Figure 2.7: One loop quark self energy.

The full electron propagator in Euclidean space can be written as

$$S(P) = \frac{1}{\not{P} + m + \Sigma} \quad (2.61)$$

Evaluation of Σ

Electron self energy in Feynman gauge is

$$\Sigma(P) = -e^2 \int_K \frac{\gamma_\mu (\not{K} - \not{P}) \gamma^\mu}{K^2 (P - K)^2} \quad (2.62)$$

In HTL approximation, we can neglect P w.r.t. K . After contracting the Dirac matrices, the electron self-energy in $d = 3$ dimension reduces to

$$\Sigma(P) \approx -2e^2 \int_K \frac{\not{K}}{K^2 (P - K)^2} \quad (2.63)$$

The necessary frequency sum can be performed using contour integration techniques and the results are

$$\begin{aligned} T \sum_{K_0} \frac{1}{K^2 (P - K)^2} = & -\frac{1}{4k|\mathbf{p} - \mathbf{k}|} \left\{ \right. \\ & \left. \left(1 + n_B(k) - n_F(|\mathbf{p} - \mathbf{k}|) \right) \left[\frac{1}{iP_0 - k - |\mathbf{p} - \mathbf{k}|} - \frac{1}{iP_0 + k + |\mathbf{p} - \mathbf{k}|} \right] \right. \\ & \left. + \left(n_B(k) + n_F(|\mathbf{p} - \mathbf{k}|) \right) \left[\frac{1}{iP_0 + k - |\mathbf{p} - \mathbf{k}|} + \frac{1}{iP_0 - k + |\mathbf{p} - \mathbf{k}|} \right] \right\}, \quad (2.64) \end{aligned}$$

and

$$\begin{aligned}
 T \sum_{K_0} \omega_n \frac{1}{K^2(P-K)^2} &= \frac{i}{4|\mathbf{p}-\mathbf{k}|} \left\{ \right. \\
 &\quad \left. \left(1 + n_B(k) - n_F(|\mathbf{p}-\mathbf{k}|)\right) \left[\frac{1}{iP_0 - k - |\mathbf{p}-\mathbf{k}|} + \frac{1}{iP_0 + k + |\mathbf{p}-\mathbf{k}|} \right] \right. \\
 &\quad \left. - \left(n_B(k) + n_F(|\mathbf{p}-\mathbf{k}|)\right) \left[\frac{1}{iP_0 + k - |\mathbf{p}-\mathbf{k}|} + \frac{1}{iP_0 - k + |\mathbf{p}-\mathbf{k}|} \right] \right\}, \quad (2.65)
 \end{aligned}$$

where $n_B(x) = 1/(\exp(\beta x) - 1)$ and $n_F(x) = 1/(\exp(\beta x) + 1)$ as before. The first term in the square bracket of Eq. (2.64) leads to a behavior that is linear in T , and the corresponding term in Eq. (2.65) is even more convergent; thus these terms are non-leading in T . Only the second terms of both the Eqs. (2.64) and (2.65) contributes to order T^2 . Using this knowledge, we can easily obtain the following results:

$$\sum_K \frac{k_i}{K^2(P-K)^2} = -\frac{T^2}{16} \int \frac{d\Omega}{4\pi} \frac{\hat{k}_i}{P \cdot \hat{K}} \quad (2.66)$$

and

$$\sum_K \frac{\omega_n}{K^2(P-K)^2} = -\frac{iT^2}{16} \int \frac{d\Omega}{4\pi} \frac{1}{P \cdot \hat{K}} \quad (2.67)$$

Which leads to

$$\begin{aligned}
 \Sigma(P) &= \frac{e^2 T^2}{8} \int \frac{\hat{K}}{P \cdot \hat{K}} & \hat{K} &= (-i, \hat{\mathbf{k}}) \\
 &= \frac{e^2 T^2}{8} \int \frac{Y}{P \cdot Y} & Y &= (-i, \hat{\mathbf{y}}) \\
 &= m_f^2 \mathcal{T}(P), \quad (2.68)
 \end{aligned}$$

where

$$\mathcal{T}^\mu(P) = - \left\langle \frac{Y^\mu}{P \cdot Y} \right\rangle_{\hat{\mathbf{Y}}} \quad Y \equiv (-i, \hat{\mathbf{y}}), \quad (2.69)$$

and m_f is the thermal electron mass

$$m_f^2 = -3e^2 \int_{\{K\}} \frac{1}{K^2} = \frac{e^2 T^2}{8}. \quad (2.70)$$

In Minkowski space $\Sigma(P)$ has same form as in Euclidean space as

$$\Sigma(P) = \frac{e^2 T^2}{8} \int \frac{Y}{P \cdot Y} \quad Y = (1, \hat{\mathbf{y}}) \quad (2.71)$$

The corresponding retarded dressed electron propagator for massless case reads

$$S(P) = \frac{i}{\not{P} - \Sigma} \quad (2.72)$$

Now, one can evaluate electron self energy in Eq. (2.71) as

$$\Sigma(p_0, p) = \frac{m_f^2}{p_0} \gamma_0 \mathcal{T}_P + \frac{m_f^2}{p} \boldsymbol{\gamma} \cdot \hat{\mathbf{p}} (1 - \mathcal{T}_P) \quad (2.73)$$

where \mathcal{T}_P is 00 component of the tensor $\mathcal{T}^{\mu\nu}(p, -p)$ and given in Eq. (2.36) as

$$\begin{aligned} \mathcal{T}_P(p, -p) &= \frac{w(\epsilon)}{2} \int_{-1}^1 dc (1 - c^2)^{-\epsilon} \frac{p_0}{p_0 - |\mathbf{p}|c} \\ &= \left\langle \frac{p_0^2}{p_0^2 - p^2 c^2} \right\rangle_c \end{aligned} \quad (2.74)$$

We can rewrite the inverse of electron propagator from Eq. (2.72) as

$$iS^{-1}(P) = \not{P} - \Sigma(P) = A_0 \gamma_0 - A_S \boldsymbol{\gamma} \cdot \hat{\mathbf{p}} \quad (2.75)$$

with

$$A_0 = p_0 - \frac{m_f^2}{p_0} \mathcal{T}_P \quad A_S = p + \frac{m_f^2}{p} (1 - \mathcal{T}_P) \quad (2.76)$$

The above expressions can be written three spatial dimension as

$$A_0 = p_0 - \frac{m_f^2}{p} \ln \frac{p_0 + p}{p_0 - p} \quad A_S = p + \frac{m_f^2}{p} \left(1 - \frac{p_0}{p} \ln \frac{p_0 + p}{p_0 - p} \right) \quad (2.77)$$

The physical interpretation of any calculation is particularly transparent if we rewrite

$$-iS(P) = \frac{\gamma_0 - \gamma \cdot \hat{\mathbf{p}}}{2D_+(p_0, p)} + \frac{\gamma_0 + \gamma \cdot \hat{\mathbf{p}}}{2D_-(p_0, p)}, \quad (2.78)$$

where

$$\begin{aligned} D_{\pm}(p_0, p) &= A_0 \mp A_S \\ &= p_0 \mp p - \frac{m_f^2}{2p} \left[\left(1 \mp \frac{p_0}{p} \right) \ln \frac{p_0 + p}{p_0 - p} \pm 2 \right] \end{aligned} \quad (2.79)$$

As $D_{\pm}(p_0, p)$ has an imaginary part for space-like values of $P(p_0^2 < p^2)$, it is useful to note the parity properties for both real and imaginary values of $D_{\pm}(p_0, p)$ as

$$\begin{aligned} \text{Re } D_+(p_0, p) &= -\text{Re } D_-(-p_0, p) \\ \text{Im } D_+(p_0, p) &= \text{Im } D_-(-p_0, p) \end{aligned} \quad (2.80)$$

The zeros of the denominators in Eq. (2.78) *i.e.* the solution of $D_{\pm}(p_0, p) = 0$ give the position of the quasi-particle poles. One finds that $D_+(p_0, p) = A_0 - A_S = 0$ has two solutions:

$$p_0 = \omega_+(p) \quad p_0 = -\omega_-(p), \quad (2.81)$$

and, from the parity properties of Eq. (2.80), the equation $D_-(p_0, p) = A_0 + A_S = 0$ has also two solutions:

$$p_0 = \omega_-(p) \quad p_0 = -\omega_+(p), \quad (2.82)$$

where $\omega_{\pm}(p)$ is chosen to be positive. The dispersion laws of $\omega_{\pm}(p)$ are illustrated in Fig. (2.8) along-with the dispersion law of free massless fermion(dashed line).

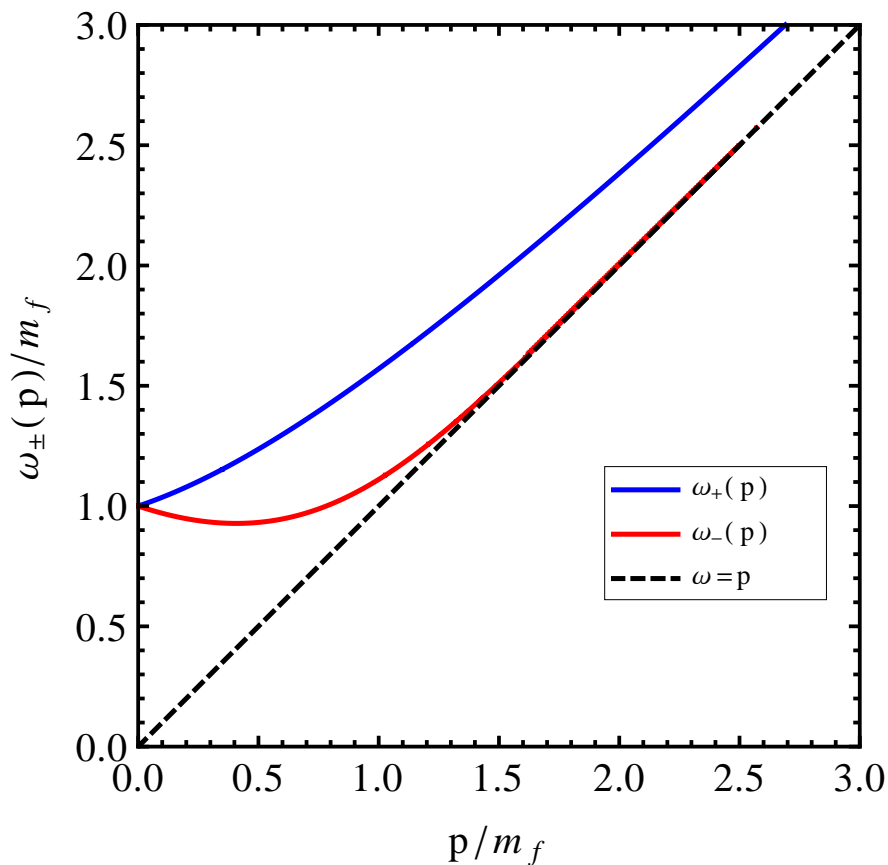


Figure 2.8: Dispersion laws for fermionic excitations.

It is possible to find approximate analytic solution of $\omega_{\pm}(p)$ as in the case of $\omega_{L,T}(p)$ for small and large values of momentum.

For small values of momentum ($p \ll m_f$) the dispersion laws are

$$\begin{aligned}\omega_+(p) &\approx m_f + \frac{1}{3}p + \frac{1}{3} \frac{p^2}{m_f^2} - \frac{16}{135} \frac{p^3}{m_f^3}, \\ \omega_-(p) &\approx m_f - \frac{1}{3}p + \frac{1}{3} \frac{p^2}{m_f^2} + \frac{16}{135} \frac{p^3}{m_f^3}\end{aligned}\quad (2.83)$$

and for large value of momentum ($m_f \ll p \ll T$),

$$\omega_+(p) \approx p + \frac{m_f^2}{p} - \frac{m_f^4}{2p^3} \ln \frac{m_f^2}{2p^2} + \frac{m_f^6}{4p^5} \left[\ln^2 \frac{m_f^2}{2p^2} + \ln \frac{m_f^2}{2p^2} - 1 \right], \quad (2.84)$$

$$\omega_-(p) \approx p + 2p \exp \left(-\frac{2p^2 + m_f^2}{m_f^2} \right). \quad (2.85)$$

Quark Self-energy(QCD)

In the previous section, we discussed about the self energy propagator for electron.

In case of QCD, quark self energy in Feynman gauge can be written as

$$\Sigma(P)\delta_{ij} = - \sum_{\vec{K}} (g\gamma_\mu(t^a)_{ik})(\not{K} - \not{P})(g\gamma^\mu(t^a)_{kj}) \frac{1}{K^2(P-K)^2} \quad (2.86)$$

Using the identity $(t^a t^a)_{ij} = \frac{N_c^2 - 1}{2N_c} \delta_{ij} = C_F \delta_{ij}$ and after doing the frequency sum, the above quark self energy expression reduces to

$$\Sigma(P) = m_q^2 \mathcal{T}(P), \quad (2.87)$$

which is the same form of electron self energy as in Eq. (2.68) but thermal electron mass m_f should be replaced with quark thermal mass and which can be derive as

$$\begin{aligned}m_q^2 &= -3C_F g^2 \sum_{\{K\}} \frac{1}{K^2} \\ &= \frac{g^2 T^2}{8} C_F (1 + 4\hat{\mu}^2).\end{aligned}\quad (2.88)$$

2.2.4 Three point quark gluon vertex

In gauge theories, there are also hard thermal loops involving vertices. For instance, the one-loop correction to the three-point function in QCD, can compactly be written as

$$\Gamma^\mu(P, Q, R) = \gamma^\mu - m_q^2 \tilde{\mathcal{T}}^\mu(P, Q, R), \quad (2.89)$$

where the tensor in the HTL correction term is only defined for $P - Q + R = 0$:

$$\tilde{\mathcal{T}}^\mu(P, Q, R) = \left\langle Y^\mu \left(\frac{\not{Y}}{(Q \cdot Y)(R \cdot Y)} \right) \right\rangle_{\hat{Y}}. \quad (2.90)$$

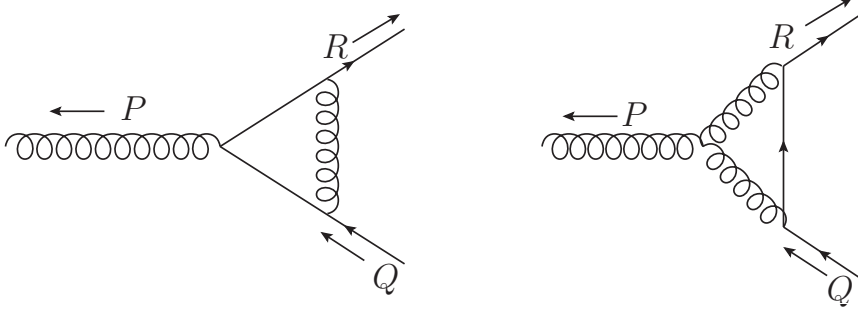


Figure 2.9: One loop correction to the three-point quark gluon vertex.

The quark-gluon vertex satisfies the Ward identity

$$P^\mu \Gamma^\mu(P, Q, R) = S^{-1}(Q) - S^{-1}(R), \quad (2.91)$$

where $S(Q)$ is the resummed effective fermion propagator.

2.2.5 Quark-gluon four-vertex

We define the quark-gluon four-point vertex with outgoing gluon momenta P and Q , incoming quark momentum R , and outgoing quark momentum S . It reads

$$\delta^{ab}\Gamma_{abij}^{\mu\nu}(P, Q, R, S) = -g^2 m_q^2 c_F \delta_{ij} \tilde{\mathcal{T}}^{\mu\nu}(P, Q, R, S) \quad (2.92)$$

$$\equiv g^2 c_F \delta_{ij} \Gamma^{\mu\nu}, \quad (2.93)$$

There is no tree-level term. The tensor in the HTL correction term is only defined for $P + Q - R + S = 0$,

$$\begin{aligned} \tilde{\mathcal{T}}^{\mu\nu}(P, Q, R, S) = & \left\langle Y^\mu Y^\nu \left(\frac{1}{R \cdot Y} + \frac{1}{S \cdot Y} \right) \right. \\ & \left. \times \frac{Y}{[(R - P) \cdot Y] [(S + P) \cdot Y]} \right\rangle. \end{aligned} \quad (2.94)$$

This tensor is symmetric in μ and ν and is traceless. It satisfies the Ward identity:

$$P_\mu \Gamma^{\mu\nu}(P, Q, R, S) = \Gamma^\nu(Q, R - P, S) - \Gamma^\nu(Q, R, S + P). \quad (2.95)$$

2.2.6 Three gluon vertex

The three-gluon vertex for gluons with outgoing momenta P , Q , and R , Lorentz indices μ , ν , and λ , and color indices a , b , and c is

$$i\Gamma_{abc}^{\mu\nu\lambda}(P, Q, R) = -gf_{abc}\Gamma^{\mu\nu\lambda}(P, Q, R), \quad (2.96)$$

where f^{abc} are the structure constants and the three-gluon vertex tensor is

$$\begin{aligned} \Gamma^{\mu\nu\lambda}(P, Q, R) = & g^{\mu\nu}(P - Q)^\lambda + g^{\nu\lambda}(Q - R)^\mu \\ & + g^{\lambda\mu}(R - P)^\nu - m_D^2 \mathcal{T}^{\mu\nu\lambda}(P, Q, R). \end{aligned} \quad (2.97)$$

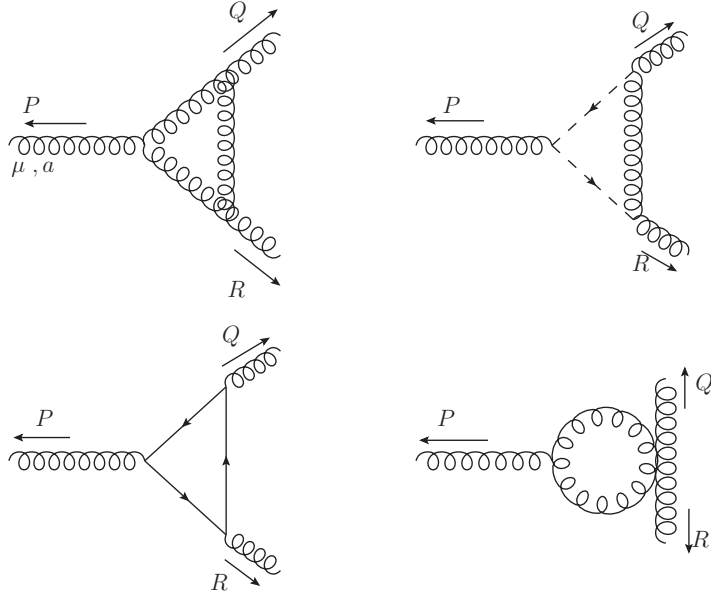


Figure 2.10: One-loop correction to three gluon vertex.

The tensor $\mathcal{T}^{\mu\nu\lambda}$ in the HTL correction term is defined only for $P + Q + R = 0$:

$$\mathcal{T}^{\mu\nu\lambda}(P, Q, R) = - \left\langle Y^\mu Y^\nu Y^\lambda \left(\frac{P \cdot n}{P \cdot Y Q \cdot Y} - \frac{R \cdot n}{R \cdot Y Q \cdot Y} \right) \right\rangle_{\hat{y}}. \quad (2.98)$$

This tensor is totally symmetric in its three indices and traceless in any pair of indices: $g_{\mu\nu} \mathcal{T}^{\mu\nu\lambda} = 0$. It is odd (even) under odd (even) permutations of the momenta P , Q , and R . It satisfies the ‘‘Ward identity’’

$$Q_\mu \mathcal{T}^{\mu\nu\lambda}(P, Q, R) = \mathcal{T}^{\nu\lambda}(P + Q, R) - \mathcal{T}^{\nu\lambda}(P, R + Q). \quad (2.99)$$

The three-gluon vertex tensor therefore satisfies the Ward identity

$$P_\mu \Gamma^{\mu\nu\lambda}(P, Q, R) = \Delta_\infty^{-1}(Q)^{\nu\lambda} - \Delta_\infty^{-1}(R)^{\nu\lambda}. \quad (2.100)$$

2.2.7 Four-gluon Vertex

The four-gluon vertex for gluons with outgoing momenta P , Q , R , and S , Lorentz indices μ , ν , λ , and σ , and color indices a , b , c , and d is

$$\begin{aligned}
 i\Gamma_{abcd}^{\mu\nu\lambda\sigma}(P, Q, R, S) &= -ig^2 \{ f_{abx} f_{xcd} (g^{\mu\lambda} g^{\nu\sigma} - g^{\mu\sigma} g^{\nu\lambda}) \\
 &\quad + 2m_D^2 \text{tr} [T^a (T^b T^c T^d + T^d T^c T^b)] \mathcal{T}^{\mu\nu\lambda\sigma}(P, Q, R, S) \} \\
 &\quad + 2 \text{ cyclic permutations } , \tag{2.101}
 \end{aligned}$$

where the cyclic permutations are of (Q, ν, b) , (R, λ, c) , and (S, σ, d) . The matrices T^a are the fundamental representation of the $SU(3)$ algebra with the standard normalization $\text{tr}(T^a T^b) = \frac{1}{2} \delta^{ab}$. The tensor $\mathcal{T}^{\mu\nu\lambda\sigma}$ in the HTL correction term is defined only for $P + Q + R + S = 0$:

$$\begin{aligned}
 \mathcal{T}^{\mu\nu\lambda\sigma}(P, Q, R, S) &= \left\langle Y^\mu Y^\nu Y^\lambda Y^\sigma \left(\frac{P \cdot n}{P \cdot Y \ Q \cdot Y \ (Q + R) \cdot Y} \right. \right. \\
 &\quad \left. \left. + \frac{(P + Q) \cdot n}{Q \cdot Y \ R \cdot Y \ (R + S) \cdot Y} + \frac{(P + Q + R) \cdot n}{R \cdot Y \ S \cdot Y \ (S + P) \cdot Y} \right) \right\rangle. \tag{2.102}
 \end{aligned}$$

This tensor is totally symmetric in its four indices and traceless in any pair of indices: $g_{\mu\nu} \mathcal{T}^{\mu\nu\lambda\sigma} = 0$. It is even under cyclic or anti-cyclic permutations of the momenta P , Q , R , and S . It satisfies the ‘‘Ward identity’’

$$q_\mu \mathcal{T}^{\mu\nu\lambda\sigma}(P, Q, R, S) = \mathcal{T}^{\nu\lambda\sigma}(P + Q, R, S) - \mathcal{T}^{\nu\lambda\sigma}(P, R + Q, S) \tag{2.103}$$

and the ‘‘Bianchi identity’’

$$\mathcal{T}^{\mu\nu\lambda\sigma}(P, Q, R, S) + \mathcal{T}^{\mu\nu\lambda\sigma}(P, R, S, Q) + \mathcal{T}^{\mu\nu\lambda\sigma}(P, S, Q, R) = 0. \tag{2.104}$$

When its color indices are traced in pairs, the four-gluon vertex becomes particularly simple:

$$\delta^{ab}\delta^{cd}i\Gamma_{abcd}^{\mu\nu\lambda\sigma}(P, Q, R, S) = -ig^2 N_c(N_c^2 - 1)\Gamma^{\mu\nu,\lambda\sigma}(P, Q, R, S), \quad (2.105)$$

where the color-traced four-gluon vertex tensor is

$$\Gamma^{\mu\nu,\lambda\sigma}(P, Q, R, S) = 2g^{\mu\nu}g^{\lambda\sigma} - g^{\mu\lambda}g^{\nu\sigma} - g^{\mu\sigma}g^{\nu\lambda} - m_D^2\mathcal{T}^{\mu\nu\lambda\sigma}(P, S, Q, R). \quad (2.106)$$

Note the ordering of the momenta in the arguments of the tensor $\mathcal{T}^{\mu\nu\lambda\sigma}$, which comes from the use of the Bianchi identity (2.104). The tensor (2.106) is symmetric under the interchange of μ and ν , under the interchange of λ and σ , and under the interchange of (μ, ν) and (λ, σ) . It is also symmetric under the interchange of P and Q , under the interchange of R and S , and under the interchange of (P, Q) and (R, S) . It satisfies the Ward identity

$$p_\mu\Gamma^{\mu\nu,\lambda\sigma}(P, Q, R, S) = \Gamma^{\nu\lambda\sigma}(Q, R + P, S) - \Gamma^{\nu\lambda\sigma}(Q, R, S + P). \quad (2.107)$$

In QED there are, in fact, infinitely many amplitudes with hard thermal loops. To be precise, there are hard thermal loops in all n -point functions with two fermion lines and $n - 2$ photon lines. In non-Abelian gauge theories such as QCD, there are in addition hard thermal loops in amplitudes with n gluon lines [150].

2.2.8 The HTL effective lagrangian in QCD

The preceding results can be summarized in a compact way by writing an effective Lagrangian: Hard-thermal-loop perturbation theory is a reorganization of in-medium perturbation theory for QCD. The HTL perturbation theory Lagrangian

density can be written as

$$\mathcal{L} = (\mathcal{L}_{\text{QCD}} + \mathcal{L}_{\text{HTL}})|_{g \rightarrow \sqrt{\delta}g} + \Delta\mathcal{L}_{\text{HTL}}, \quad (2.108)$$

where the QCD Lagrangian density \mathcal{L}_{QCD} is defined in Eq. (1.10) of chapter 1. The HTL improvement term \mathcal{L}_{HTL} can be written as [155]

$$\begin{aligned} \mathcal{L}_{\text{HTL}} = & (1 - \delta)im_q^2 \bar{\psi} \gamma^\mu \left\langle \frac{Y_\mu}{Y \cdot D} \right\rangle_{\hat{y}} \psi \\ & - \frac{1}{2}(1 - \delta)m_D^2 \text{Tr} \left(F_{\mu\alpha} \left\langle \frac{Y^\alpha Y_\beta}{(Y \cdot D)^2} \right\rangle_{\hat{y}} F^{\mu\beta} \right), \end{aligned} \quad (2.109)$$

where $Y^\mu = (1, \hat{y})$ is a light-like four-vector with \hat{y} being a three-dimensional unit vector and the angular bracket indicates an average over the direction of \hat{y} and $\Delta\mathcal{L}_{\text{HTL}}$ contains the counterterms necessary to cancel additional ultraviolet divergences generated by HTL perturbation theory. The two parameters m_D and m_q can be identified with the Debye screening mass and the thermal quark mass, respectively, and account for screening effects. There are various prescription to choose the parameters m_D and m_q . In one loop QCD thermodynamic calculations in Chapter 3, one loop perturbative mass prescription as given in Eq (2.42) for m_D and in Eq (2.88) for m_q , will be used. In two loop QCD thermodynamic calculations in Chapter 4, we will see that thermodynamical quantities are correct up to g^3 order if one expand for small running coupling. So one can use variational or two loop perturbative mass prescription instead of one loop perturbative mass. The variational mass prescription, which will be discussed in Chapter 4 in details, will be used for NLO calculations. But for the computation of various thermodynamic quantities in three loop HTL perturbation theory, variational mass equations give the imaginary result for m_D , so we have only left with two loop perturbative mass prescription for m_D and that would be used in NNLO computation. We don't have any existing two loop perturbative m_q in literature, so we will use $m_q = 0$ (which is a variational

solution in NNLO) and we will test our result with one loop perturbative m_q also.

HTL perturbation theory is defined by treating δ as a formal expansion parameter. By coupling the HTL improvement term (2.109) to the QCD Lagrangian (1.10), HTL perturbation theory systematically shifts the perturbative expansion from being around an ideal gas of massless particles to being around a gas of massive quasi-particles which are the appropriate physical degrees of freedom at high temperature and/or chemical potential. The HTL perturbation theory Lagrangian (2.108) reduces to the QCD Lagrangian (1.10) if we set $\delta = 1$. Physical observables are calculated in HTL perturbation theory by expanding in powers of δ , truncating at some specified order, and then setting $\delta = 1$. This defines a reorganization of the perturbative series in which the effects of m_D^2 and m_q^2 terms in (2.109) are included to leading order but then systematically subtracted out at higher orders in perturbation theory by the δm_D^2 and δm_q^2 terms in (2.109). To obtain leading order (LO), next-to-leading order (NLO), and next-to-next-leading order (NNLO) results, one expands to orders δ^0 , δ^1 , δ^2 , respectively. This Lagrangian is manifestly gauge invariant. An explicit, but tedious, computation shows that it generates the two- and three-point functions correctly, which is sufficient to ensure that it is also correct for all N -point functions.

Hard thermal loop perturbation has been extensively used to calculate various thermodynamical quantities over almost two decades. It has been used to study one loop thermodynamic potential (or pressure) both at zero and finite chemical potential but at finite temperature in Refs. [163–165, 246, 247] and to study one loop conserved charge fluctuations in Refs. [14, 18, 19, 157, 158, 166, 168–170, 246–249]. HTL perturbation theory has also been used to study next-to-leading order thermodynamic potential (or pressure) in Refs. [15, 172, 173] and hence second and fourth order conserved charge fluctuations in Ref. [20]. Recently, HTL perturbation has been used to calculate three thermodynamic potential for pure gluonic medium in

Refs. [174, 175], for QED in Ref. [176] and also for QCD medium in Ref. [177, 178]. Very recently these calculations have been extended in Refs. [16, 17] at finite chemical potential to calculate pressure, energy density, entropy density, speed of sound, trace anomaly at finite temperature and finite chemical potential and various order diagonal and off-diagonal quark number susceptibilities.

In addition to calculations of the thermodynamic potential, hard-thermal-loop perturbation theory has been used to calculate various physical quantities which are relevant to the deconfined state of matter. Quantities such as the dilepton production rate [22, 250], photon production rate [251], single quark and quark anti-quark potentials [252–261], fermion damping rate [262–264], photon damping rate [265], gluon damping rate [156, 266], jet energy loss [267–278], plasma instabilities [279–285], and lepton asymmetry during leptogenesis [286, 287] have also been calculated using HTL perturbation theory. In the next chapter we discuss about leading order thermodynamics and conserved density fluctuations (quark number susceptibility) and temporal component of the Euclidean correlation function in the vector channel within HTL perturbation theory.

CHAPTER 3

One loop HTL thermodynamics

In this chapter we discuss about leading order thermodynamic functions *viz.* number density, entropy density, pressure and hence leading order conserved density fluctuations (quark number susceptibility) and temporal component of the Euclidean correlation function in the vector channel within HTL perturbation theory. This chapter is based on: 1. *Quark Number Susceptibility and Thermodynamics in HTL approximation*, Najmul Haque, Munshi G. Mustafa, **Nucl. Phys. A** **862-863**, **271** (2011); 2. *Conserved Density Fluctuation and Temporal Correlation Function in HTL Perturbation Theory*, Najmul Haque, Munshi G. Mustafa, Markus H. Thoma, **Phys. Rev. D** **84**, **054009** (2011).

3.1 Introduction

Dynamical properties of many particle system can generally be studied by employing an external perturbation, which disturbs the system only slightly from its equilibrium state, and thus measuring the spontaneous response/fluctuations of the system to this external perturbation. In general, the fluctuations are related to the correlation function through the symmetry of the system, which provides important inputs

for quantitative calculations of complicated many-body system. Also, many of the properties (*e.g.* real and virtual photon production, various transport coefficients etc.) of the deconfined strongly interacting matter are reflected in the structure of the correlation and the spectral functions [288, 289] of the vector current.

The static thermal dilepton rate describing the production of lepton pairs is related to the spectral function in the vector current [217, 290]. Within the Hard thermal loop perturbation theory (HTLpt) the vector spectral function has been obtained [290–296], which is found to diverge due to its spatial part at the low energy regime. This is due to the fact that the HTL quark-photon vertex is inversely proportional to the photon energy and it sharply rises at zero photon energy. On the other hand, the fluctuations of conserved quantities, such as baryon number and electric charge, are considered to be a signal [297–301] for quark-gluon plasma (QGP) formation in heavy-ion experiments. These conserved density fluctuations are closely related to the temporal correlation function in the vector channel through derivatives of a thermodynamic quantity associated with the symmetry, known as the thermodynamic sum rule [302–304]. It is expected that the temporal part of the spectral function associated with the symmetry should be a finite quantity and would not encounter any such infrared divergence unlike the spatial part at low energy. A very recent lattice calculation [305] has obtained the temporal part of the Euclidean correlation function associated with the response of the conserved density fluctuations, which is found to be a finite quantity. In view of this we compute the temporal correlation function in the vector channel from the quark number susceptibility associated with the quark number density fluctuations within the HTLpt [14] and to compare it with recent lattice data [305].

This chapter is organized as follows. In Sec. (3.2) we briefly discuss some generalities on correlation functions, fluctuation and its response (susceptibility) associated with conserved charges. In this section we also obtain the relation between the response of

the density fluctuation of the conserved charge and the corresponding temporal part of the Euclidean correlation function in the vector current. In Sec. (3.3) we present leading order quark number susceptibility (QNS) in HTL perturbation theory. Next using QNS in leading order (LO) within HTL perturbation theory we compute temporal part of the Euclidean correlation function in the vector current in HTL perturbation theory and compare with lattice data. In Sec. (3.4) we present the results of LO QNS and temporal correlation function and compare them with lattice QCD data. Finally, we conclude in Sec. (3.5).

3.2 Generalities

In this section we summarize some of the basic relations and also describe in details their important features relevant as well as required for our purpose.

3.2.1 Correlation Functions

The two-point correlation function [217, 288–290] of the vector current, $J_\mu = \bar{\psi}(\tau, \vec{x})\Gamma_\mu\psi(\tau, \vec{x})$ with three point function Γ_μ , is defined at fixed momentum $\vec{\mathbf{p}}$ as

$$G_{\mu\nu}(\tau, \vec{\mathbf{p}}) = \int d^3x \langle J_\mu(\tau, \vec{x})J_\nu^\dagger(0, \vec{\mathbf{0}}) \rangle e^{i\vec{\mathbf{p}}\cdot\vec{x}} , \quad (3.1)$$

where the Euclidean time τ is restricted to the interval $[0, \beta = 1/T]$ and three point function $\Gamma_\mu = \gamma_\mu$ for vector channel. The thermal two-point vector correlation function in coordinate space, $G_{\mu\nu}(\tau, \vec{x})$, can be written as

$$G_{\mu\nu}(\tau, \vec{x}) = \langle J_\mu(\tau, \vec{x})J_\nu^\dagger(0, \vec{\mathbf{0}}) \rangle = T \sum_{n=-\infty}^{\infty} \int \frac{d^3p}{(2\pi)^3} e^{-i(w_n\tau + \vec{\mathbf{p}}\cdot\vec{x})} G_{\mu\nu}(w_n, \vec{\mathbf{p}}) , \quad (3.2)$$

where the Fourier transformed correlation function $G_{\mu\nu}(w_n, \vec{\mathbf{p}})$ is given at the discrete Matsubara modes, $w_n = 2\pi nT$.

The imaginary part of the momentum space correlator gives the spectral function $\sigma(\omega, \vec{\mathbf{p}})$ as

$$\begin{aligned} G_H(w_n, \vec{\mathbf{p}}) &= - \int_{-\infty}^{\infty} d\omega \frac{\sigma_H(\omega, \vec{\mathbf{p}})}{iw_n - \omega} \\ \Rightarrow \sigma_H(\omega, \vec{\mathbf{p}}) &= \frac{1}{\pi} \text{Im} G_H(\omega, \vec{\mathbf{p}}), \end{aligned} \quad (3.3)$$

where $H = (00, ii, V)$ denotes (temporal, spatial, vector). We have also introduced the vector spectral function as $\sigma_V = \sigma_{00} + \sigma_{ii}$, where σ_{ii} is the sum over the three space-space components and σ_{00} is the time-time component of $\sigma_{\mu\nu}$.

Using (3.2) and (3.3) in (3.1) the spectral representation of the thermal correlation functions at fixed momentum can be obtained [290] as

$$G_H(\tau, \vec{\mathbf{p}}) = \int_0^{\infty} d\omega \sigma_H(\omega, \vec{\mathbf{p}}) \frac{\cosh[\omega(\tau - \beta/2)]}{\sinh[\omega\beta/2]}. \quad (3.4)$$

We note that in the analysis of lattice gauge theory, the Euclidean correlation function is usually restricted to vanishing three momentum, $\vec{\mathbf{p}} = 0$, and one can write $G_H(\tau T) = G_H(\tau, \vec{\mathbf{0}})$. Because of the problem of analytic continuation in the lattice gauge theory can not calculate spectral function $\sigma_H(\omega, \vec{\mathbf{p}})$ directly from Eq. (3.3), instead it uses Eq. (3.4) to extract spectral function as discussed briefly below.

A finite temperature lattice gauge theory calculation is performed on lattices with finite temporal extent N_τ , which provides information on the Euclidean correlation function, $G_H(\tau T)$, only for a discrete and finite set of Euclidean times $\tau = k/(N_\tau T)$, $k = 1, \dots, N_\tau$. The vector correlation function, $G_V(\tau T)$, had been computed [217] within the quenched approximation of QCD using non-perturbative improved clover fermions [306, 307] for temporal extent $N_\tau = 16$ and spatial extent

$N_\sigma = 64$. Then by inverting the integral in (3.4) through a probabilistic application based on the maximum entropy method (MEM) [308–310], the spectral function was reconstructed [217] in lattice QCD.

3.2.2 Density Fluctuation and its Response

Let \mathcal{O}_α be a Heisenberg operator where α may be associated with a degree of freedom in the system. In a static and uniform external field \mathcal{F}_α , the (induced) expectation value of the operator $\mathcal{O}_\alpha(0, \vec{x})$ is written [39, 40, 302–304] as

$$\phi_\alpha \equiv \langle \mathcal{O}_\alpha(0, \vec{x}) \rangle_{\mathcal{F}} = \frac{\text{Tr} [\mathcal{O}_\alpha(0, \vec{x}) e^{-\beta(\mathcal{H} + \mathcal{H}_{ex})}]}{\text{Tr} [e^{-\beta(\mathcal{H} + \mathcal{H}_{ex})}]} = \frac{1}{V} \int d^3x \langle \mathcal{O}_\alpha(0, \vec{x}) \rangle, \quad (3.5)$$

where translational invariance is assumed, V is the volume of the system and \mathcal{H}_{ex} is given by

$$\mathcal{H}_{ex} = - \sum_{\alpha} \int d^3x \mathcal{O}_\alpha(0, \vec{x}) \mathcal{F}_\alpha. \quad (3.6)$$

The (static) susceptibility $\chi_{\alpha\sigma}$ is defined as the rate with which the expectation value changes in response to that external field,

$$\chi_{\alpha\sigma}(T) = \left. \frac{\partial \phi_\alpha}{\partial \mathcal{F}_\sigma} \right|_{\mathcal{F}=0} = \beta \int d^3x \langle \mathcal{O}_\alpha(0, \vec{x}) \mathcal{O}_\sigma(0, \vec{0}) \rangle, \quad (3.7)$$

where $\langle \mathcal{O}_\alpha(0, \vec{x}) \mathcal{O}_\sigma(0, \vec{0}) \rangle$ is the two point correlation function with operators evaluated at equal times. There is no broken symmetry as

$$\langle \mathcal{O}_\alpha(0, \vec{x}) \rangle|_{\mathcal{F} \rightarrow 0} = \langle \mathcal{O}_\sigma(0, \vec{0}) \rangle|_{\mathcal{F} \rightarrow 0} = 0. \quad (3.8)$$

3.2.3 Thermodynamics functions and quark number susceptibility

The pressure of a given system is defined as

$$\mathcal{P} = \frac{T}{V} \ln \mathcal{Z} \quad (3.9)$$

where T is temperature, V is the volume and \mathcal{Z} is the partition function of a system containing quark-antiquark gas. The entropy density is defined as

$$S = \frac{\partial \mathcal{P}}{\partial T} \quad (3.10)$$

The number density for a given quark flavor can be written as

$$\rho = \frac{\partial \mathcal{P}}{\partial \mu} = \frac{1}{V} \frac{\text{Tr}[\mathcal{N} e^{-\beta(\mathcal{H} - \mu \mathcal{N})}]}{\text{Tr}[e^{-\beta(\mathcal{H} - \mu \mathcal{N})}]} = \frac{\langle \mathcal{N} \rangle}{V} \quad (3.11)$$

with \mathcal{N} is the quark number operator and μ is the chemical potential. If $\mu \rightarrow 0$, the quark number density vanishes due to CP invariance. Then the QNS for a given quark flavor follows can be written as

$$\chi_q(T) = \left. \frac{\partial \rho}{\partial \mu} \right|_{\mu=0} = \left. \frac{\partial^2 \mathcal{P}}{\partial \mu^2} \right|_{\mu=0} \quad (3.12)$$

3.2.4 QNS and Temporal Euclidean Correlation Function

The QNS is a measure of the response of the quark number density with infinitesimal change in the quark chemical potential, $\mu + \delta\mu$. Under such a situation the external field, \mathcal{F}_α , in Eq. (3.6) can be identified as the quark chemical potential and the operator \mathcal{O}_α as the temporal component (J_0) of the vector current, $J_\sigma(t, \vec{x}) = \bar{\psi} \Gamma_\sigma \psi$,

where Γ^σ is in general a three point function.

Then the QNS for a given quark flavor can be written from Eq. (3.7) as

$$\begin{aligned}\chi_q(T) &= \int d^4x \langle J_0(0, \vec{x}) J_0(0, \vec{0}) \rangle \\ &= -\lim_{\vec{p} \rightarrow 0} \text{Re} G_{00}^R(0, \vec{p}),\end{aligned}\tag{3.13}$$

where G_{00}^R is the retarded correlation function. To obtain (3.13) in concise form, we have used the fluctuation-dissipation theorem given as

$$G_{00}(\omega, \vec{p}) = -\frac{2}{1 - e^{-\omega/T}} \text{Im} G_{00}^R(\omega, \vec{p}),\tag{3.14}$$

and the Kramers-Kronig dispersion relation

$$\text{Re} G_{00}^R(\omega, \vec{p}) = \int_{-\infty}^{\infty} \frac{d\omega'}{2\pi} \frac{\text{Im} G_{00}^R(\omega', \vec{p})}{\omega' - \omega},\tag{3.15}$$

where $\lim_{\vec{p} \rightarrow 0} \text{Im} G_{00}^R(\omega, \vec{p})$ is proportional to $\delta(\omega)$ due to the quark number conservation [39, 40, 302–304].

Now, (3.7) or (3.13) indicates that the thermodynamic derivatives with respect to the external source are related to the temporal component of the static correlation function associated with the number conservation of the system. This relation in (3.13) is known as *the thermodynamic sum rule* [302–304].

Owing to the quark number conservation the temporal spectral function $\sigma_{00}(\omega, \vec{0})$ in (3.3) becomes

$$\sigma_{00}(\omega, \vec{0}) = \frac{1}{\pi} \text{Im} G_{00}^R(\omega, \vec{0}) = -\omega \delta(\omega) \chi_q(T).\tag{3.16}$$

Using Eq. (3.16) in Eq. (3.4), it is straight forward to obtain the temporal correlation

function as

$$G_{00}(\tau T) = -T\chi_q(T), \quad (3.17)$$

which is proportional to the QNS χ_q and T , but independent of τ .

In the next section we present LO QNS in HTLpt for our purpose.

3.3 Leading order QNS in HTLpt

The partition function including HTL improvement term can be written as

$$\mathcal{Z}[\mu] = \int \mathcal{D}[\psi] \mathcal{D}[\bar{\psi}] \mathcal{D}[\mathcal{A}] e^{i \int d^4x (\mathcal{L}_{QCD} + \mathcal{L}_{HTL})(\psi, \bar{\psi}, \mu)}, \quad (3.18)$$

where we have considered the external source as μ , the quark chemical potential, and \mathcal{A} is a background gauge field. The HTL improvement term \mathcal{L}_{HTL} is defined in Eq. (2.109) of Chapter 2.

Using the Eqs. (3.9), (3.11) and (3.18), one could now write the number density as

$$\begin{aligned} \rho(T, \mu) &= N_c N_f \int \frac{d^4K}{(2\pi)^4} \text{Tr} [S(K) \Gamma_0(K, -K; 0)] \\ &= i N_c N_f T \int \frac{d^3k}{(2\pi)^3} \sum_{k_0} \text{Tr} [S(K) \Gamma_0(K, -K; 0)], \end{aligned} \quad (3.19)$$

where ‘Tr’ is over Dirac indices. The quark Matsubara modes are given as $k_0 = (2m + 1)\pi iT + \mu$, where $m = 0, 1, 2, \dots$; N_f is the number of massless flavors and N_c is the number of color. The quark propagator $S(K \equiv (k_0, k))$ and temporal component of three-point quark gluon vertex can be found in (2.78) and (2.89), respectively. The zero momentum limit of the 3-point HTL function can also be obtained from the Ward identity as

$$\Gamma^0(K, -K; 0) = \frac{\partial}{\partial k_0} (-iS(k_0, k)^{-1}) = a\gamma^0 + b\vec{\gamma} \cdot \hat{k}, \quad (3.20)$$

where

$$a \pm b = D'_{\pm}(k_0, k), \quad (3.21)$$

with $D_{\pm}(k_0, k)$ defined in Eq. (2.79) and leads to

$$D'_{\pm} = \frac{D_{\pm}}{k_0 \mp k} + \frac{2m_q^2}{k_0^2 - k^2}. \quad (3.22)$$

After performing the trace over Dirac matrices, the number density (3.19) in terms of $D_{\pm}(k_0, k)$ can be written as

$$\begin{aligned} \rho^{HTL}(T, \mu) &= 2N_c N_f T \int \frac{d^3k}{(2\pi)^3} \sum_{k_0} \left[\frac{D'_+}{D_+} + \frac{D'_-}{D_-} \right] \\ &= 2N_c N_f T \int \frac{d^3k}{(2\pi)^3} \sum_{k_0} \left[\frac{1}{k_0 - k} + \frac{1}{k_0 + k} + \frac{2m_q^2}{k_0^2 - k^2} \left(\frac{1}{D_+} + \frac{1}{D_-} \right) \right]. \end{aligned} \quad (3.23)$$

Apart from the various poles due to quasiparticle (QP) in Eq. (3.23) it has Landau damping (LD) part as $D_{\pm}(k_0, k)$ contain logarithmic terms which generate discontinuity for $k_0^2 < k^2$. Eq. (3.23) can be decomposed in individual contribution as

$$\rho^{HTL}(T, \mu) = \rho^{QP}(T, \mu) + \rho^{LD}(T, \mu). \quad (3.24)$$

3.3.1 Quasiparticle part (QP)

The pole part of the number density can be calculated using the contour integration method introduced in Chapter 1 and calculating the residues of each term of Eq. (3.23), one can obtain the HTL quasiparticle contributions to the quark number density as

$$\begin{aligned}
 \rho^{QP}(T, \mu) &= -N_c N_f \int \frac{d^3 k}{(2\pi)^3} \left[\tanh \frac{\beta(\omega_+ - \mu)}{2} + \tanh \frac{\beta(\omega_- - \mu)}{2} - \tanh \frac{\beta(k - \mu)}{2} \right. \\
 &\quad \left. - \tanh \frac{\beta(\omega_+ + \mu)}{2} - \tanh \frac{\beta(\omega_- + \mu)}{2} + \tanh \frac{\beta(k + \mu)}{2} \right] \\
 &= 2N_c N_f \int \frac{d^3 k}{(2\pi)^3} [n(\omega_+ - \mu) + n(\omega_- - \mu) - n(k - \mu) - n(\omega_+ + \mu) \\
 &\quad - n(\omega_- + \mu) + n(k + \mu)] \quad , \quad (3.25)
 \end{aligned}$$

where $n(y)$ is the Fermi-Dirac distribution, ω_{\pm} is defined in Chapter 2. Eq. (H6) agrees with that of the two-loop approximately self-consistent Φ -derivable HTL resummation of Ref. [157] in leading order mass prescription.

Now, the pressure is obtained by integrating the first line of (3.25) w.r.t. μ as

$$\begin{aligned}
 \mathcal{P}^{QP}(T, \mu) &= 2N_f N_c T \int \frac{d^3 k}{(2\pi)^3} \left[\ln(1 + e^{-\beta(\omega_+ - \mu)}) + \ln\left(\frac{1 + e^{-\beta(\omega_- - \mu)}}{1 + e^{-\beta(k - \mu)}}\right) \right. \\
 &\quad \left. + \ln(1 + e^{-\beta(\omega_+ + \mu)}) + \ln\left(\frac{1 + e^{-\beta(\omega_- + \mu)}}{1 + e^{-\beta(k + \mu)}}\right) + \beta\omega_+ + \beta(\omega_- - k) \right], \quad (3.26)
 \end{aligned}$$

where both quasiparticles with energies ω_+ and ω_- generate T dependent ultraviolet (UV) divergences in LO HTL pressure due to quasiparticles. This also agrees with the *quasiparticle* contribution as obtained in Ref. [165] for $\mu = 0$ and adopting the same technique prescribed therein one can remove the UV divergences. At very high temperature, Eq. (3.26) reduces to free case as

$$\mathcal{P}(T, \mu) = 2N_f N_c T \int \frac{d^3 k}{(2\pi)^3} [\beta k + \ln(1 + e^{-\beta(k - \mu)}) + \ln(1 + e^{-\beta(k + \mu)})]. \quad (3.27)$$

The corresponding HTL QP entropy density in LO can be obtained as

$$\begin{aligned}
 \mathcal{S}^{QP}(T, \mu) &= \frac{\partial \mathcal{P}_I^{QP}}{\partial T} = 2N_c N_f \int \frac{d^3 k}{(2\pi)^3} \left[\ln(1 + e^{-\beta(\omega_+ - \mu)}) + \ln\left(\frac{1 + e^{-\beta(\omega_- - \mu)}}{1 + e^{-\beta(k - \mu)}}\right) \right. \\
 &+ \ln(1 + e^{-\beta(\omega_+ + \mu)}) + \ln\left(\frac{1 + e^{-\beta(\omega_- + \mu)}}{1 + e^{-\beta(k + \mu)}}\right) + \frac{\beta(\omega_+ - \mu)}{e^{\beta(\omega_+ - \mu)} + 1} + \frac{\beta(\omega_- - \mu)}{e^{\beta(\omega_- - \mu)} + 1} \\
 &\left. - \frac{\beta(k - \mu)}{e^{\beta(k - \mu)} + 1} + \frac{\beta(\omega_+ + \mu)}{e^{\beta(\omega_+ + \mu)} + 1} + \frac{\beta(\omega_- + \mu)}{e^{\beta(\omega_- + \mu)} + 1} - \frac{\beta(k + \mu)}{e^{\beta(k + \mu)} + 1} \right]. \quad (3.28)
 \end{aligned}$$

The QNS in LO due to HTL QP can also be obtained from (3.25) as

$$\begin{aligned}
 \chi^{QP}(T) &= \left. \frac{\partial}{\partial \mu} [\rho^{QP}] \right|_{\mu=0} \\
 &= 4N_c N_f \beta \int \frac{d^3 k}{(2\pi)^3} [n(\omega_+) (1 - n(\omega_+)) + n(\omega_-) (1 - n(\omega_-)) \\
 &\quad - n(k) (1 - n(k))] , \quad (3.29)
 \end{aligned}$$

where the μ derivative is performed only to the explicit μ dependence. Obviously (3.29) agrees well with that of the 2-loop approximately self-consistent Φ -derivable HTL resummation [157]. The above thermodynamical quantities in LO due to HTL *quasiparticles* with excitation energies ω_{\pm} are similar in form to those of free case but the hard and soft contributions are clearly separated out and one does not need an ad hoc separating scale as used in Ref. [158].

3.3.2 Landau Damping part (LD)

The LD part of the quark number density in LO follows from (3.23) as

$$\rho^{LD}(T, \mu) = N_c N_f \int \frac{d^3 k}{(2\pi)^3} \int_{-k}^k d\omega \left(\frac{2m_q^2}{\omega^2 - k^2} \right) \beta_+(\omega, k) [n(\omega - \mu) - n(\omega + \mu)]. \quad (3.30)$$

where $\beta_{\pm}(\omega, k)$ is discontinuity for quark propagator $D_{\pm}(k_0, k)$ for $k_0^2 < k^2$ and can be obtained as

$$\begin{aligned} \beta_{\pm}(\omega, k) &= \frac{1}{\pi} \text{Disc} \frac{1}{D_{\pm}(k_0, k)} = \frac{1}{\pi} \text{Im} \frac{1}{D_{\pm}(k_0, k)} \Big|_{\substack{k_0 \rightarrow \omega + i\epsilon \\ \epsilon \rightarrow 0}} \\ &= \frac{\frac{m_q^2}{2k} (-1 \pm \frac{\omega}{k}) \Theta(k^2 - \omega^2)}{\left[\omega \mp k - \frac{m_q^2}{k} (\pm 1 - \frac{\omega \mp k}{2k} \ln \frac{k+\omega}{k-\omega}) \right]^2 + \left[\pi \frac{m_q^2}{2k} (1 \mp \frac{\omega}{k}) \right]^2}. \end{aligned} \quad (3.31)$$

One can obtain the pressure due to LD contribution by integrating (3.30) w.r.t. μ , while considering m_q is an implicit function of T and μ , as

$$\begin{aligned} \mathcal{P}^{LD}(T, \mu) &= N_c N_f T \int \frac{d^3 k}{(2\pi)^3} \int_{-k}^k d\omega \left(\frac{2m_q^2}{\omega^2 - k^2} \right) \beta_+(\omega, k) \left[\ln(1 + e^{-\beta(\omega - \mu)}) \right. \\ &\quad \left. + \ln(1 + e^{-\beta(\omega + \mu)}) + \beta\omega \right], \end{aligned} \quad (3.32)$$

which has UV divergence like [165] and can be removed using the prescription therein.

The corresponding LD part of entropy density can be obtained as

$$\begin{aligned} \mathcal{S}^{LD}(T, \mu) &= N_c N_f \int \frac{d^3 k}{(2\pi)^3} \int_{-k}^k d\omega \left(\frac{2m_q^2}{\omega^2 - k^2} \right) \beta_+(\omega, k) \left[\ln(1 + e^{-\beta(\omega - \mu)}) \right. \\ &\quad \left. + \ln(1 + e^{-\beta(\omega + \mu)}) + \frac{\beta(\omega - \mu)}{e^{\beta(\omega - \mu)} + 1} + \frac{\beta(\omega + \mu)}{e^{\beta(\omega + \mu)} + 1} \right]. \end{aligned} \quad (3.33)$$

Also the LD part of the QNS becomes

$$\begin{aligned} \chi^{LD}(T) &= \frac{\partial}{\partial \mu} [\rho_I^{LD}(T, \mu)] \Big|_{\mu=0} = 2N_c N_f \beta \int \frac{d^3 k}{(2\pi)^3} \int_{-k}^k d\omega \left(\frac{2m_q^2}{\omega^2 - k^2} \right) \\ &\quad \times \beta_+(\omega, k) n(\omega) (1 - n(\omega)), \end{aligned} \quad (3.34)$$

where the μ derivative is again performed only to the explicit μ dependence. It is also

to be noted that the LD contribution is of the order of m_q^4 . The LD contribution can not be compared with that of the 2-loop approximately self-consistent Φ -derivable HTL resummation [157] as it does not have any closed form for the final expression.

So total QNS can be written from Eqs. (3.29) and (3.34) as

$$\begin{aligned}
 \chi_q^{HTL}(T) &= \chi_q^{QP} + \chi_q^{LD} \\
 &= 4N_c N_f \beta \int \frac{d^3k}{(2\pi)^3} \left[n(\omega_+) (1 - n(\omega_+)) + n(\omega_-) (1 - n(\omega_-)) \right. \\
 &\quad \left. - n(k) (1 - n(k)) \right] \\
 &\quad + 2N_c N_f \beta \int \frac{d^3k}{(2\pi)^3} \int_{-k}^k d\omega \left(\frac{2m_q^2}{\omega^2 - k^2} \right) \beta_+(\omega, k) n(\omega) (1 - n(\omega)) \quad (3.35)
 \end{aligned}$$

The QP part results in (3.29) is identical to that of the 2-loop approximately self-consistent Φ -derivable HTL resummation approach [157, 169] within LO mass prescription. The LD part (3.34) cannot be compared directly to the LD part of Ref. [157, 169] as no closed expression is given there. However, numerical results of the both QNS agree very well. We also note that Ref. [158] used HTLpt but did not take into account properly the effect of the variation of the external field to the density fluctuation, which resulted in an over-counting in the LO QNS. Moreover, it required an ad hoc separation scale is required to distinguish between soft and hard momenta. In the HTLpt approach in Ref. [166, 168] the HTL N-point functions were used uniformly for all momenta scale, *i.e.*, both soft and hard momenta, which resulted in an over-counting within the LO contribution [157, 169]. The reason is that the HTL action is accurate only for soft momenta and for hard ones only in the vicinity of light cone.

3.4 Results and Discussions:

In Fig. (3.1) we plot LO QNS in HTLpt for two-flavor system along-with perturbative and various lattice QCD data.

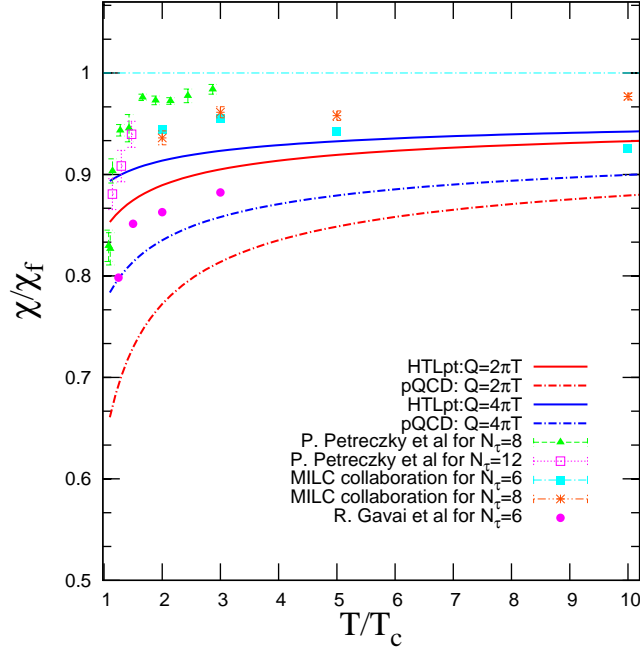


Figure 3.1: The 2-flavor scaled QNS with that of free one as a function of T/T_C . The solid lines are for LO in HTLpt whereas the dashed lines are for LO in pQCD [133, 157, 169, 234]. The different choices of the renormalization scale are $Q = 2\pi T$ (red), and $4\pi T$ (blue). The symbols represent the various lattice data [102–104, 109–111, 116].

It is clear from Fig. (3.1) that the dependence on renormalization scale in case of HTLpt is less than that of pQCD [133, 157, 169, 234] results of order g^2 . Also the 2 flavor LO QNS in HTLpt is higher in all temperature range than pQCD results and HTLpt results are in good agreement with lattice QCD data. Moreover, it also shows the same trend as the available lattice results for $(2+1)$ -flavors [109–112, 116, 117] as well as for 2-flavors [102–104], though there is a large variation among the various lattice results. In Fig. (3.1), the green triangles (with $T_c = 191$ MeV) and purple squares (with $T_c = 185$ MeV) represent $p4$ lattice QCD data [110, 116], the

squares (cyan) and stars (saffron) are from asqtad lattice QCD data [111] for (2+1)-flavor, $m = 0.2m_s$ and $T_c = 186 \pm 4$ MeV. The solid circles (purple) represent lattice QCD data [102–104] for $T_c = 0.49\Lambda_{\overline{MS}}$. The quark mass ranges between (0.1 to 0.2) m_s , where m_s is the strange quark mass near its physical value. Note that further lowering the quark mass to its physical value seems to have a small effect [117] for $T > 200$ MeV. The details of these lattice results are also summarized in Ref. [112]. A detailed analysis on uncertainties of the ingredients in the lattice QCD calculations is presented in Refs. [110,117]. This calls for further investigation both on the analytic side by improving the HTL resummation schemes and on the lattice side by refining the various lattice ingredients.

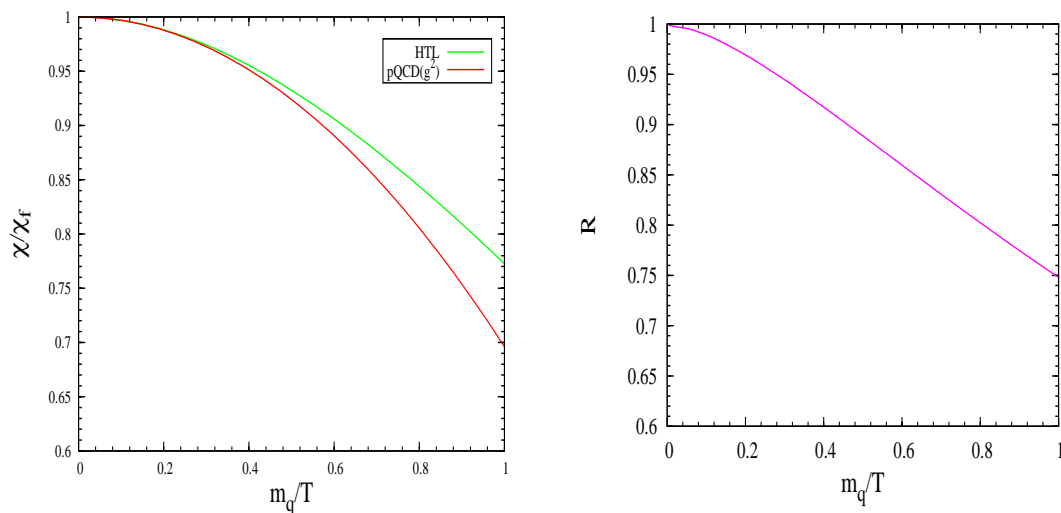


Figure 3.2: (Color online) *Left panel:* The ratio of 2-flavour HTL to free quark QNS and also that of LO perturbative one as a function of m_q/T . *Right panel:* R as a function of m_q/T .

In the left panel of Fig. 3.2 we display the LO HTL and perturbative QNS [157] scaled with free one vs m_q/T . In the weak coupling limit both approach unity whereas HTL has a little slower deviation from ideal gas value. Now, in the right panel we plot a ratio [157, 169], $R \equiv (\chi_{htl} - \chi_f)/(\chi_{p(g^2)} - \chi_f)$, which measures the deviation of interaction of χ_{htl} from that of pQCD in order g^2 . It approaches unity in the weak coupling limit implying the correct inclusion [157, 169] of order g^2 in our approach in a truly perturbative sense.

Recently, an improved lattice calculation [305] has been performed within the quenched approximation of QCD where the temporal correlation function is determined. Using the LO HTLpt QNS in Eq. (3.35) we now obtain the temporal correlation function in Eq. (3.17) and compare with the recent lattice data [305]. In Fig. (3.3) the scaled

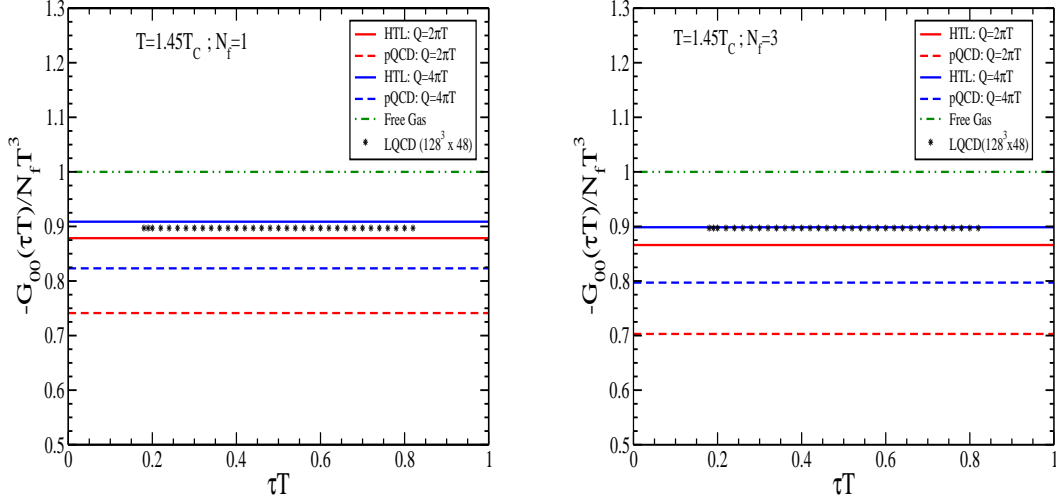


Figure 3.3: The scaled temporal correlation function with T^3 for $N_f = 1$ (left panel) and $N_f = 3$ (right panel) at $T = 1.45T_c$ for $Q = 2\pi T$ (red) and $4\pi T$ (blue) as a function of scaled Euclidean time, τT . The symbols represent the recent lattice data [305] on lattices of size $128^3 \times 48$ for quark mass $0.1T$ in quenched QCD.

temporal correlation function with T^3 is shown for $N_f = 1$ (left panel) and $N_f = 3$ (right panel) at $T = 1.45T_c$. We first note that the correlation functions both in HTLpt and pQCD have weak flavor dependence due to the temperature dependent coupling, α_s as discussed before. The LO HTLpt result indicates an improvement over that of the pQCD one [133, 157, 169, 234] for different choices of the renormalization scale as shown in Fig. (3.3). Also, the HTLpt result shows a good agreement to that of recent lattice gauge theory calculation [305] performed on lattices up to size $128^3 \times 48$ in quenched approximation for a quark mass $\sim 0.1T$. We also note that unlike the dynamical spatial part of the correlation function in the vector channel the temporal part does not encounter any infrared problem in the low energy part as it is related to the static quantity through the thermodynamic sum rule associated

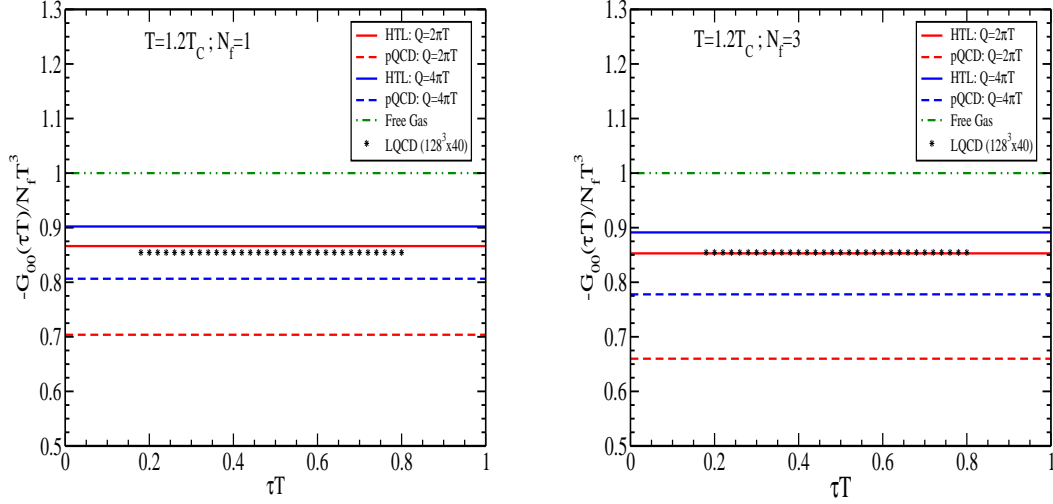


Figure 3.4: Same as Fig. (3.3) but at $T = 1.2T_C$ and the corresponding lattice data are preliminary [311] with lattice size $148^3 \times 40$.

with the corresponding symmetry, *viz.*, the number conservation of the system.

We also presented two extreme cases of HTLpt temporal correlation function at $T = 1.2T_C$ in Fig. (3.4) and at $T \sim 3T_C$ in Fig. (3.5), respectively, for two different flavors and compare with the corresponding preliminary lattice data [311], which are also found to be in good agreement.

3.5 Conclusion

The LO QNS as a response of the conserved density fluctuation in HTLpt when compared with the available lattice data [102–104, 109–111, 116] in the literature within their wide variation shows the same trend but deviates from those in certain extent. The same HTL QNS is used to compute the temporal part of the Euclidean correlation in vector current which agrees quite well with that of improved lattice gauge theory calculations [305, 311] recently performed within quenched approximation on lattices up to size $128^3 \times 48$ for a quark mass $\sim 0.1T$. Leaving aside the difference in ingredients in various lattice calculations, one can expect that the HTLpt and

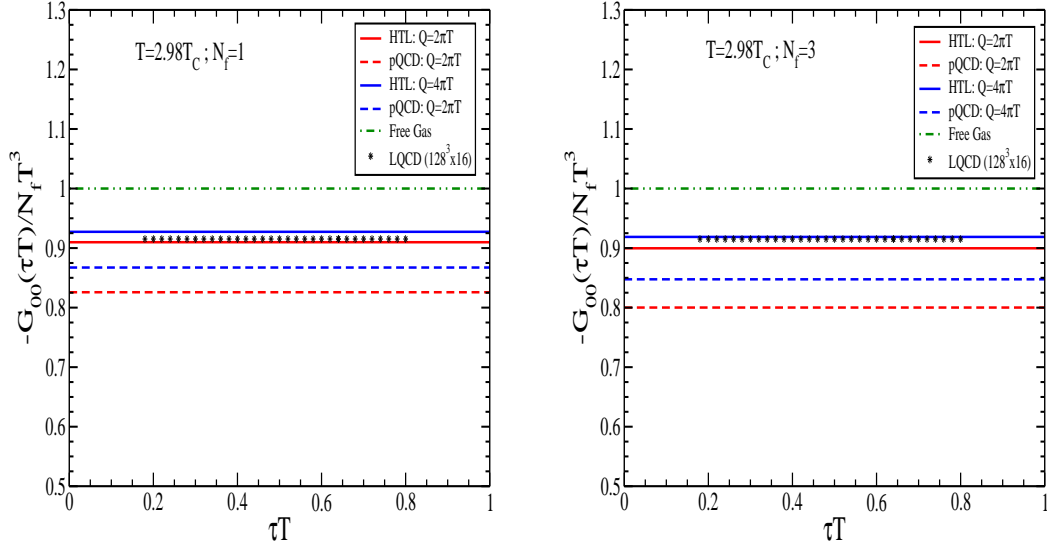


Figure 3.5: Same as Fig. (3.3) but at $T = 2.98T_C$ and the corresponding lattice data are preliminary [311] with lattice size $148^3 \times 16$.

lattice calculations are in close proximity for quantities associated with the conserved density fluctuation. The leading order quark number susceptibility in HTL perturbation theory produces correct $\mathcal{O}(g^2)$ perturbative results when expanded in a strict power series in g . So make the results more reliable for heavy-ion-collisions experiments, we need to go beyond leading order calculations. In the following two chapters, we will discuss about thermodynamic calculations beyond leading order.

CHAPTER 4

Two-loop HTL Thermodynamics

In this chapter, we study the two-loop pressure and also second and fourth order quark number susceptibility of QCD using the hard-thermal-loop perturbation theory. This chapter is based on: *Two-loop HTL pressure at finite temperature and chemical potential*, N. Haque, M. G. Mustafa, and M. Strickland, **Phys. Rev. D** **87** (2013) 105007 and *Quark Number Susceptibilities from Two-Loop Hard Thermal Loop Perturbation Theory*, N. Haque, M. G. Mustafa, and M. Strickland, **JHEP** **1307** (2013) 184.

4.1 Introduction

In Chapter 3, HTL perturbation theory has been applied to calculate LO thermodynamics to the case of finite temperature and finite chemical potential and also to calculate LO QNS. As discussed in Chapter 3, LO QNS in HTLpt produced correct perturbative order up to g^2 in strict perturbative expansion, it will be interesting to go beyond leading order at finite temperature and finite chemical potential in HTLpt.

In HTL perturbation theory the next-to-leading order (NLO) thermodynamic po-

tential was computed in [172,173] at finite temperature and zero chemical potential. But in view of the ongoing RHIC beam energy scan and planned FAIR experiments, one is motivated to reliably determine the thermodynamic functions at finite chemical potential. In this chapter we discuss the NLO pressure of quarks and gluons at finite T and μ . The computation utilizes a high temperature expansion through fourth order in the ratio of the chemical potential to temperature. This allows us to reliably access the region of high temperature and small chemical potential. We compare our final result for the NLO HTLpt pressure at finite temperature and chemical potential with state-of-the-art perturbative quantum chromodynamics (QCD) calculations and available lattice QCD results.

Having the full thermodynamic potential as a function of chemical potential(s) and temperature allows us to compute the quark number susceptibilities. For massless quark flavors the QNS are usually defined as

$$\chi_n(T) \equiv \left. \frac{\partial^n \mathcal{P}}{\partial \mu^n} \right|_{\mu=0}, \quad (4.1)$$

where \mathcal{P} is the pressure of system, μ is the quark chemical potential and T is the temperature of the system.

This chapter is organized as follows. In Sec. (4.2) we discuss various quantities required to be calculated at finite chemical potential based on prior calculations of the NLO thermodynamic at zero chemical potential [172,173]. In Sec. (4.3) we reduce the sum of various diagrams to scalar sum-integrals. A high temperature expansion is made in Sec. (4.4) to obtain analytic expressions for both the LO and NLO thermodynamic potential. In Secs. (4.5) and (4.6) we calculate the various sum-integrals and d -dimensional integrals that appear in Sec. (4.4). We then use the results of Secs. (4.4), (4.5) and (4.6) to compute the pressure in Sec. (4.7). We compute second and fourth order quark number susceptibilities in Sec. (4.8). We finally conclude in Sec. (4.9).

4.2 Ingredients for the NLO Thermodynamic potential in HTLpt

The LO HTLpt thermodynamic potential, Ω_{LO} , for an $SU(N_c)$ gauge theory with N_f massless quarks in the fundamental representation can be written as [164, 172, 173]

$$\Omega_{\text{LO}} = d_A \mathcal{F}_g + d_F \mathcal{F}_q + \Delta_0 \mathcal{E}_0, \quad (4.2)$$

where $d_F = N_f N_c$ and $d_A = N_c^2 - 1$ with N_c is the number of colors. \mathcal{F}_q and \mathcal{F}_g are the one loop contributions to quark and gluon free energies, respectively. The LO counter-term is the same as in the case of zero chemical potential [164]

$$\Delta_0 \mathcal{E}_0 = \frac{d_A}{128\pi^2\epsilon} m_D^4. \quad (4.3)$$

At NLO one must consider the diagrams shown in Fig. (4.1). The resulting NLO

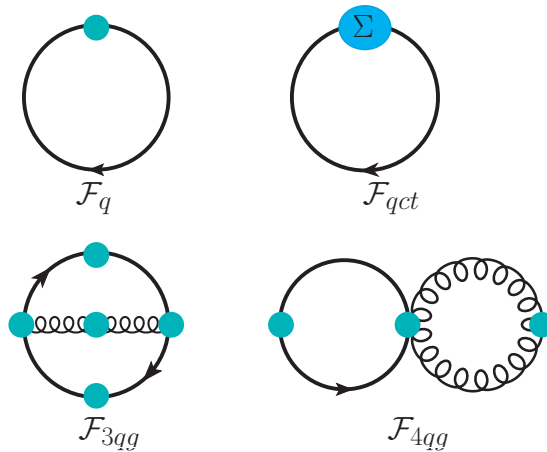


Figure 4.1: Diagrams containing fermionic lines relevant for NLO thermodynamics potential in HTLpt with finite chemical potential. Shaded circles indicate HTL n -point functions.

HTLpt thermodynamic potential can be written in the following general form [173]

$$\begin{aligned} \Omega_{\text{NLO}} = & \Omega_{\text{LO}} + d_A [\mathcal{F}_{3g} + \mathcal{F}_{4g} + \mathcal{F}_{gh} + \mathcal{F}_{gct}] + d_{AS_F} [\mathcal{F}_{3qg} + \mathcal{F}_{4qg}] \\ & + d_F \mathcal{F}_{qct} + \Delta_1 \mathcal{E}_0 + \Delta_1 m_D^2 \frac{\partial}{\partial m_D^2} \Omega_{\text{LO}} + \Delta_1 m_q^2 \frac{\partial}{\partial m_q^2} \Omega_{\text{LO}} , \end{aligned} \quad (4.4)$$

where $s_F = N_f/2$. At NLO the terms that depend on the chemical potential are \mathcal{F}_q , \mathcal{F}_{3qg} , \mathcal{F}_{4qg} , \mathcal{F}_{qct} , $\Delta_1 m_q^2$, and $\Delta_1 m_D^2$ as displayed in Fig. (4.1). The other terms, e.g. \mathcal{F}_g , \mathcal{F}_{3g} , \mathcal{F}_{4g} , \mathcal{F}_{gh} and \mathcal{F}_{gct} coming from gluon and ghost loops remain the same as the $\mu = 0$ case [172, 173]. We also add that the vacuum energy counter-term, $\Delta_1 \mathcal{E}_0$, remains the same as the $\mu = 0$ case whereas the mass counter-terms, $\Delta_1 m_D^2$ and $\Delta_1 m_q^2$, have to be computed for $\mu \neq 0$. These counter-terms are of order δ . This completes a general description of contributions one needs to compute in order to determine NLO HTLpt thermodynamic potential at finite chemical potential. We now proceed to the scalarization of the necessary diagrams.

4.3 Scalarization of the fermionic diagrams

The one-loop quark contribution coming from the first diagram in Fig. (4.1) can be written as

$$\mathcal{F}_q = - \sum_{\{P\}} \log \det [\not{P} - \Sigma(P)] = -2 \sum_{\{P\}} \log P^2 - 2 \sum_{\{P\}} \log \left[\frac{A_S^2 - A_0^2}{P^2} \right], \quad (4.5)$$

where A_0 and A_S are defined in Eq. (2.76) of Chapter 2 in Minkowski space. We can write it in Euclidean space as

$$A_0(P) = iP_0 - \frac{m_q^2}{iP_0} \mathcal{T}_P, \quad (4.6)$$

$$A_S(P) = |\mathbf{p}| + \frac{m_q^2}{|\mathbf{p}|} [1 - \mathcal{T}_P], \quad (4.7)$$

and \mathcal{T}_P is defined by the following integral [172, 173] in Euclidean space as

$$\mathcal{T}_P = \left\langle \frac{P_0^2}{P_0^2 + p^2 c^2} \right\rangle_c = \frac{\omega(\epsilon)}{2} \int_{-1}^1 dc (1 - c^2)^{-\epsilon} \frac{iP_0}{iP_0 - |\mathbf{p}|c}, \quad (4.8)$$

with $w(\epsilon) = 2^{2\epsilon} \Gamma(2 - 2\epsilon)/\Gamma^2(1 - \epsilon)$. In three dimensions *i.e.* for $\epsilon \rightarrow 0$, Eq. (4.8) reduces to

$$\mathcal{T}_P = \frac{iP_0}{2|\mathbf{p}|} \log \frac{iP_0 + |\mathbf{p}|}{iP_0 - |\mathbf{p}|}, \quad (4.9)$$

with $P \equiv (P_0, \mathbf{p})$. In practice, one must use the general form and only take the limit $\epsilon \rightarrow 0$ after regularization/renormalization.

The HTL quark counter-term at one-loop order can be rewritten from the second diagram in Fig. (4.1) as

$$\mathcal{F}_{qct} = -4 \sum_{\{P\}} \frac{P^2 + m_q^2}{A_S^2 - A_0^2}. \quad (4.10)$$

The two-loop contributions coming from the third and fourth diagrams in Fig. (4.1) are given, respectively, by

$$\mathcal{F}_{3qg} = \frac{1}{2} g^2 \sum_{P\{Q\}} \text{Tr} [\Gamma^\mu(P, Q, R) S(Q) \times \Gamma^\nu(P, Q, R) S(R)] \Delta_{\mu\nu}(P), \quad (4.11)$$

$$\mathcal{F}_{4qg} = \frac{1}{2} g^2 \sum_{P\{Q\}} \text{Tr} [\Gamma^{\mu\nu}(P, -P, Q, Q) S(Q)] \Delta_{\mu\nu}(P), \quad (4.12)$$

where S is the quark propagator which is given by $S = (\gamma^\mu \mathcal{A}_\mu)^{-1}$ with $\mathcal{A}_\mu = (A_0(P), A_S(P) \hat{\mathbf{p}})$ and $\Delta^{\mu\nu}$ is the gluon propagator. The general covariant gauge $\Delta^{\mu\nu}$ can be found in Eq. (2.54) of Chapter 2 in Minkowski space. Also above Γ^μ and $\Gamma^{\mu\nu}$ are HTL-resummed 3- and 4-point functions can be found in Chapter 2. Many more details concerning the HTL n -point functions including the general Coulomb

gauge propagator etc. can be found in Chapter 2 and also in appendices of Refs. [164, 172, 173].

In general covariant gauge, the sum of (4.11) and (4.12) reduces to

$$\mathcal{F}_{3qg+4qg} = \frac{1}{2}g^2 \sum_{P\{Q\}} \left\{ \Delta_X(P) \text{Tr} [\Gamma^{00} S(Q)] - \Delta_T(P) \text{Tr} [\Gamma^\mu S(Q) \Gamma^\mu S(R')] \right. \\ \left. + \Delta_X(P) \text{Tr} [\Gamma^0 S(Q) \Gamma^0 S(R')] \right\}, \quad (4.13)$$

where Δ_T is the transverse gluon propagator, Δ_X is a combination of the longitudinal and transverse gluon propagators [172, 173], and $R' = Q - P$. After performing the traces of the γ -matrices one obtains [172, 173]

$$\mathcal{F}_{3qg+4qg} = -g^2 \sum_{P\{Q\}} \frac{1}{A_S^2(Q) - A_0^2(Q)} \left[2(d-1) \Delta_T(P) \frac{\hat{\mathbf{q}} \cdot \hat{\mathbf{r}} A_S(Q) A_S(R) - A_0(Q) A_0(R)}{A_S^2(R) - A_0^2(R)} \right. \\ - 2 \Delta_X(P) \frac{A_0(Q) A_0(R) + A_S(Q) A_S(R) \hat{\mathbf{q}} \cdot \hat{\mathbf{r}}}{A_S^2(R) - A_0^2(R)} \\ - 4m_q^2 \Delta_X(P) \left\langle \frac{A_0(Q) - A_S(Q) \hat{\mathbf{q}} \cdot \hat{\mathbf{y}}}{(P \cdot Y)^2 - (Q \cdot Y)^2} \frac{1}{(Q \cdot Y)} \right\rangle_{\hat{\mathbf{y}}} \\ + \frac{8m_q^2 \Delta_T(P)}{A_S^2(R) - A_0^2(R)} \left\langle \frac{(A_0(Q) - A_S(Q) \hat{\mathbf{q}} \cdot \hat{\mathbf{y}})(A_0(R) - A_S(R) \hat{\mathbf{r}} \cdot \hat{\mathbf{y}})}{(Q \cdot Y)(R \cdot Y)} \right\rangle_{\hat{\mathbf{y}}} \\ + \frac{4m_q^2 \Delta_X(P)}{A_S^2(R) - A_0^2(R)} \left\langle \frac{2A_0(R) A_S(Q) \hat{\mathbf{q}} \cdot \hat{\mathbf{y}} - A_0(Q) A_0(R) - A_S(Q) A_S(R) \hat{\mathbf{q}} \cdot \hat{\mathbf{r}}}{(Q \cdot Y)(R \cdot Y)} \right\rangle_{\hat{\mathbf{y}}} \\ \left. + O(g^2 m_q^4), \right] \quad (4.14)$$

where A_0 and A_S are defined in (4.6) and (4.7), respectively. We add that the exact evaluation of two-loop free energy could be performed numerically and would involve 5-dimensional integrations; however, one would need to be able to identify all divergences and regulate the numerical integration appropriately. Short of this, one can calculate the sum-integrals by expanding in a power series in m_D/T , m_q/T , and μ/T in order to obtain semi-analytic expressions.

4.4 High temperature expansion

As discussed above, we make an expansion of two-loop free energies in a power series of m_D/T and m_q/T to obtain a series which is nominally accurate to order g^5 . By “nominally accurate” we mean that we expand the scalar integrals treating m_D and m_q as $\mathcal{O}(g)$ keeping all terms which contribute through $\mathcal{O}(g^5)$; however, the resulting series is accurate to order g^5 in name only.

In practice, the HTL n -point functions can have both hard and soft momenta scales on each leg. At one-loop order the contributions can be classified “hard” or “soft” depending on whether the loop momenta are order T or gT , respectively; however, since the lowest fermionic Matsubara mode corresponds to $P_0 = \pi T$, fermion loops are always hard. The two-loop contributions to the thermodynamic potential can be grouped into hard-hard (hh), hard-soft (hs), and soft-soft (ss) contributions. However, we note that one of the momenta contributing is always hard since it corresponds to a fermionic loop and therefore there will be no two-loop soft-soft contribution. Below we calculate the various contributions to the sum-integrals presented in Sec. (4.3).

4.4.1 One-loop sum-integrals

The one-loop sum-integrals (4.5) and (4.10) correspond to the first two diagrams in Fig. (4.1). They represent the leading-order quark contribution and order- δ HTL counterterm. We will expand the sum-integrals through order m_q^4 taking m_q to be of (leading) order g . This gives a result which is nominally accurate (at one-loop) through order g^5 .¹

¹Of course, this won't reproduce the full g^5 pQCD result in the limit $g \rightarrow 0$. In order to reproduce all known coefficients through $\mathcal{O}(g^5)$, one would need to perform a NNLO HTLpt calculation.

Hard Contribution

The hard contribution to the one-loop quark self-energy in (4.5) can be expanded in powers of m_q^2 as

$$\mathcal{F}_q^{(h)} = -2 \sum_{\{P\}} \log P^2 - 4m_q^2 \sum_{\{P\}} \frac{1}{P^2} + 2m_q^4 \sum_{\{P\}} \left[\frac{2}{P^4} - \frac{1}{p^2 P^2} + \frac{2\mathcal{T}_P}{p^2 P^2} - \frac{(\mathcal{T}_P)^2}{p^2 P_0^2} \right]. \quad (4.15)$$

Note that the function \mathcal{T}_P does not appear in m_q^2 term. The expressions for the sum-integrals in (4.15) are listed in Sec.(4.5). Using those expressions, the hard contribution to the quark free energy becomes

$$\begin{aligned} \mathcal{F}_q^{(h)} &= -\frac{7\pi^2}{180} T^4 \left(1 + \frac{120}{7} \hat{\mu}^2 + \frac{240}{7} \hat{\mu}^4 \right) + \left(\frac{\Lambda}{4\pi T} \right)^{2\epsilon} \frac{m_q^2 T^2}{6} \left[(1 + 12\hat{\mu}^2) \right. \\ &\quad \left. + \epsilon \left(2 - 2 \ln 2 + 2 \frac{\zeta'(-1)}{\zeta(-1)} + 24(\gamma_E + 2 \ln 2) \hat{\mu}^2 - 28\zeta(3) \hat{\mu}^4 + \mathcal{O}(\hat{\mu}^6) \right) \right] \\ &\quad + \frac{m_q^4}{12\pi^2} (\pi^2 - 6). \end{aligned} \quad (4.16)$$

Expanding the HTL quark counter-term in (4.10) one can write

$$\mathcal{F}_{\text{qct}}^{(h)} = 4m_q^2 \sum_{\{P\}} \frac{1}{P^2} - 4m_q^4 \sum_{\{P\}} \left[\frac{2}{P^4} - \frac{1}{p^2 P^2} + \frac{2}{p^2 P^2} \mathcal{T}_P - \frac{1}{p^2 P_0^2} (\mathcal{T}_P)^2 \right], \quad (4.17)$$

where the expressions for various sum-integrals in (4.17) are listed in Sec. (4.5). Using those expressions, the hard contribution to the HTL quark counter-term becomes

$$\mathcal{F}_{\text{qct}}^{(h)} = -\frac{m_q^2 T^2}{6} (1 + 12\hat{\mu}^2) - \frac{m_q^4}{6\pi^2} (\pi^2 - 6). \quad (4.18)$$

We note that the first term in (4.18) cancels the order- ϵ^0 term in the coefficient of m_q^2 in (4.16). There are no soft contributions either from the leading-order quark term in (4.5) or from the HTL quark counter-term in (4.10).

4.4.2 Two-loop sum-integrals

Since the two-loop sum-integrals given in (4.13) contain an explicit factor of g^2 , we only require an expansion to order $m_q^2 m_D / T^3$ and m_D^3 / T^3 in order to determine all terms contributing through order g^5 . We note that the soft scales are given by m_q and m_D whereas the hard scale is given by T , which leads to two different phase-space regions as discussed in Sec. 4.4.1. In the hard-hard region, all three momenta P , Q , and R are hard whereas in the hard-soft region, two of the three momenta are hard and the other one is soft.

The hh contribution

The self-energies for hard momenta are suppressed [150, 155, 156, 172, 173] by m_D^2 / T^2 or m_q^2 / T^2 relative to the propagators. For hard momenta, one just needs to expand in powers of gluon self-energies Π_T , Π_L , and quark self-energy Σ . So, the hard-hard contribution of \mathcal{F}_{3qg} and \mathcal{F}_{4qg} in (4.13) can be written as

$$\begin{aligned}
 \mathcal{F}_{3qg+4qg}^{(hh)} &= (d-1)g^2 \left[\sum_{\{PQ\}} \frac{1}{P^2 Q^2} - 2 \sum_{P\{Q\}} \frac{1}{P^2 Q^2} \right] \\
 &+ 2m_D^2 g^2 \sum_{P\{Q\}} \left[\frac{1}{p^2 P^2 Q^2} \mathcal{T}_P + \frac{1}{P^4 Q^2} - \frac{d-2}{d-1} \frac{1}{p^2 P^2 Q^2} \right] \\
 &+ m_D^2 g^2 \sum_{\{PQ\}} \left[\frac{d+1}{d-1} \frac{1}{P^2 Q^2 r^2} - \frac{4d}{d-1} \frac{q^2}{P^2 Q^2 r^4} - \frac{2d}{d-1} \frac{P \cdot Q}{P^2 Q^2 r^4} \right] \mathcal{T}_R \\
 &+ m_D^2 g^2 \sum_{\{PQ\}} \left[\frac{3-d}{d-1} \frac{1}{P^2 Q^2 R^2} + \frac{2d}{d-1} \frac{P \cdot Q}{P^2 Q^2 r^4} - \frac{d+2}{d-1} \frac{1}{P^2 Q^2 r^2} \right. \\
 &\quad \left. + \frac{4d}{d-1} \frac{q^2}{P^2 Q^2 r^4} - \frac{4}{d-1} \frac{q^2}{P^2 Q^2 r^2 R^2} \right] \\
 &+ 2m_q^2 g^2 (d-1) \sum_{\{PQ\}} \left[\frac{1}{P^2 Q_0^2 Q^2} + \frac{p^2 - r^2}{q^2 P^2 Q_0^2 R^2} \right] \mathcal{T}_Q
 \end{aligned}$$

$$\begin{aligned}
 & + 2m_q^2 g^2 (d-1) \sum_{P\{Q\}} \left[\frac{2}{P^2 Q^4} - \frac{1}{P^2 Q_0^2 Q^2} \mathcal{T}_Q \right] \\
 & + 2m_q^2 g^2 (d-1) \sum_{\{PQ\}} \left[\frac{d+3}{d-1} \frac{1}{P^2 Q^2 R^2} - \frac{2}{P^2 Q^4} - \frac{p^2 - r^2}{q^2 P^2 Q^2 R^2} \right], \quad (4.19)
 \end{aligned}$$

where the various sum-integrals and integrals are evaluated in Sec. (4.5) and (4.6).

Using those results, the hh contribution becomes

$$\begin{aligned}
 \mathcal{F}_{3qg+4qg}^{(hh)} & = \frac{5\pi^2}{72} \frac{\alpha_s}{\pi} T^4 \left[1 + \frac{72}{5} \hat{\mu}^2 + \frac{144}{5} \hat{\mu}^4 \right] \\
 & - \frac{1}{72} \frac{\alpha_s}{\pi} \left(\frac{\Lambda}{4\pi T} \right)^{4\epsilon} \left[\frac{1 + 6(4 - 3\zeta(3)) \hat{\mu}^2 - 120(\zeta(3) - \zeta(5)) \hat{\mu}^4 + \mathcal{O}(\hat{\mu}^6)}{\epsilon} \right. \\
 & + 1.3035 - 59.9055 \hat{\mu}^2 - 75.4564 \hat{\mu}^4 + \mathcal{O}(\hat{\mu}^6) \left. \right] m_D^2 T^2 \\
 & + \frac{1}{8} \frac{\alpha_s}{\pi} \left(\frac{\Lambda}{4\pi T} \right)^{4\epsilon} \left[\frac{1 - 12 \hat{\mu}^2}{\epsilon} + 8.9807 - 152.793 \hat{\mu}^2 \right. \\
 & \left. + 115.826 \hat{\mu}^4 + \mathcal{O}(\hat{\mu}^6) \right] m_q^2 T^2. \quad (4.20)
 \end{aligned}$$

The hs contribution

Following Ref. [172, 173] one can extract the hard-soft contribution from (4.13) as the momentum P is soft whereas momenta Q and R are always hard. The function associated with the soft propagator $\Delta_T(0, \mathbf{p})$ or $\Delta_X(0, \mathbf{p})$ can be expanded in powers of the soft momentum \mathbf{p} . For $\Delta_T(0, \mathbf{p})$, the resulting integrals over \mathbf{p} are not associated with any scale and they vanish in dimensional regularization. The integration measure $\int_{\mathbf{p}}$ scales like m_D^3 , the soft propagator $\Delta_X(0, \mathbf{p})$ scales like $1/m_D^2$, and every power of p in the numerator scales like m_D .

The contributions that survive only through order $g^2 m_D^3 T$ and $m_q^2 m_D g^3 T$ from \mathcal{F}_{3qg} and \mathcal{F}_{4qg} in (4.13) are

$$\mathcal{F}_{3qg+4qg}^{(hs)} = g^2 T \int_{\mathbf{p}} \frac{1}{p^2 + m_D^2} \sum_{\{Q\}} \left[\frac{2}{Q^2} - \frac{4q^2}{Q^4} \right]$$

$$\begin{aligned}
 & + 2m_D^2 g^2 T \int_{\mathbf{p}} \frac{1}{p^2 + m_D^2} \not{\sum}_{\{Q\}} \left[\frac{1}{Q^4} - \frac{2(3+d)}{d} \frac{q^2}{Q^6} + \frac{8}{d} \frac{q^4}{Q^8} \right] \\
 & - 4m_q^2 g^2 T \int_{\mathbf{p}} \frac{1}{p^2 + m_D^2} \not{\sum}_{\{Q\}} \left[\frac{3}{Q^4} - \frac{4q^2}{Q^6} - \frac{4}{Q^4} \mathcal{T}_Q - \frac{2}{Q^2} \left\langle \frac{1}{(Q \cdot Y)^2} \right\rangle_{\hat{\mathbf{y}}} \right]. \quad (4.21)
 \end{aligned}$$

Using the sum-integrals and integrals contained in Sec. (4.5) and (4.6), the hard-soft contribution becomes

$$\begin{aligned}
 \mathcal{F}_{3qg+4qg}^{(hs)} & = -\frac{1}{6} \alpha_s m_D T^3 (1 + 12 \hat{\mu}^2) - \frac{\alpha_s}{2\pi^2} m_q^2 m_D T + \left(\frac{\Lambda}{4\pi T} \right)^{2\epsilon} \left(\frac{\Lambda}{2m_D} \right)^{2\epsilon} m_D^3 T \\
 & \times \frac{\alpha_s}{24\pi^2} \left[\frac{1}{\epsilon} + 1 + 2\gamma_E + 4 \ln 2 - 14\zeta(3) \hat{\mu}^2 + 62\zeta(5) \hat{\mu}^4 + \mathcal{O}(\hat{\mu}^6) \right]. \quad (4.22)
 \end{aligned}$$

The ss contribution

As discussed earlier in Sec. (4.4) there is no soft-soft contribution from the diagrams in Fig. (4.1) since at least one of the loops is fermionic.

4.4.3 Thermodynamic potential

Now we can obtain the thermodynamic potential through two-loop order in HTL perturbation theory for which the contributions involving quark lines are computed here whereas the ghost and gluon contributions are computed in Refs. [172,173]. We also follow the variational mass prescription as discussed in Chapter 3 to determine the mass parameter m_D and m_q from respective gap equations. The details about the variational mass prescription will be discussed in Sec. 4.7.2.

Leading order thermodynamic potential

Using the expressions of \mathcal{F}_q with finite quark chemical potential in (4.16) and \mathcal{F}_g from Ref. [172,173], the total contributions from the one-loop diagrams including

all terms through order g^5 becomes

$$\begin{aligned}
 \Omega_{\text{one loop}} &= -d_A \frac{\pi^2 T^4}{45} \left\{ 1 + \frac{7 d_F}{4 d_A} \left(1 + \frac{120}{7} \hat{\mu}^2 + \frac{240}{7} \hat{\mu}^4 \right) \right. \\
 &\quad - \frac{15}{2} \left[1 + \epsilon \left(2 + 2 \frac{\zeta'(-1)}{\zeta(-1)} + 2 \ln \frac{\hat{\Lambda}}{2} \right) \right] \hat{m}_D^2 \\
 &\quad - 30 \frac{d_F}{d_A} \left[\left(1 + 12 \hat{\mu}^2 \right) + \epsilon \left(2 - 2 \ln 2 + 2 \frac{\zeta'(-1)}{\zeta(-1)} + 2 \ln \frac{\hat{\Lambda}}{2} + 24(\gamma_E + 2 \ln 2) \hat{\mu}^2 \right. \right. \\
 &\quad \left. \left. - 28 \zeta(3) \hat{\mu}^4 + \mathcal{O}(\hat{\mu}^6) \right) \right] \hat{m}_q^2 + 30 \left(\frac{\Lambda}{2m_D} \right)^{2\epsilon} \left[1 + \frac{8}{3} \epsilon \right] \hat{m}_D^3 \\
 &\quad \left. + \frac{45}{8} \left(\frac{1}{\epsilon} + 2 \ln \frac{\hat{\Lambda}}{2} - 7 + 2\gamma_E + \frac{2\pi^2}{3} \right) \hat{m}_D^4 - 60 \frac{d_F}{d_A} (\pi^2 - 6) \hat{m}_q^4 \right\}, \quad (4.23)
 \end{aligned}$$

where \hat{m}_D , \hat{m}_q , $\hat{\Lambda}$, and $\hat{\mu}$ are dimensionless variables:

$$\hat{m}_D = \frac{m_D}{2\pi T}, \quad (4.24)$$

$$\hat{m}_q = \frac{m_q}{2\pi T}, \quad (4.25)$$

$$\hat{\Lambda} = \frac{\Lambda}{2\pi T}, \quad (4.26)$$

$$\hat{\mu} = \frac{\mu}{2\pi T}. \quad (4.27)$$

Adding the counterterm in (4.3), we obtain the thermodynamic potential at leading order in the δ -expansion:

$$\begin{aligned}
 \Omega_{\text{LO}} &= -d_A \frac{\pi^2 T^4}{45} \left\{ 1 + \frac{7 d_F}{4 d_A} \left(1 + \frac{120}{7} \hat{\mu}^2 + \frac{240}{7} \hat{\mu}^4 \right) \right. \\
 &\quad - \frac{15}{2} \left[1 + \epsilon \left(2 + 2 \frac{\zeta'(-1)}{\zeta(-1)} + 2 \ln \frac{\hat{\Lambda}}{2} \right) \right] \hat{m}_D^2 \\
 &\quad - 30 \frac{d_F}{d_A} \left[\left(1 + 12 \hat{\mu}^2 \right) + \epsilon \left(2 - 2 \ln 2 + 2 \frac{\zeta'(-1)}{\zeta(-1)} + 2 \ln \frac{\hat{\Lambda}}{2} + 24(\gamma_E + 2 \ln 2) \hat{\mu}^2 \right. \right. \\
 &\quad \left. \left. - 28 \zeta(3) \hat{\mu}^4 + \mathcal{O}(\hat{\mu}^6) \right) \right] \hat{m}_q^2 + 30 \left(\frac{\Lambda}{2m_D} \right)^{2\epsilon} \left[1 + \frac{8}{3} \epsilon \right] \hat{m}_D^3 \\
 &\quad \left. + \frac{45}{8} \left(2 \ln \frac{\hat{\Lambda}}{2} - 7 + 2\gamma_E + \frac{2\pi^2}{3} \right) \hat{m}_D^4 - 60 \frac{d_F}{d_A} (\pi^2 - 6) \hat{m}_q^4 \right\}, \quad (4.28)
 \end{aligned}$$

where we have kept terms of $\mathcal{O}(\epsilon)$ since they will be needed for the two-loop renormalization.

Next-to-leading order thermodynamic potential

The complete expression for the next-to-leading order correction to the thermodynamic potential is the sum of the contributions from all two-loop diagrams, the quark and gluon counter-terms, and renormalization counterterms. Adding the contributions of the two-loop diagrams, $\mathcal{F}_{3qg+4qg}$, involving a quark line in (4.20) and (4.22) and the contributions of $\mathcal{F}_{3g+4g+gh}$ from Ref. [172, 173], one obtains

$$\begin{aligned}
 \Omega_{\text{two loop}} = & -d_A \frac{\pi^2 T^4 \alpha_s}{45 \pi} \left\{ -\frac{5}{4} \left[c_A + \frac{5}{2} s_F \left(1 + \frac{72}{5} \hat{\mu}^2 + \frac{144}{5} \hat{\mu}^4 \right) \right] \right. \\
 & + 15 (c_A + s_F (1 + 12 \hat{\mu}^2)) \hat{m}_D - \frac{55}{8} \left[\left(c_A - \frac{4}{11} s_F \left[1 + 6(4 - 3\zeta(3)) \hat{\mu}^2 \right. \right. \right. \\
 & \left. \left. \left. - 120(\zeta(3) - \zeta(5)) \hat{\mu}^4 + \mathcal{O}(\hat{\mu}^6) \right) \right] \left(\frac{1}{\epsilon} + 4 \ln \frac{\hat{\Lambda}}{2} \right) \right. \\
 & \left. - s_F (0.471 - 34.876 \hat{\mu}^2 - 21.021 \hat{\mu}^4 + \mathcal{O}(\hat{\mu}^6)) \right. \\
 & \left. - c_A \left(\frac{72}{11} \ln \hat{m}_D - 1.969 \right) \right] \hat{m}_D^2 - \frac{45}{2} s_F \left[(1 - 12 \hat{\mu}^2) \left(\frac{1}{\epsilon} + 4 \ln \frac{\hat{\Lambda}}{2} \right) \right. \\
 & \left. + 8.981 - 152.793 \hat{\mu}^2 + 115.826 \hat{\mu}^4 + \mathcal{O}(\hat{\mu}^6) \right] \hat{m}_q^2 \\
 & + 180 s_F \hat{m}_D \hat{m}_q^2 + \frac{165}{4} \left[\left(c_A - \frac{4}{11} s_F \right) \left(\frac{1}{\epsilon} + 4 \ln \frac{\hat{\Lambda}}{2} - 2 \ln \hat{m}_D \right) \right. \\
 & \left. + c_A \left(\frac{27}{11} + 2\gamma_E \right) - \frac{4}{11} s_F (1 + 2\gamma_E + 4 \ln 2 - 14\zeta(3)) \hat{\mu}^2 \right. \\
 & \left. + 62\zeta(5) \hat{\mu}^4 + \mathcal{O}(\hat{\mu}^6) \right] \hat{m}_D^3 \left. \right\}, \tag{4.29}
 \end{aligned}$$

where $c_A = N_c$ and $s_F = N_f/2$.

The HTL gluon counter-term is the same as obtained at zero chemical potential in Refs. [172, 173] and can be written as

$$\Omega_{\text{gct}} = -d_A \frac{\pi^2 T^4}{45} \left[\frac{15}{2} \hat{m}_D^2 - 45 \hat{m}_D^3 - \frac{45}{4} \left(\frac{1}{\epsilon} + 2 \ln \frac{\hat{\Lambda}}{2} - 7 + 2\gamma_E + \frac{2\pi^2}{3} \right) \hat{m}_D^4 \right]. \quad (4.30)$$

The HTL quark counterterm as given by (4.18) is

$$\Omega_{\text{qct}} = -d_F \frac{\pi^2 T^4}{45} \left[30(1 + 12 \hat{\mu}^2) \hat{m}_q^2 + 120(\pi^2 - 6) \hat{m}_q^4 \right]. \quad (4.31)$$

The ultraviolet divergences that remain after adding (4.29), (4.30), and (4.31) can be removed by renormalization of the vacuum energy density \mathcal{E}_0 and the HTL mass parameter m_D and m_q . The renormalization contributions [172, 173] at first order in δ are

$$\Delta\Omega = \Delta_1 \mathcal{E}_0 + \Delta_1 m_D^2 \frac{\partial}{\partial m_D^2} \Omega_{LO} + \Delta_1 m_q^2 \frac{\partial}{\partial m_q^2} \Omega_{LO}. \quad (4.32)$$

The counterterm $\Delta_1 \mathcal{E}_0$ at first order in δ will be same as the zero chemical potential counterterm

$$\Delta_1 \mathcal{E}_0 = -\frac{d_A}{64\pi^2 \epsilon} m_D^4. \quad (4.33)$$

The mass counterterms necessary at first order in δ are found to be

$$\begin{aligned} \Delta_1 \hat{m}_D^2 &= -\frac{\alpha_s}{3\pi\epsilon} \left[\frac{11}{4} c_A - s_F - s_F (1 + 6\hat{m}_D) \right. \\ &\quad \left. \times \left[(24 - 18\zeta(3)) \hat{\mu}^2 + 120(\zeta(5) - \zeta(3)) \hat{\mu}^4 + \mathcal{O}(\hat{\mu}^6) \right] \right] \hat{m}_D^2 \end{aligned} \quad (4.34)$$

and

$$\Delta_1 \hat{m}_q^2 = -\frac{\alpha_s}{3\pi\epsilon} \left[\frac{9 d_A}{8 c_A} \right] \frac{1 - 12 \hat{\mu}^2}{1 + 12 \hat{\mu}^2} \hat{m}_q^2. \quad (4.35)$$

Using the above counterterms, the complete contribution from the counterterms in (4.32) at first order in δ at finite chemical potential becomes

$$\begin{aligned}
 \Delta\Omega = & -d_A \frac{\pi^2 T^4}{45} \left\{ \frac{45}{4\epsilon} \hat{m}_D^4 + \frac{\alpha_s}{\pi} \left[\frac{55}{8} \left(c_A - \frac{4}{11} s_F \left[1 + (24 - 18\zeta(3)) \hat{\mu}^2 \right. \right. \right. \right. \\
 & + \left. \left. \left. 120(\zeta(5) - \zeta(3)) \hat{\mu}^4 + \mathcal{O}(\hat{\mu}^6) \right] \right) \left(\frac{1}{\epsilon} + 2 + 2 \frac{\zeta'(-1)}{\zeta(-1)} + 2 \ln \frac{\hat{\Lambda}}{2} \right) \hat{m}_D^2 \right. \\
 & - \frac{165}{4} \left(c_A - \frac{4}{11} s_F \right) \left(\frac{1}{\epsilon} + 2 + 2 \ln \frac{\hat{\Lambda}}{2} - 2 \ln \hat{m}_D \right) \hat{m}_D^3 \\
 & - \frac{165}{4} \frac{4}{11} s_F \left[(24 - 18\zeta(3)) \hat{\mu}^2 + 120(\zeta(5) - \zeta(3)) \hat{\mu}^4 + \mathcal{O}(\hat{\mu}^6) \right] \\
 & \times \left(2 \frac{\zeta'(-1)}{\zeta(-1)} + 2 \ln \hat{m}_D \right) \hat{m}_D^3 \\
 & + \frac{45}{2} s_F \frac{1 - 12 \hat{\mu}^2}{1 + 12 \hat{\mu}^2} \left(\frac{1 + 12 \hat{\mu}^2}{\epsilon} + 2 + 2 \ln \frac{\hat{\Lambda}}{2} - 2 \ln 2 + 2 \frac{\zeta'(-1)}{\zeta(-1)} \right. \\
 & \left. + 24(\gamma_E + 2 \ln 2) \hat{\mu}^2 - 28\zeta(3) \hat{\mu}^4 + \mathcal{O}(\hat{\mu}^6) \right) \hat{m}_q^2 \left. \right\}. \tag{4.36}
 \end{aligned}$$

Adding the contributions from the two-loop diagrams in (4.29), the HTL gluon and quark counterterms in (4.30) and (4.31), the contribution from vacuum and mass renormalizations in (4.36), and the leading-order thermodynamic potential in (4.28) we obtain the complete expression for the QCD thermodynamic potential at next-to-leading order in HTLpt:

$$\begin{aligned}
 \Omega_{\text{NLO}} = & -d_A \frac{\pi^2 T^4}{45} \left\{ 1 + \frac{7 d_F}{4 d_A} \left(1 + \frac{120}{7} \hat{\mu}^2 + \frac{240}{7} \hat{\mu}^4 \right) - 15 \hat{m}_D^3 \right. \\
 & - \frac{45}{4} \left(\log \frac{\hat{\Lambda}}{2} - \frac{7}{2} + \gamma_E + \frac{\pi^2}{3} \right) \hat{m}_D^4 + 60 \frac{d_F}{d_A} (\pi^2 - 6) \hat{m}_q^4 \\
 & + \frac{\alpha_s}{\pi} \left[-\frac{5}{4} \left(c_A + \frac{5 s_F}{2} \left(1 + \frac{72}{5} \hat{\mu}^2 + \frac{144}{5} \hat{\mu}^4 \right) \right) + 15 (c_A + s_F (1 + 12 \hat{\mu}^2)) \hat{m}_D \right. \\
 & - \frac{55}{4} \left\{ c_A \left(\log \frac{\hat{\Lambda}}{2} - \frac{36}{11} \log \hat{m}_D - 2.001 \right) - \frac{4}{11} s_F \left[\left(\log \frac{\hat{\Lambda}}{2} - 2.337 \right) \right. \right. \\
 & + (24 - 18 \zeta(3)) \left(\log \frac{\hat{\Lambda}}{2} - 15.662 \right) \hat{\mu}^2 + 120 (\zeta(5) - \zeta(3)) \\
 & \times \left. \left. \left(\log \frac{\hat{\Lambda}}{2} - 1.0811 \right) \hat{\mu}^4 + \mathcal{O}(\hat{\mu}^6) \right] \right\} \hat{m}_D^2 - 45 s_F \left\{ \log \frac{\hat{\Lambda}}{2} + 2.198 - 44.953 \hat{\mu}^2 \right. \\
 & - \left. \left(288 \ln \frac{\hat{\Lambda}}{2} + 19.836 \right) \hat{\mu}^4 + \mathcal{O}(\hat{\mu}^6) \right\} \hat{m}_q^2 + \frac{165}{2} \left\{ c_A \left(\log \frac{\hat{\Lambda}}{2} + \frac{5}{22} + \gamma_E \right) \right. \\
 & - \left. \frac{4}{11} s_F \left(\log \frac{\hat{\Lambda}}{2} - \frac{1}{2} + \gamma_E + 2 \ln 2 - 7 \zeta(3) \hat{\mu}^2 + 31 \zeta(5) \hat{\mu}^4 + \mathcal{O}(\hat{\mu}^6) \right) \right\} \hat{m}_D^3 \\
 & + 15 s_F \left(2 \frac{\zeta'(-1)}{\zeta(-1)} + 2 \ln \hat{m}_D \right) \left[(24 - 18 \zeta(3)) \hat{\mu}^2 \right. \\
 & \left. + 120 (\zeta(5) - \zeta(3)) \hat{\mu}^4 + \mathcal{O}(\hat{\mu}^6) \right] \hat{m}_D^3 + 180 s_F \hat{m}_D \hat{m}_q^2 \left. \right\}. \tag{4.37}
 \end{aligned}$$

4.5 The necessary Sum-Integrals

In the imaginary-time (Euclidean time) formalism for the field theory of a hot and dense medium, the 4-momentum $P = (P_0, \mathbf{p})$ is Euclidean with $P^2 = P_0^2 + \mathbf{p}^2$. The Euclidean energy P_0 has discrete values: $P_0 = 2n\pi T$ for bosons and $P_0 = (2n + 1)\pi T - i\mu$ for fermions, where n is an integer running from $-\infty$ to ∞ , μ is the quark chemical potential, and $T = 1/\beta$ is the temperature of the medium. Loop diagrams usually then involve sums over P_0 and integrals over \mathbf{p} . In dimensional regularization, the integral over spatial momentum is generalized to $d = 3 - 2\epsilon$ spatial

dimensions. The dimensionally regularized bosonic and fermionic sum-integrals are defined in Eq. (1.18). All other frequency sums that appear in this chapter can be evaluated using the contour integration technique as discussed in Chapter 2 and are listed below:

4.5.1 Simple one loop sum-integrals

The specific fermionic one-loop sum-integrals needed are

$$\sum_{\{P\}} \ln P^2 = \frac{7\pi^2}{360} T^4 \left(1 + \frac{120}{7} \hat{\mu}^2 + \frac{240}{7} \hat{\mu}^4 \right). \quad (4.38)$$

$$\begin{aligned} \sum_{\{P\}} \frac{1}{P^2} = & -\frac{T^2}{24} \left(\frac{\Lambda}{4\pi T} \right)^{2\epsilon} \left[1 + 12\hat{\mu}^2 + \epsilon \left(2 - 2\ln 2 + 2\frac{\zeta'(-1)}{\zeta(-1)} \right. \right. \\ & + \left. \left. 24(\gamma_E + 2\ln 2)\hat{\mu}^2 - 28\zeta(3)\hat{\mu}^4 + \mathcal{O}(\hat{\mu}^6) \right) \right. \\ & + \left. \epsilon^2 \left(4 + \frac{\pi^2}{4} - 4\ln 2 + 4(1 - \ln 2)\frac{\zeta'(-1)}{\zeta(-1)} - 2\ln^2 2 \right. \right. \\ & \left. \left. + 2\frac{\zeta''(-1)}{\zeta(-1)} + 94.5749\hat{\mu}^2 - 143.203\hat{\mu}^4 + \mathcal{O}(\hat{\mu}^6) \right) \right]. \quad (4.39) \end{aligned}$$

$$\begin{aligned} \sum_{\{P\}} \frac{1}{P^4} = & \frac{1}{(4\pi)^2} \left(\frac{\Lambda}{4\pi T} \right)^{2\epsilon} \left[\frac{1}{\epsilon} + 2\gamma_E + 4\ln 2 - 14\zeta(3)\hat{\mu}^2 \right. \\ & + \left. 62\zeta(5)\hat{\mu}^4 + \mathcal{O}(\hat{\mu}^6) + \epsilon \left(4(2\gamma_E + \ln 2)\ln 2 \right. \right. \\ & \left. \left. - 4\gamma_1 + \frac{\pi^2}{4} - 71.6013\hat{\mu}^2 + 356.329\hat{\mu}^4 + \mathcal{O}(\hat{\mu}^6) \right) \right]. \quad (4.40) \end{aligned}$$

$$\begin{aligned} \sum_{\{P\}} \frac{p^2}{P^4} = & -\frac{T^2}{16} \left(\frac{\Lambda}{4\pi T} \right)^{2\epsilon} \left[1 + 12\hat{\mu}^2 + \epsilon \left(\frac{4}{3} - 2\ln 2 + 2\frac{\zeta'(-1)}{\zeta(-1)} \right. \right. \\ & \left. \left. + 8(3\gamma_E + 6\ln 2 - 1)\hat{\mu}^2 - 28\zeta(3)\hat{\mu}^4 + \mathcal{O}(\hat{\mu}^6) \right) \right]. \quad (4.41) \end{aligned}$$

$$\begin{aligned} \sum_{\{P\}} \frac{p^2}{P^6} &= \frac{3}{4(4\pi)^2} \left(\frac{\Lambda}{4\pi T} \right)^{2\epsilon} \left[\frac{1}{\epsilon} + 2\gamma_E - \frac{2}{3} + 4 \ln 2 \right. \\ &\quad \left. - 14\zeta(3)\hat{\mu}^2 + 62\zeta(5)\hat{\mu}^4 + \mathcal{O}(\hat{\mu}^6) \right]. \end{aligned} \quad (4.42)$$

$$\begin{aligned} \sum_{\{P\}} \frac{p^4}{P^6} &= -\frac{5T^2}{64} \left(\frac{\Lambda}{4\pi T} \right)^{2\epsilon} \left[1 + 12\hat{\mu}^2 + \epsilon \left(\frac{14}{15} - 2 \ln 2 + 2 \frac{\zeta'(-1)}{\zeta(-1)} \right) \right. \\ &\quad \left. + 8 \left(-\frac{8}{5} + 3\gamma_E + 6 \ln 2 \right) \hat{\mu}^2 - 28 \zeta(3) \hat{\mu}^4 + \mathcal{O}(\hat{\mu}^6) \right]. \end{aligned} \quad (4.43)$$

$$\begin{aligned} \sum_{\{P\}} \frac{p^4}{P^8} &= \frac{1}{(4\pi)^2} \left(\frac{\Lambda}{4\pi T} \right)^{2\epsilon} \frac{5}{8} \left[\frac{1}{\epsilon} + \left(2\gamma_E - \frac{16}{15} + 4 \ln 2 - 14 \zeta(3) \hat{\mu}^2 \right. \right. \\ &\quad \left. \left. + 62 \zeta(5) \hat{\mu}^4 + \mathcal{O}(\hat{\mu}^6) \right) \right]. \end{aligned} \quad (4.44)$$

$$\begin{aligned} \sum_{\{P\}} \frac{1}{p^2 P^2} &= \frac{1}{(4\pi)^2} \left(\frac{\Lambda}{4\pi T} \right)^{2\epsilon} 2 \left[\frac{1}{\epsilon} + \left(2 + 2\gamma_E + 4 \ln 2 - 14 \zeta(3) \hat{\mu}^2 \right. \right. \\ &\quad \left. \left. + 62 \zeta(5) \hat{\mu}^4 + \mathcal{O}(\hat{\mu}^6) \right) + \epsilon \left(4 + 8 \ln 2 + 4 \ln^2 2 + 4\gamma_E \right. \right. \\ &\quad \left. \left. + 8\gamma_E \ln 2 + \frac{\pi^2}{4} - 4\gamma_1 - 105.259 \hat{\mu}^2 + 484.908 \hat{\mu}^4 + \mathcal{O}(\hat{\mu}^6) \right) \right]. \end{aligned} \quad (4.45)$$

where γ_1 , appearing in Eqs. (4.40) and (4.45), is the first Stieltjes gamma constant defined by the equation

$$\zeta(1+z) = \frac{1}{z} + \gamma_E - \gamma_1 z + \mathcal{O}(z^2). \quad (4.46)$$

and the numerical value of $\gamma_1 \approx -0.0728158$.

4.5.2 HTL one loop sum-integrals

We also need some more difficult one-loop sum-integrals that involve the HTL function defined in (4.8). The specific fermionic sum-integrals needed are

$$\sum_{\{P\}} \frac{1}{P^4} \mathcal{T}_P = \frac{1}{(4\pi)^2} \left(\frac{\Lambda}{4\pi T} \right)^{2\epsilon} \frac{1}{2} \left[\frac{1}{\epsilon} + \left(1 + 2\gamma_E + 4 \ln 2 - 14 \zeta(3) \hat{\mu}^2 \right. \right. \\ \left. \left. + 62 \zeta(5) \hat{\mu}^4 + \mathcal{O}(\hat{\mu}^6) \right) \right]. \quad (4.47)$$

$$\sum_{\{P\}} \frac{1}{p^2 P^2} \mathcal{T}_P = \frac{2}{(4\pi)^2} \left(\frac{\Lambda}{4\pi T} \right)^{2\epsilon} \left[\frac{\ln 2}{\epsilon} + \frac{\pi^2}{6} + 2\gamma_E \ln 2 \right. \\ \left. + \ln 2 \left(5 \ln 2 - 14 \zeta(3) \hat{\mu}^2 + 62 \zeta(5) \hat{\mu}^4 + \mathcal{O}(\hat{\mu}^6) \right) \right. \\ \left. + \epsilon \left(17.5137 - 85.398 \hat{\mu}^2 + 383.629 \hat{\mu}^4 + \mathcal{O}(\hat{\mu}^6) \right) \right]. \quad (4.48)$$

$$\sum_{\{P\}} \frac{1}{P^2 P_0^2} \mathcal{T}_P = \frac{1}{(4\pi)^2} \left(\frac{\Lambda}{4\pi T} \right)^{2\epsilon} \left[\frac{1}{\epsilon^2} + \frac{2}{\epsilon} \left(\gamma_E + 2 \ln 2 - 7 \zeta(3) \hat{\mu}^2 \right. \right. \\ \left. \left. + 31 \zeta(5) \hat{\mu}^4 + \mathcal{O}(\hat{\mu}^6) \right) + \frac{\pi^2}{4} + 4 \ln^2 2 \right. \\ \left. + 8\gamma_E \ln 2 - 4\gamma_1 - 71.601 \hat{\mu}^2 + 356.329 \hat{\mu}^4 + \mathcal{O}(\hat{\mu}^6) \right]. \quad (4.49)$$

$$\sum_{\{P\}} \frac{1}{p^2 P_0^2} (\mathcal{T}_P)^2 = \frac{4}{(4\pi)^2} \left(\frac{\Lambda}{4\pi T} \right)^{2\epsilon} \ln 2 \left[\frac{1}{\epsilon} + (2\gamma_E + 5 \ln 2) - 14 \zeta(3) \hat{\mu}^2 \right. \\ \left. + 62 \zeta(5) \hat{\mu}^4 + \mathcal{O}(\hat{\mu}^6) \right]. \quad (4.50)$$

$$\sum_{\{P\}} \frac{1}{P^2} \left\langle \frac{1}{(P \cdot Y)^2} \right\rangle_{\hat{\mathbf{y}}} = -\frac{1}{(4\pi)^2} \left(\frac{\Lambda}{4\pi T} \right)^{2\epsilon} \left[\frac{1}{\epsilon} - 1 + 2\gamma_E + 4 \ln 2 - 14 \zeta(3) \hat{\mu}^2 \right. \\ \left. + 62 \zeta(5) \hat{\mu}^4 + \mathcal{O}(\hat{\mu}^6) \right]. \quad (4.51)$$

4.5.3 Simple two loop sum-integrals

$$\sum_{\{PQ\}} \frac{1}{P^2 Q^2 R^2} = \frac{T^2}{(4\pi)^2} \left(\frac{\Lambda}{4\pi T} \right)^{4\epsilon} \left[\frac{\hat{\mu}^2}{\epsilon} + 2(4 \ln 2 + 2\gamma_E + 1) \hat{\mu}^2 - \frac{28}{3} \zeta(3) \hat{\mu}^4 + \mathcal{O}(\hat{\mu}^6) \right]. \quad (4.52)$$

$$\begin{aligned} \sum_{\{PQ\}} \frac{1}{P^2 Q^2 r^2} = & -\frac{T^2}{(4\pi)^2} \left(\frac{\Lambda}{4\pi T} \right)^{4\epsilon} \frac{1}{6} \left[\frac{1}{\epsilon} (1 + 12\hat{\mu}^2) + 4 - 2 \ln 2 + 4 \frac{\zeta'(-1)}{\zeta(-1)} \right. \\ & \left. + 48(1 + \gamma_E + \ln 2) \hat{\mu}^2 - 76\zeta(3) \hat{\mu}^4 + \mathcal{O}(\hat{\mu}^6) \right]. \quad (4.53) \end{aligned}$$

$$\begin{aligned} \sum_{\{PQ\}} \frac{p^2}{P^2 Q^2 r^4} = & \frac{T^2}{(4\pi)^2} \left(\frac{\Lambda}{4\pi T} \right)^{4\epsilon} \left(-\frac{1}{12} \right) \left[\frac{1}{\epsilon} (1 + 12\hat{\mu}^2) + \frac{11}{3} + 2\gamma_E \right. \\ & - 2 \ln 2 + 2 \frac{\zeta'(-1)}{\zeta(-1)} + 4(7 + 12\gamma_E + 12 \ln 2 - 3\zeta(3)) \hat{\mu}^2 \\ & \left. - 4(27\zeta(3) - 20\zeta(5)) \hat{\mu}^4 + \mathcal{O}(\hat{\mu}^6) \right]. \quad (4.54) \end{aligned}$$

$$\begin{aligned} \sum_{\{PQ\}} \frac{P \cdot Q}{P^2 Q^2 r^4} = & -\frac{T^2}{(4\pi)^2} \left(\frac{\Lambda}{4\pi T} \right)^{4\epsilon} \frac{1}{36} \left[1 - 6\gamma_E + 6 \frac{\zeta'(-1)}{\zeta(-1)} + 24 \{2 + 3\zeta(3)\} \hat{\mu}^2 \right. \\ & \left. + 48(7\zeta(3) - 10\zeta(5)) \hat{\mu}^4 + \mathcal{O}(\hat{\mu}^6) \right]. \quad (4.55) \end{aligned}$$

$$\begin{aligned} \sum_{\{PQ\}} \frac{p^2}{r^2 P^2 Q^2 R^2} = & -\frac{T^2}{(4\pi)^2} \left(\frac{\Lambda}{4\pi T} \right)^{4\epsilon} \frac{1}{72} \left[\frac{1}{\epsilon} (1 - 12(1 - 3\zeta(3)) \hat{\mu}^2 \right. \\ & + 240(\zeta(3) - \zeta(5)) \hat{\mu}^4 + \mathcal{O}(\hat{\mu}^6) \\ & \left. - (7.001 - 108.218 \hat{\mu}^2 - 304.034 \hat{\mu}^4 + \mathcal{O}(\hat{\mu}^6)) \right]. \quad (4.56) \end{aligned}$$

$$\begin{aligned}
 \sum_{\{PQ\}} \frac{p^2}{q^2 P^2 Q^2 R^2} &= \frac{T^2}{(4\pi)^2} \left(\frac{\Lambda}{4\pi T} \right)^{4\epsilon} \frac{5}{72} \left[\frac{1}{\epsilon} \left(1 - \frac{12}{5} (1 + 7\zeta(3)) \hat{\mu}^2 \right. \right. \\
 &\quad \left. \left. - \frac{24}{5} (14\zeta(3) - 31\zeta(5)) \hat{\mu}^4 + \mathcal{O}(\hat{\mu}^6) \right) \right. \\
 &\quad \left. + (9.5424 - 185.706 \hat{\mu}^2 + 916.268 \hat{\mu}^4 + \mathcal{O}(\hat{\mu}^6)) \right]. \quad (4.57)
 \end{aligned}$$

$$\begin{aligned}
 \sum_{\{PQ\}} \frac{r^2}{q^2 P^2 Q^2 R^2} &= -\frac{T^2}{(4\pi)^2} \left(\frac{\Lambda}{4\pi T} \right)^{4\epsilon} \frac{1}{18} \left[\frac{1}{\epsilon} \left(1 + 3(-2 + 7\zeta(3)) \hat{\mu}^2 \right. \right. \\
 &\quad \left. \left. + 6(14\zeta(3) - 31\zeta(5)) \hat{\mu}^4 + \mathcal{O}(\hat{\mu}^6) \right) \right. \\
 &\quad \left. + (8.143 + 96.935 \hat{\mu}^2 - 974.609 \hat{\mu}^4 + \mathcal{O}(\hat{\mu}^6)) \right]. \quad (4.58)
 \end{aligned}$$

The generalized two loop sum-integrals can be written from [173] as

$$\begin{aligned}
 \sum_{\{PQ\}} |F(P)G(Q)H(R)| &= \int_{PQ} F(P)G(Q)H(R) \\
 &- \int_{p_0, \mathbf{p}} \epsilon(p_0) n_F(|p_0|) 2 \operatorname{Im} F(-ip_0 + \epsilon, \mathbf{p}) \operatorname{Re} \int_Q G(Q)H(R) \Big|_{P_0 = -ip_0 + \epsilon} \\
 &- \int_{p_0, \mathbf{p}} \epsilon(p_0) n_F(|p_0|) 2 \operatorname{Im} G(-ip_0 + \epsilon, \mathbf{p}) \operatorname{Re} \int_Q H(Q)F(R) \Big|_{P_0 = -ip_0 + \epsilon} \\
 &+ \int_{p_0, \mathbf{p}} \epsilon(p_0) n_B(|p_0|) 2 \operatorname{Im} H(-ip_0 + \epsilon, \mathbf{p}) \operatorname{Re} \int_Q F(Q)G(R) \Big|_{P_0 = -ip_0 + \epsilon} \\
 &+ \int_{p_0, \mathbf{p}} \epsilon(p_0) n_F(|p_0|) 2 \operatorname{Im} F(-ip_0 + \epsilon, \mathbf{p}) \int_{q_0, \mathbf{q}} \epsilon(q_0) n_F(|q_0|) 2 \operatorname{Im} G(-iq_0 + \epsilon, \mathbf{q}) \operatorname{Re} H(R) \Big|_{R_0 = i(p_0 + q_0) + \epsilon} \\
 &- \int_{p_0, \mathbf{p}} \epsilon(p_0) n_F(|p_0|) 2 \operatorname{Im} G(-ip_0 + \epsilon, \mathbf{p}) \int_{q_0, \mathbf{q}} \epsilon(q_0) n_B(|q_0|) 2 \operatorname{Im} H(-iq_0 + \epsilon, \mathbf{q}) \operatorname{Re} F(R) \Big|_{R_0 = i(p_0 + q_0) + \epsilon} \\
 &- \int_{p_0, \mathbf{p}} \epsilon(p_0) n_B(|p_0|) 2 \operatorname{Im} H(-ip_0 + \epsilon, \mathbf{p}) \int_{q_0, \mathbf{q}} \epsilon(q_0) n_F(|q_0|) 2 \operatorname{Im} F(-iq_0 + \epsilon, \mathbf{q}) \operatorname{Re} G(R) \Big|_{R_0 = i(p_0 + q_0) + \epsilon}.
 \end{aligned} \quad (4.59)$$

After applying Eq. (4.59) and using the delta function to calculate the P_0 and Q_0 integrations, the sum-integral (4.56) reduces to

$$\sum_{\{PQ\}} \frac{1}{P^2 Q^2 R^2} = \int_{\mathbf{p}\mathbf{q}} \frac{n_F^-(p) - n_F^+(p)}{2p} \frac{n_F^-(q) - n_F^+(q)}{2q} \frac{2p q}{\Delta(p, q, r)}, \quad (4.60)$$

where

$$n_F^\pm(p) = \frac{1}{e^{\beta(p \pm \mu)} + 1} \quad (4.61)$$

and

$$\Delta(p, q, r) = p^4 + q^4 + r^4 - 2(p^2 q^2 + q^2 r^2 + p^2 r^2) = -4p^2 q^2 (1 - x^2), \quad (4.62)$$

and using the result of Eq. (4.92), we get sum-integral (4.52) and agree with [13].

After applying Eq. (4.59), the sum-integral (4.53) reduces to

$$\sum_{\{PQ\}} \frac{1}{P^2 Q^2 r^2} = -2 \int_{\mathbf{p}} \frac{n_F(p)}{2p} \int_{\mathbf{Q}} \frac{1}{Q^2 r^2} + \int_{\mathbf{p}\mathbf{q}} \frac{n_F(p) n_F(q)}{4pq} \frac{1}{r^2}, \quad (4.63)$$

where $n_F(p) = n_F^-(p) + n_F^+(p)$. Now using the result of 4-dimensional integrals from [173] and applying Eq. (4.85) and Eq. (4.87), we can calculate sum-integral Eq. (4.53). The sum-integrals (4.54) can be calculated in same way:

$$\sum_{\{PQ\}} \frac{p^2}{P^2 Q^2 r^4} = -2 \int_{\mathbf{p}} \frac{n_F(p)}{2p} \int_{\mathbf{Q}} \frac{p^2}{Q^2 r^4} + \int_{\mathbf{p}\mathbf{q}} \frac{n_F(p) n_F(q)}{4pq} \frac{p^2}{r^4}. \quad (4.64)$$

The sum-integral (4.55) can be written as

$$\sum_{\{PQ\}} \frac{P \cdot Q}{P^2 Q^2 r^4} = \sum_{\{PQ\}} \frac{P_0 Q_0}{P^2 Q^2 r^4} + \frac{1}{2} \sum_{\{PQ\}} \frac{1}{P^2 Q^2 r^2} - \sum_{\{PQ\}} \frac{p^2}{P^2 Q^2 r^4} \quad (4.65)$$

Using Eq. (4.59) and after doing P_0 and Q_0 integrations, first sum-integral above reduces to

$$\sum_{\{PQ\}} \frac{P_0 Q_0}{P^2 Q^2 r^4} = \int_{\mathbf{pq}} \frac{n_F^-(p) - n_F^+(p)}{2p} \frac{n_F^-(q) - n_F^+(q)}{2q} \frac{pq}{r^4}, \quad (4.66)$$

and the result is given in Eq. (4.91). The second term and third terms sum-integrals above are linear combinations of Eq. (4.53) and Eq. (4.54). Adding all of them, we get required sum-integral.

Similarly after applying Eq. (4.59), the sum-integral (4.56) reduces to

$$\begin{aligned} \sum_{\{PQ\}} \frac{p^2}{r^2 P^2 Q^2 R^2} &= \int_{\mathbf{p}} \frac{n_B(p)}{p} \int_Q \frac{r^2}{p^2 Q^2 R^2} \Big|_{P_0=-ip} \\ &- \int_{\mathbf{p}} \frac{n_F(p)}{2p} \int_Q \frac{1}{Q^2 R^2} \left(\frac{q^2}{r^2} + \frac{p^2}{q^2} \right) \Big|_{P_0=-ip} \\ &+ \int_{\mathbf{pq}} \frac{n_F(p)n_F(q)}{4pq} \frac{q^2}{r^2} \frac{r^2 - p^2 - q^2}{\Delta(p, q, r)} \\ &- \int_{\mathbf{pq}} \frac{n_F(p)n_B(q)}{4pq} \frac{p^2 + r^2}{q^2} \frac{r^2 - p^2 - q^2}{\Delta(p, q, r)}. \end{aligned} \quad (4.67)$$

So

$$\left\langle \frac{p^2 + r^2}{q^2} \frac{r^2 - p^2 - q^2}{\Delta(p, q, r)} \right\rangle_{\hat{p}\hat{q}} = \frac{1}{2q^2 \epsilon}, \quad (4.68)$$

and

$$\begin{aligned} \left\langle \frac{q^2}{r^2} \frac{r^2 - p^2 - q^2}{\Delta(p, q, r)} \right\rangle_{\hat{p}\hat{q}} &= \left\langle \frac{q^2}{\Delta(p, q, r)} \right\rangle_x - \left\langle \frac{q^2(p^2 + q^2)}{\Delta(p, q, r)} \right\rangle_x, \\ &= \frac{1 - 2\epsilon}{8\epsilon} \frac{1}{p^2} - \frac{1}{2\epsilon} \left\langle \frac{q^2}{r^4} \right\rangle_x - \frac{1 - 2\epsilon}{8\epsilon} \frac{1}{p^2} \\ &= -\frac{1}{2\epsilon} \left\langle \frac{q^2}{r^4} \right\rangle_x. \end{aligned} \quad (4.69)$$

Using the above angular integration, Eq. (4.67) becomes

$$\begin{aligned}
 \sum_{\{PQ\}} \frac{p^2}{r^2 P^2 Q^2 R^2} &= \int_{\mathbf{p}} \frac{n_B(p)}{p} \int_Q \frac{r^2}{p^2 Q^2 R^2} \Big|_{P_0=-ip} \\
 &- \int_{\mathbf{p}} \frac{n_F(p)}{2p} \int_Q \frac{1}{Q^2 R^2} \left(\frac{q^2}{r^2} + \frac{p^2}{q^2} \right) \Big|_{P_0=-ip} \\
 &- \frac{1}{2\epsilon} \int_{\mathbf{pq}} \frac{n_F(p)n_F(q)}{4pq} \frac{p^2}{r^4} - \frac{1}{2\epsilon} \int_{\mathbf{pq}} \frac{n_F(p)n_B(q)}{4pq} \frac{1}{q^2}. \quad (4.70)
 \end{aligned}$$

Using the 4-dimensional integrals from [173] and Eqs. (4.84), (4.85), (4.86) and (4.88), we obtain the sum-integral (4.56).

Similarly after applying Eq. (4.59), the sum-integral (4.57) reduces to

$$\begin{aligned}
 \sum_{\{PQ\}} \frac{p^2}{q^2 P^2 Q^2 R^2} &= \int_{\mathbf{p}} \frac{n_B(p)}{p} \int_Q \frac{q^2}{Q^2 r^2 R^2} \Big|_{P_0=-ip} \\
 &- \int_{\mathbf{p}} \frac{n_F(p)}{2p} \int_Q \frac{1}{Q^2 R^2} \left(\frac{p^2}{q^2} + \frac{q^2}{p^2} \right) \Big|_{P_0=-ip} \\
 &+ \int_{\mathbf{pq}} \frac{n_F(p)n_F(q)}{4pq} \frac{p^2}{q^2} \frac{r^2 - p^2 - q^2}{\Delta(p, q, r)} \\
 &- \int_{\mathbf{pq}} \frac{n_F(p)n_B(q)}{4pq} \left(\frac{p^2}{r^2} + \frac{r^2}{p^2} \right) \frac{r^2 - p^2 - q^2}{\Delta(p, q, r)}. \quad (4.71)
 \end{aligned}$$

Now

$$\left\langle \frac{p^2}{q^2} \frac{r^2 - p^2 - q^2}{\Delta(p, q, r)} \right\rangle_{\hat{p}\hat{q}} = 0, \quad (4.72)$$

and

$$\left\langle \left(\frac{p^2}{r^2} + \frac{r^2}{p^2} \right) \frac{r^2 - p^2 - q^2}{\Delta(p, q, r)} \right\rangle_{\hat{p}\hat{q}} = \frac{1}{2\epsilon} \frac{1}{p^2} - \frac{1}{2\epsilon} \left\langle \frac{p^2}{r^4} \right\rangle_x. \quad (4.73)$$

Using the above angular average, we find

$$\begin{aligned}
 \sum_{\{PQ\}} \frac{p^2}{q^2 P^2 Q^2 R^2} &= \int_{\mathbf{p}} \frac{n_B(p)}{p} \int_Q \frac{q^2}{Q^2 r^2 R^2} \Big|_{P_0=-ip} \\
 &- \int_{\mathbf{p}} \frac{n_F(p)}{2p} \int_Q \frac{1}{Q^2 R^2} \left(\frac{p^2}{q^2} + \frac{q^2}{p^2} \right) \Big|_{P_0=-ip} \\
 &- \frac{1}{2\epsilon} \int_{\mathbf{p}\mathbf{q}} \frac{n_F(p)n_B(q)}{2pq} \frac{1}{p^2} + \frac{1}{2\epsilon} \int_{\mathbf{p}\mathbf{q}} \frac{n_F(p)n_B(q)}{2pq} \frac{p^2}{r^4}. \quad (4.74)
 \end{aligned}$$

Using the 4-dimensional integrals from [173] and Eqs. (4.84), (4.85), (4.86) and (4.89), we obtain the sum-integral (4.57).

Similarly after applying Eq. (4.59), the sum-integral (4.58) reduces to

$$\begin{aligned}
 \sum_{\{PQ\}} \frac{r^2}{p^2 P^2 Q^2 R^2} &= \int_{\mathbf{p}} \frac{n_B(p)}{p} \int_Q \frac{p^2}{Q^2 r^2 R^2} \Big|_{P_0=-ip} \\
 &- \int_{\mathbf{p}} \frac{n_F(p)}{2p} \int_Q \frac{1}{Q^2 R^2} \left(\frac{r^2}{p^2} + \frac{r^2}{q^2} \right) \Big|_{P_0=-ip} \\
 &+ \int_{\mathbf{p}\mathbf{q}} \frac{n_F(p)n_F(q)}{4pq} \frac{r^2}{p^2} \frac{r^2 - p^2 - q^2}{\Delta(p, q, r)} \\
 &- \int_{\mathbf{p}\mathbf{q}} \frac{n_F(p)n_B(q)}{4pq} \left(\frac{q^2}{r^2} + \frac{q^2}{p^2} \right) \frac{r^2 - p^2 - q^2}{\Delta(p, q, r)}. \quad (4.75)
 \end{aligned}$$

Now

$$\left\langle \frac{r^2}{p^2} \frac{r^2 - p^2 - q^2}{\Delta(p, q, r)} \right\rangle_{\hat{p}\hat{q}} = \frac{1}{2p^2\epsilon}, \quad (4.76)$$

and

$$\left\langle \left(\frac{q^2}{r^2} + \frac{q^2}{p^2} \right) \frac{r^2 - p^2 - q^2}{\Delta(p, q, r)} \right\rangle_{\hat{p}\hat{q}} = -\frac{1}{2\epsilon} \left\langle \frac{q^2}{r^4} \right\rangle_x. \quad (4.77)$$

Using the above angular average, we have

$$\begin{aligned}
 \not\int_{\{PQ\}} \frac{p^2}{q^2 P^2 Q^2 R^2} &= \int_{\mathbf{p}} \frac{n_B(p)}{p} \int_Q \frac{q^2}{Q^2 r^2 R^2} \Big|_{P_0=-ip} \\
 &- \int_{\mathbf{p}} \frac{n_F(p)}{2p} \int_Q \frac{1}{Q^2 R^2} \left(\frac{p^2}{q^2} + \frac{q^2}{p^2} \right) \Big|_{P_0=-ip} \\
 &+ \frac{1}{2\epsilon} \int_{\mathbf{p}\mathbf{q}} \frac{n_F(p)n_B(q)}{2pq} \frac{1}{p^2} + \frac{1}{2\epsilon} \int_{\mathbf{p}\mathbf{q}} \frac{n_F(p)n_B(q)}{2pq} \frac{q^2}{r^4}. \quad (4.78)
 \end{aligned}$$

Using the 4-dimensional integrals from [173] and Eqs. (4.84), (4.85), (4.86) and (4.90), we obtain the sum-integral (4.57).

4.5.4 HTL two loop sum-integrals

$$\begin{aligned}
 \not\int_{\{PQ\}} \frac{1}{P^2 Q^2 r^2} \mathcal{T}_R &= -\frac{T^2}{(4\pi)^2} \left(\frac{\Lambda}{4\pi T} \right)^{4\epsilon} \frac{1}{48} \left[\frac{1}{\epsilon^2} \right. \\
 &+ \left(2 + 12(1 + 8 \hat{\mu}^2) \ln 2 + 4 \frac{\zeta'(-1)}{\zeta(-1)} \right) \frac{1}{\epsilon} \\
 &\left. + (136.362 + 460.23 \hat{\mu}^2 - 273.046 \hat{\mu}^4 + \mathcal{O}(\hat{\mu}^6)) \right]. \quad (4.79)
 \end{aligned}$$

$$\begin{aligned}
 \not\int_{\{PQ\}} \frac{p^2}{P^2 Q^2 r^4} \mathcal{T}_R &= -\frac{1}{576} \frac{T^2}{(4\pi)^2} \left(\frac{\Lambda}{4\pi T} \right)^{4\epsilon} \left[\frac{1}{\epsilon^2} + \left(\frac{26}{3} + 4(13 + 144 \hat{\mu}^2) \ln 2 + 4 \frac{\zeta'(-1)}{\zeta(-1)} \right) \frac{1}{\epsilon} \right. \\
 &\left. + (446.397 + 2717.86 \hat{\mu}^2 - 1735.61 \hat{\mu}^4 + \mathcal{O}(\hat{\mu}^6)) \right]. \quad (4.80)
 \end{aligned}$$

$$\begin{aligned}
 \not\int_{\{PQ\}} \frac{P \cdot Q}{P^2 Q^2 r^4} \mathcal{T}_R &= \frac{T^2}{(4\pi)^2} \left(\frac{\Lambda}{4\pi T} \right)^{4\epsilon} \left(-\frac{1}{96} \right) \left[\frac{1}{\epsilon^2} + \left(4 \ln 2 + 4 \frac{\zeta'(-1)}{\zeta(-1)} \right) \frac{1}{\epsilon} \right. \\
 &\left. + (69.1737 + 118.244 \hat{\mu}^2 + 136.688 \hat{\mu}^4 + \mathcal{O}(\hat{\mu}^6)) \right]. \quad (4.81)
 \end{aligned}$$

$$\begin{aligned}
 \sum_{\{PQ\}} \frac{r^2 - p^2}{P^2 q^2 Q_0^2 R^2} \mathcal{T}_Q &= -\frac{T^2}{(4\pi)^2} \left(\frac{\Lambda}{4\pi T} \right)^{4\epsilon} \frac{1}{8} \left[\frac{1}{\epsilon^2} (1 + 4 \hat{\mu}^2) \right. \\
 &+ \frac{1}{\epsilon} \left(2 + 2\gamma_E + \frac{10}{3} \ln 2 + 2 \frac{\zeta'(-1)}{\zeta(-1)} \right) \\
 &+ 2 (8\gamma_E + 16 \ln 2 - 7\zeta(3)) \hat{\mu}^2 \\
 &- \frac{2}{3} (98\zeta(3) - 93\zeta(5)) \hat{\mu}^4 + \mathcal{O}(\hat{\mu}^6) \left. \right] \\
 &+ 46.8757 - 41.1192 \hat{\mu}^2 + 64.0841 \hat{\mu}^4 + \mathcal{O}(\hat{\mu}^6) \left. \right]. \quad (4.82)
 \end{aligned}$$

4.6 Integrals

4.6.1 Three dimensional integrals

We require one integral that does not involve the Bose-Einstein distribution function. The momentum scale in these integrals is set by the mass $m = m_D$. The one-loop integral is

$$\int_{\mathbf{p}} \frac{1}{p^2 + m^2} = -\frac{m}{4\pi} \left(\frac{\Lambda}{2m} \right)^{2\epsilon} [1 + 2\epsilon]. \quad (4.83)$$

4.6.2 Thermal Integrals

$$\begin{aligned}
 \frac{\Lambda^{2\epsilon}}{(4\pi)^2} \int_{\mathbf{p}} \frac{n_B(p)}{p} p^{-2\epsilon} &= \frac{T^2}{(4\pi)^2} \left(\frac{\Lambda}{4\pi T} \right)^{4\epsilon} \left(\frac{1}{12} \right) \left[1 + \epsilon \left(2 - 2 \ln 2 + 4 \frac{\zeta'(-1)}{\zeta(-1)} \right) \right. \\
 &+ 2\epsilon^2 \left(\frac{7\pi^2}{8} - 2 + \ln^2 2 - 2 \ln 2 + 4(1 + \ln 2) \right. \\
 &\left. \left. + 4(1 + \ln 2) \frac{\zeta'(-1)}{\zeta(-1)} + 4 \frac{\zeta''(-1)}{\zeta(-1)} \right) \right]. \quad (4.84)
 \end{aligned}$$

$$\begin{aligned}
 \frac{\Lambda^{2\epsilon}}{(4\pi)^2} \int_{\mathbf{p}} \frac{n_F(p)}{2p} p^{-2\epsilon} &= \frac{T^2}{(4\pi)^2} \left(\frac{\Lambda}{4\pi T} \right)^{4\epsilon} \left(\frac{1}{24} \right) \left[(1 + 12\hat{\mu}^2) \right. \\
 &+ \epsilon \left\{ 2 - 2 \ln 2 + 4 \frac{\zeta'(-1)}{\zeta(-1)} + 24(2\gamma_E + 5 \ln 2 - 1) \hat{\mu}^2 \right. \\
 &\left. \left. - 56\zeta(3) \hat{\mu}^4 + \mathcal{O}(\hat{\mu}^6) \right\} \right]. \quad (4.85)
 \end{aligned}$$

$$\begin{aligned}
 \frac{\Lambda^{2\epsilon}}{(4\pi)^2} \int_{\mathbf{p}} \frac{n_F(p)}{2p} \frac{1}{p^2} p^{-2\epsilon} &= -\frac{T^2}{(4\pi)^2} \left(\frac{\Lambda}{4\pi T} \right)^{4\epsilon} \left[\frac{1}{\epsilon} + 2 + 2\gamma_E + 10 \ln 2 \right. \\
 &\left. - 28\zeta(3) \hat{\mu}^2 + 124\zeta(5) \hat{\mu}^4 + \mathcal{O}(\hat{\mu}^6) \right]. \quad (4.86)
 \end{aligned}$$

$$\int_{\mathbf{p}\mathbf{q}} \frac{n_F(p)n_F(q)}{4pq} \frac{1}{r^2} = \frac{T^2}{(4\pi)^2} \left[\frac{1}{3}(1 - \ln 2) + 4(2 \ln 2 - 1)\hat{\mu}^2 + \frac{10}{3}\zeta(3) \hat{\mu}^4 + \mathcal{O}(\hat{\mu}^6) \right]. \quad (4.87)$$

$$\begin{aligned}
 \int_{\mathbf{p}\mathbf{q}} \frac{n_F(p)n_F(q)}{4pq} \frac{p^2}{r^4} &= \frac{T^2}{(4\pi)^2} \left(-\frac{1}{36} \right) \left[\left(5 + 6\gamma_E + 6 \ln 2 - 6 \frac{\zeta'(-1)}{\zeta(-1)} \right. \right. \\
 &- 12(12 \ln 2 - 13 + 3\zeta(3))\hat{\mu}^2 \\
 &+ 12(20\zeta(5) - 13\zeta(3))\hat{\mu}^4 + \mathcal{O}(\hat{\mu}^6) \left. \right) \\
 &\left. + \epsilon(3.0747 + 31.2624 \hat{\mu}^2 + 262.387 \hat{\mu}^4 + \mathcal{O}(\hat{\mu}^6)) \right]. \quad (4.88)
 \end{aligned}$$

$$\begin{aligned}
 \int_{\mathbf{p}\mathbf{q}} \frac{n_B(p)n_F(q)}{2pq} \frac{p^2}{r^4} &= -\frac{1}{36} \frac{T^2}{(4\pi)^2} \left[\left\{ 7 - 6\gamma_E - 18 \ln 2 + 6 \frac{\zeta'(-1)}{\zeta(-1)} + 6(21\zeta(3) - 21)\hat{\mu}^2 \right. \right. \\
 &+ 6(126\zeta(3) - 155\zeta(5)) \hat{\mu}^4 + \mathcal{O}(\hat{\mu}^6) \left. \right\} \\
 &\left. + \epsilon(29.5113 + 158.176 \hat{\mu}^2 - 557.189 \hat{\mu}^4 + \mathcal{O}(\hat{\mu}^6)) \right]. \quad (4.89)
 \end{aligned}$$

$$\begin{aligned}
 \int_{\mathbf{pq}} \frac{n_B(p)n_F(q)}{2pq} \frac{q^2}{r^4} &= \frac{T^2}{(4\pi)^2} \left(\frac{1}{18} \right) \left[\left(1 - 6\gamma_E - 12 \ln 2 + 6 \frac{\zeta'(-1)}{\zeta(-1)} + 12\hat{\mu}^2 \right. \right. \\
 &\quad \left. \left. - 6(28\zeta(3) - 31\zeta(5)) \hat{\mu}^4 + \mathcal{O}(\hat{\mu}^6) \right) \right. \\
 &\quad \left. + \epsilon \left(31.0735 + 222.294 \hat{\mu}^2 - 416.474 \hat{\mu}^4 + \mathcal{O}(\hat{\mu}^6) \right) \right]. \quad (4.90)
 \end{aligned}$$

$$\begin{aligned}
 \int_{\mathbf{pq}} \frac{n_F^-(p) - n_F^+(p)}{2p} \frac{n_F^-(q) - n_F^+(q)}{2q} \frac{pq}{r^4} \\
 = \frac{T^2}{(4\pi)^2} \frac{1}{3} \left[(1 - 3\zeta(3)) \hat{\mu}^2 - 20(\zeta(3) - \zeta(5)) \hat{\mu}^4 + \mathcal{O}(\hat{\mu}^6) \right]. \quad (4.91)
 \end{aligned}$$

Thermal integrals containing the triangle function:

$$\begin{aligned}
 \int_{\mathbf{pq}} \frac{n_F^-(p) - n_F^+(p)}{2p} \frac{n_F^-(q) - n_F^+(q)}{2q} \frac{2pq}{\Delta(p, q, r)} \\
 = \frac{T^2}{(4\pi)^2} \left(\frac{\Lambda}{4\pi T} \right)^{4\epsilon} \left[\frac{\hat{\mu}^2}{\epsilon} + 2(4 \ln 2 + 2\gamma_E + 1) \hat{\mu}^2 - \frac{28}{3} \zeta(3) \hat{\mu}^4 + \mathcal{O}(\hat{\mu}^6) \right]. \quad (4.92)
 \end{aligned}$$

Thermal integrals containing both the triangle function and HTL average are listed below:

$$\begin{aligned}
 \int_{\mathbf{pq}} \frac{n_F(p)n_F(q)}{4pq} \operatorname{Re} \left\langle c^2 \frac{r^2 c^2 - p^2 - q^2}{\Delta(p + i\varepsilon, q, rc)} \right\rangle_c \\
 = \frac{T^2}{(4\pi)^2} \left[0.01458 + 0.23807 \hat{\mu}^2 + 0.82516 \hat{\mu}^4 + \mathcal{O}(\hat{\mu}^6) \right]. \quad (4.93)
 \end{aligned}$$

$$\begin{aligned}
 \int_{\mathbf{pq}} \frac{n_F(p)n_F(q)}{4pq} \operatorname{Re} \left\langle c^4 \frac{r^2 c^2 - p^2 - q^2}{\Delta(p + i\varepsilon, q, rc)} \right\rangle_c \\
 = \frac{T^2}{(4\pi)^2} \left[0.017715 + 0.28015 \hat{\mu}^2 + 0.87321 \hat{\mu}^4 + \mathcal{O}(\hat{\mu}^6) \right]. \quad (4.94)
 \end{aligned}$$

$$\begin{aligned}
 & \int_{\mathbf{p}\mathbf{q}} \frac{n_F(p)n_F(q)}{4pq} \operatorname{Re} \left\langle \frac{q^2}{r^2} c^2 \frac{r^2 c^2 - p^2 - q^2}{\Delta(p + i\varepsilon, q, rc)} \right\rangle_c \\
 &= -\frac{T^2}{(4\pi)^2} [0.01158 + 0.17449 \hat{\mu}^2 + 0.45566 \hat{\mu}^4 + \mathcal{O}(\hat{\mu}^6)]. \quad (4.95)
 \end{aligned}$$

$$\begin{aligned}
 & \int_{\mathbf{p}\mathbf{q}} \frac{n_B(p)n_F(q)}{2pq} \operatorname{Re} \left\langle \frac{p^2 - q^2}{r^2} \frac{r^2 c^2 - p^2 - q^2}{\Delta(p + i\varepsilon, q, rc)} \right\rangle_c \\
 &= \frac{T^2}{(4\pi)^2} [0.17811 + 1.43775 \hat{\mu}^2 - 2.45413 \hat{\mu}^4 + \mathcal{O}(\hat{\mu}^6)]. \quad (4.96)
 \end{aligned}$$

Second set of integrals involve the variables $r_c = |\mathbf{p} + \mathbf{q}/c|$:

$$\begin{aligned}
 & \int_{\mathbf{p}\mathbf{q}} \frac{n_F(p)n_B(q)}{2pq} \operatorname{Re} \left\langle c^{-1+2\varepsilon} \frac{r_c^2 - p^2 - q^2}{\Delta(p + i\varepsilon, q, r_c)} \right\rangle_c \\
 &= \frac{T^2}{(4\pi)^2} [0.19678 + 1.07745 \hat{\mu}^2 - 2.63486 \hat{\mu}^4 + \mathcal{O}(\hat{\mu}^6)]. \quad (4.97)
 \end{aligned}$$

$$\begin{aligned}
 & \int_{\mathbf{p}\mathbf{q}} \frac{n_F(p)n_B(q)}{2pq} \operatorname{Re} \left\langle c^{1+2\varepsilon} \frac{r_c^2 - p^2 - q^2}{\Delta(p + i\varepsilon, q, r_c)} \right\rangle_c \\
 &= \frac{T^2}{(4\pi)^2} [0.048368 + 0.23298 \hat{\mu}^2 - 0.65074 \hat{\mu}^4 + \mathcal{O}(\hat{\mu}^6)]. \quad (4.98)
 \end{aligned}$$

$$\begin{aligned}
 & \int_{\mathbf{p}\mathbf{q}} \frac{n_F(p)n_B(q)}{2pq} \frac{p^2}{q^2} \operatorname{Re} \left\langle c^{1+2\varepsilon} \frac{r_c^2 - p^2 - q^2}{\Delta(p + i\varepsilon, q, r_c)} \right\rangle_c = \frac{1}{96} \frac{T^2}{(4\pi)^2} \left(\frac{\Lambda}{4\pi T} \right)^{4\varepsilon} \\
 & \quad \times \left[\frac{(1 + 12 \hat{\mu}^2)}{\varepsilon} + (7.7724 + 81.1057 \hat{\mu}^2 - 48.5858 \hat{\mu}^4 + \mathcal{O}(\hat{\mu}^6)) \right]. \quad (4.99)
 \end{aligned}$$

$$\begin{aligned}
 & \int_{\mathbf{p}\mathbf{q}} \frac{n_F(p)n_B(q)}{2pq} \operatorname{Re} \left\langle c^{1+2\varepsilon} \frac{r_c^2}{q^2} \frac{r_c^2 - p^2 - q^2}{\Delta(p + i\varepsilon, q, r_c)} \right\rangle_c = \frac{T^2}{(4\pi)^2} \left(\frac{\Lambda}{4\pi T} \right)^{4\varepsilon} \frac{11 - 8 \ln 2}{288} \\
 & \quad \times \left[\frac{1}{\varepsilon} (1 + 12 \hat{\mu}^2) + (7.799 + 70.516 \hat{\mu}^2 - 57.928 \hat{\mu}^4 + \mathcal{O}(\hat{\mu}^6)) \right]. \quad (4.100)
 \end{aligned}$$

$$\begin{aligned}
 \int_{\mathbf{pq}} \frac{n_F(p)n_F(q)}{4pq} \operatorname{Re} \frac{1}{24} \left\langle c^{-1+2\epsilon} \frac{r_c^2 - p^2}{q^2} \frac{r_c^2 - p^2 - q^2}{\Delta(p + i\varepsilon, q, r_c)} \right\rangle_c &= -\frac{T^2}{(4\pi)^2} \left(\frac{\Lambda}{4\pi T} \right)^{4\epsilon} \\
 &\times \left[(1 + 12 \hat{\mu}^2) \frac{1}{\epsilon^2} + \frac{2}{\epsilon} \left(1 + \gamma_E + \ln 2 + \frac{\zeta'(-1)}{\zeta(-1)} \right) \right. \\
 &+ (24\gamma_E + 48 \ln 2 - 7\zeta(3))\hat{\mu}^2 + (31\zeta(5) - 98\zeta(3))\hat{\mu}^4 + \mathcal{O}(\hat{\mu}^6) \Big) \\
 &+ \left. (40.3158 + 261.822 \hat{\mu}^2 - 1310.69 \hat{\mu}^4 + \mathcal{O}(\hat{\mu}^6)) \right]. \quad (4.101)
 \end{aligned}$$

$$\begin{aligned}
 \int_{\mathbf{pq}} \frac{n_B(p)n_F(q)}{2pq} \operatorname{Re} \left\langle c^{-1+2\epsilon} \frac{r_c^2 - p^2}{q^2} \frac{r_c^2 - p^2 - q^2}{\Delta(p + i\varepsilon, q, r_c)} \right\rangle_c &= -\frac{T^2}{(4\pi)^2} \left(\frac{\Lambda}{4\pi T} \right)^{4\epsilon} \frac{1}{12} \left[\frac{1}{\epsilon^2} \right. \\
 &+ \frac{1}{\epsilon} \left(2 + 2\gamma_E + 4 \ln 2 + 2 \frac{\zeta'(-1)}{\zeta(-1)} - 14\zeta(3)\hat{\mu}^2 + 62\zeta(5)\hat{\mu}^4 + \mathcal{O}(\hat{\mu}^6) \right) \\
 &+ \left. (52.953 - 190.103 \hat{\mu}^2 + 780.921 \hat{\mu}^4 + \mathcal{O}(\hat{\mu}^6)) \right]. \quad (4.102)
 \end{aligned}$$

The integral (4.94) can be evaluated directly in three dimensions at finite chemical potential. The other integrals Eqs. (4.95)–(4.102) can be evaluated following the same procedure as discussed in [173] at finite chemical potential.

4.7 Pressure

In the previous section we have computed both LO and NLO thermodynamic potential in presence of quark chemical potential and temperature. All other thermodynamic quantities can be calculated using standard thermodynamic relations. The pressure is defined as

$$P = -\Omega(T, \mu, m_q, m_D), \quad (4.103)$$

4.7.1 LO Pressure

The LO HTLpt pressure through $\mathcal{O}(g^4)$ at any μ can be written in leading order of ϵ from eqn. (4.28) as

$$\begin{aligned}
 \mathcal{P}_{\text{LO}} = & d_A \frac{\pi^2 T^4}{45} \left[1 + \frac{7 d_F}{4 d_A} \left(1 + \frac{120}{7} \hat{\mu}^2 + \frac{240}{7} \hat{\mu}^4 \right) \right. \\
 & - \frac{15}{2} \hat{m}_D^2 - 30 \frac{d_F}{d_A} (1 + 12 \hat{\mu}^2) \hat{m}_q^2 + 30 \hat{m}_D^3 \\
 & \left. + \frac{45}{4} \left(\ln \frac{\hat{\Lambda}}{2} - \frac{7}{2} + \gamma_E + \frac{\pi^2}{3} \right) \hat{m}_D^4 - 60 \frac{d_F}{d_A} (\pi^2 - 6) \hat{m}_q^4 \right]. \quad (4.104)
 \end{aligned}$$

At leading order, the weak coupling expressions for the mass parameters are

$$m_D^2 = \frac{g^2 T^2}{3} [c_A + s_F (1 + 12 \hat{\mu}^2)] ; \quad m_q^2 = \frac{g^2 T^2 c_F}{4} \frac{c_F}{2} (1 + 4 \hat{\mu}^2) . \quad (4.105)$$

4.7.2 NLO HTLpt Pressure and Variational Mass Gap Equations

The NLO HTLpt pressure through $\mathcal{O}[(\mu/T)^4]$ can be obtain from Eq. (4.37) using (4.103) as

$$\begin{aligned}
 \mathcal{P}_{\text{NLO}} = & d_A \frac{\pi^2 T^4}{45} \left\{ 1 + \frac{7 d_F}{4 d_A} \left(1 + \frac{120}{7} \hat{\mu}^2 + \frac{240}{7} \hat{\mu}^4 \right) - 15 \hat{m}_D^3 \right. \\
 & - \frac{45}{4} \left(\log \frac{\hat{\Lambda}}{2} - \frac{7}{2} + \gamma_E + \frac{\pi^2}{3} \right) \hat{m}_D^4 + 60 \frac{d_F}{d_A} (\pi^2 - 6) \hat{m}_q^4 \\
 & + \frac{\alpha_s}{\pi} \left[-\frac{5}{4} \left(c_A + \frac{5 s_F}{2} \left(1 + \frac{72}{5} \hat{\mu}^2 + \frac{144}{5} \hat{\mu}^4 \right) \right) + 15 (c_A + s_F (1 + 12 \hat{\mu}^2)) \hat{m}_D \right. \\
 & - \frac{55}{4} \left\{ c_A \left(\log \frac{\hat{\Lambda}}{2} - \frac{36}{11} \log \hat{m}_D - 2.001 \right) - \frac{4}{11} s_F \left[\left(\log \frac{\hat{\Lambda}}{2} - 2.337 \right) \right. \right. \\
 & + (24 - 18 \zeta(3)) \left(\log \frac{\hat{\Lambda}}{2} - 15.662 \right) \hat{\mu}^2 + 120 (\zeta(5) - \zeta(3)) \\
 & \left. \left. \times \left(\log \frac{\hat{\Lambda}}{2} - 1.0811 \right) \hat{\mu}^4 + \mathcal{O}(\hat{\mu}^6) \right] \right\} \hat{m}_D^2 - 45 s_F \left\{ \log \frac{\hat{\Lambda}}{2} + 2.198 - 44.953 \hat{\mu}^2 \right. \\
 & - \left. \left(288 \ln \frac{\hat{\Lambda}}{2} + 19.836 \right) \hat{\mu}^4 + \mathcal{O}(\hat{\mu}^6) \right\} \hat{m}_q^2 + \frac{165}{2} \left\{ c_A \left(\log \frac{\hat{\Lambda}}{2} + \frac{5}{22} + \gamma_E \right) \right. \\
 & - \left. \frac{4}{11} s_F \left(\log \frac{\hat{\Lambda}}{2} - \frac{1}{2} + \gamma_E + 2 \ln 2 - 7 \zeta(3) \hat{\mu}^2 + 31 \zeta(5) \hat{\mu}^4 + \mathcal{O}(\hat{\mu}^6) \right) \right\} \hat{m}_D^3 \\
 & + 15 s_F \left(2 \frac{\zeta'(-1)}{\zeta(-1)} + 2 \ln \hat{m}_D \right) \left[(24 - 18 \zeta(3)) \hat{\mu}^2 \right. \\
 & \left. + 120 (\zeta(5) - \zeta(3)) \hat{\mu}^4 + \mathcal{O}(\hat{\mu}^6) \right] \hat{m}_D^3 + 180 s_F \hat{m}_D \hat{m}_q^2 \left. \right\}. \tag{4.106}
 \end{aligned}$$

which is accurate up to $\mathcal{O}(g^3)$ and nominally accurate to $\mathcal{O}(g^5)$ since it was obtained from an expansion of two-loop thermodynamic potential in a power series in m_D/T and m_q/T treating both m_D and m_q having leading terms proportional to g . Using the result above, the mass parameters m_D and m_q can be obtained by solving the two variational equations:

$$\begin{aligned}
 \left. \frac{\partial \Omega_{\text{NLO}}}{\partial \hat{m}_D} \right|_{m_q = \text{constant}} &= 0, \\
 \left. \frac{\partial \Omega_{\text{NLO}}}{\partial \hat{m}_q} \right|_{m_D = \text{constant}} &= 0. \tag{4.107}
 \end{aligned}$$

This leads to the following two gap equations which will be solved numerically

$$\begin{aligned}
 & 45\hat{m}_D^2 \left[1 + \left(\ln \frac{\hat{\Lambda}}{2} - \frac{7}{2} + \gamma_E + \frac{\pi^2}{3} \right) \hat{m}_D \right] \\
 &= \frac{\alpha_s}{\pi} \left\{ 15(c_A + s_F(1 + 12\hat{\mu}^2)) - \frac{55}{2} \left[c_A \left(\ln \frac{\hat{\Lambda}}{2} - \frac{36}{11} \ln \hat{m}_D - 3.637 \right) \right. \right. \\
 &- \frac{4}{11} s_F \left\{ \ln \frac{\hat{\Lambda}}{2} - 2.333 + (24 - 18\zeta(3)) \left(\ln \frac{\hat{\Lambda}}{2} - 15.662 \right) \hat{\mu}^2 \right. \\
 &+ \left. \left. 120(\zeta(5) - \zeta(3)) \left(\ln \frac{\hat{\Lambda}}{2} - 1.0811 \right) \hat{\mu}^4 \right\} \right] \hat{m}_D + \frac{495}{2} \left[c_A \left(\ln \frac{\hat{\Lambda}}{2} + \frac{5}{22} + \gamma_E \right) \right. \\
 &- \frac{4}{11} s_F \left\{ \ln \frac{\hat{\Lambda}}{2} - \frac{1}{2} + \gamma_E + 2 \ln 2 - 7\zeta(3)\hat{\mu}^2 + 31\zeta(5)\hat{\mu}^4 \right. \\
 &- \left. \left. \left(\frac{\zeta'(-1)}{\zeta(-1)} + \ln \hat{m}_D + \frac{1}{3} \right) ((24 - 18\zeta(3))\hat{\mu}^2 + 120(\zeta(5) - \zeta(3))\hat{\mu}^4) \right\} \right] \hat{m}_D^2 \\
 &+ \left. 180s_F\hat{m}_q^2 \right\}, \tag{4.108}
 \end{aligned}$$

and

$$\begin{aligned}
 \hat{m}_q^2 = \frac{d_A}{8d_F(\pi^2 - 6)} \frac{\alpha_s s_F}{\pi} \left[3 \left(\ln \frac{\hat{\Lambda}}{2} + 2.198 - 44.953 \hat{\mu}^2 \right. \right. \\
 \left. \left. - \left(288 \ln \frac{\hat{\Lambda}}{2} + 19.836 \right) \hat{\mu}^4 \right) - 12\hat{m}_D \right]. \tag{4.109}
 \end{aligned}$$

For convenience and comparison with lattice data [10], we define the pressure difference

$$\Delta P(T, \mu) = P(T, \mu) - P(T, 0). \tag{4.110}$$

where we note that we have discarded terms of $\mathcal{O}(\hat{\mu}^6)$ and higher above. In figs. (4.2) and (4.3) we present a comparison of NLO HTLpt pressure with that of four-loop

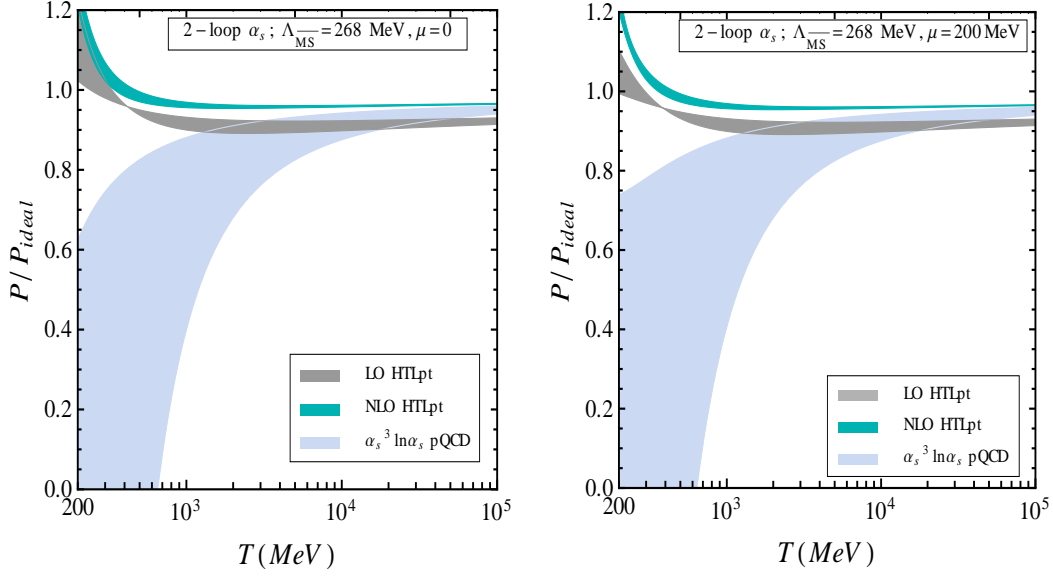


Figure 4.2: The NLO HTLpt pressure scaled with ideal gas pressure plotted along with four-loop pQCD pressure [13, 146] for two different values of chemical potential with $N_f = 3$ and 2-loop running coupling constant α_s . The bands are obtained by varying the renormalization scale by a factor of 2 around its central value $\Lambda = 2\pi\sqrt{T^2 + \mu^2/\pi^2}$ [13, 68, 146, 226–228]. We use $\Lambda_{\overline{\text{MS}}} = 290$ MeV based on recent lattice calculations [229] of the three-loop running of α_s .

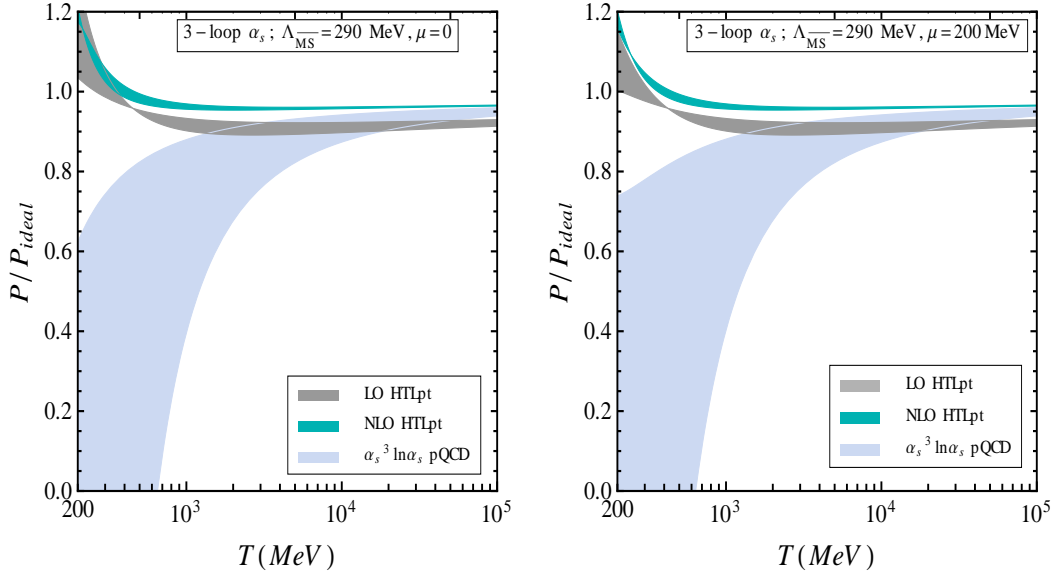


Figure 4.3: Same as Fig. 4.2 but for 3-loop α_s .

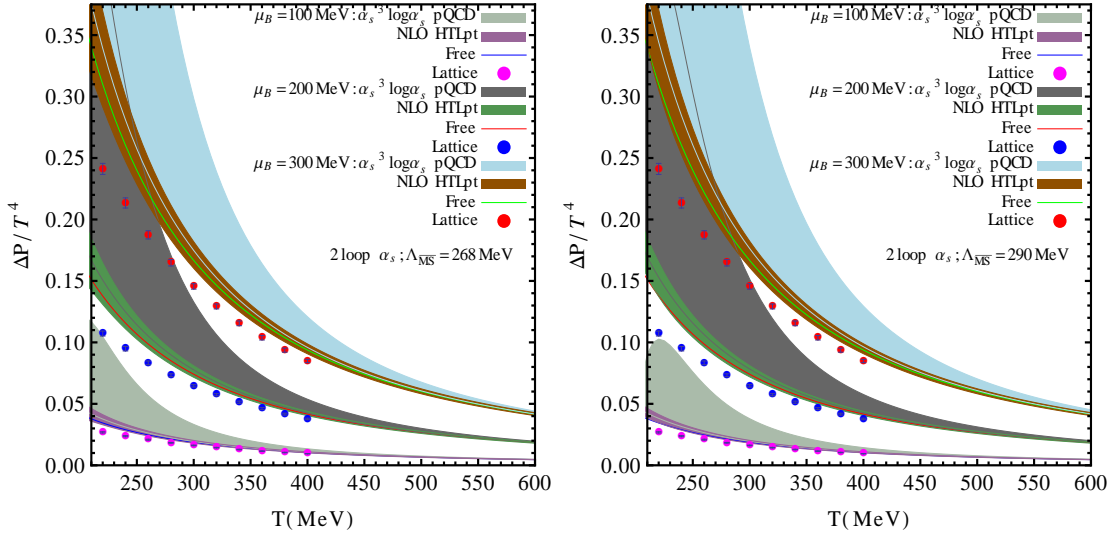


Figure 4.4: (Left panel) ΔP for $N_f = 3$ is plotted as a function of T for two-loop HTLpt result along with those of four-loop pQCD up to $\alpha_s^3 \ln \alpha_s$ [13, 146] and lattice QCD [10] up to $\mathcal{O}(\mu^2)$ using 2-loop running coupling constant α_s . (Right panel) Same as left panel but using 3-loop running coupling. In both cases three different values of μ are shown as specified in the legend. The bands in both HTLpt and pQCD are obtained by varying the renormalization scale by a factor of 2 around its central value $\Lambda = 2\pi\sqrt{T^2 + \mu^2/\pi^2}$ [13, 68, 146, 226–228].

pQCD [13, 146] as a function of the temperature for two and three loop running of α_s . The only difference between Figs. (4.2) and (4.3) is the choice of order of the running coupling used. As can be seen from these figures, the dependence on the order of the running coupling is quite small. However, we note that in both figures even at extremely large temperatures there is a sizable correction when going from LO to NLO. This was already seen in the $\mu = 0$ results of Ref. [172, 173] where it was found that due to the logarithmic running of the coupling, it was necessary to go to very large temperatures in order for the LO and NLO predictions to overlap. This is due to over-counting problems at LO which lead to an order- g^2 perturbative coefficient which is twice as large as it should be [20, 172, 173]. This problem is corrected at NLO, but the end result is that there is a reasonably large correction ($\sim 5\%$) at the temperatures shown.

The NLO HTLpt result differs from the pQCD result through order $\alpha_s^3 \ln \alpha_s$ at low temperatures. A NNLO HTLpt calculation at finite μ would agree better with

pQCD $\alpha_s^3 \ln \alpha_s$ as found in $\mu = 0$ case [178]. The HTLpt result clearly indicates a modest improvement over pQCD in respect of convergence and sensitivity of the renormalization scale. In Fig. 4.4 the pressure difference, ΔP , is also compared with the same quantity computed using pQCD [13, 146] and lattice QCD [10]. Both LO and NLO HTLpt results are less sensitive to the choice of the renormalization scale than the weak coupling results with the inclusion of successive orders of approximation. Comparison with available lattice QCD data [10] suggests that HTLpt and pQCD cannot accurately account for the lattice QCD results below approximately $3T_c$; however, the results are in very good qualitative agreement with the lattice QCD results without any fine tuning.

4.8 Quark Number Susceptibility

We are now in a position to obtain the second and fourth-order HTLpt QNS following Eq. (4.1). We note that the pure gluonic loops at any order do not contribute to QNS, however, gluons contribute through the dynamical fermions through fermionic loops. This makes QNS proportional to only quark degrees of freedom. Below we present (semi-)analytic expressions for both LO and NLO QNS.

To obtain the second and fourth-order quark number susceptibilities in HTLpt, one requires expressions for m_D , $\frac{\partial^2}{\partial \mu^2} m_D$, m_q , and $\frac{\partial^2}{\partial \mu^2} m_q$ at $\mu = 0$ from Eqs. (4.108) and (4.109).² We list these here for completeness. The result for the limit of the m_D

²Note that odd derivatives with respect to μ vanish at $\mu = 0$. Fourth-order derivatives at $\mu = 0$ are nonzero, however, they appear as multiplicative factors of the gap equations and are therefore not required, as we will see below.

gap equation necessary is

$$\begin{aligned}
 & 45\hat{m}_D^2(0) \left[1 + \left(\ln \frac{\hat{\Lambda}}{2} - \frac{7}{2} + \gamma_E + \frac{\pi^2}{3} \right) \hat{m}_D(0) \right] \\
 &= \frac{\alpha_s}{\pi} \left\{ 15(c_A + s_F) - \frac{55}{2} \left[c_A \left(\ln \frac{\hat{\Lambda}}{2} - \frac{36}{11} \ln \hat{m}_D(0) - 3.637 \right) \right. \right. \\
 &\quad - \frac{4}{11} s_F \left. \left. \left\{ \ln \frac{\hat{\Lambda}}{2} - 2.333 \right\} \right] \hat{m}_D(0) + \frac{495}{2} \left[c_A \left(\ln \frac{\hat{\Lambda}}{2} + \frac{5}{22} + \gamma_E \right) \right. \right. \\
 &\quad \left. \left. - \frac{4}{11} s_F \left(\ln \frac{\hat{\Lambda}}{2} - \frac{1}{2} + \gamma_E + 2 \ln 2 \right) \right] \hat{m}_D^2(0) + 180 s_F \hat{m}_q^2(0) \right\}. \quad (4.111)
 \end{aligned}$$

For m_q one obtains

$$\hat{m}_q^2(0) = \frac{d_A}{8d_F(\pi^2 - 6)} \frac{\alpha_s s_F}{\pi} \left[3 \left(\ln \frac{\hat{\Lambda}}{2} + 2.198 \right) - 12\hat{m}_D(0) \right]. \quad (4.112)$$

For $\frac{\partial^2}{\partial \mu^2} m_D$ one obtains

$$\begin{aligned}
 & 45 \left[2 + 3 \left(\ln \frac{\hat{\Lambda}}{2} - \frac{7}{2} + \gamma_E + \frac{\pi^2}{3} \right) \hat{m}_D(0) \right] \hat{m}_D(0) \hat{m}_D''(0) \\
 &= \frac{\alpha_s}{\pi} \left\{ 360 s_F - \frac{55}{2} \hat{m}_D''(0) \left[c_A \left(\ln \frac{\hat{\Lambda}}{2} - \frac{36}{11} \ln \hat{m}_D(0) - 6.9097 \right) - \frac{4}{11} s_F \left(\ln \frac{\hat{\Lambda}}{2} - 2.333 \right) \right] \right. \\
 &\quad + 495 \hat{m}_D''(0) \left[c_A \left(\frac{5}{22} + \gamma_E + \ln \frac{\hat{\Lambda}}{2} \right) - \frac{4}{11} s_F \left(\ln \frac{\hat{\Lambda}}{2} - \frac{1}{2} + \gamma_E + 2 \ln 2 \right) \right] \hat{m}_D(0) \\
 &\quad + 20 s_F \left(\ln \frac{\hat{\Lambda}}{2} - 15.662 \right) (24 - 18\zeta(3)) \hat{m}_D(0) \\
 &\quad + 180 s_F \hat{m}_D(0)^2 \left[7\zeta(3) + \left(\frac{\zeta'(-1)}{\zeta(-1)} + \ln \hat{m}_D(0) + \frac{1}{3} \right) (24 - 18\zeta(3)) \right] \\
 &\quad \left. + 360 s_F \hat{m}_q(0) \hat{m}_q''(0) \right\}. \quad (4.113)
 \end{aligned}$$

For $\frac{\partial^2}{\partial \mu^2} m_q$ one obtains

$$\hat{m}_q(0) \hat{m}_q''(0) = -\frac{3d_A}{8d_F(\pi^2 - 6)} \frac{\alpha_s s_F}{\pi} [44.953 + 2\hat{m}_D''(0)]. \quad (4.114)$$

In the expressions above, $m_D(0) \equiv m_D(T, \Lambda, \mu = 0)$, $m_D''(0) \equiv \frac{\partial^2}{\partial \mu^2} m_D(T, \Lambda, \mu) \Big|_{\mu=0}$ and similarly for m_q .

4.8.1 LO HTLpt second-order QNS

An analytic expression for the LO HTLpt second-order QNS can be obtained using Eq. (4.104)

$$\begin{aligned}
 \chi_2^{\text{LO}}(T) &= \frac{\partial^2}{\partial \mu^2} \mathcal{P}_{\text{LO}}(T, \Lambda, \mu) \Big|_{\mu=0} = \frac{1}{(2\pi T)^2} \frac{\partial^2}{\partial \hat{\mu}^2} \mathcal{P}_{\text{LO}}(T, \Lambda, \hat{\mu}) \Big|_{\hat{\mu}=0} \\
 &= \frac{d_F T^2}{3} \left[1 - \frac{3c_F}{4} \left(\frac{g}{\pi}\right)^2 + \frac{c_F}{4} \sqrt{3(c_A + s_F)} \left(\frac{g}{\pi}\right)^3 - \frac{c_F^2}{64} (\pi^2 - 6) \left(\frac{g}{\pi}\right)^4 \right. \\
 &\quad \left. + \frac{c_F}{16} (c_A + s_F) \left(\log \frac{\hat{\Lambda}}{2} - \frac{7}{2} + \gamma_E + \frac{\pi^2}{3} \right) \left(\frac{g}{\pi}\right)^4 \right], \tag{4.115}
 \end{aligned}$$

where the LO Debye and quark masses listed in Eqs. (4.105) and their μ derivatives have been used.

4.8.2 LO HTLpt fourth-order QNS

An analytic expression for the LO HTLpt fourth-order QNS can also be obtained using Eq. (4.104)

$$\begin{aligned}
 \chi_4^{\text{LO}}(T) &= \frac{\partial^4}{\partial \mu^4} \mathcal{P}_{\text{LO}}(T, \Lambda, \mu) \Big|_{\mu=0} = \frac{1}{(2\pi T)^4} \frac{\partial^4}{\partial \hat{\mu}^4} \mathcal{P}_{\text{LO}}(T, \Lambda, \hat{\mu}) \Big|_{\hat{\mu}=0} \\
 &= \frac{2d_F}{\pi^2} \left[1 - \frac{3}{4} c_F \left(\frac{g}{\pi}\right)^2 + \frac{3}{8} c_F s_F \sqrt{\frac{3}{c_A + s_F}} \left(\frac{g}{\pi}\right)^3 - \frac{c_F^2 (\pi^2 - 6)}{64} \left(\frac{g}{\pi}\right)^4 \right. \\
 &\quad \left. + \frac{3}{16} c_F s_F \left(\log \frac{\hat{\Lambda}}{2} - \frac{7}{2} + \gamma_E + \frac{\pi^2}{3} \right) \left(\frac{g}{\pi}\right)^4 \right], \tag{4.116}
 \end{aligned}$$

where, once again, the LO Debye and quark masses listed in Eqs. (4.105) and their μ derivatives have been used. We note that both χ_2^{LO} in (4.115) and χ_4^{LO} in (4.116)

are the same as those recently obtained by Andersen et al. [170]; however, the closed-form expressions obtained here have not been explicitly listed therein.

4.8.3 NLO HTLpt second-order QNS

A semi-analytic expression for the NLO HTLpt second-order QNS can be obtained from Eq. (4.106)

$$\begin{aligned}
 \chi_2^{\text{NLO}}(T) &= \left. \frac{\partial^2}{\partial \mu^2} \mathcal{P}_{\text{NLO}}(T, \Lambda, \mu) \right|_{\mu=0} = \frac{1}{(2\pi T)^2} \left. \frac{\partial^2}{\partial \hat{\mu}^2} \mathcal{P}_{\text{NLO}}(T, \Lambda, \hat{\mu}) \right|_{\hat{\mu}=0} \\
 &= \frac{d_A T^2}{2} \left[\frac{2}{3} \frac{d_F}{d_A} + \frac{\alpha_s}{\pi} s_F \left\{ -1 + 4 \hat{m}_D(0) + \frac{2}{3} \left(\ln \frac{\hat{\Lambda}}{2} - 15.662 \right) \right. \right. \\
 &\quad \times (4 - 3\zeta(3)) \hat{m}_D^2(0) + 44.953 \hat{m}_q^2(0) \\
 &\quad \left. \left. + \left[\frac{14}{3} \zeta(3) + \left(\frac{\zeta'(-1)}{\zeta(-1)} + \ln \hat{m}_D(0) \right) (16 - 12\zeta(3)) \right] \hat{m}_D^3(0) \right\} \right]. \quad (4.117)
 \end{aligned}$$

We note that no μ derivatives of the mass parameters appear in (4.117) and, as a result, $\chi_2^{\text{NLO}}(T)$ reduces to such a simple and compact form. This is because the second derivatives of the mass parameters with respect to μ always appear as multiplicative factors of the gap equations (4.111) and (4.112) and hence these contributions vanish. Numerically solving for the variational masses using Eq. (4.111) and (4.112) one can directly compute $\chi_2^{\text{NLO}}(T)$ from (4.117). Alternatively, we have also computed $\chi_2^{\text{NLO}}(T)$ by performing numerical differentiation of the pressure in (4.106) which leads to the same result within numerical errors.

In Fig. (4.5) we have plotted the $N_f = 3$ second-order QNS scaled by the corresponding free gas limit as a function of the temperature. As discussed above, the bands shown for the HTLpt and pQCD [13] results indicate the sensitivity of χ_2 to the choice of the renormalization scale Λ . However, χ_2 in both HTLpt and pQCD depends only weakly on the chosen order of the running of the strong coupling and in turn only depends weakly on Λ_{MS} , as can be seen clearly from both

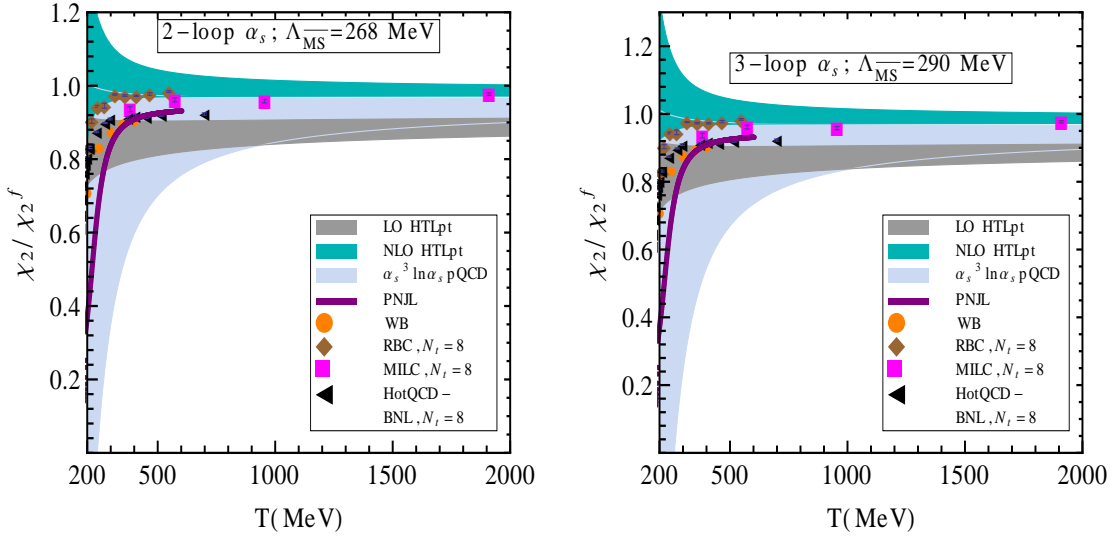


Figure 4.5: *Left panel:* χ_2 scaled by the free field value for LO (grey band) and NLO (sea green band) in 2-loop HTLpt, 4-loop pQCD (sky blue band) [13], LQCD (various symbols) [10, 111, 116, 118], and PNJL model (thick purple line) [52, 53] are plotted as a function of the temperature. The bands in HTLpt and pQCD are obtained by varying the $\overline{\text{MS}}$ renormalization scale (Λ) around its central value by a factor of two. We also used $\Lambda_{\overline{\text{MS}}} = 268$ MeV and 2-loop α_s for HTLpt and pQCD. *Right panel:* Same as left panel but using 3-loop α_s and $\Lambda_{\overline{\text{MS}}} = 290$ MeV.

panels of Fig. (4.5). The LO HTLpt prediction for χ_2 seems to agree reasonably well with the available Wuppertal-Budapest LQCD data which are obtained using the tree-level improved Symanzik action and a stout smeared staggered fermionic action with light quark masses $\sim 0.035 m_s$, with m_s being the strange quark mass near its physical value; however, there is a sizable variation among different lattice computations [10, 111, 116] considering improved lattice actions and a range of quark masses. However, lowering the quark mass ($0.035 m_s$, m_s is the strange quark mass) nearer to its physical value [10] seems to have a very small effect in the temperature range, as seen from the LQCD data. Note that for the Wuppertal-Budapest (WB) lattice data shown in Fig. (4.5), Ref. [10] provided a parameterization of their χ_2 data

$$\chi_2(T) = e^{-(h_3/t + h_4/t^2)} f_3 [\tanh(f_4 t + f_5) + 1], \quad (4.118)$$

where $t = T/(200\text{MeV})$, $h_3 = 0.5022$, $h_4 = 0.5950$, $f_3 = 0.1359$, $f_4 = 6.3290$, and $f_5 = 4.8303$. The authors of Ref. [10] performed the fit for data [11] in the temperature range $125 \text{ MeV} < T \leq 400 \text{ MeV}$. Using the parameterization above, we display their data up to 400 MeV with a step size of 50 MeV. The RBC-Bielefeld collaboration [118] data for χ_2 shown in Fig. (4.5) used a p4 action whereas the MILC collaboration [111] used an asqtad action. In both cases the light quark mass ranges from $(0.1-0.2) m_s$. The results for χ_2 obtained using a nonperturbative PNJL model [52, 53] which includes an six-quark interaction are only available very close to the phase transition temperature. We see in Fig. (4.5) that NLO HTLpt (4.117) exhibits a modest improvement over the pQCD calculation shown, which is accurate to $\mathcal{O}(\alpha_s^3 \ln \alpha_s)$. However, the NLO χ_2 is higher than the LO one at higher temperature and it goes beyond the free gas value at lower temperatures. It should be mentioned that, although the 2-loop calculation improves upon the LO results by rectifying over-counting which causes incorrect coefficients in the weak coupling limit, it does so by pushing the problem to higher order in g . The reason can be understood in the following way: in HTLpt the loop and coupling expansion are not symmetrical, therefore at a given loop order there are contributions from higher orders in coupling. Since the NLO HTL pressure and thus QNS is only strictly accurate to order $\mathcal{O}(g^3)$ there is over-counting occurring at higher orders in g , namely at $\mathcal{O}(g^4)$ and $\mathcal{O}(g^5)$. A next-to-next-to-leading order (NNLO) HTLpt calculation would fix the problem through $\mathcal{O}(g^5)$ thereby guaranteeing that, when expanded in a strict power series in g , the HTLpt result would reproduce the perturbative result order-by-order through $\mathcal{O}(g^5)$.

4.8.4 NLO HTLpt fourth-order QNS

A semi-analytic expression for the NLO HTLpt fourth-order QNS can also be obtained from Eq. (4.106)

$$\begin{aligned}
 \chi_4^{\text{NLO}}(T) &= \left. \frac{\partial^4}{\partial \mu^4} \mathcal{P}_{\text{NLO}}(T, \Lambda, \mu) \right|_{\mu=0} = \frac{1}{(2\pi T)^4} \left. \frac{\partial^4}{\partial \hat{\mu}^4} \mathcal{P}_{\text{NLO}}(T, \Lambda, \hat{\mu}) \right|_{\hat{\mu}=0} \\
 &= \frac{d_A}{4\pi^2} \left[8 \frac{d_F}{d_A} + \frac{\alpha_s}{\pi} s_F \left\{ -12 + 6\hat{m}_D''(0) \right. \right. \\
 &\quad + 3\hat{m}_D^2(0) \left[\left(\frac{\zeta'(-1)}{\zeta(-1)} + \ln \hat{m}_D(0) + \frac{1}{3} \right) (24 - 18\zeta(3)) + 7\zeta(3) \right] \hat{m}_D''(0) \\
 &\quad + \hat{m}_D(0)\hat{m}_D''(0) \left(\ln \frac{\hat{\Lambda}}{2} - 15.662 \right) (8 - 6\zeta(3)) \\
 &\quad - 4\hat{m}_D^3(0) \left[31\zeta(5) - 120 \left(\frac{\zeta'(-1)}{\zeta(-1)} + \ln \hat{m}_D(0) \right) (\zeta(5) - \zeta(3)) \right] \\
 &\quad \left. \left. + 80\hat{m}_D^2(0) \left(\ln \frac{\hat{\Lambda}}{2} - 1.0811 \right) (\zeta(5) - \zeta(3)) + 134.859 \hat{m}_q(0)\hat{m}_q''(0) \right\} \right], \quad (4.119)
 \end{aligned}$$

where the double derivatives of the mass parameters with respect to μ survive, but the fourth derivatives of the mass parameters disappear as discussed earlier. One can now directly compute the fourth-order susceptibility by using numerical solutions of the gap equations in (4.111) and (4.114). Alternatively, we have also computed $\chi_4^{\text{NLO}}(T)$ by performing numerical differentiation of the pressure in (4.106) which leads to the same result within numerical errors.

In Fig. (4.6) we plot the fourth-order QNS (χ_4) scaled by the corresponding free gas value for HTLpt as given in (4.116) and (4.119), pQCD, and LQCD. Both the HTLpt and pQCD results exhibit a very weak dependence on the choice of order of the running of α_s and thus $\Lambda_{\overline{\text{MS}}}$. Nevertheless, the HTLpt results are found to be far below the pQCD result [13] which is accurate to $\mathcal{O}(\alpha_s^3 \ln(\alpha_s))$ and the LQCD results [116, 126]. Also, the correction to χ_4 when going from LO to NLO is quite large. This is due to the fact that the fourth order susceptibility is highly sensitive to the erroneous $\mathcal{O}(g^4)$ and $\mathcal{O}(g^5)$ terms which appear at NLO. It is expected that carrying the HTLpt calculation to NNLO would improve this situation; however, only explicit calculation can prove this. We note additionally that although the

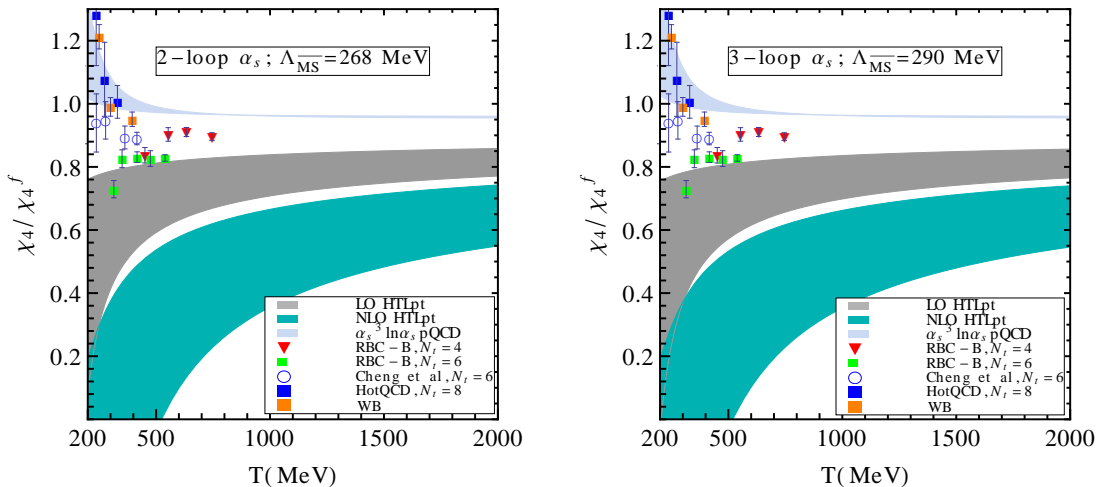


Figure 4.6: Left panel: χ_4 scaled by the free field value for LO and NLO HTLpt as given, respectively, in (4.116) and (4.119), 4-loop pQCD [13], and LQCD [116, 126] are plotted as a function of the temperature. The bands in HTLpt and pQCD are obtained by varying the $\overline{\text{MS}}$ renormalization scale (Λ) around its central value by a factor of two. We used $\Lambda_{\overline{\text{MS}}} = 268$ MeV and 2-loop α_s for HTLpt and pQCD. Lattice QCD results [116, 126] are represented by symbols. The Wuppertal-Budapest (WB) lattice data are taken from Ref. [82]. Right panel: Same as left panel but using 3-loop α_s and $\Lambda_{\overline{\text{MS}}} = 290$ MeV.

pQCD result is very close to the Stefan-Boltzmann limit, the dimensional-reduction resummation method yields a fourth-order QNS which is approximately 20% below the Stefan-Boltzmann limit [170] which places it slightly higher than the LO HTLpt result shown in Fig. (4.6).

4.9 Conclusions and Outlook

In this chapter we have generalized the zero chemical potential NLO HTLpt calculation of the QCD thermodynamic potential [172, 173] to finite chemical potential. We have obtained (semi-)analytic expressions for the thermodynamic potential at both LO and NLO in HTL perturbation theory. We have also obtained second and fourth order quark number susceptibilities at both LO and NLO from that (semi-)analytic expressions for the thermodynamic potential. The results for ther-

modynamic potential obtained here are trustworthy at high temperatures and small chemical potential since we performed an expansion in the ratio of the chemical potential over the temperature.

This NLO thermodynamic potential will be useful for the study of finite temperature and chemical potential QCD matter. This is important in view of the ongoing RHIC beam energy scan and proposed heavy-ion experiments at FAIR. Using the NLO HTLpt thermodynamic potential, we have obtained a variational solution for both mass parameters, m_q and m_D , and we have used this to obtain the pressure at finite temperature and chemical potential. When compared with the weak coupling expansion of QCD, the HTLpt pressure helps somewhat with the problem of oscillation of successive approximations found in pQCD. Furthermore, the scale variation of the NLO HTLpt result for pressure is smaller than that obtained with the weak coupling result.

The LO result for χ_2 obtained here shows reasonable agreement with available LQCD data; however, at this point in time there is still a fairly sizable variation of this quantity between the different lattice groups. Moving forward it would seem that a detailed analysis of the uncertainties in the various LQCD calculations is necessary before detailed conclusions can be drawn. Unlike the LO results, our NLO calculation takes into account dynamical quark contributions by including two-loop graphs which involve fermion loops; however, they suffer from the same problem that NLO HTLpt calculations at zero chemical potential faced: the NLO χ_2 in Eq. (4.117) gets $\mathcal{O}(g^3)$ correct but the $\mathcal{O}(g^4)$ and $\mathcal{O}(g^5)$ contributions are incorrect if they are expanded out in a strict power series in g . As a result, our NLO result for χ_2 scaled to the free limit is closer to unity than the corresponding LO result and only shows a weak dependence on the chosen value of the renormalization scale. Our NLO result for χ_4 (Eq. (4.119)) in which μ derivatives of the variational mass parameters survive is significantly below the pQCD and lattice data.

As was the case with the pressure at zero chemical potential, it seems that fixing this problem will require going to NNLO. In the case of the zero chemical potential pressure, performing such a calculation resulted in much improved agreement between HTL perturbation theory and LQCD calculations above $\sim 2T_c$. At the very least a NNLO calculation will fix the over-counting problems through $\mathcal{O}(g^5)$ and NNLO calculation at finite temperature and chemical potential will be discussed in the next Chapter 5.

CHAPTER 5

Three-loop HTLpt thermodynamics

In this chapter, we study the three loop thermodynamics of QCD using the hard thermal loop perturbation theory. We show that at three loop order hard thermal loop perturbation theory results are compatible with lattice results for the pressure, energy density, entropy density, various order diagonal and off-diagonal susceptibilities, speed of sound down to temperatures $T \sim 250$ MeV. This chapter is based on: *Three-loop HTLpt Pressure and Susceptibilities at Finite Temperature and Density*, N. Haque, J. O. Andersen, M. G. Mustafa, M. Strickland, and N. Su, **Phys. Rev. D** **89** (2014) **061701** and *Three-loop HTLpt thermodynamics at finite temperature and chemical potential*, N. Haque, A. Bandyopadhyay, J. O. Andersen, M. G. Mustafa, M. Strickland, and N. Su, **JHEP** **1405** (2014) **027**.

As we discussed in Chapter 4, at leading order thermodynamic potential is only correct g^0 and g^3 terms when one expands in a strict power series in g . Similarly, at next-to-leading order thermodynamic potential one obtains correct g^0 , g^2 and g^3 terms when one expands in a strict power series in g . So to make the results more reliable at moderate coupling constant g , one needs to calculate thermodynamic functions beyond next-to-leading order in HTL perturbation theory. In this chapter we calculate the thermodynamic potential at finite temperature (T) and chemical

potential (μ) to three-loop order in HTLpt. The three-loop thermodynamic potential is renormalized using only known vacuum, mass, and coupling constant counterterms and the final result is completely analytic. The resulting analytic thermodynamic potential is then used to obtain expressions for the pressure, energy density, entropy density, trace anomaly, speed of sound, and various quark number susceptibilities. We find that there is good agreement between our NNLO HTLpt results and lattice data down to temperatures on the order of 250 MeV.

This chapter is organized as follows. In Sec. (5.1) we discuss the diagrams that contribute to the HTL perturbation theory thermodynamic potential through NNLO. In Sec. (5.2) the necessary diagrams are reduced to scalar sum-integrals and expanded in powers of m_D/T and m_q/T . We list the necessary non-trivial sum-integrals and d -dimensional integrals in Secs. (5.3) and (5.4) respectively. In Sec. (5.5) we present our final results for the NNLO thermodynamic potential. In Sec. (5.6) we discuss the mass prescription for the in-medium masses m_D and m_q . We present our results for the thermodynamic functions and compare them with results from lattice gauge simulations in Sec. (5.7). In Sec. (5.8) we present our results for the second-, fourth-, and sixth-order baryon and quark number susceptibilities and compare them with results from lattice QCD data. In Sec. (5.9) we summarize and conclude.

5.1 Contributions to the HTLpt thermodynamic potential through NNLO

The diagrams needed for the computation of the HTLpt thermodynamic potential through NNLO are listed in Figs. (5.1) and (5.2). The shorthand notations used in Fig. (5.2) have been explained in Fig. (5.3).

In Ref. [178] the authors computed the NNLO thermodynamic potential at zero

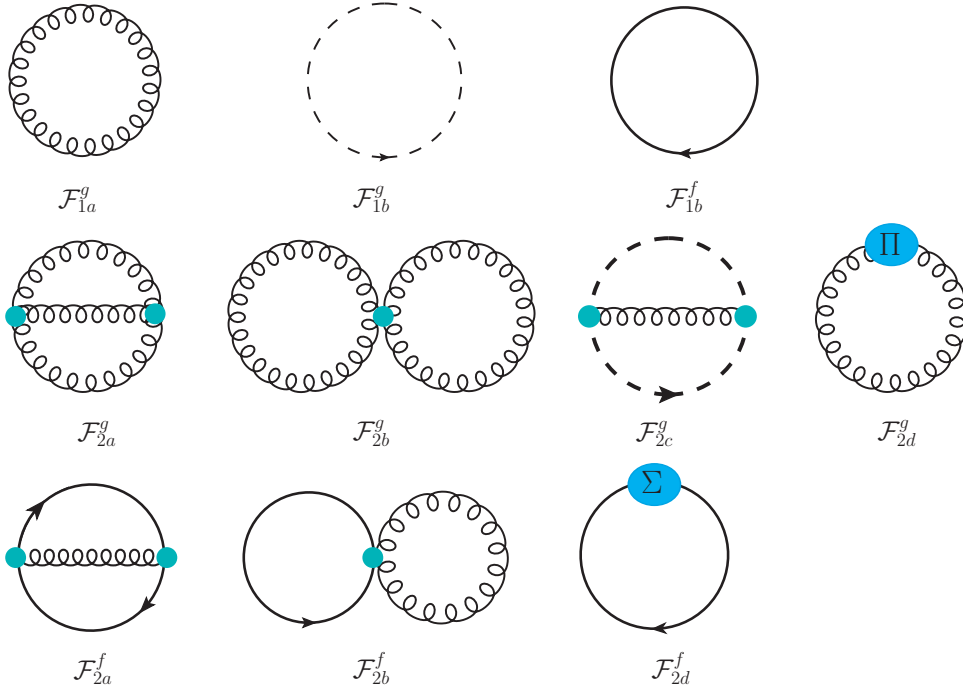


Figure 5.1: One and two loop Feynman diagrams that will contribute to the thermodynamic potential.

chemical potential. Here we extend the NNLO calculation to finite chemical potential. For this purpose, one needs to only consider diagrams which contain at least one quark propagator; however, for completeness we also list the purely gluonic contributions below. In the results we will express thermodynamic quantities in terms of dimensionless variables: $\hat{m}_D = m_D/(2\pi T)$, $\hat{m}_q = m_q/(2\pi T)$, $\hat{\mu} = \mu/(2\pi T)$, $\hat{\Lambda} = \Lambda/(2\pi T)$ and $\hat{\Lambda}_g = \Lambda_g/(2\pi T)$ where Λ and Λ_g are renormalization scale scales for gluon and fermion respectively as discussed in Sec. (5.7.1).

The complete NNLO HTLpt thermodynamic potential can be expressed in terms of each diagrams of Figs. (5.1) and (5.2) as

$$\begin{aligned}
 \Omega_{\text{NNLO}} = & d_A [\mathcal{F}_{1a}^g + \mathcal{F}_{1b}^g + \mathcal{F}_{2d}^g + \mathcal{F}_{3m}^g] + d_F [\mathcal{F}_{1b}^f + \mathcal{F}_{2d}^f + \mathcal{F}_{3i}^f] \\
 & + d_{ACA} [\mathcal{F}_{2a}^g + \mathcal{F}_{2b}^g + \mathcal{F}_{2c}^g + \mathcal{F}_{3h}^g + \mathcal{F}_{3i}^g + \mathcal{F}_{3j}^g + \mathcal{F}_{3k}^g + \mathcal{F}_{3l}^g] \\
 & + d_{ASF} [\mathcal{F}_{2a}^f + \mathcal{F}_{2b}^f + \mathcal{F}_{3d}^f + \mathcal{F}_{3e}^f + \mathcal{F}_{3f}^f + \mathcal{F}_{3g}^f + \mathcal{F}_{3k}^f + \mathcal{F}_{3l}^f] \\
 & + d_{AC_A^2} [\mathcal{F}_{3a}^g + \mathcal{F}_{3b}^g + \mathcal{F}_{3c}^g + \mathcal{F}_{3d}^g + \mathcal{F}_{3e}^g + \mathcal{F}_{3f}^g + \mathcal{F}_{3g}^g] + d_{AS_{2F}} [\mathcal{F}_{3a}^f + \mathcal{F}_{3b}^f] \\
 & + d_{ACA_{SF}} \left[-\frac{1}{2} \mathcal{F}_{3a}^f + \mathcal{F}_{3m}^f + \mathcal{F}_{3n}^f + \mathcal{F}_{3o}^f \right] + d_{AS_F^2} [\mathcal{F}_{3c}^f + \mathcal{F}_{3j}^f] \\
 & + \Delta_0 \mathcal{E}_0 + \Delta_1 \mathcal{E}_0 + \Delta_2 \mathcal{E}_0 + \Delta_1 m_D^2 \frac{\partial}{\partial m_D^2} \Omega_{\text{LO}} + \Delta_1 m_q^2 \frac{\partial}{\partial m_q^2} \Omega_{\text{LO}} \\
 & + \Delta_2 m_D^2 \frac{\partial}{\partial m_D^2} \Omega_{\text{LO}} + \Delta_2 m_q^2 \frac{\partial}{\partial m_q^2} \Omega_{\text{LO}} + \Delta_1 m_D^2 \frac{\partial}{\partial m_D^2} \Omega_{\text{NLO}} \\
 & + \Delta_1 m_q^2 \frac{\partial}{\partial m_q^2} \Omega_{\text{NLO}} + \frac{1}{2} \left[\frac{\partial^2}{(\partial m_D^2)^2} \Omega_{\text{LO}} \right] (\Delta_1 m_D^2)^2 \\
 & + \frac{1}{2} \left[\frac{\partial^2}{(\partial m_q^2)^2} \Omega_{\text{LO}} \right] (\Delta_1 m_q^2)^2 + d_A \left[\frac{c_A \mathcal{F}_{2a+2b+2c}^g + s_F \mathcal{F}_{2a+2b}^f}{\alpha_s} \right] \Delta_1 \alpha_s, \quad (5.1)
 \end{aligned}$$

where the necessary counterterms at any order in δ can be calculated using the following counter terms

$$\Delta \mathcal{E}_0 = \frac{d_A}{128\pi^2\epsilon} (1-\delta)^2 m_D^4, \quad (5.2)$$

$$\Delta m_D^2 = \frac{11c_A - 4s_F}{12\pi\epsilon} \alpha_s \delta (1-\delta) m_D^2, \quad (5.3)$$

$$\Delta m_q^2 = \frac{3}{8\pi\epsilon} \frac{d_A}{c_A} \alpha_s \delta (1-\delta) m_q^2, \quad (5.4)$$

$$\delta \Delta \alpha_s = -\frac{11c_A - 4s_F}{12\pi\epsilon} \alpha_s^2 \delta^2, \quad (5.5)$$

The expressions for the one- and two-loop diagrams above can be found in Refs. [172, 173]. The expressions for the three-loop bosonic diagrams $\mathcal{F}_{3a}^g - \mathcal{F}_{3m}^g$ are presented in section 3 of Ref. [175]. The three-loop diagrams specific to QCD, i.e. the non-

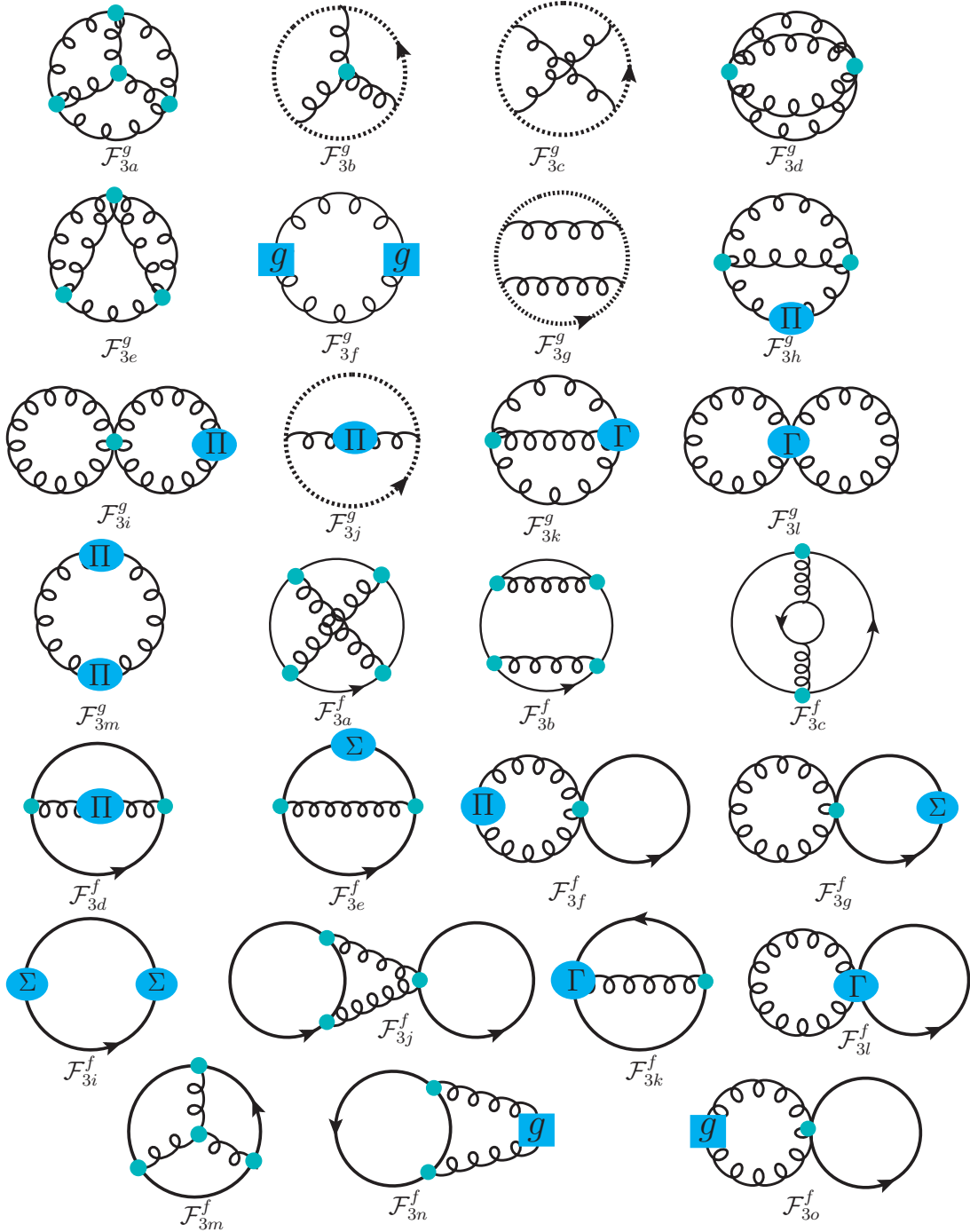


Figure 5.2: Three loop HTL Feynman diagrams that will contribute to the thermodynamic potential.

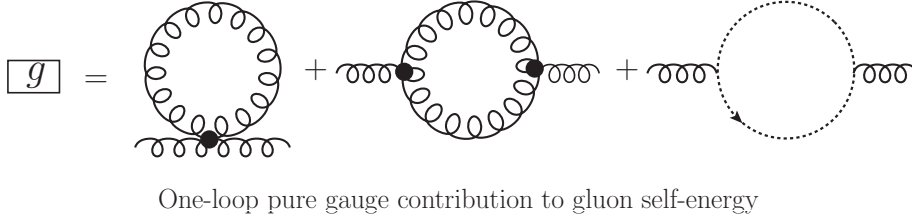
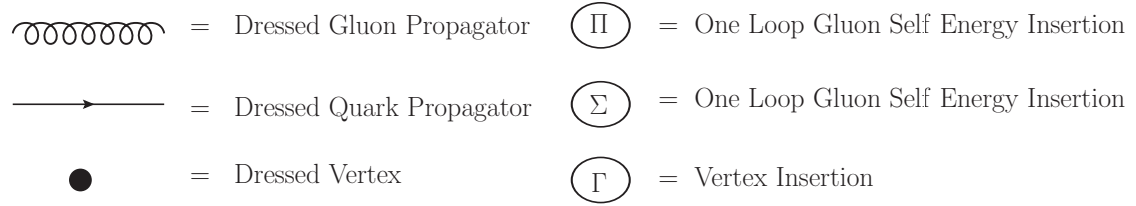


Figure 5.3: The shorthand notations used in Fig. (5.2).

Abelian diagrams involving quarks, are given by

$$\mathcal{F}_{3a}^f = \frac{1}{4}g^4 \sum_{P\{QR\}} \text{Tr} [\Gamma^\mu(-P, Q-P, Q)S(Q)\Gamma^\alpha(Q-R, Q, R)S(R)\Gamma^\nu(P, R, R-P) \\ \times S(R-P)\Gamma^\beta(-Q+R, R-P, Q-P)S(Q-P)] \Delta_{\mu\nu}(P)\Delta_{\alpha\beta}(Q-R), \quad (5.6)$$

$$\mathcal{F}_{3b}^f = \frac{1}{2}g^4 \sum_{P\{QR\}} \text{Tr} [\Gamma^\mu(P, P+Q, Q)S(Q)\Gamma^\beta(-R+Q, Q, R)S(R)\Gamma^\alpha(R-Q, R, Q) \\ \times S(Q)\Gamma^\nu(-P, Q, P+Q)S(P+Q)] \Delta_{\mu\nu}(P)\Delta_{\alpha\beta}(R-Q), \quad (5.7)$$

$$\mathcal{F}_{3c}^f = -\frac{1}{4}g^4 \sum_{P\{QR\}} \text{Tr} [\Gamma^\mu(P, P+Q, Q)S(Q)\Gamma^\beta(-P, Q, P+Q)S(P+Q)] \\ \times \text{Tr} [\Gamma^\nu(-P, R, P+R)S(P+R)\Gamma^\alpha(P, P+R, R)S(R)] \Delta^{\mu\nu}(P)\Delta^{\alpha\beta}(P), \quad (5.8)$$

$$\mathcal{F}_{3j}^f = -\frac{1}{2}g^4 \sum_{P\{QR\}} \text{Tr} [\Gamma^{\alpha\beta}(P, -P, R, R)S(R)] \Delta^{\alpha\mu}(P)\Delta^{\beta\nu}(P) \\ \times \text{Tr} [\Gamma^\mu(P, P+Q, Q)S(Q)\Gamma^\nu(-P, Q, P+Q)S(P+Q)], \quad (5.9)$$

$$\mathcal{F}_{3m}^f = \frac{1}{6} \sum_{\{PQR\}} \text{Tr} [\Gamma^\alpha(R-P, R, P)S(P)\Gamma^\beta(P-Q, P, Q)S(Q)\Gamma^\gamma(Q-R, Q, R)S(R)] \\ \times \Gamma^{\mu\nu\delta}(P-R, Q-P, R-Q)\Delta^{\alpha\mu}(P-R)\Delta^{\beta\nu}(Q-P)\Delta^{\gamma\delta}(R-Q), \quad (5.10)$$

$$\mathcal{F}_{3n}^f = - \sum_P \bar{\Pi}_g^{\mu\nu}(P)\Delta^{\nu\alpha}(P)\bar{\Pi}_f^{\alpha\beta}(P)\Delta^{\beta\mu}(P), \quad (5.11)$$

$$\mathcal{F}_{3o}^f = -\frac{1}{2}g^2 \sum_{P\{Q\}} \text{Tr} [\Gamma^{\alpha\beta}(P, -P, Q, Q)S(Q)] \Delta^{\alpha\mu}(P)\Delta^{\beta\nu}(P)\bar{\Pi}_g^{\mu\nu}(P), \quad (5.12)$$

where

$$\begin{aligned}
 \bar{\Pi}_g^{\mu\nu}(P) &= \frac{1}{2}g^2 \not\int_Q \Gamma^{\mu\nu,\alpha\beta}(P, -P, Q, -Q)\Delta^{\alpha\beta}(Q) \\
 &+ \frac{1}{2}g^2 \not\int_Q \Gamma^{\mu\alpha\beta}(P, Q, -P - Q)\Delta^{\alpha\beta}(Q)\Gamma^{\nu\gamma\delta}(P, Q, -P - Q)\Delta^{\gamma\delta}(-P - Q) \\
 &+ g^2 \not\int_Q \frac{Q^\mu(P + Q)^\nu}{Q^2(P + Q)^2}, \tag{5.13}
 \end{aligned}$$

$$\bar{\Pi}_f^{\mu\nu}(P) = -g^2 \not\int_{\{Q\}} \text{Tr} [\Gamma^\mu(P, Q, Q - P)S(Q)\Gamma^\nu(P, Q, Q - P)S(Q - P)]. \tag{5.14}$$

Thus $\bar{\Pi}^{\mu\nu}(P)$ is the one-loop gluon self-energy with HTL-resummed propagators and vertices:

$$\bar{\Pi}^{\mu\nu}(P) = c_A \bar{\Pi}_g^{\mu\nu}(P) + s_F \bar{\Pi}_f^{\mu\nu}(P). \tag{5.15}$$

5.2 Expansion in mass parameters

In Refs. [172, 173] the NLO HTLpt thermodynamic potential was reduced to scalar sum-integrals. Evaluating these scalar sum-integrals exactly seems intractable, however, the sum-integrals can be calculated approximately by expanding them in powers of m_D/T and m_q/T following the method developed in Ref. [188]. We will adopt the same strategy in this chapter and include all terms through order g^5 assuming that m_D and m_q are $\mathcal{O}(g)$ at leading order. At each loop order, the contributions can be divided into those coming from hard and soft momenta, which are the momenta proportional to the scales T and gT respectively. In the one-loop diagrams, the contributions are either hard (h) or soft (s), while at the two-loop level, there are hard-hard (hh), hard-soft (hs), and soft-soft (ss) contributions. At three loops there are hard-hard-hard (hhh), hard-hard-soft (hhs), hard-soft-soft (hss), and soft-soft-soft (sss) contributions.

5.2.1 One-loop sum-integrals

We now review the mass expansion of the necessary one-loop sum-integrals considering separately the contributions from hard and soft momenta. We list the purely gluonic contributions when they are necessary for simpler exposition of the final result. Note that in order to simplify the results, when possible, it is best to add the corresponding iterated polarization and self-energy insertions that appear at higher order in δ , e.g. below we will also include \mathcal{F}_{2d}^g , \mathcal{F}_{2d}^f , \mathcal{F}_{3m}^g , and \mathcal{F}_{3i}^f as “one-loop” contributions.

Hard contributions

For one loop gluon (\mathcal{F}_{1a}^g) and one loop ghost (\mathcal{F}_{1b}^g) diagrams, we need to expand in order m_D^2 :

$$\begin{aligned} \mathcal{F}_{1a+1b}^{g(h)} &= \frac{1}{2}(d-1) \not\sum_P \ln P^2 + \frac{1}{2}m_D^2 \not\sum_P \frac{1}{P^2} \\ &- \frac{1}{4(d-1)}m_D^4 \not\sum_P \left[\frac{1}{P^4} - \frac{2}{p^2P^2} - \frac{2d}{p^4}\mathcal{T}_P + \frac{2}{p^2P^2}\mathcal{T}_P + \frac{d}{p^4}\mathcal{T}_P^2 \right]. \end{aligned} \quad (5.16)$$

The one-loop graph with a gluon self-energy insertion (\mathcal{F}_{2d}^g) has an explicit factor of m_D^2 and, therefore, we only need to expand the sum-integral to first order in m_D^2 :

$$\begin{aligned} \mathcal{F}_{2d}^{g(h)} &= -\frac{1}{2}m_D^2 \not\sum_P \frac{1}{P^2} \\ &+ \frac{1}{2(d-1)}m_D^4 \not\sum_P \left[\frac{1}{P^4} - \frac{2}{p^2P^2} - \frac{2d}{p^4}\mathcal{T}_P + \frac{2}{p^2P^2}\mathcal{T}_P + \frac{d}{p^4}\mathcal{T}_P^2 \right]. \end{aligned} \quad (5.17)$$

The one-loop graph with two gluon self-energy insertions (\mathcal{F}_{3m}^g) must be expanded to zeroth order in m_D^2

$$\mathcal{F}_{3m}^{g(h)} = -\frac{1}{4(d-1)}m_D^4 \not\sum_P \left[\frac{1}{P^4} - \frac{2}{p^2P^2} - \frac{2d}{p^4}\mathcal{T}_P + \frac{2}{p^2P^2}\mathcal{T}_P + \frac{d}{p^4}\mathcal{T}_P^2 \right]. \quad (5.18)$$

The sum of Eqs. (5.16)-(5.18) is very simple

$$\mathcal{F}_{1a+1b+2d+3m}^{g(h)} = \frac{1}{2}(d-1) \sum_P \ln(P^2) = -\frac{\pi^2}{45} T^4. \quad (5.19)$$

This is the free energy of an ideal gas consisting of a single massless boson.

The one-loop fermionic graph \mathcal{F}_{1b}^f needs to be expanded to second order in m_q^2 :

$$\begin{aligned} \mathcal{F}_{1b}^{f(h)} &= -2 \sum_{\{P\}} \ln P^2 - 4m_q^2 \sum_{\{P\}} \frac{1}{P^2} \\ &\quad + 2m_q^4 \sum_{\{P\}} \left[\frac{2}{P^4} - \frac{1}{p^2 P^2} + \frac{2}{p^2 P^2} \mathcal{T}_P - \frac{1}{p^2 P_0^2} \mathcal{T}_P^2 \right]. \end{aligned} \quad (5.20)$$

The one-loop fermion loop with a fermion self-energy insertion \mathcal{F}_{2d}^f must be expanded to first order in m_q^2 :

$$\mathcal{F}_{2d}^{f(h)} = 4m_q^2 \sum_{\{P\}} \frac{1}{P^2} - 4m_q^4 \sum_{\{P\}} \left[\frac{2}{P^4} - \frac{1}{p^2 P^2} + \frac{2}{p^2 P^2} \mathcal{T}_P - \frac{1}{p^2 P_0^2} \mathcal{T}_P^2 \right]. \quad (5.21)$$

The one-loop fermion loop with two self-energy insertions \mathcal{F}_{3i}^f must be expanded to zeroth order in m_q^2 :

$$\mathcal{F}_{3i}^{f(h)} = 2m_q^4 \sum_{\{P\}} \left[\frac{2}{P^4} - \frac{1}{p^2 P^2} + \frac{2}{p^2 P^2} \mathcal{T}_P - \frac{1}{p^2 P_0^2} \mathcal{T}_P^2 \right]. \quad (5.22)$$

The sum of Eqs. (5.20)-(5.22) is particularly simple

$$\begin{aligned} \mathcal{F}_{1b+2d+3i}^{f(h)} &= -2 \sum_{\{P\}} \ln P^2 \\ &= -\frac{7\pi^2}{180} T^4 \left[1 + \frac{120}{7} \hat{\mu}^2 + \frac{240}{7} \hat{\mu}^4 \right]. \end{aligned} \quad (5.23)$$

This is the free energy of an ideal gas consisting of a single massless fermion.

Soft contributions

The soft contributions in the diagrams \mathcal{F}_{1a+1b}^g , \mathcal{F}_{2d}^g , and \mathcal{F}_{3m}^g arise from the $P_0 = 0$ term in the sum-integral. At soft momentum $P = (0, \mathbf{p})$, the HTL self-energy functions reduce to $\Pi_T(P) = 0$ and $\Pi_L(P) = m_D^2$. The transverse term vanishes in dimensional regularization because there is no momentum scale in the integral over \mathbf{p} . Thus the soft contributions come from the longitudinal term only and read

$$\mathcal{F}_{1a+1b}^{g(s)} = \frac{1}{2}T \int_p \ln(p^2 + m_D^2) = -\frac{m_D^3 T}{12\pi} \left(\frac{\Lambda_g}{2m_D}\right)^{2\epsilon} \left[1 + \frac{8}{3}\epsilon\right], \quad (5.24)$$

$$\mathcal{F}_{2d}^{g(s)} = -\frac{1}{2}m_D^2 T \int_p \frac{1}{p^2 + m_D^2} = \frac{m_D^3 T}{8\pi} \left(\frac{\Lambda_g}{2m_D}\right)^{2\epsilon} [1 + 2\epsilon], \quad (5.25)$$

$$\mathcal{F}_{3m}^{g(s)} = -\frac{1}{4}m_D^4 T \int_p \frac{1}{(p^2 + m_D^2)^2} = -\frac{m_D^3 T}{32\pi}. \quad (5.26)$$

The total soft contribution from Eqs. (5.24)-(5.26) is

$$\mathcal{F}_{1a+1b+2d+3m}^{g(s)} = -\frac{m_D^3 T}{96\pi} \left(\frac{\Lambda_g}{2m_D}\right)^{2\epsilon} \left[1 + \frac{8}{3}\epsilon\right]. \quad (5.27)$$

There are no soft contributions from the leading-order fermion diagrams or HTL counterterms (polarization and self-energy insertions).

5.2.2 Two-loop sum-integrals

For hard momenta, the self-energies are suppressed by m_D/T and m_q/T relative to the inverse free propagators, so we can expand in powers of Π_T , Π_L , and Σ . As was the case for the one-loop contributions, we once again treat the polarization and self-energy insertion NNLO diagrams as two-loop graphs in order to simplify the resulting expressions.

Hard-hard (hh) contribution

We first consider the contribution from fermionic diagrams. The (hh) contribution from \mathcal{F}_{2a}^f and \mathcal{F}_{2b}^f reads

$$\begin{aligned}
 \mathcal{F}_{2a+2b}^{f(hh)} = & (d-1)g^2 \left[\sum_{\{PQ\}} \frac{1}{P^2Q^2} - \sum_{P\{Q\}} \frac{2}{P^2Q^2} \right] \\
 & + 2m_D^2g^2 \sum_{P\{Q\}} \left[\frac{1}{p^2P^2Q^2} \mathcal{T}_P + \frac{1}{P^4Q^2} - \frac{d-2}{d-1} \frac{1}{p^2P^2Q^2} \right] \\
 & + m_D^2g^2 \sum_{\{PQ\}} \left[\frac{d+1}{d-1} \frac{1}{P^2Q^2r^2} - \frac{4d}{d-1} \frac{q^2}{P^2Q^2r^4} - \frac{2d}{d-1} \frac{P \cdot Q}{P^2Q^2r^4} \right] \mathcal{T}_R \\
 & + m_D^2g^2 \sum_{\{PQ\}} \left[\frac{3-d}{d-1} \frac{1}{P^2Q^2R^2} + \frac{2d}{d-1} \frac{P \cdot Q}{P^2Q^2r^4} - \frac{d+2}{d-1} \frac{1}{P^2Q^2r^2} \right. \\
 & \left. + \frac{4d}{d-1} \frac{q^2}{P^2Q^2r^4} - \frac{4}{d-1} \frac{q^2}{P^2Q^2r^2R^2} \right] + 2m_q^2g^2(d-1) \sum_{\{PQ\}} \left[\frac{d+3}{d-1} \frac{1}{P^2Q^2R^2} \right. \\
 & \left. - \frac{2}{P^2Q^4} + \frac{r^2-p^2}{q^2P^2Q^2R^2} \right] + 2m_q^2g^2(d-1) \sum_{\{PQ\}} \left[\frac{1}{P^2Q_0^2Q^2} + \frac{p^2-r^2}{P^2q^2Q_0^2R^2} \right] \mathcal{T}_Q \\
 & + 2m_q^2g^2(d-1) \sum_{P\{Q\}} \left[\frac{2}{P^2Q^4} - \frac{1}{P^2Q_0^2Q^2} \mathcal{T}_Q \right]. \tag{5.28}
 \end{aligned}$$

We consider next the (hh) contributions from \mathcal{F}_{3d}^f and \mathcal{F}_{3f}^f . The easiest way to calculate these term, is to expand the two-loop diagrams \mathcal{F}_{2a}^f and \mathcal{F}_{2b}^f to first order in m_D^2 . This yields

$$\begin{aligned}
 \mathcal{F}_{3d+3f}^{f(hh)} = & -2m_D^2g^2 \sum_{P\{Q\}} \left[\frac{1}{p^2P^2Q^2} \mathcal{T}_P + \frac{1}{P^4Q^2} - \frac{d-2}{d-1} \frac{1}{p^2P^2Q^2} \right] \\
 & - m_D^2g^2 \sum_{\{PQ\}} \left[\frac{d+1}{d-1} \frac{1}{P^2Q^2r^2} - \frac{4d}{d-1} \frac{q^2}{P^2Q^2r^4} - \frac{2d}{d-1} \frac{P \cdot Q}{P^2Q^2r^4} \right] \mathcal{T}_R \\
 & - m_D^2g^2 \sum_{\{PQ\}} \left[\frac{3-d}{d-1} \frac{1}{P^2Q^2R^2} + \frac{2d}{d-1} \frac{P \cdot Q}{P^2Q^2r^4} - \frac{d+2}{d-1} \frac{1}{P^2Q^2r^2} \right. \\
 & \left. + \frac{4d}{d-1} \frac{q^2}{P^2Q^2r^4} - \frac{4}{d-1} \frac{q^2}{P^2Q^2r^2R^2} \right]. \tag{5.29}
 \end{aligned}$$

Next we consider the (hh) contribution from the diagrams $\mathcal{F}_{3e}^f, \mathcal{F}_{3g}^f, \mathcal{F}_{3k}^f$ and \mathcal{F}_{3l}^f

$$\begin{aligned}
 \mathcal{F}_{3e+3g+3k+3l}^{f(hh)} &= -2m_q^2 g^2 (d-1) \sum_{\{PQ\}} \left[\frac{1}{P^2 Q_0^2 Q^2} + \frac{p^2 - r^2}{P^2 q^2 Q_0^2 R^2} \right] \mathcal{T}_Q \\
 &\quad - 2m_q^2 g^2 (d-1) \sum_{P\{Q\}} \left[\frac{2}{P^2 Q^4} + \frac{1}{P^2 Q_0^2 Q^2} \mathcal{T}_Q \right] \\
 &\quad - 2m_q^2 g^2 (d-1) \sum_{\{PQ\}} \left[\frac{d+3}{d-1} \frac{1}{P^2 Q^2 R^2} - \frac{2}{P^2 Q^4} + \frac{r^2 - p^2}{q^2 P^2 Q^2 R^2} \right]. \quad (5.30)
 \end{aligned}$$

The sum of Eqs.(5.28)-(5.30) is

$$\begin{aligned}
 \mathcal{F}_{2a+2b+3d+3e+3f+3g+3k+3l}^{f(hh)} &= (d-1)g^2 \left[\sum_{\{PQ\}} \frac{1}{P^2 Q^2} - \sum_{P\{Q\}} \frac{2}{P^2 Q^2} \right] \\
 &= \frac{\pi^2}{72} \frac{\alpha_s}{\pi} T^4 (1 + 12\hat{\mu}^2) (5 + 12\hat{\mu}^2). \quad (5.31)
 \end{aligned}$$

For completeness, the (hh) contribution coming from two-loop pure-gluon diagrams is [175]

$$\mathcal{F}_{2a+2b+2c+3h+3i+3j+3k+3l}^{g(hh)} = \frac{1}{4} (d-1)^2 g^2 \sum_{PQ} \frac{1}{P^2 Q^2} = \frac{\pi^2}{36} \frac{\alpha_s}{\pi} T^4 \quad (5.32)$$

Hard-soft (hs) contribution

In the (hs) region, one gluon momentum is soft but the fermionic momentum is always hard. The terms that contribute through order $g^2 m_D^3 T$ and $g^2 m_q^2 m_D T$ from \mathcal{F}_{2a}^f and \mathcal{F}_{2b}^f were calculated in Ref. [15, 172, 173] and read

$$\begin{aligned}
 \mathcal{F}_{2a+2b}^{f(hs)} &= 2g^2 T \int_p \frac{1}{p^2 + m_D^2} \sum_{\{Q\}} \left[\frac{1}{Q^2} - \frac{2q^2}{Q^4} \right] \\
 &\quad + 2m_D^2 g^2 T \int_p \frac{1}{p^2 + m_D^2} \sum_{\{Q\}} \left[\frac{1}{Q^4} - \frac{2}{d} (3+d) \frac{q^2}{Q^6} + \frac{8}{d} \frac{q^4}{Q^8} \right] \\
 &\quad - 4m_q^2 g^2 T \int_p \frac{1}{p^2 + m_D^2} \sum_{\{Q\}} \left[\frac{3}{Q^4} - \frac{4q^2}{Q^6} - \frac{4}{Q^4} \mathcal{T}_Q - \frac{2}{Q^2} \left\langle \frac{1}{(Q \cdot Y)^2} \right\rangle_{\hat{y}} \right]. \quad (5.33)
 \end{aligned}$$

The (hs) contribution from diagrams \mathcal{F}_{3d}^f and \mathcal{F}_{3f}^f can again be calculated from the diagrams \mathcal{F}_{2a}^f and \mathcal{F}_{2b}^f by Taylor expanding their contribution to first order in m_D^2 .

This yields

$$\begin{aligned} \mathcal{F}_{3d+3f}^{f(hs)} &= 2m_D^2 g^2 T \int_p \frac{1}{(p^2 + m_D^2)^2} \not\sum_{\{Q\}} \left[\frac{1}{Q^2} - \frac{2q^2}{Q^4} \right] \\ &\quad - 2m_D^2 g^2 T \int_p \frac{p^2}{(p^2 + m_D^2)^2} \not\sum_{\{Q\}} \left[\frac{1}{Q^4} - \frac{2}{d}(3+d) \frac{q^2}{Q^6} + \frac{8}{d} \frac{q^4}{Q^8} \right] \\ &\quad - 4m_D^2 m_q^2 g^2 T \int_p \frac{1}{(p^2 + m_D^2)^2} \not\sum_{\{Q\}} \left[\frac{3}{Q^4} - \frac{4q^2}{Q^6} - \frac{4}{Q^4} \mathcal{T}_Q - \frac{2}{Q^2} \left\langle \frac{1}{(Q \cdot Y)^2} \right\rangle_{\hat{y}} \right]. \end{aligned} \quad (5.34)$$

We also need the (hs) contributions from the diagrams $\mathcal{F}_{3e}^f, \mathcal{F}_{3g}^f, \mathcal{F}_{3k}^f$ and \mathcal{F}_{3l}^f . Again we calculate these contributions by expanding the two-loop diagrams \mathcal{F}_{2a}^f and \mathcal{F}_{2b}^f to first order in m_q^2 . This yields

$$\mathcal{F}_{3e+3g+3k+3l}^{f(hs)} = 4m_q^2 g^2 T \int_p \frac{1}{p^2 + m_D^2} \not\sum_{\{Q\}} \left[\frac{3}{Q^4} - \frac{4q^2}{Q^6} - \frac{4}{Q^4} \mathcal{T}_Q - \frac{2}{Q^2} \left\langle \frac{1}{(Q \cdot Y)^2} \right\rangle_{\hat{y}} \right]. \quad (5.35)$$

The sum of Eqs. (5.33)-(5.35) is

$$\begin{aligned} &\mathcal{F}_{2a+2b+3d+3e+3f+3g+3k+3l}^{f(hs)} \\ &= 2g^2 T \left[\int_p \frac{1}{p^2 + m_D^2} + m_D^2 \int_p \frac{1}{(p^2 + m_D^2)^2} \right] \not\sum_{\{Q\}} \left[\frac{1}{Q^2} - \frac{2q^2}{Q^4} \right] \\ &\quad + 2g^2 m_D^2 T \left[\int_p \frac{1}{p^2 + m_D^2} - \int_p \frac{p^2}{(p^2 + m_D^2)^2} \right] \not\sum_{\{Q\}} \left[\frac{1}{Q^4} - \frac{2}{d}(3+d) \frac{q^2}{Q^6} + \frac{8}{d} \frac{q^4}{Q^8} \right] \\ &\quad - 4m_q^2 m_D^2 T \int_p \frac{1}{(p^2 + m_D^2)^2} \not\sum_{\{Q\}} \left[\frac{3}{Q^4} - \frac{4q^2}{Q^6} - \frac{4}{Q^4} \mathcal{T}_Q - \frac{2}{Q^2} \left\langle \frac{1}{(Q \cdot Y)^2} \right\rangle_{\hat{y}} \right] \\ &= -2(d-1)g^2 T \left[\int_p \frac{1}{p^2 + m_D^2} + m_D^2 \int_p \frac{1}{(p^2 + m_D^2)^2} \right] \not\sum_{\{Q\}} \frac{1}{Q^2} \\ &\quad - \frac{d-1}{3} g^2 m_D^4 T \int_p \frac{1}{(p^2 + m_D^2)^2} \not\sum_{\{Q\}} \frac{1}{Q^4} - 8 \frac{d-3}{d-1} g^2 m_q^2 m_D^2 T \int_p \frac{1}{(p^2 + m_D^2)^2} \not\sum_{\{Q\}} \frac{1}{Q^4}. \end{aligned} \quad (5.36)$$

Using the results from Secs. (5.3) and (5.4), Eq. (5.36) can be written as

$$\begin{aligned} \mathcal{F}_{2a+2b+3d+3e+3f+3g+3k+3l}^{f(hs)} &= -\frac{1}{12}\alpha_s (1 + 12\hat{\mu}^2) m_D T^3 - \frac{\alpha_s}{4\pi^2} m_q^2 m_D^2 T \\ &\quad - \frac{\alpha_s}{48\pi^2} \left[\frac{1}{\epsilon} - 1 - \aleph(z) \right] \left(\frac{\Lambda}{4\pi T} \right)^{2\epsilon} \left(\frac{\Lambda}{2m_D} \right)^{2\epsilon} \end{aligned} \quad (5.37)$$

where $\aleph(z) = \Psi(z) + \Psi(z^*)$ with $z = 1/2 - i\hat{\mu}$ and Ψ being the digamma function (see app. A for more details and useful properties of $\aleph(z)$).

5.2.3 Three-loop sum-integrals

We now list the mass-expanded sum-integrals necessary at three-loops. As before we organize the contributions according to whether the momentum flowing in a given propagator is hard or soft.

Hard-hard-hard (hhh) contribution

The (hhh) contributions from diagrams \mathcal{F}_{3a}^f and \mathcal{F}_{3b}^f which are defined in Eqs. (5.6) and (5.7) can be written as

$$\begin{aligned} \mathcal{F}_{3a}^{f(hhh)} &= g^4(d-1) \left[4 \left(\not\int_P \frac{1}{P^2} - 2 \not\int_{\{P\}} \frac{1}{P^2} \right) \not\int_{\{QR\}} \frac{1}{Q^2 R^2 (Q+R)^2} \right. \\ &\quad \left. - \frac{1}{2}(d-7) \not\int_{\{PQR\}} \frac{1}{P^2 Q^2 R^2 (P+Q+R)^2} \right. \\ &\quad \left. + (d-3) \not\int_{\{PQR\}} \frac{1}{P^2 Q^2 (P-R)^2 (Q-R)^2} + 2 \not\int_{\{PQ\}R} \frac{(P-Q)^2}{P^2 Q^2 R^2 (P-R)^2 (Q-R)^2} \right] \\ &= g^4(d-1) \left\{ 4 \left(\mathcal{I}_1^0 - 2\tilde{\mathcal{I}}_1^0 \right) \tilde{\tau} - \frac{1}{2} (d-7) \mathcal{N}_{0,0} + (d-3) \widetilde{\mathcal{M}}_{0,0} + 2\mathcal{N}_{1,-1} \right\}. \end{aligned} \quad (5.38)$$

$$\begin{aligned}
 \mathcal{F}_{3b}^{f(hhh)} &= -g^4(d-1)^2 \left[\left(\sum_P \frac{1}{P^2} - \sum_{\{P\}} \frac{1}{P^2} \right)^2 \sum_{\{P\}} \frac{1}{P^4} - 2 \sum_{\{PQR\}} \frac{1}{P^2 Q^2 R^2 (Q+R)^2} \right. \\
 &\quad \left. + \sum_{\{PQR\}} \frac{1}{P^2 Q^2 (P-R)^2 (Q-R)^2} + \sum_{\{PQR\}} \frac{(P-Q)^2}{P^2 Q^2 R^2 (P-R)^2 (Q-R)^2} \right] \\
 &= -g^4(d-1)^2 \left\{ \left(\mathcal{I}_1^0 - \tilde{\mathcal{I}}_1^0 \right)^2 \tilde{\mathcal{I}}_2^0 - 2\tilde{\mathcal{I}}_1^0 \tilde{\tau} + \tilde{\mathcal{M}}_{0,0} + \tilde{\mathcal{M}}_{1,-1} \right\}. \quad (5.39)
 \end{aligned}$$

Using the results of sum-integrals from Sec. (5.3), the hhh contribution of the sum of \mathcal{F}_{3a}^f and \mathcal{F}_{3b}^f from Eqs. (5.38) and (5.39) can be written as

$$\begin{aligned}
 \mathcal{F}_{3a}^{f(hhh)} + \mathcal{F}_{3b}^{f(hhh)} &= \frac{\alpha_s^2 T^4}{192} \left[35 - 32 \frac{\zeta'(-1)}{\zeta(-1)} + 472 \hat{\mu}^2 + 384 \frac{\zeta'(-1)}{\zeta(-1)} \hat{\mu}^2 + 1328 \hat{\mu}^4 \right. \\
 &\quad \left. - 64 \left(36i \hat{\mu} \aleph(2, z) - 6(1 + 8\hat{\mu}^2) \aleph(1, z) - 3i \hat{\mu} (1 + 4\hat{\mu}^2) \aleph(0, z) \right) \right]. \quad (5.40)
 \end{aligned}$$

where $\aleph(n, z)$ is defined in appendix (A).

Hard-hard-hard contribution from the term \mathcal{F}_{3c}^f that has been defined in Eq. (5.8) can be written as

$$\begin{aligned}
 \mathcal{F}_{3c}^{f(hhh)} &= -\frac{5\alpha_s^2}{216} T^4 \left(\frac{\Lambda}{4\pi T} \right)^{6\epsilon} \left[\left(1 + \frac{72}{5} \hat{\mu}^2 + \frac{144}{5} \hat{\mu}^4 \right) \frac{1}{\epsilon} + \frac{31}{10} + \frac{6}{5} \gamma_E \right. \\
 &\quad - \frac{68}{25} \frac{\zeta'(-3)}{\zeta(-3)} + \frac{12}{5} (25 + 12\gamma_E) \hat{\mu}^2 + 120 \hat{\mu}^4 - \frac{8}{5} (1 + 12\hat{\mu}^2) \frac{\zeta'(-1)}{\zeta(-1)} \\
 &\quad - \frac{144}{5} \left[8\aleph(3, z) + 3\aleph(3, 2z) + 12i\hat{\mu} (\aleph(2, z) + \aleph(2, 2z)) \right. \\
 &\quad \left. \left. - (3 + 20\hat{\mu}^2) \aleph(1, z) - i\hat{\mu} (1 + 12\hat{\mu}^2) \aleph(0, z) - 12\hat{\mu}^2 \aleph(1, 2z) \right] \right], \quad (5.41)
 \end{aligned}$$

The (hhh) contribution of the term, which is proportional to c_{ASF} is

$$\begin{aligned}
 & -\frac{1}{2}\mathcal{F}_{3a}^{f(hhh)} + \mathcal{F}_{3m+3n}^{f(hhh)} \\
 = & g^2(d-1) \left\{ 2(d-5) \int\!\!\!\int_{PQ\{R\}} \frac{1}{P^4Q^2R^2} + \frac{1}{2}(d-3) \int\!\!\!\int_{\{PQR\}} \frac{1}{P^2Q^2(P-Q)^2(Q-R)^2} \right. \\
 & -\frac{1}{4}(d-7) \int\!\!\!\int_{\{PQ\}R} \frac{1}{P^2Q^2(P-R)^2(Q-R)^2} + \int\!\!\!\int_{\{PQ\}R} \frac{(P-Q)^2}{P^2Q^2R^2(P-R)^2(Q-R)^2} \\
 & -(d-3) \int\!\!\!\int_{P\{QR\}} \frac{1}{P^2Q^2R^2(Q-R)^2} - 2 \int\!\!\!\int_{\{PQR\}} \frac{1}{P^2Q^2R^2(Q-R)^2} \\
 & \left. + 2 \int\!\!\!\int_{\{PQR\}} \frac{R^4}{P^2Q^2(P-Q)^4(Q-R)^4} \right\} \\
 = & g^2(d-1) \left[2(d-5)\mathcal{I}_2^0\mathcal{I}_1^0\tilde{\mathcal{I}}_1^0 + \frac{1}{2}(d-3)\tilde{\mathcal{M}}_{00} - \frac{1}{4}(d-7)\mathcal{N}_{00} \right. \\
 & \left. + \mathcal{N}_{1,-1} - (d-3)\mathcal{I}_1^0\tilde{\tau} - 2\tilde{\mathcal{I}}_1^0\tilde{\tau} \right] \\
 = & -\frac{25\alpha_s^2T^4}{864} \left[\left(1 + \frac{72}{25}\hat{\mu}^2 - \frac{1584}{25}\hat{\mu}^4 \right) \left(\frac{1}{\epsilon} + 6\ln\frac{\hat{\Lambda}}{2} \right) \right. \\
 & - \frac{369}{250} \left(1 + \frac{2840}{123}\hat{\mu}^2 + \frac{28720}{123}\hat{\mu}^4 \right) + \frac{48}{25} (1 + 12\hat{\mu}^2) \gamma_E \\
 & + \frac{536}{125} \frac{\zeta'(-3)}{\zeta(-3)} + \frac{32}{25} (1 + 6\hat{\mu}^2) \frac{\zeta'(-1)}{\zeta(-1)} + \frac{288}{25} \left[26\mathfrak{N}(3, z) \right. \\
 & \left. \left. + (3 - 68\hat{\mu}^2) \mathfrak{N}(1, z) + 72i\hat{\mu}\mathfrak{N}(2, z) + 2i\hat{\mu}\mathfrak{N}(0, z) \right] \right], \tag{5.42}
 \end{aligned}$$

where the integrals appearing above are evaluated in Sec. (5.3.3). Finally, we note that there is no (hhh) contribution from \mathcal{F}_{3o}^f since this is a purely HTL diagram.

hhs contribution

The (*hhs*) contribution to the \mathcal{F}_{3a}^f , \mathcal{F}_{3b}^f , and \mathcal{F}_{3c+3j}^f are

$$\mathcal{F}_{3a}^{f(hhs)} = 2(d-1)g^4T \int_p \frac{1}{p^2 + m_D^2} \left[\sum_{Q\{R\}} \frac{4Q_0R_0}{Q^2R^4(Q+R)^2} - \sum_{\{QR\}} \frac{1}{Q^2R^2(Q-R)^2} + \sum_{\{QR\}} \frac{2Q_0R_0}{Q^4R^4} \right], \quad (5.43)$$

$$\mathcal{F}_{3b}^{f(hhs)} = 2(d-1)g^4T \int_p \frac{1}{p^2 + m_D^2} \left[\sum_{Q\{R\}} -\frac{4Q_0R_0}{Q^2R^4(Q+R)^2} + \sum_{\{QR\}} \frac{1}{Q^2R^2(Q-R)^2} + (d-3) \sum_{\{Q\}} \frac{1}{Q^4} \left(\sum_R \frac{1}{R^2} - \sum_{\{R\}} \frac{1}{R^2} \right) \right], \quad (5.44)$$

$$\begin{aligned} \mathcal{F}_{3c+3j}^{f(hhs)} &= -4g^4T \int_p \frac{1}{(p^2 + m_D^2)^2} \left[\sum_{\{Q\}} \left(\frac{1}{Q^2} - \frac{2q^2}{Q^4} \right) \right]^2 \\ &+ 8g^4T \int_p \frac{p^2}{(p^2 + m_D^2)^2} \sum_{\{Q\}} \left[\frac{1}{Q^2} - \frac{2q^2}{Q^4} \right] \sum_{\{R\}} \left[\frac{1}{R^4} - \frac{2}{d}(3+d) \frac{r^2}{R^6} + \frac{8}{d} \frac{r^4}{R^8} \right] \\ &- 16m_q^2g^4T \int_p \frac{1}{(p^2 + m_D^2)^2} \sum_{\{Q\}} \left[\frac{1}{Q^2} - \frac{2q^2}{Q^4} \right] \sum_{\{R\}} \left[\frac{3}{R^4} - \frac{4r^2}{R^6} - \frac{4}{R^4} \mathcal{T}_R - \frac{2}{R^2} \left\langle \frac{1}{(R \cdot Y)^2} \right\rangle_{\hat{y}} \right] \\ &= -4g^4T(d-1)^2 \int_p \frac{1}{(p^2 + m_D^2)^2} \sum_{\{QR\}} \frac{1}{Q^2R^2} + \frac{4}{3}g^4T(d-1)^2 \int_p \frac{p^2}{(p^2 + m_D^2)^2} \sum_{\{QR\}} \frac{1}{Q^2R^4} \\ &+ 32m_q^2g^4T(d-3) \int_p \frac{1}{(p^2 + m_D^2)^2} \sum_{\{QR\}} \frac{1}{Q^2R^4}. \end{aligned} \quad (5.45)$$

Computing the necessary sum-integrals one finds

$$\mathcal{F}_{3a+3b}^{f(hhs)} = \frac{\alpha_s^2 m_D T^3}{4\pi} (1 + 12\hat{\mu}^2), \quad (5.46)$$

$$\begin{aligned}
 \mathcal{F}_{3c+3j}^{f(hhs)} &= \frac{\alpha_s^2 m_D T^3}{12\pi} \left[\frac{1 + 12\hat{\mu}^2}{\epsilon} + (1 + 12\hat{\mu}^2) \left(\frac{4}{3} - \aleph(z) \right) + 24\aleph(1, z) \right] \\
 &- \frac{\pi \alpha_s^2 T^5}{18m_D} (1 + 12\hat{\mu}^2)^2 - \frac{\alpha_s^2 m_q^2 T^3}{3\pi m_D} (1 + 12\hat{\mu}^2). \quad (5.47)
 \end{aligned}$$

Similarly, one obtains

$$\begin{aligned}
 &-\frac{1}{2} \mathcal{F}_{3a}^{f(hhs)} + \mathcal{F}_{3m+3n+3o}^{f(hhs)} \\
 &= g^2 T (d-1) \left\{ 2(d-1)^2 \int_p \frac{1}{(p^2 + m_D^2)^2} \not\int_{Q\{R\}} \frac{1}{Q^2 R^2} \right. \\
 &\quad + \frac{1}{2} (d-3) \int_p \frac{1}{(p^2 + m_D^2)} \not\int_{\{QR\}} \frac{1}{Q^2 R^2 (Q-R)^2} \\
 &\quad - \int_p \frac{1}{(p^2 + m_D^2)} \not\int_{\{QR\}} \frac{2Q_0 R_0}{Q^4 R^4} - \frac{1}{3} (d^2 - 11d + 46) \int_p \frac{p^2}{(p^2 + m_D^2)^2} \not\int_{Q\{R\}} \frac{1}{Q^4 R^2} \\
 &\quad - \frac{1}{3} (d-1)^2 \int_p \frac{p^2}{(p^2 + m_D^2)^2} \not\int_{Q\{R\}} \frac{1}{Q^2 R^4} \\
 &\quad \left. + 4m_q^2 (d-1) \int_p \frac{1}{(p^2 + m_D^2)^2} \not\int_Q \frac{1}{Q^2} \not\int_{\{R\}} \left[\frac{3}{R^4} - \frac{4r^2}{R^6} - \frac{4}{R^4} \mathcal{T}_R - \frac{2}{R^2} \left\langle \frac{1}{(R.Y)^2} \right\rangle_{\hat{y}} \right] \right\}, \\
 &= g^2 T (d-1) \left\{ 2(d-1)^2 \int_p \frac{1}{(p^2 + m_D^2)^2} \not\int_{Q\{R\}} \frac{1}{Q^2 R^2} \right. \\
 &\quad - \frac{1}{3} (d^2 - 11d + 46) \int_p \frac{p^2}{(p^2 + m_D^2)} \not\int_{Q\{R\}} \frac{1}{Q^4 R^2} \\
 &\quad \left. - \frac{1}{3} (d-1)^2 \int_p \frac{p^2}{(p^2 + m_D^2)^2} \not\int_{Q\{R\}} \frac{1}{Q^2 R^4} + 8m_q^2 (d-3) \int_p \frac{1}{(p^2 + m_D^2)^2} \not\int_{Q\{R\}} \frac{1}{Q^2 R^4} \right\} \\
 &= -\frac{\alpha_s m_D T^3}{48\pi} \left(\frac{\Lambda}{2m_D} \right)^{2\epsilon} \left(\frac{\Lambda}{4\pi T} \right)^{4\epsilon} \left[\frac{1}{\epsilon} (7 + 132\hat{\mu}^2) + \frac{88}{3} + 440\hat{\mu}^2 + 22(1 + 12\hat{\mu}^2) \gamma_E \right. \\
 &\quad \left. - 8 \frac{\zeta'(-1)}{\zeta(-1)} + 4\aleph(z) + 264\aleph(1, z) \right] - \frac{\pi \alpha_s^2 T^5}{9m_D} (1 + 12\hat{\mu}^2) - \frac{\alpha_s^2}{3\pi m_D} m_q^2 T^3. \quad (5.48)
 \end{aligned}$$

hss contribution

The only three loop diagram involving a fermionic line that has a (*hss*) contribution is \mathcal{F}_{3n}^f which can be written as

$$\begin{aligned}
 \mathcal{F}_{3n}^{f(hss)} &= g^4 T^2 \int_{pq} \left[\frac{4}{(p^2 + m_D^2)(q^2 + m_D^2)(\mathbf{p} + \mathbf{q})^2} - \frac{2}{(p^2 + m_D^2)(q^2 + m_D^2)^2} \right. \\
 &\quad \left. - \frac{8m_D^2}{(\mathbf{p} + \mathbf{q})^2(p^2 + m_D^2)(q^2 + m_D^2)^2} \right] \sum_{\{R\}} \left(\frac{1}{R^2} - \frac{2r^2}{R^4} \right) \\
 &= -g^4 T^2 (d-1) \int_{pq} \left[\frac{4}{(p^2 + m_D^2)(q^2 + m_D^2)(\mathbf{p} + \mathbf{q})^2} - \frac{2}{(p^2 + m_D^2)(q^2 + m_D^2)^2} \right. \\
 &\quad \left. - \frac{8m_D^2}{(\mathbf{p} + \mathbf{q})^2(p^2 + m_D^2)(q^2 + m_D^2)^2} \right] \sum_{\{R\}} \frac{1}{R^2} \\
 &= \frac{\alpha_s^2 T^4}{12} \left[\frac{1 + 12\hat{\mu}^2}{\epsilon} + 2(1 + 12\hat{\mu}^2 + 12\mathcal{N}(1, z)) \right] \left(\frac{\Lambda}{2m_D} \right)^{4\epsilon} \left(\frac{\Lambda}{4\pi T} \right)^{2\epsilon} \quad (5.49)
 \end{aligned}$$

5.3 Sum-Integrals

In Sec (4.5) of Chapter 4 we have listed all the one and two loop sum-integrals at small chemical potential up to $\mathcal{O}(\mu/T)^4$. In this chapter we are calculating thermodynamic potential at general value of chemical potential. So we are enlisting here all the necessary one, two and three loop sum-integrals at any value of temperature and chemical potential.

We can define a set of “master” sum integral as in [13, 146]

$$\mathcal{I}_n^m = \sum_P \frac{P_0^m}{P^{2n}}, \quad (5.50)$$

$$\tilde{\mathcal{I}}_n^m = \sum_{\{P\}} \frac{P_0^m}{P^{2n}}, \quad (5.51)$$

$$\tilde{\tau} = \sum_{\{PQ\}} \frac{1}{P^2 Q^2 (P+Q)^2}, \quad (5.52)$$

$$\mathcal{M}_{m,n} = \sum_{PQR} \frac{1}{P^2 Q^2 (R^2)^m [(P-Q)^2]^n (P-R)^2 (Q-R)^2}, \quad (5.53)$$

$$\widetilde{\mathcal{M}}_{m,n} = \sum_{\{PQR\}} \frac{1}{P^2 Q^2 (R^2)^m [(P-Q)^2]^n (P-R)^2 (Q-R)^2}, \quad (5.54)$$

$$\mathcal{N}_{m,n} = \sum_{\{PQ\}R} \frac{1}{P^2 Q^2 (R^2)^m [(P-Q)^2]^n (P-R)^2 (Q-R)^2}. \quad (5.55)$$

5.3.1 One loop sum-integrals

The specific bosonic sun-integrals needed are

$$\mathcal{I}_1^0 = \sum_P \frac{1}{P^2} = \frac{T^2}{12} \left(\frac{\Lambda_g}{4\pi T} \right)^{2\epsilon} \left[1 + 2\epsilon \left(1 + \frac{\zeta'(-1)}{\zeta(-1)} \right) \right], \quad (5.56)$$

$$\mathcal{I}_2^0 = \sum_P \frac{1}{P^4} = \frac{1}{(4\pi)^2} \left(\frac{\Lambda_g}{4\pi T} \right)^{2\epsilon} \left[\frac{1}{\epsilon} + 2\gamma_E \right]. \quad (5.57)$$

The specific fermionic sun-integrals needed are

$$\widetilde{\mathcal{I}}_1^0 = \sum_{\{P\}} \frac{1}{P^2} = -\frac{T^2}{24} \left(\frac{\Lambda}{4\pi T} \right)^{2\epsilon} \left[1 + 12\hat{\mu}^2 + 2\epsilon (1 + 12\hat{\mu}^2 + 12\aleph(1, z)) \right], \quad (5.58)$$

and

$$\widetilde{\mathcal{I}}_2^0 = \sum_{\{P\}} \frac{1}{P^4} = \frac{1}{(4\pi)^2} \left(\frac{\Lambda}{4\pi T} \right)^{2\epsilon} \left[\frac{1}{\epsilon} - \aleph(z) \right]. \quad (5.59)$$

Using the two basic one-loop sum-integrals above, we can construct other one-loop sum-integrals that will be necessary here as follows:

$$\sum_{\{P\}} \frac{1}{P^2} = \frac{2}{d} \sum_{\{P\}} \frac{p^2}{P^4} \quad (5.60)$$

$$\begin{aligned}
 \sum_{\{P\}} \frac{1}{P^4} &= \frac{4}{d} \sum_{\{P\}} \frac{p^2}{P^6} = \frac{24}{d(d+2)} \sum_{\{P\}} \frac{p^4}{P^8}, \\
 &= (d-1) \sum_{\{P\}} \frac{1}{P^4} \mathcal{T}_P = -\frac{2}{d-1} \sum_{\{P\}} \frac{1}{P^2} \left\langle \frac{1}{(P.Y)^2} \right\rangle_{\hat{y}}. \quad (5.61)
 \end{aligned}$$

This allows us to compute the following sum-integrals

$$\sum_{\{P\}} \frac{p^2}{P^4} = -\frac{T^2}{16} \left(\frac{\Lambda}{4\pi T} \right)^{2\epsilon} \left[1 + 12\hat{\mu}^2 + \frac{4}{3}\epsilon (1 + 12\hat{\mu}^2 + 18\aleph(1, z)) \right], \quad (5.62)$$

$$\sum_{\{P\}} \frac{1}{P^4} \mathcal{T}_P = \frac{1}{2} \frac{1}{(4\pi)^2} \left(\frac{\Lambda}{4\pi T} \right)^{2\epsilon} \left[\frac{1}{\epsilon} + 1 - \aleph(z) \right], \quad (5.63)$$

$$\sum_{\{P\}} \frac{p^2}{P^6} = \frac{3}{4} \frac{1}{(4\pi)^2} \left(\frac{\Lambda}{4\pi T} \right)^{2\epsilon} \left[\frac{1}{\epsilon} - \frac{2}{3} - \aleph(z) \right], \quad (5.64)$$

$$\sum_{\{P\}} \frac{p^4}{P^8} = \frac{5}{8} \frac{1}{(4\pi)^2} \left(\frac{\Lambda}{4\pi T} \right)^{2\epsilon} \left[\frac{1}{\epsilon} - \frac{16}{15} - \aleph(z) \right], \quad (5.65)$$

$$\sum_{\{P\}} \frac{1}{P^2} \left\langle \frac{1}{(P.Y)^2} \right\rangle_{\hat{y}} = -\frac{1}{(4\pi)^2} \left(\frac{\Lambda}{4\pi T} \right)^{2\epsilon} \left[\frac{1}{\epsilon} - 1 - \aleph(z) \right], \quad (5.66)$$

$$\sum_{\{P\}} \frac{P_0}{P^4} = \frac{1}{(4\pi)} \left(\frac{\Lambda}{4\pi T} \right)^{2\epsilon} [i\hat{\mu} + \aleph(0, z)\epsilon]. \quad (5.67)$$

5.3.2 Two loop sum-integrals

For the purposes of this chapter we only need one new two-loop sum-integral

$$\tilde{\tau} = \sum_{\{PQ\}} \frac{1}{P^2 Q^2 (P+Q)^2} = -\frac{T^2}{(4\pi)^2} \left(\frac{\Lambda}{4\pi T} \right)^{4\epsilon} \left[\frac{\hat{\mu}^2}{\epsilon} + 2\hat{\mu}^2 - 2i\hat{\mu}\mathfrak{N}[0, z] \right]. \quad (5.68)$$

5.3.3 Three loop sum-integrals

The three-loop sum-integrals necessary are

$$\begin{aligned} \mathcal{M}_{00} &= \sum_{PQR} \frac{1}{P^2 Q^2 R^2 (P+Q+R)^2} \\ &= \frac{1}{(4\pi)^2} \left(\frac{T^2}{12} \right)^2 \left(\frac{\Lambda_g}{4\pi T} \right)^{6\epsilon} \left[\frac{6}{\epsilon} + \frac{182}{5} - 12 \frac{\zeta'(-3)}{\zeta(-3)} + 48 \frac{\zeta'(-1)}{\zeta(-1)} \right]. \end{aligned} \quad (5.69)$$

$$\begin{aligned} \mathcal{N}_{00} &= \sum_{\{PQR\}} \frac{1}{P^2 Q^2 R^2 (P+Q+R)^2} \\ &= \frac{1}{(4\pi)^2} \left(\frac{T^2}{12} \right)^2 \left(\frac{\Lambda}{4\pi T} \right)^{6\epsilon} \left[\frac{3}{2\epsilon} (1 + 12\hat{\mu}^2)^2 + \frac{173}{20} + 210\hat{\mu}^2 \right. \\ &\quad + 1284\hat{\mu}^4 - \frac{24}{5} \frac{\zeta'(-3)}{\zeta(-3)} + 144 \left((1 + 8\hat{\mu}^2)\mathfrak{N}(1, z) + 4\hat{\mu}^2\mathfrak{N}(1, 2z) \right. \\ &\quad \left. \left. - 4i\hat{\mu}[\mathfrak{N}(2, z) + \mathfrak{N}(2, 2z)] - 2\mathfrak{N}(3, z) - \mathfrak{N}(3, 2z) \right) \right]. \end{aligned} \quad (5.70)$$

$$\begin{aligned} \tilde{\mathcal{M}}_{00} &= \sum_{PQ\{R\}} \frac{1}{P^2 Q^2 R^2 (P+Q+R)^2} \\ &= -\frac{1}{(4\pi)^2} \left(\frac{T^2}{12} \right)^2 \left(\frac{\Lambda}{4\pi T} \right)^{6\epsilon} \left[\frac{3}{4\epsilon} (1 + 24\hat{\mu}^2 - 48\hat{\mu}^4) + \frac{179}{40} \right. \\ &\quad + 111\hat{\mu}^2 - 210\hat{\mu}^4 + 48 \frac{\zeta'(-1)}{\zeta(-1)} \hat{\mu}^2 + \frac{24}{5} \frac{\zeta'(-3)}{\zeta(-3)} \\ &\quad \left. + 72 \left((1 - 8\hat{\mu}^2)\mathfrak{N}(1, z) + 6\mathfrak{N}(3, z) + 12i\hat{\mu}\mathfrak{N}(2, z) \right) \right]. \end{aligned} \quad (5.71)$$

$$\begin{aligned}
 \mathcal{N}_{1,-1} &= -\frac{1}{2(4\pi)^2} \left(\frac{T^2}{12}\right)^2 \left(\frac{\Lambda}{4\pi T}\right)^{6\epsilon} \left[\frac{3}{2\epsilon} (1 + 12\hat{\mu}^2) (1 - 4\hat{\mu}^2) \right. \\
 &+ \frac{173}{20} + 114\hat{\mu}^2 + 132\hat{\mu}^4 - \frac{12}{5} \frac{\zeta'(-3)}{\zeta(-3)} - 96\hat{\mu}^2 \frac{\zeta'(-1)}{\zeta(-1)} \\
 &- 144 \left[2\mathfrak{N}(3, z) + 2\mathfrak{N}(3, 2z) - 4i\hat{\mu} \mathfrak{N}(2, z) + 8i\hat{\mu} \mathfrak{N}(2, 2z) \right. \\
 &\left. \left. - (1 - 4\hat{\mu}^2) \mathfrak{N}(1, z) - 8\hat{\mu}^2 \mathfrak{N}(1, 2z) - \frac{1}{3} i\hat{\mu} (1 + 12\hat{\mu}^2) \mathfrak{N}(0, z) \right] \right]. \quad (5.72)
 \end{aligned}$$

$$\begin{aligned}
 H_3 &= \sum_{\{P\}QR} \frac{Q \cdot R}{P^2 Q^2 R^2 (P+Q)^2 (P+R)^2} \\
 &= \frac{1}{(4\pi)^2} \left(\frac{T^2}{12}\right)^2 \left(\frac{\Lambda}{4\pi T}\right)^{6\epsilon} \left[\frac{3}{8\epsilon} (1 + 12\hat{\mu}^2)^2 + \frac{361}{160} - \frac{3}{5} \frac{\zeta'(-3)}{\zeta(-3)} \right. \\
 &+ \frac{141}{4} \hat{\mu}^2 + \frac{501}{2} \hat{\mu}^4 - 9 \left\{ \left(\frac{1}{8} + \hat{\mu}^2 + 2\hat{\mu}^4 \right) \mathfrak{N}(z) + 2i\hat{\mu} (1 + 4\hat{\mu}^2) \mathfrak{N}(0, z) \right. \\
 &\left. \left. + 2(1 - 12\hat{\mu}^2) \mathfrak{N}(1, z) + 24i\hat{\mu} \mathfrak{N}(2, z) + 16\mathfrak{N}(3, z) \right\} \right]. \quad (5.73)
 \end{aligned}$$

$$\begin{aligned}
 \widetilde{\mathcal{M}}_{-2,2} &= \sum_{\{PQR\}} \frac{R^4}{P^2 Q^2 (P-Q)^4 (Q-R)^2 (R-P)^2} \\
 &= -\frac{1}{(4\pi)^2} \left(\frac{T^2}{12}\right)^2 \left(\frac{\Lambda}{4\pi T}\right)^{6\epsilon} \left[\frac{1}{12\epsilon} (29 + 288\hat{\mu}^2 - 144\hat{\mu}^4) + \frac{89}{12} + 4\gamma_E \right. \\
 &+ 2(43 + 24\gamma_E) \hat{\mu}^2 - 68\hat{\mu}^4 + \frac{10}{3} \left(1 + \frac{84}{5} \hat{\mu}^2 \right) \frac{\zeta'(-1)}{\zeta(-1)} + \frac{8}{3} \frac{\zeta'(-3)}{\zeta(-3)} \\
 &\left. + 24 \left[10\mathfrak{N}(3, z) + 18i\hat{\mu} \mathfrak{N}(2, z) + 2(2 - 5\hat{\mu}^2) \mathfrak{N}(1, z) + i\hat{\mu} \mathfrak{N}(0, z) \right] \right]. \quad (5.74)
 \end{aligned}$$

5.4 Three-dimensional integrals

Dimensional regularization can be used to regularize both the ultraviolet divergences and infrared divergences in 3-dimensional integrals over momenta. The spatial dimension is generalized to $d = 3 - 2\epsilon$ dimensions. Integrals are evaluated at a value of d for which they converge and then analytically continued to $d = 3$. We use the integration measure

$$\int_p \equiv \left(\frac{e^{\gamma_E} \Lambda^2}{4\pi} \right)^\epsilon \int \frac{d^{3-2\epsilon} p}{(2\pi)^{3-2\epsilon}} . \quad (5.75)$$

5.4.1 One-loop integrals

The general one-loop integral is given by

$$\begin{aligned} I_n &\equiv \int_p \frac{1}{(p^2 + m^2)^n} \\ &= \frac{1}{8\pi} (e^{\gamma_E} \Lambda^2)^\epsilon \frac{\Gamma(n - \frac{3}{2} + \epsilon)}{\Gamma(\frac{1}{2})\Gamma(n)} m^{3-2n-2\epsilon} . \end{aligned} \quad (5.76)$$

Specifically, we need

$$\begin{aligned} I'_0 &\equiv \int_p \ln(p^2 + m^2) \\ &= -\frac{m^3}{6\pi} \left(\frac{\Lambda}{2m} \right)^{2\epsilon} \left[1 + \frac{8}{3}\epsilon + \mathcal{O}(\epsilon^2) \right] , \end{aligned} \quad (5.77)$$

$$I_1 = -\frac{m}{4\pi} \left(\frac{\Lambda}{2m} \right)^{2\epsilon} [1 + 2\epsilon + \mathcal{O}(\epsilon^2)] , \quad (5.78)$$

$$I_2 = \frac{1}{8\pi m} \left(\frac{\Lambda}{2m} \right)^{2\epsilon} [1 + \mathcal{O}(\epsilon)] . \quad (5.79)$$

5.4.2 Two-loop integrals

We also need a few two-loop integrals on the form

$$J_n = \int_{pq} \frac{1}{p^2 + m^2} \frac{1}{(q^2 + m^2)^n} \frac{1}{(\mathbf{p} + \mathbf{q})^2} . \quad (5.80)$$

Specifically, we need J_1 and J_2 which were calculated in Ref. [175]:

$$J_1 = \frac{1}{4(4\pi)^2} \left(\frac{\Lambda}{2m} \right)^{4\epsilon} \left[\frac{1}{\epsilon} + 2 + \mathcal{O}(\epsilon) \right] , \quad (5.81)$$

$$J_2 = \frac{1}{4(4\pi)^2 m^2} \left(\frac{\Lambda}{2m} \right)^{4\epsilon} [1 + \mathcal{O}(\epsilon)] . \quad (5.82)$$

5.5 NNLO HTLpt thermodynamic potential

In Sec. (5.2) we expanded each term of Eq. (5.1) form small m_D/T and m_q/T . In Sec. (5.3) and Sec. (5.4) we calculated necessary sum-integrals and three dimensional integrals that arise in Sec. (5.2). In this section we will summarized the results from Secs. (5.2), (5.3) and (5.4) to get final thermodynamic potential.

We consider first the case that all quarks have the same chemical potential $\mu_f = \mu = \mu_B/N_f$ where f is a flavor index with $f \in \{\mu_u, \mu_d, \mu_s, \dots, \mu_{N_f}\}$. Here we are considering $N_f = 3$, so $\mu_f = \mu = \mu_B/3$. After presenting the steps needed for this case, we give the general result with separate chemical potentials for each flavor.

5.5.1 NNLO result for equal chemical potentials

When all quarks have the same chemical potential $\mu_i = \mu = \mu_B/3$ we can straightforwardly combine the results for the various sum-integrals. In this case, the unrenormalized three-loop HTLpt thermodynamic potential is

$$\begin{aligned}
 \frac{\Omega_{3\text{loop}}}{\Omega_0} = & \frac{7 d_F}{4 d_A} \left(1 + \frac{120}{7} \hat{\mu}^2 + \frac{240}{7} \hat{\mu}^4 \right) + \frac{s_F \alpha_s}{\pi} \left[-\frac{5}{8} (1 + 12 \hat{\mu}^2) (5 + 12 \hat{\mu}^2) \right. \\
 & + \frac{15}{2} (1 + 12 \hat{\mu}^2) \hat{m}_D + \frac{15}{2} \left(\frac{1}{\epsilon} - 1 - \aleph(z) + 4 \ln \frac{\hat{\Lambda}}{2} - 2 \ln \hat{m}_D \right) \hat{m}_D^3 \\
 & - 90 \hat{m}_q^2 \hat{m}_D \left. \right] + s_{2F} \left(\frac{\alpha_s}{\pi} \right)^2 \left[\frac{15}{64} \left\{ 35 - 32 \frac{\zeta'(-1)}{\zeta(-1)} + 472 \hat{\mu}^2 \right. \right. \\
 & + 384 \frac{\zeta'(-1)}{\zeta(-1)} \hat{\mu}^2 + 1328 \hat{\mu}^4 + 64 \left(-36 i \hat{\mu} \aleph(2, z) + 6(1 + 8 \hat{\mu}^2) \aleph(1, z) \right. \\
 & \left. \left. + 3 i \hat{\mu} (1 + 4 \hat{\mu}^2) \aleph(0, z) \right) \right\} - \frac{45}{2} \hat{m}_D (1 + 12 \hat{\mu}^2) \left. \right] \\
 & + \left(\frac{s_F \alpha_s}{\pi} \right)^2 \left[\frac{5}{4 \hat{m}_D} (1 + 12 \hat{\mu}^2)^2 + 30 (1 + 12 \hat{\mu}^2) \frac{\hat{m}_q^2}{\hat{m}_D} \right. \\
 & + \frac{25}{24} \left\{ \left(1 + \frac{72}{5} \hat{\mu}^2 + \frac{144}{5} \hat{\mu}^4 \right) \left(\frac{1}{\epsilon} + 6 \ln \frac{\hat{\Lambda}}{2} \right) + \frac{31}{10} + \frac{6}{5} \gamma_E - \frac{68}{25} \frac{\zeta'(-3)}{\zeta(-3)} \right. \\
 & + \frac{12}{5} (25 + 12 \gamma_E) \hat{\mu}^2 + \frac{24}{5} (61 + 36 \gamma_E) \hat{\mu}^4 - \frac{8}{5} (1 + 12 \hat{\mu}^2) \frac{\zeta'(-1)}{\zeta(-1)} \\
 & - \frac{144}{5} \left[8 \aleph(3, z) + 3 \aleph(3, 2z) + 12 i \hat{\mu} (\aleph(2, z) + \aleph(2, 2z)) - 12 \hat{\mu}^2 \aleph(1, 2z) \right. \\
 & \left. \left. - i \hat{\mu} (1 + 12 \hat{\mu}^2) \aleph(0, z) - (3 + 20 \hat{\mu}^2) \aleph(1, z) \right] \right\} \\
 & - \frac{15}{2} \left\{ (1 + 12 \hat{\mu}^2) \left(\frac{1}{\epsilon} + 4 \ln \frac{\hat{\Lambda}}{2} - 2 \ln \hat{m}_D \right) + (1 + 12 \hat{\mu}^2) \left(\frac{4}{3} - \aleph(z) \right) \right. \\
 & + 24 \aleph(1, z) \left. \right\} \hat{m}_D \left. \right] + \left(\frac{c_A \alpha_s}{3\pi} \right) \left(\frac{s_F \alpha_s}{\pi} \right) \left[\frac{15}{2 \hat{m}_D} (1 + 12 \hat{\mu}^2) \right. \\
 & - \frac{235}{32} \left\{ \left(1 + \frac{792}{47} \hat{\mu}^2 + \frac{1584}{47} \hat{\mu}^4 \right) \left(\frac{1}{\epsilon} + 6 \ln \frac{\hat{\Lambda}}{2} \right) - \frac{48 \gamma_E}{47} (1 + 12 \mu^2) \right. \\
 & + \frac{1809}{470} \left(1 + \frac{8600}{603} \hat{\mu}^2 + \frac{28720}{603} \hat{\mu}^4 \right) - \frac{32}{47} (1 + 6 \mu^2) \frac{\zeta'(-1)}{\zeta(-1)} \\
 & - \frac{464}{235} \frac{\zeta'(-3)}{\zeta(-3)} - \frac{288}{47} (1 + 12 \hat{\mu}^2) \ln \hat{m}_D - \frac{288}{47} \left[2 i \hat{\mu} \aleph(0, z) \right. \\
 & \left. \left. - (3 + 68 \hat{\mu}^2) \aleph(1, z) + 72 i \hat{\mu} \aleph(2, z) + 26 \aleph(3, z) \right] \right\} \\
 & + \frac{315}{8} \left\{ \left(1 + \frac{132}{7} \mu^2 \right) \left(\frac{1}{\epsilon} + 6 \ln \frac{\hat{\Lambda}}{2} - 2 \ln \hat{m}_D \right) + \frac{88}{21} + \frac{22}{7} (1 + 12 \hat{\mu}^2) \gamma_E \right. \\
 & \left. + \frac{440}{7} \hat{\mu}^2 - \frac{8}{7} \frac{\zeta'(-1)}{\zeta(-1)} + \frac{4}{7} \aleph(z) + \frac{264}{7} \aleph(1, z) \right\} \hat{m}_D + 90 \frac{\hat{m}_q}{\hat{m}_D} \left. \right], \quad (5.83)
 \end{aligned}$$

where $\Omega_0 = -d_A \pi^2 T^4 / 45$.

The sum of all counterterms through order δ^2 is

$$\begin{aligned}
 \frac{\Delta\Omega}{\Omega_0} &= \frac{\Delta\Omega_1 + \Delta\Omega_2}{\Omega_0} \\
 &= \frac{s_F \alpha_s}{\pi} \left[-\frac{15}{2} \left(\frac{1}{\epsilon} + 2 \ln \frac{\hat{\Lambda}}{2} - 2 \ln \hat{m}_D \right) \hat{m}_D^3 \right] \\
 &+ \left(\frac{c_A \alpha_s}{3\pi} \right) \left(\frac{s_F \alpha_s}{\pi} \right) \left[\frac{235}{32} \left\{ \left(1 + \frac{792}{47} \hat{\mu}^2 + \frac{1584}{47} \hat{\mu}^4 \right) \left(\frac{1}{\epsilon} + 4 \ln \frac{\hat{\Lambda}}{2} \right) + \frac{56}{47} \frac{\zeta'(-1)}{\zeta(-1)} \right. \right. \\
 &+ \left. \frac{149}{47} \left(1 + \frac{2376}{149} \hat{\mu}^2 + \frac{4752}{149} \hat{\mu}^4 \right) + \frac{1584}{47} (1 + 4\hat{\mu}^2) \aleph(1, z) + \frac{1056}{47} \frac{\zeta'(-1)}{\zeta(-1)} \hat{\mu}^2 \right\} \\
 &- \frac{315}{8} \left\{ \left(1 + \frac{132}{7} \hat{\mu}^2 \right) \left(\frac{1}{\epsilon} + 4 \ln \frac{\hat{\Lambda}}{2} - 2 \ln \hat{m}_D \right) - \frac{8}{7} \frac{\zeta'(-1)}{\zeta(-1)} + \frac{61}{21} + 44\hat{\mu}^2 \right. \\
 &+ \left. \frac{264}{7} \aleph(1, z) \right\} \hat{m}_D \left. \right] + \left(\frac{s_F \alpha_s}{\pi} \right)^2 \left[-\frac{25}{24} \left\{ \left(1 + \frac{72}{5} \hat{\mu}^2 + \frac{144}{5} \hat{\mu}^4 \right) \left(\frac{1}{\epsilon} + 4 \ln \frac{\hat{\Lambda}}{2} + 3 \right) \right. \right. \\
 &+ \left. \frac{144}{5} (1 + 4\hat{\mu}^2) \aleph(1, z) + \frac{8}{5} (1 + 12\hat{\mu}^2) \frac{\zeta'(-1)}{\zeta(-1)} \right\} \\
 &+ \left. \frac{15}{2} \left\{ (1 + 12\hat{\mu}^2) \left(\frac{1}{\epsilon} + 4 \ln \frac{\hat{\Lambda}}{2} - 2 \ln \hat{m}_D + \frac{7}{3} \right) + 24 \aleph(1, z) \right\} \hat{m}_D \right] + \frac{\Delta\Omega^{\text{YM}}}{\Omega_0}, \tag{5.84}
 \end{aligned}$$

where $\Delta\Omega^{\text{YM}}$ is the pure-gluon three-loop HTLpt counterterm [178]

$$\begin{aligned}
 \frac{\Delta\Omega^{\text{YM}}}{\Omega_0} &= \frac{45}{8\epsilon} \hat{m}_D^4 + \frac{495}{8} \left(\frac{c_A \alpha_s}{3\pi} \right) \left(\frac{1}{\epsilon} + 2 \ln \frac{\hat{\Lambda}_g}{2} - 2 \ln \hat{m}_D \right) \hat{m}_D^3 \\
 &+ \left(\frac{c_A \alpha_s}{3\pi} \right)^2 \left[\frac{165}{16} \left(\frac{1}{\epsilon} + 4 \ln \frac{\hat{\Lambda}_g}{2} + 2 + 4 \frac{\zeta'(-1)}{\zeta(-1)} \right) \right. \\
 &- \left. \frac{1485}{8} \left(\frac{1}{\epsilon} + 4 \ln \frac{\hat{\Lambda}_g}{2} - 2 \ln \hat{m}_D + \frac{4}{3} + 2 \frac{\zeta'(-1)}{\zeta(-1)} \right) \hat{m}_D \right]. \tag{5.85}
 \end{aligned}$$

Adding the total three-loop HTLpt counterterm (5.84) to the unrenormalized three-loop HTLpt thermodynamic potential (5.83) we obtain our final result for the NNLO HTLpt thermodynamic potential in the case that all quarks have the same chemical

potential

$$\begin{aligned}
 \frac{\Omega_{\text{NNLO}}}{\Omega_0} &= \frac{7 d_F}{4 d_A} \left(1 + \frac{120}{7} \hat{\mu}^2 + \frac{240}{7} \hat{\mu}^4 \right) - \frac{s_F \alpha_s}{\pi} \left[\frac{5}{8} (1 + 12 \hat{\mu}^2) (5 + 12 \hat{\mu}^2) \right. \\
 &\quad \left. - \frac{15}{2} (1 + 12 \hat{\mu}^2) \hat{m}_D - \frac{15}{2} \left(2 \ln \frac{\hat{\Lambda}}{2} - 1 - \aleph(z) \right) \hat{m}_D^3 + 90 \hat{m}_q^2 \hat{m}_D \right] \\
 &+ s_{2F} \left(\frac{\alpha_s}{\pi} \right)^2 \left[\frac{15}{64} \left\{ 35 - 32 (1 - 12 \hat{\mu}^2) \frac{\zeta'(-1)}{\zeta(-1)} + 472 \hat{\mu}^2 + 1328 \hat{\mu}^4 \right. \right. \\
 &+ \left. \left. 64 \left(-36 i \hat{\mu} \aleph(2, z) + 6(1 + 8 \hat{\mu}^2) \aleph(1, z) + 3i \hat{\mu} (1 + 4 \hat{\mu}^2) \aleph(0, z) \right) \right\} \right. \\
 &\quad \left. - \frac{45}{2} \hat{m}_D (1 + 12 \hat{\mu}^2) \right] + \left(\frac{s_F \alpha_s}{\pi} \right)^2 \left[\frac{5}{4 \hat{m}_D} (1 + 12 \hat{\mu}^2)^2 + 30 (1 + 12 \hat{\mu}^2) \frac{\hat{m}_q^2}{\hat{m}_D} \right. \\
 &+ \frac{25}{12} \left\{ \left(1 + \frac{72}{5} \hat{\mu}^2 + \frac{144}{5} \hat{\mu}^4 \right) \ln \frac{\hat{\Lambda}}{2} + \frac{1}{20} (1 + 168 \hat{\mu}^2 + 2064 \hat{\mu}^4) \right. \\
 &+ \frac{3}{5} (1 + 12 \hat{\mu}^2)^2 \gamma_E - \frac{8}{5} (1 + 12 \hat{\mu}^2) \frac{\zeta'(-1)}{\zeta(-1)} - \frac{34}{25} \frac{\zeta'(-3)}{\zeta(-3)} \\
 &\quad \left. - \frac{72}{5} \left[8 \aleph(3, z) + 3 \aleph(3, 2z) + 12 i \hat{\mu} (\aleph(2, z) + \aleph(2, 2z)) \right. \right. \\
 &\quad \left. \left. - 12 \hat{\mu}^2 \aleph(1, 2z) - i \hat{\mu} (1 + 12 \hat{\mu}^2) \aleph(0, z) - 2(1 + 8 \hat{\mu}^2) \aleph(1, z) \right] \right\} \\
 &\quad \left. - \frac{15}{2} (1 + 12 \hat{\mu}^2) \left(2 \ln \frac{\hat{\Lambda}}{2} - 1 - \aleph(z) \right) \hat{m}_D \right] \\
 &+ \left(\frac{c_A \alpha_s}{3\pi} \right) \left(\frac{s_F \alpha_s}{\pi} \right) \left[\frac{15}{2 \hat{m}_D} (1 + 12 \hat{\mu}^2) - \frac{235}{16} \left\{ \left(1 + \frac{792}{47} \hat{\mu}^2 + \frac{1584}{47} \hat{\mu}^4 \right) \ln \frac{\hat{\Lambda}}{2} \right. \right. \\
 &\quad \left. \left. - \frac{144}{47} (1 + 12 \hat{\mu}^2) \ln \hat{m}_D + \frac{319}{940} \left(1 + \frac{2040}{319} \hat{\mu}^2 + \frac{38640}{319} \hat{\mu}^4 \right) - \frac{24 \gamma_E}{47} (1 + 12 \hat{\mu}^2) \right. \right. \\
 &\quad \left. \left. - \frac{44}{47} \left(1 + \frac{156}{11} \hat{\mu}^2 \right) \frac{\zeta'(-1)}{\zeta(-1)} - \frac{268}{235} \frac{\zeta'(-3)}{\zeta(-3)} - \frac{72}{47} \left[4 i \hat{\mu} \aleph(0, z) \right. \right. \right. \\
 &\quad \left. \left. \left. + (5 - 92 \hat{\mu}^2) \aleph(1, z) + 144 i \hat{\mu} \aleph(2, z) + 52 \aleph(3, z) \right] \right\} + 90 \frac{\hat{m}_q^2}{\hat{m}_D} \right. \\
 &+ \frac{315}{4} \left\{ \left(1 + \frac{132}{7} \hat{\mu}^2 \right) \ln \frac{\hat{\Lambda}}{2} + \frac{11}{7} (1 + 12 \hat{\mu}^2) \gamma_E + \frac{9}{14} \left(1 + \frac{132}{9} \hat{\mu}^2 \right) \right. \\
 &\quad \left. \left. + \frac{2}{7} \aleph(z) \right\} \hat{m}_D \right] + \frac{\Omega_{\text{NNLO}}^{\text{YM}}}{\Omega_0}. \tag{5.86}
 \end{aligned}$$

where $\Omega_{\text{NNLO}}^{\text{YM}}$ is the NNLO pure glue thermodynamic potential [175]

$$\begin{aligned} \frac{\Omega_{\text{NNLO}}^{\text{YM}}}{\Omega_0} &= 1 - \frac{15}{4} \hat{m}_D^3 + \frac{c_A \alpha_s}{3\pi} \left[-\frac{15}{4} + \frac{45}{2} \hat{m}_D - \frac{135}{2} \hat{m}_D^2 - \frac{495}{4} \left(\ln \frac{\hat{\Lambda}_g}{2} + \frac{5}{22} + \gamma_E \right) \hat{m}_D^3 \right] \\ &\quad - \left(\frac{c_A \alpha_s}{3\pi} \right)^2 \left[\frac{165}{8} \left(\ln \frac{\hat{\Lambda}_g}{2} - \frac{72}{11} \ln \hat{m}_D - \frac{84}{55} - \frac{6}{11} \gamma_E - \frac{74}{11} \frac{\zeta'(-1)}{\zeta(-1)} + \frac{19}{11} \frac{\zeta'(-3)}{\zeta(-3)} \right) \right. \\ &\quad \left. - \frac{1485}{4} \left(\ln \frac{\hat{\Lambda}_g}{2} - \frac{79}{44} + \gamma_E + \ln 2 - \frac{\pi^2}{11} \right) \hat{m}_D - \frac{45}{4 \hat{m}_D} \right], \end{aligned} \quad (5.87)$$

It is worth to mention here that the NNLO pure glue thermodynamic potential in Eq. (5.87) looks like chemical potential independent as there are no explicit chemical potential dependence, but the chemical potential implicitly present within Debye mass m_D . It appears in pure glue diagrams from the internal quark loop in effective gluon propagators and effective vertices.

Note that the full thermodynamic potential (5.86) reduces to thermodynamic potential of Ref. [178] in the limit $\mu \rightarrow 0$. In addition, the above thermodynamic potential produces the correct $\mathcal{O}(g^5)$ perturbative result when expanded in a strict power series in g [13, 146].

5.5.2 NNLO result – General case

It is relatively straightforward to generalize the previously obtained result (5.86) to the case that each quark has a separate chemical potential μ_f . The final result is

$$\begin{aligned} \frac{\Omega_{\text{NNLO}}}{\Omega_0} &= \frac{7}{4} \frac{d_F}{d_A} \frac{1}{N_f} \sum_f \left(1 + \frac{120}{7} \hat{\mu}_f^2 + \frac{240}{7} \hat{\mu}_f^4 \right) - \frac{s_F \alpha_s}{\pi} \frac{1}{N_f} \sum_f \left[\frac{5}{8} (5 + 72 \hat{\mu}_f^2 + 144 \hat{\mu}_f^4) \right. \\ &\quad \left. - \frac{15}{2} (1 + 12 \hat{\mu}_f^2) \hat{m}_D - \frac{15}{2} \left(2 \ln \frac{\hat{\Lambda}}{2} - 1 - \mathfrak{N}(z_f) \right) \hat{m}_D^3 + 90 \hat{m}_q^2 \hat{m}_D \right] \end{aligned}$$

$$\begin{aligned}
 & + \frac{s_{2F}}{N_f} \left(\frac{\alpha_s}{\pi} \right)^2 \sum_f \left[\frac{15}{64} \left\{ 35 - 32 (1 - 12\hat{\mu}_f^2) \frac{\zeta'(-1)}{\zeta(-1)} + 472\hat{\mu}_f^2 + 1328\hat{\mu}_f^4 \right. \right. \\
 & + 64 \left(-36i\hat{\mu}_f \mathfrak{N}(2, z_f) + 6(1 + 8\hat{\mu}_f^2) \mathfrak{N}(1, z_f) + 3i\hat{\mu}_f(1 + 4\hat{\mu}_f^2) \mathfrak{N}(0, z_f) \right) \left. \right\} \\
 & - \left. \frac{45}{2} \hat{m}_D (1 + 12\hat{\mu}_f^2) \right] \\
 & + \left(\frac{s_F \alpha_s}{\pi} \right)^2 \frac{1}{N_f} \sum_f \frac{5}{16} \left[96 (1 + 12\hat{\mu}_f^2) \frac{\hat{m}_q^2}{\hat{m}_D} + \frac{4}{3} (1 + 12\hat{\mu}_f^2) (5 + 12\hat{\mu}_f^2) \ln \frac{\hat{\Lambda}}{2} \right. \\
 & + \frac{1}{3} + 4\gamma_E + 8(7 + 12\gamma_E)\hat{\mu}_f^2 + 112\hat{\mu}_f^4 - \frac{64}{15} \frac{\zeta'(-3)}{\zeta(-3)} - \frac{32}{3} (1 + 12\hat{\mu}_f^2) \frac{\zeta'(-1)}{\zeta(-1)} \\
 & - \left. 96 \left\{ 8\mathfrak{N}(3, z_f) + 12i\hat{\mu}_f \mathfrak{N}(2, z_f) - 2(1 + 2\hat{\mu}_f^2) \mathfrak{N}(1, z_f) - i\hat{\mu}_f \mathfrak{N}(0, z_f) \right\} \right] \\
 & + \left(\frac{s_F \alpha_s}{\pi} \right)^2 \frac{1}{N_f^2} \sum_{f,g} \left[\frac{5}{4\hat{m}_D} (1 + 12\hat{\mu}_f^2) (1 + 12\hat{\mu}_g^2) + 90 \left\{ 2(1 + \gamma_E) \hat{\mu}_f^2 \hat{\mu}_g^2 \right. \right. \\
 & - \left\{ \mathfrak{N}(3, z_f + z_g) + \mathfrak{N}(3, z_f + z_g^*) + 4i\hat{\mu}_f [\mathfrak{N}(2, z_f + z_g) + \mathfrak{N}(2, z_f + z_g^*)] \right. \\
 & - 4\hat{\mu}_g^2 \mathfrak{N}(1, z_f) - (\hat{\mu}_f + \hat{\mu}_g)^2 \mathfrak{N}(1, z_f + z_g) - (\hat{\mu}_f - \hat{\mu}_g)^2 \mathfrak{N}(1, z_f + z_g^*) \\
 & \left. \left. - 4i\hat{\mu}_f \hat{\mu}_g^2 \mathfrak{N}(0, z_f) \right\} \right] - \frac{15}{2} (1 + 12\hat{\mu}_f^2) \left(2 \ln \frac{\hat{\Lambda}}{2} - 1 - \mathfrak{N}(z_g) \right) \hat{m}_D \left. \right] \\
 & + \left(\frac{c_A \alpha_s}{3\pi} \right) \left(\frac{s_F \alpha_s}{\pi N_f} \right) \sum_f \left[-\frac{235}{16} \left\{ \left(1 + \frac{792}{47} \hat{\mu}_f^2 + \frac{1584}{47} \hat{\mu}_f^4 \right) \ln \frac{\hat{\Lambda}}{2} \right. \right. \\
 & - \frac{144}{47} (1 + 12\hat{\mu}_f^2) \ln \hat{m}_D + \frac{319}{940} \left(1 + \frac{2040}{319} \hat{\mu}_f^2 + \frac{38640}{319} \hat{\mu}_f^4 \right) \\
 & - \frac{24\gamma_E}{47} (1 + 12\hat{\mu}_f^2) - \frac{44}{47} \left(1 + \frac{156}{11} \hat{\mu}_f^2 \right) \frac{\zeta'(-1)}{\zeta(-1)} - \frac{268}{235} \frac{\zeta'(-3)}{\zeta(-3)} \\
 & - \left. \frac{72}{47} \left[4i\hat{\mu}_f \mathfrak{N}(0, z_f) + (5 - 92\hat{\mu}_f^2) \mathfrak{N}(1, z_f) + 144i\hat{\mu}_f \mathfrak{N}(2, z_f) + 52\mathfrak{N}(3, z_f) \right] \right\} \\
 & + \frac{15}{2\hat{m}_D} (1 + 12\hat{\mu}_f^2) + 90 \frac{\hat{m}_q^2}{\hat{m}_D} + \frac{315}{4} \left\{ \left(1 + \frac{132}{7} \hat{\mu}_f^2 \right) \ln \frac{\hat{\Lambda}}{2} \right. \\
 & \left. + \frac{11}{7} (1 + 12\hat{\mu}_f^2) \gamma_E + \frac{9}{14} \left(1 + \frac{132}{9} \hat{\mu}_f^2 \right) + \frac{2}{7} \mathfrak{N}(z_f) \right\} \hat{m}_D \left. \right] + \frac{\Omega_{\text{NNLO}}^{\text{YM}}}{\Omega_0}, \quad (5.88)
 \end{aligned}$$

where the sums over f and g include all quark flavors, $z_f = 1/2 - i\hat{\mu}_f$, and $\Omega_{\text{NNLO}}^{\text{YM}}$ is the pure-gluon contribution as before.

5.6 Mass prescription

As discussed in Sec. (2.2.8) of Chapter 2 and also in Ref. [178], the two-loop perturbative electric gluon mass, first introduced by Braaten and Nieto in [139, 144] is the most suitable for three-loop HTLpt calculations. We use the Braaten-Nieto (BN) mass prescription for m_D in the remainder of the chapter. Originally, the two-loop perturbative mass was calculated in Refs. [139, 144] for zero chemical potential, however, Vuorinen has generalized it to finite chemical potential. The resulting expression for m_D^2 is [13, 146]

$$\begin{aligned} \hat{m}_D^2 = & \frac{\alpha_s}{3\pi} \left\{ c_A + \frac{c_A^2 \alpha_s}{12\pi} \left(5 + 22\gamma_E + 22 \ln \frac{\hat{\Lambda}_g}{2} \right) + \frac{1}{N_f} \sum_f \left[s_F (1 + 12\hat{\mu}_f^2) \right. \right. \\ & + \left. \frac{c_A s_F \alpha_s}{12\pi} \left((9 + 132\hat{\mu}_f^2) + 22 (1 + 12\hat{\mu}_f^2) \gamma_E + 2 (7 + 132\hat{\mu}_f^2) \ln \frac{\hat{\Lambda}}{2} + 4\aleph(z_f) \right) \right. \\ & \left. \left. + \frac{s_F^2 \alpha_s}{3\pi} (1 + 12\hat{\mu}_f^2) \left(1 - 2 \ln \frac{\hat{\Lambda}}{2} + \aleph(z_f) \right) - \frac{3 s_{2F} \alpha_s}{2\pi} (1 + 12\hat{\mu}_f^2) \right] \right\}. \quad (5.89) \end{aligned}$$

The effect of the in-medium quark mass parameter m_q in thermodynamic functions is small and following Ref. [178] we take $m_q = 0$ which is the three loop variational solution. The maximal effect on the susceptibilities comparing the perturbative quark mass, $\hat{m}_q^2 = c_F \alpha_s (T^2 + \mu^2/\pi^2)/8\pi$, with the variational solution, $m_q = 0$, is approximately 0.2% at $T = 200$ MeV. At higher temperatures, the effect is much smaller, e.g. 0.02% at $T = 1$ GeV.

5.7 Thermodynamic functions

In this section we present our final results for the NNLO HTLpt pressure, energy density, entropy density, trace anomaly, and speed of sound. We will plot our NNLO result both using one loop (1.35) and three loop (1.36) running cou-

pling. For both one- and three-loop running we fix the scale $\Lambda_{\overline{\text{MS}}}$ by requiring that $\alpha_s(1.5 \text{ GeV}) = 0.326$ which is obtained from lattice measurements [229]. For one-loop running, this procedure gives $\Lambda_{\overline{\text{MS}}} = 176 \text{ MeV}$, and for three-loop running, one obtains $\Lambda_{\overline{\text{MS}}} = 316 \text{ MeV}$.

5.7.1 Scales

For the renormalization scale we use separate scales, Λ_g and Λ , for purely-gluonic and fermionic graphs, respectively. We take the central values of these renormalization scales to be $\Lambda_g = 2\pi T$ and $\Lambda = 2\pi\sqrt{T^2 + \mu^2/\pi^2}$. In all plots the thick lines indicate the result obtained using these central values and the light-blue band indicates the variation of the result under variation of both of these scales by a factor of two, e.g. $\pi T \leq \Lambda_g \leq 4\pi T$. For all numerical results below we use $c_A = N_c = 3$ and $N_f = 3$.

5.7.2 Pressure

The QGP pressure can be obtained directly from the thermodynamic potential (5.86)

$$\mathcal{P}(T, \Lambda, \mu) = -\Omega_{\text{NNLO}}(T, \Lambda, \mu), \quad (5.90)$$

where Λ above is understood to include both scales Λ_g and Λ .

We note that in the ideal gas limit, the pressure becomes

$$\mathcal{P}_{\text{ideal}}(T, \mu) = \frac{d_A \pi^2 T^4}{45} \left[1 + \frac{7}{4} \frac{d_F}{d_A} \left(1 + \frac{120}{7} \hat{\mu}^2 + \frac{240}{7} \hat{\mu}^4 \right) \right]. \quad (5.91)$$

In Figs. (5.4) and (5.5) we compare the scaled NNLO HTLpt pressure for $\mu_B = 0$ (left) and $\mu_B = 400 \text{ MeV}$ (right) with lattice data from Refs. [8, 9, 110]. The deviations below $T \sim 200 \text{ MeV}$ are due to the fact that our calculation does not

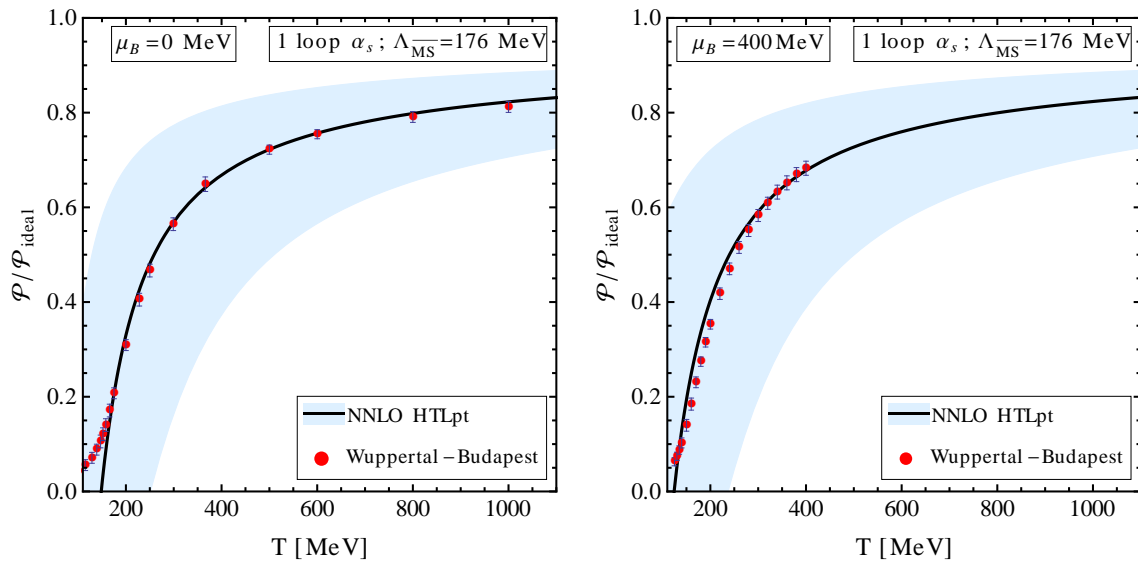


Figure 5.4: Comparison of the $N_f = 2 + 1$, $\mu_B = 0$ (left) and $\mu_B = 400$ MeV (right) NNLO HTLpt pressure with lattice data from Borsanyi et al. [8, 9]. For the HTLpt results a one-loop running coupling constant was used.

include hadronic degrees of freedom which dominate at low temperatures (see e.g. fits in [312]) or nonperturbative effects [313–319]. Further, in order to gauge the sensitivity of the results to the order of the running coupling, in Fig. (5.4) we show the results obtained using a one-loop running and in Fig. (5.5) the results obtained using a three-loop running. As can be seen by comparing these two sets, the sensitivity of the results to the order of the running coupling is small for $T \gtrsim 250$ MeV. As a result, unless the order of the running coupling turns out to have a significant effect on a given observable (see e.g. the fourth-order baryon number susceptibility), we will show the results obtained using a one-loop running coupling consistent with the counterterms necessary to renormalize the NNLO thermodynamic potential (5.5).

For an additional comparison we can compute the change in the pressure

$$\Delta\mathcal{P} = \mathcal{P}(T, \Lambda, \mu) - \mathcal{P}(T, \Lambda, 0). \quad (5.92)$$

In Fig. (5.6) we plot $\Delta\mathcal{P}$ as a function of the temperature for $\mu_B = 300$ MeV and $\mu_B = 400$ MeV. The solid lines are the NNLO HTLpt result and the dashed lines

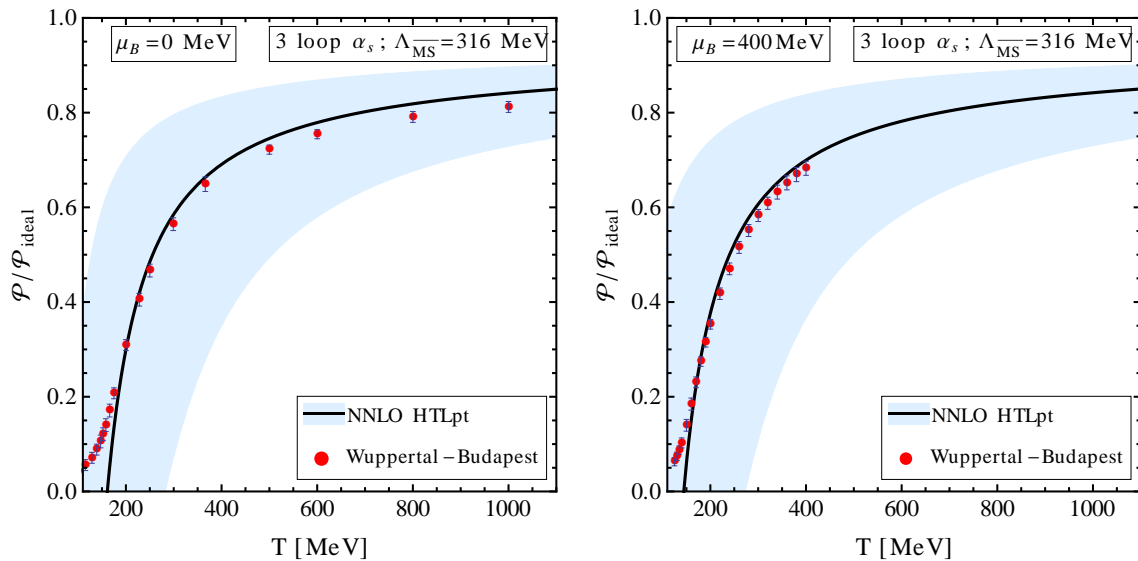


Figure 5.5: Same as Fig. (5.4) except with a three-loop running coupling constant.

are the result obtained in the Stefan-Boltzmann limit. We note that in Fig. (5.6) the lattice data from the Wuppertal-Budapest group [9] is computed up to $\mathcal{O}(\mu_B^2)$, whereas the HTLpt result includes all orders in μ_B . As can be seen from this figure, the NNLO HTLpt result is quite close to the result obtained in the Stefan-Boltzmann limit. Note that the small correction in going from the Stefan-Boltzmann limit to NNLO HTLpt indicates that the fermionic sector is, to good approximation, weakly coupled for $T \gtrsim 300$ MeV.

5.7.3 Energy density

Once the pressure is known, it is straightforward to compute other thermodynamic functions such as the energy density by computing derivatives of the pressure with respect to the temperature and chemical potential. The energy density can be obtained via

$$\mathcal{E} = T \frac{\partial \mathcal{P}}{\partial T} + \mu \frac{\partial \mathcal{P}}{\partial \mu} - \mathcal{P}. \quad (5.93)$$

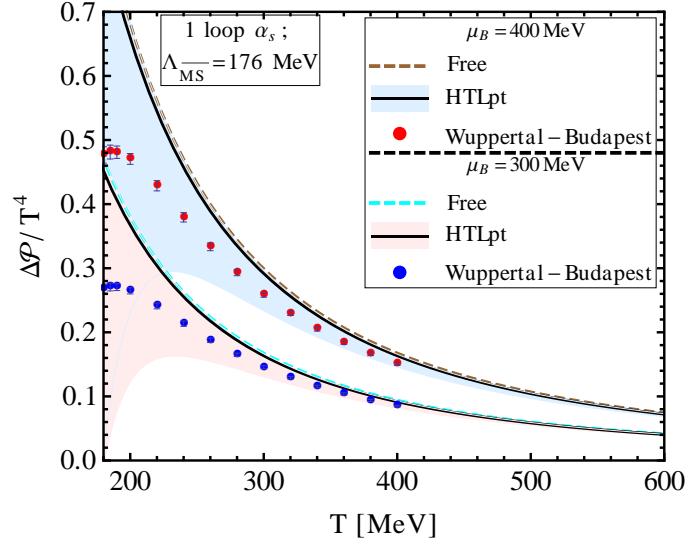


Figure 5.6: Comparison of the Stefan-Boltzmann limit (dashed lines) and NNLO HTLpt (solid lines) results for the scaled pressure difference with lattice data from Borsanyi et al. [9].

We note that in the ideal gas limit, the entropy density becomes

$$\mathcal{E}_{\text{ideal}}(T, \mu) = \frac{d_A \pi^2 T^4}{15} \left[1 + \frac{7}{4} \frac{d_F}{d_A} \left(1 + \frac{120}{7} \hat{\mu}^2 + \frac{240}{7} \hat{\mu}^4 \right) \right]. \quad (5.94)$$

In Fig. (5.7) we plot the scaled NNLO HTLpt energy density for $\mu_B = 0$ (left) and $\mu_B = 400$ MeV (right) together with $\mu_B = 0$ lattice data from Ref. [8]. As we can see from this figure, there is reasonable agreement between the NNLO HTLpt energy density and the lattice data when the central value of the scale is used.

5.7.4 Entropy density

Similarly, we can compute the entropy density

$$\mathcal{S}(T, \mu) = \frac{\partial \mathcal{P}}{\partial T}. \quad (5.95)$$

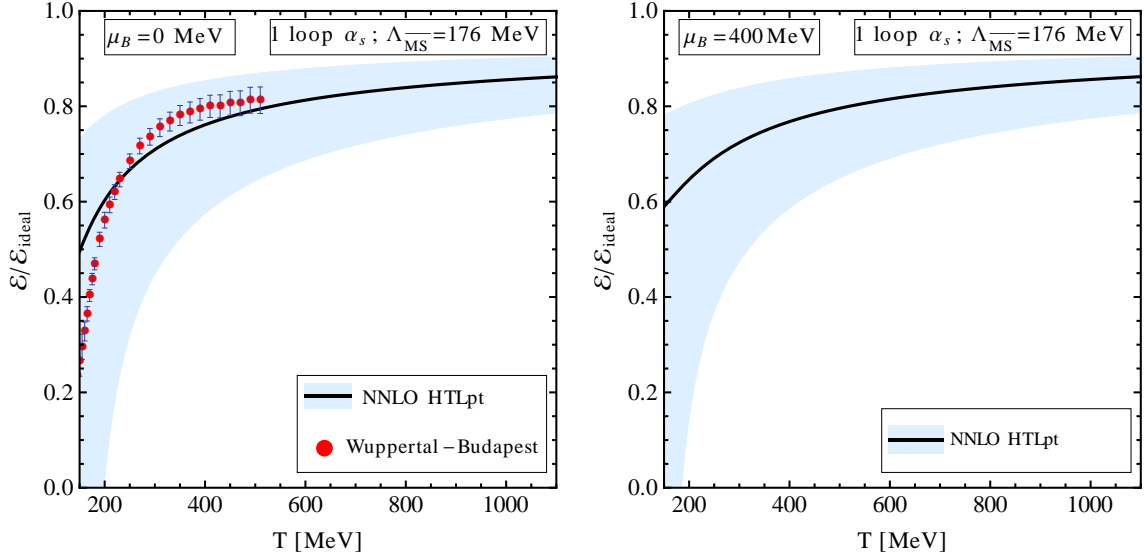


Figure 5.7: Comparison of the $N_f = 2 + 1$, $\mu_B = 0$ (left) and $\mu_B = 400$ MeV (right) NNLO HTLpt energy density with lattice data. The $\mu_B = 0$ lattice data are from [8]. For the HTLpt results a one-loop running coupling constant was used.

We note that in the ideal gas limit, the entropy density becomes

$$\mathcal{S}_{\text{ideal}}(T, \mu) = \frac{4d_A\pi^2 T^3}{45} \left[1 + \frac{7}{4} \frac{d_F}{d_A} \left(1 + \frac{60}{7} \hat{\mu}^2 \right) \right]. \quad (5.96)$$

In Fig (5.8) we plot the scaled NNLO HTLpt entropy density for $\mu_B = 0$ (left) and $\mu_B = 400$ MeV (right) together with $\mu_B = 0$ lattice data from Ref. [8]. As we can see from this figure, there is quite good agreement between the NNLO HTLpt entropy density and the lattice data when the central value of the scale is used.

5.7.5 Trace anomaly

Since it is typically the trace anomaly itself which is computed on the lattice and then integrated to obtain the other thermodynamic functions, it is interesting to compare directly with lattice data for the trace anomaly. The trace anomaly is simply $\mathcal{I} = \mathcal{E} - 3\mathcal{P}$. In the ideal gas limit, the trace anomaly goes to zero since

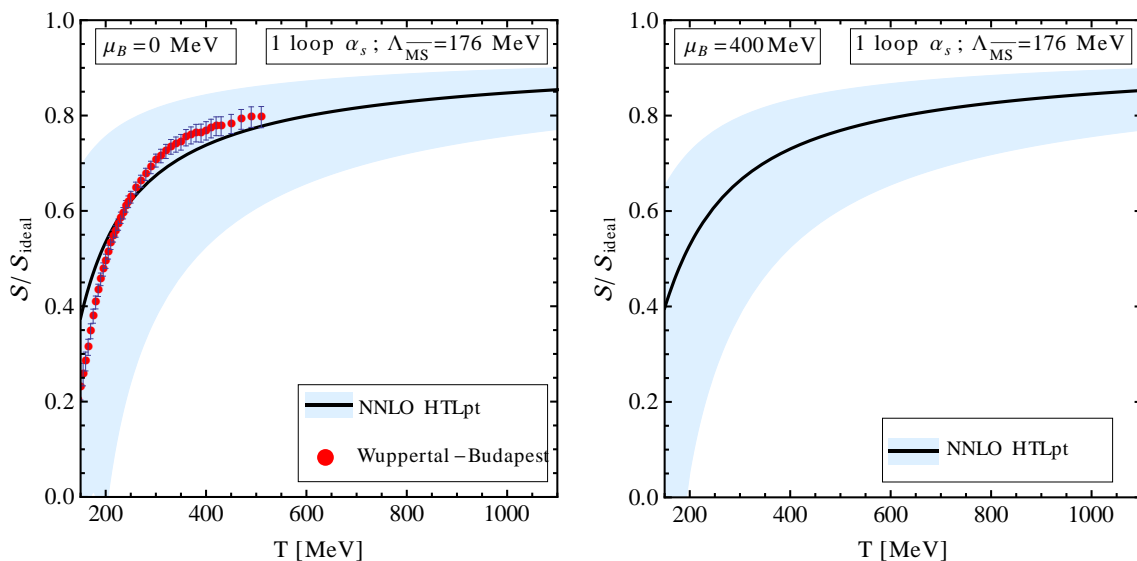


Figure 5.8: Comparison of the $N_f = 2 + 1$, $\mu_B = 0$ (left) and $\mu_B = 400$ MeV (right) NNLO HTLpt entropy density with lattice data. The $\mu_B = 0$ lattice data are from [8]. For the HTLpt results a one-loop running coupling constant was used.

$\mathcal{E} = 3\mathcal{P}$. When interactions are included, however, the trace anomaly (interaction measure) becomes non-zero.

In Fig. (5.9) we plot the scaled NNLO HTLpt trace anomaly for $\mu_B = 0$ (left) and $\mu_B = 400$ MeV (right) together with lattice data from Refs. [8] and [10]. As we can see from this figure, there is quite good agreement between the NNLO HTLpt trace anomaly and the lattice data for $T \gtrsim 220$ MeV when the central value of the scale is used.

5.7.6 Speed of sound

Another quantity which is phenomenologically interesting is the speed of sound. The speed of sound is defined as

$$c_s^2 = \frac{\partial \mathcal{P}}{\partial \mathcal{E}}. \quad (5.97)$$

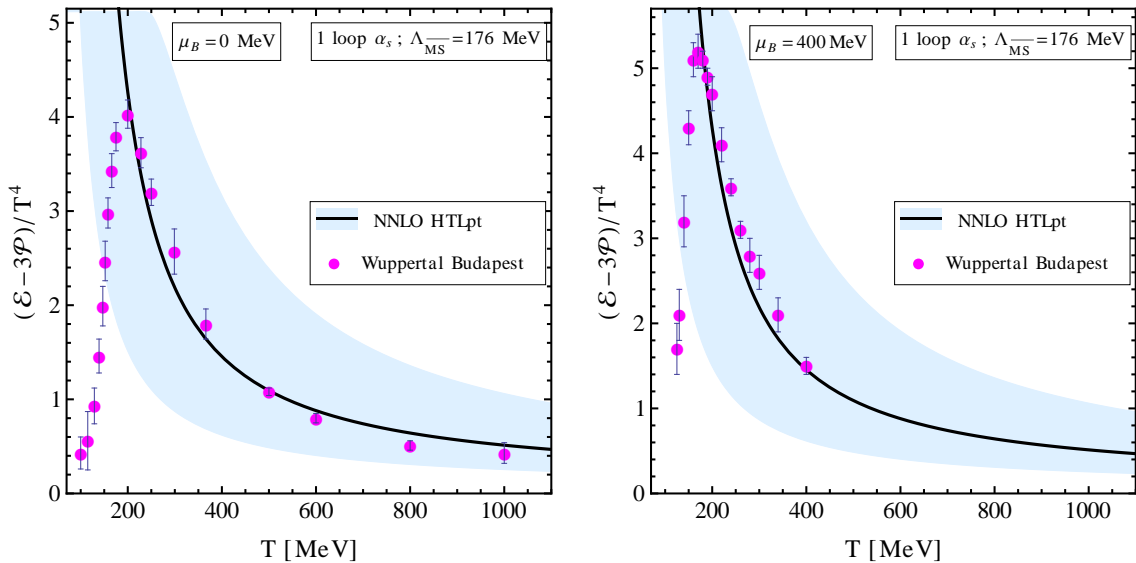


Figure 5.9: Comparison of the $N_f = 2 + 1$, $\mu_B = 0$ (left) and $\mu_B = 400$ MeV (right) NNLO HTLpt trace anomaly with lattice data. The $\mu_B = 0$ lattice data are from [8] and the $\mu_B = 400$ MeV lattice data are from [10]. For the HTLpt results a one-loop running coupling constant was used.

In Fig. (5.10) we plot the NNLO HTLpt speed of sound for $\mu_B = 0$ (left) and $\mu_B = 400$ MeV (right) together with lattice data from Refs. [8] and [10]. As we can see from this figure, there is quite good agreement between the NNLO HTLpt speed of sound and the lattice data when the central value of the scale is used.

5.8 Quark number susceptibilities

Having the full thermodynamic potential as a function of chemical potential(s) and temperature allows us to compute the quark number susceptibilities. In general, one can introduce a separate chemical potential for each quark flavor giving a N_f -dimensional vector $\boldsymbol{\mu} \equiv (\mu_1, \mu_2, \dots, \mu_{N_f})$. By taking derivatives of the pressure with respect to chemical potentials in this set, we obtain the quark number susceptibili-

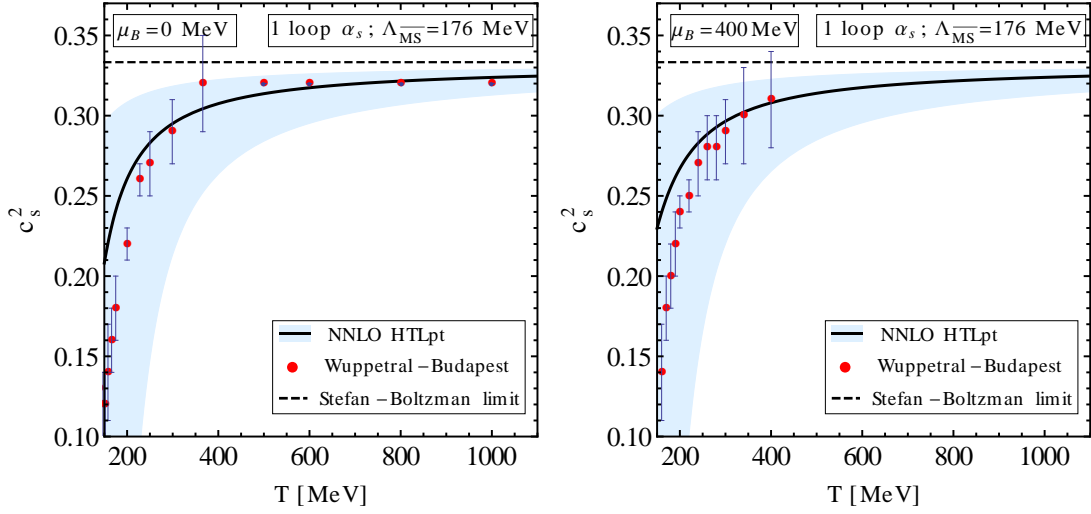


Figure 5.10: Comparison of the $N_f = 2+1$, $\mu_B = 0$ (left) and $\mu_B = 400$ MeV (right) NNLO HTLpt speed of sound squared with lattice data. The $\mu_B = 0$ lattice data are from [8] and the $\mu_B = 400$ MeV lattice data are from [10]. For the HTLpt results a one-loop running coupling constant was used.

ties¹

$$\chi_{ijk\dots}(T) \equiv \left. \frac{\partial^{i+j+k+\dots} \mathcal{P}(T, \boldsymbol{\mu})}{\partial \mu_u^i \partial \mu_d^j \partial \mu_s^k \dots} \right|_{\boldsymbol{\mu}=0}. \quad (5.98)$$

Below we will use a shorthand notation for the susceptibilities by specifying derivatives by a string of quark flavors in superscript form, e.g. $\chi_2^{uu} = \chi_{200}$, $\chi_2^{ds} = \chi_{011}$, $\chi_4^{uudd} = \chi_{220}$, etc.

When computing the derivatives with respect to the chemical potentials we treat Λ as being a constant and only put the chemical potential dependence of the Λ in after the derivatives are taken. We have done this in order to more closely match the procedure used to compute the susceptibilities using resummed dimensional reduction [246].²

¹We have specified that the derivatives should be evaluated at $\boldsymbol{\mu} = 0$. In general, one could define the susceptibilities at $\boldsymbol{\mu} = \boldsymbol{\mu}_0$.

²One could instead put the chemical potential dependence of the Λ in prior to taking the derivatives with respect to the chemical potentials. If this is done, the central lines obtained are very close to the ones obtained using the fixed- Λ prescription, however, the scale variation typically increases in this case.

5.8.1 Baryon number susceptibilities

We begin by considering the baryon number susceptibilities. The n^{th} -order baryon number susceptibility is defined as

$$\chi_B^n(T) \equiv \left. \frac{\partial^n \mathcal{P}}{\partial \mu_B^n} \right|_{\mu_B=0}. \quad (5.99)$$

For a three flavor system consisting of (u, d, s) , the baryon number susceptibilities can be related to the quark number susceptibilities [118]

$$\chi_2^B = \frac{1}{9} [\chi_2^{uu} + \chi_2^{dd} + \chi_2^{ss} + 2\chi_2^{ud} + 2\chi_2^{ds} + 2\chi_2^{us}], \quad (5.100)$$

and

$$\begin{aligned} \chi_4^B = \frac{1}{81} & \left[\chi_4^{uuuu} + \chi_4^{dddd} + \chi_4^{ssss} + 4\chi_4^{uudd} + 4\chi_4^{uus} \right. \\ & + 4\chi_4^{dddu} + 4\chi_4^{ddds} + 4\chi_4^{sssu} + 4\chi_4^{sssd} + 6\chi_4^{uudd} \\ & \left. + 6\chi_4^{ddss} + 6\chi_4^{uus} + 12\chi_4^{uuds} + 12\chi_4^{ddus} + 12\chi_4^{ssud} \right]. \quad (5.101) \end{aligned}$$

If we treat all quarks as having the same chemical potential $\mu_u = \mu_d = \mu_s = \mu = \frac{1}{3}\mu_B$, Eqs. (5.100) and (5.101) reduce to $\chi_2^B = \chi_2^{uu}$ and $\chi_4^B = \chi_4^{uuuu}$. This allows us to straightforwardly compute the baryon number susceptibility by computing derivatives of (5.86) with respect to μ . In Fig. (5.11) we compare the NNLO HTLpt result for the second order baryon number susceptibility with lattice data from various groups. In the left panel of this figure we used the one-loop running and on the right we used the three-loop running. As one can see, for this quantity, the size of the light-blue band becomes larger if one uses the three-loop running, however, the central value obtained is very close in both cases.

Comparing to the lattice data we see that the NNLO HTLpt prediction is approx-

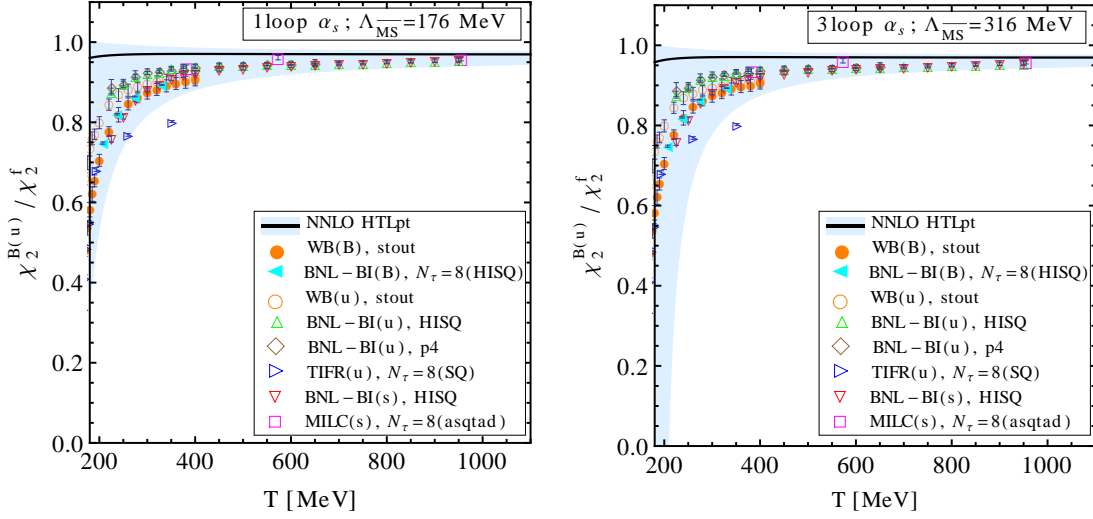


Figure 5.11: The scaled second order baryon number susceptibility compared with various lattice data using one loop running (left) and three-loop running (right). The lattice data labeled WB, BNL-BI(B), BNL-BI(u,s), MILC, and TIFR come from Refs. [11], [122], [123], [111], and [320], respectively.

imately 10% higher than the lattice data at $T = 250$ MeV and approximately 2% higher at $T = 800$ MeV. We note in this context that recently the four-loop second-order baryon number susceptibility has been computed in Ref. [246] using the resummed dimensional reduction method. The result from this approach lies within the NNLO HTLpt scale variation band and is even closer to the lattice data with the error at $T = 250$ MeV being approximately 2% and $\lesssim 1\%$ at $T = 800$ MeV. Our result, taken together with the resummed dimensional reduction results seem to indicate that the quark sector of the QGP can be quite accurately described using resummed perturbation theory for temperatures above approximately 300 MeV. In Fig. (5.12) we compare the NNLO HTLpt result for the fourth order baryon number susceptibility with lattice data. Once again we show in the left and right panels, the result obtain using the one-loop running coupling and three-loop running coupling, respectively. Both the one- and three-loop running results are consistent with the lattice data shown; however, the lattice error bars on this quantity are somewhat large and the data are restricted to temperatures below 400 MeV, making it difficult

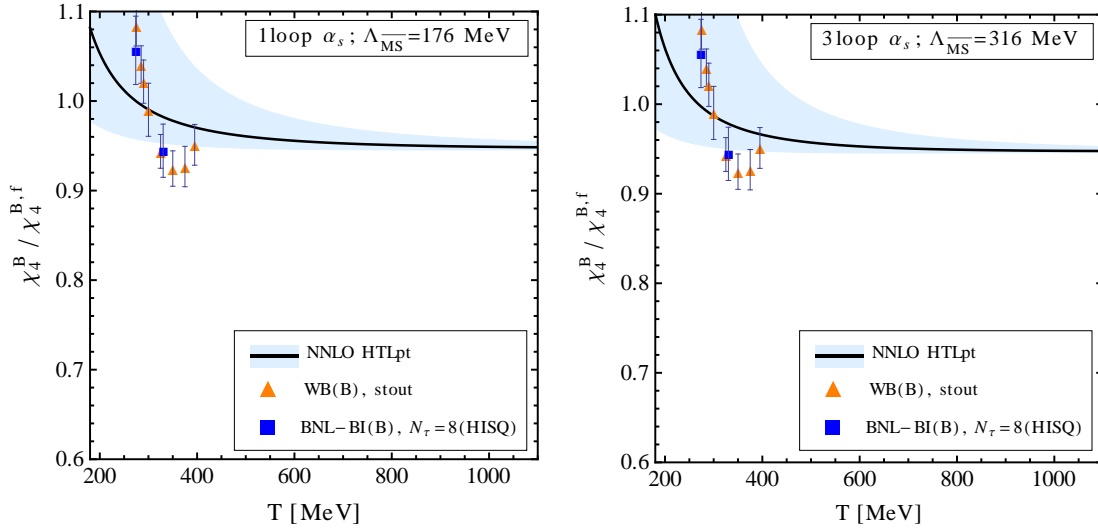


Figure 5.12: The scaled fourth order baryon number susceptibility compared with various lattice data using one loop running (left) and three-loop running (right). The lattice data labeled WB, BNL-BI(B), BNL-BI(u,s), MILC, and TIFR come from Refs. [11], [122], [123], [111], and [320], respectively.

to draw firm conclusions from this comparison. That being said, HTLpt makes a clear prediction for the temperature dependence of the fourth order baryon number susceptibility. It will be very interesting to see if future lattice data agree with this prediction.

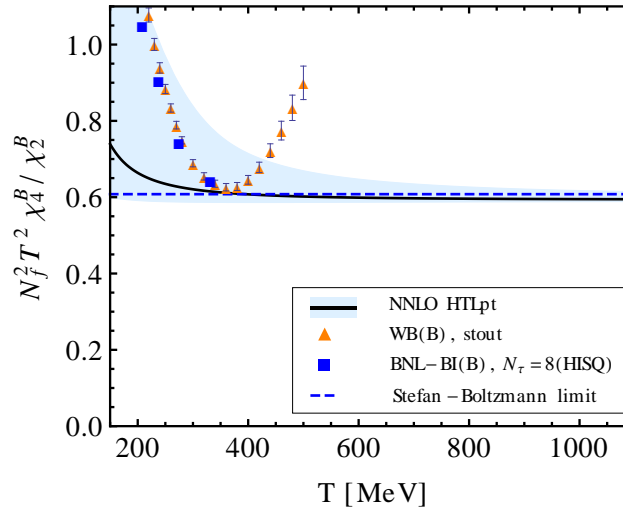


Figure 5.13: Comparison of the $N_f = 2 + 1$ NNLO HTLpt ratio of the fourth to second order baryon susceptibility with lattice data. For the HTLpt results a one-loop running coupling constant was used. The data labeled WB and BNL-BI(B) come from Refs. [82, 119] and [122], respectively.

In Fig. (5.13) we plot the scaled ratio of the fourth and second order baryon number susceptibilities as a function of temperature along with lattice data for this ratio. As we can see from this figure, this ratio very rapidly approaches the Stefan-Boltzmann limit if one considers the central NNLO HTLpt line. Comparing with the lattice data we see that the NNLO HTLpt result is below the lattice data for temperatures less than approximately 300 MeV. Without lattice data at higher temperatures, it's hard to draw a firm conclusion regarding the temperature at which HTLpt provides a good description of this quantity. In Fig. (5.14) we show the NNLO

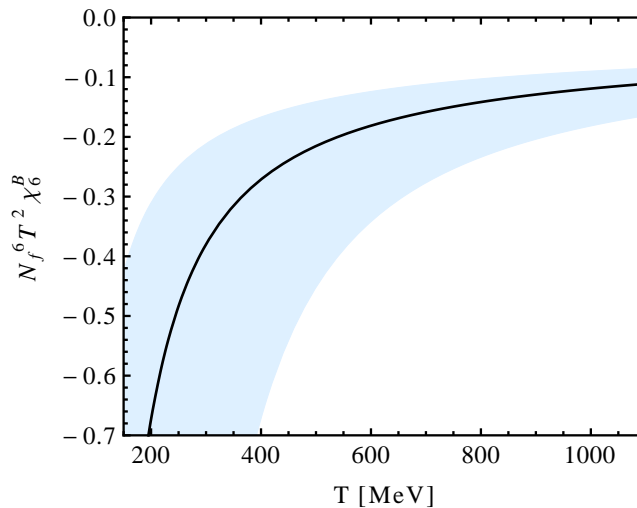


Figure 5.14: The $N_f = 2 + 1$ NNLO HTLpt scaled sixth-order baryon susceptibility as a function of temperature.

HTLpt prediction for the sixth order baryon number susceptibility. To the best of our knowledge there is currently no publicly available lattice data for this quantity. It will be very interesting to see if these NNLO HTLpt predictions agree with lattice data as they becomes available.

5.8.2 Single quark number susceptibilities

We now consider the single quark number susceptibilities (5.98). For these we use the general expression for the NNLO thermodynamic potential with different quark chemical potentials (5.88). The resulting susceptibilities can either be diagonal

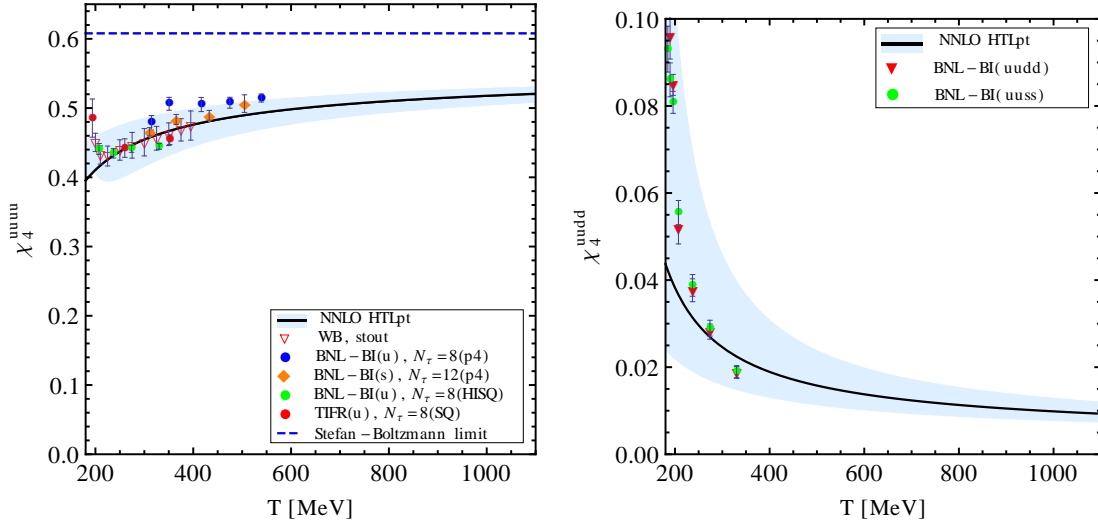


Figure 5.15: Comparison of the $N_f = 2 + 1$ NNLO HTLpt ratio of the fourth order diagonal single quark number susceptibility (left) and the only non-vanishing fourth order off-diagonal quark number susceptibility (right) with lattice data. In the left figure the dashed blue line indicates the Stefan-Boltzmann limit for this quantity. For the HTLpt results a one-loop running coupling constant was used. The data labeled BNL-BI(uudd), BNL-BI(u,s), BNL-BI(uuss), and TIFR come from Refs. [122], [123], [124], and [320], respectively.

(same flavor on all derivatives) or off-diagonal (different flavor on some or all indices). In HTLpt there are off-diagonal susceptibilities emerging explicitly from graphs \mathcal{F}_{3c}^f and \mathcal{F}_{3j}^f ; however, the latter vanishes when we use the variational mass prescription for the quark mass ($m_q = 0$), so we need only consider the \mathcal{F}_{3c}^f graph. Additionally, there are potential off-diagonal contributions coming from all HTL terms since the Debye mass receives contributions from all quark flavors. In practice, however, because we evaluate derivatives with respect to the various chemical potentials and then take $\mu_i \rightarrow 0$, one finds that all off-diagonal second order susceptibilities vanish in HTLpt. Therefore, for the three-flavor case one has

$$\chi_2^{ud} = \chi_2^{ds} = \chi_2^{su} = 0, \quad (5.102)$$

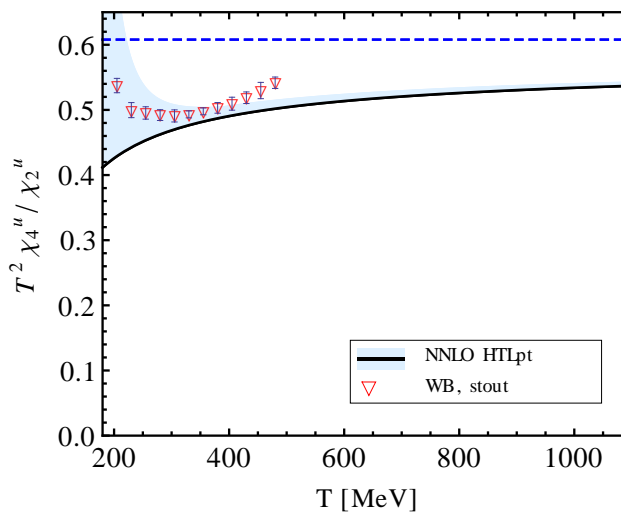


Figure 5.16: Comparison of the $N_f = 2 + 1$ NNLO HTLpt ratio of the fourth to second order single quark susceptibility with lattice data. For the HTLpt results a one-loop running coupling constant was used. The data labeled WB come from Refs. [82, 119].

and, as a result, the single quark second order susceptibility is proportional to the baryon number susceptibility

$$\chi_2^{uu} = \frac{1}{3}\chi_2^B. \quad (5.103)$$

For the fourth order susceptibility, there is only one non-zero off-diagonal susceptibility, namely $\chi_4^{uudd} = \chi_4^{uuss} = \chi_4^{ddss}$, which is related to the diagonal susceptibility, e.g. $\chi_4^{uuuu} = \chi_4^{dddd} = \chi_4^{ssss}$, as

$$\chi_4^{uuuu} = 27\chi_4^B - 6\chi_4^{uudd}. \quad (5.104)$$

As a consequence, one can compute χ_4^{uuuu} directly from (5.88) or by computing χ_4^B using (5.86) and χ_4^{uudd} using (5.88) and applying the above relation. In our final plots we compute χ_4^{uuuu} directly from (5.88), however, we have checked that we obtain the same result if we use (5.104) instead.

In Fig. (5.15) (left) we plot our result for the fourth order single quark susceptibility

χ_4^{uuuu} compared to lattice data from Refs. [123], [122], [124], and [320]. As we can see from this figure, for the fourth order susceptibility there is very good agreement with available lattice data. In addition, the scale variation of the HTLpt result is quite small for this particular quantity. In Fig. (5.15) (right) we plot our result for the fourth order off-diagonal single quark susceptibility χ_4^{uudd} compared to lattice data. From this right panel we also see reasonably good agreement between the NNLO HTLpt result and the available lattice data.

In Fig. (5.16) we plot the scaled ratio of the fourth- and second-order single quark susceptibilities. Once again we see good agreement between the NNLO HTLpt result and lattice data. Once again, for both Figs. (5.15) and (5.16), the lattice data are confined to relatively low temperatures. It will be interesting to compare higher temperature lattice data with the NNLO HTLpt prediction as they become available.

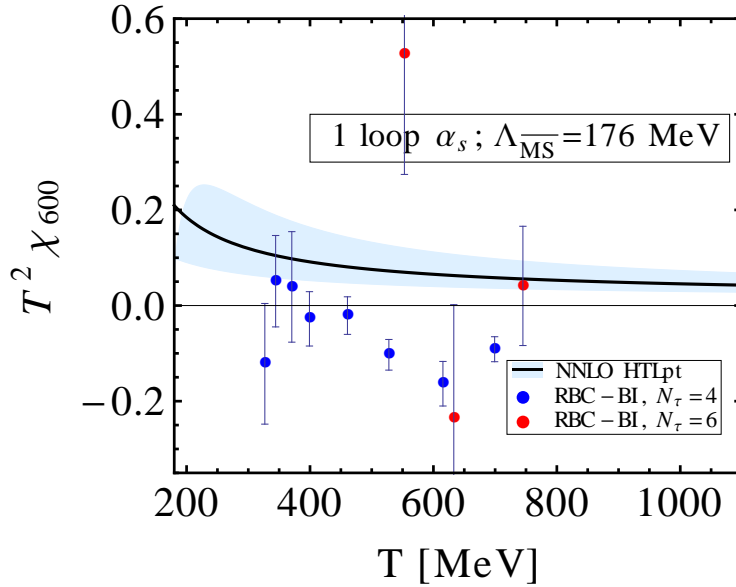


Figure 5.17: The $N_f = 2 + 1$ NNLO HTLpt scaled sixth-order diagonal single quark susceptibility χ_{600} as a function of temperature.

Finally, in Fig. (5.17) we plot the diagonal sixth-order quark number susceptibilities χ_{600} with available lattice data. In this figure we show lattice data available from

the RBC-Bielefeld collaboration [116]. At this point in time the lattice sizes are small and the errors bars for χ_{600} are large, so it is hard to draw a firm conclusion from this comparison.

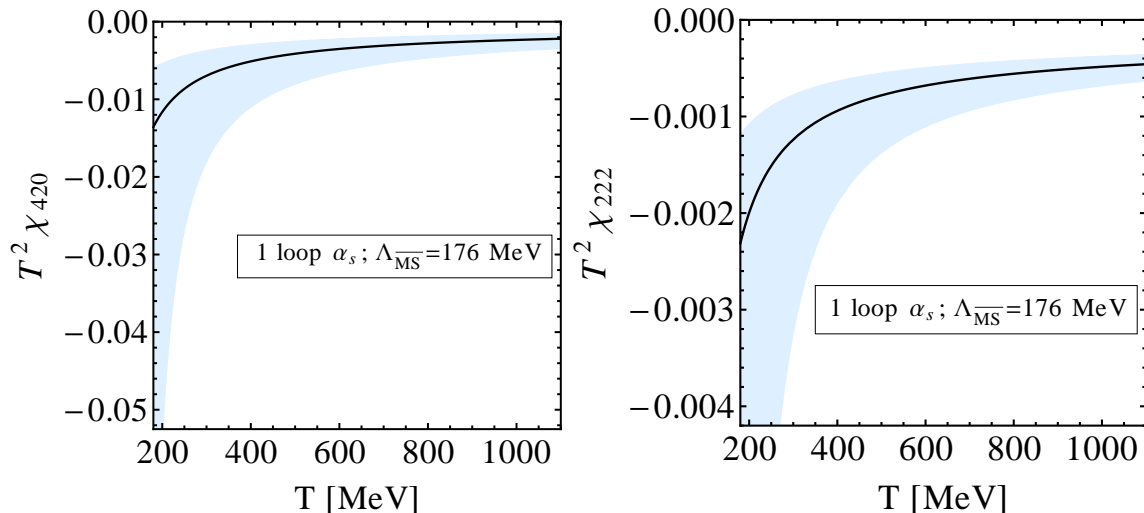


Figure 5.18: The $N_f = 2 + 1$ NNLO HTLpt scaled sixth-order off-diagonal single quark susceptibilities χ_{420} (left), and χ_{222} (right) as a function of temperature.

In Fig. (5.18) we plot off-diagonal sixth-order quark number susceptibilities χ_{420} (left), and χ_{222} (right). We are unaware of any lattice data for off-diagonal susceptibilities. As before, it will be very interesting to see if these NNLO HTLpt predictions agree with lattice data as they becomes available.

5.9 Conclusions and outlook

In this chapter, we presented the results of a NNLO (three-loop) HTLpt calculation of the thermodynamic potential of QCD at finite temperature and chemical potential(s). Our final result (5.88) is completely analytic and should be valid in the region of the phase diagram for which $\mu_i \lesssim 2\pi T$. Based on the resulting thermodynamic potential we proceeded to calculate the pressure, energy density, entropy density, trace anomaly, and speed of sound of the QGP. In all cases we found very good agreement between the results obtained using the central values of the renor-

malization scales and available lattice data. Additionally, we have made predictions for the diagonal and off-diagonal sixth-order baryon number and single quark susceptibilities.

Looking to the future there are still many avenues for improvement in the HTLpt approach: (1) inclusion of the effects of finite quark masses (2) extension of results to $\mu_i \gtrsim 2\pi T$ and eventually to $T = 0$, and (3) to potentially resum logarithms in order to reduce the scale variation of the final results (light-blue bands in all figures). Of these three, the second task is the most straightforward; however, in order to make more definitive and constrained statements it now seems necessary to start moving in directions (1) and (3) as well. In closing, we emphasize that HTLpt provides a gauge invariant reorganization of perturbation theory for calculating static quantities in thermal field theory. Since the NNLO HTLpt results are in good agreement with lattice data for various thermodynamic quantities down to temperatures that are relevant for LHC, it would therefore be interesting and challenging to apply HTLpt to the calculation of dynamic quantities, especially transport coefficients, at these temperatures.

CHAPTER 6

Dilepton Production Rate

In this chapter we study the low mass dilepton rate from deconfined state of matter using both perturbative and non-perturbative method. This chapter is based on: *Low Mass Dilepton Rate from the Deconfined Phase*, C. Greiner, N. Haque, M. G. Mustafa and M. H. Thoma, **Phys.Rev. C83 (2011) 014908**.

6.1 Introduction

The prime intention for ultra relativistic heavy-ion collisions is to study the behavior of nuclear or hadronic matter at extreme conditions like very high temperatures and/or high densities. A particular goal lies in the identification of a new state of matter formed in such collisions, the quark-gluon plasma (QGP), where the quarks and gluons are liberated from the nucleons and move freely over an extended space-time region. Various measurements taken in CERN-SPS [27] and BNL-RHIC [1–4, 28–32] do lead to ‘circumstantial evidence’ for the formation of QGP. Evidence is (or can only be) ‘circumstantial’ because only indirect diagnostic probes exist.

Electromagnetic probes, such as real photon and dileptons, are a particular example, and accordingly thermal dileptons have been theoretically proposed long time

ago [21]. At SPS energies [190–193] there was an indication for an enhancement of the dilepton production at low invariant mass ($0.2 \leq M(\text{GeV}) \leq 0.8$) compared to all known sources of electromagnetic decay of the hadronic particles and the contribution of a radiating simple hadronic fireball (for comprehensive reviews see Refs. [194–196]). One of the possible explanations of this is the modification of the in-medium properties of the vector meson (*viz.*, ρ -meson) by rescattering in a hadronic phase along with only the lowest order perturbative rate, *i.e.*, $q\bar{q}$ annihilation from a QGP [194–213]. Also at RHIC energies [28] a substantial amount of excess of electron pairs was reported in the low invariant mass region. Models taking into account in-medium properties of hadrons with various ingredients (see for details [214, 215]) can not explain the data from RHIC in the range $0.15 \leq M(\text{GeV}) \leq 0.5$, whereas they fit the SPS data more satisfactorily, indicating that a possible non-hadronic source becomes important at RHIC.

On the other hand, the higher order perturbative calculations [216] are also not very reliable at temperatures within the reach of the heavy-ion collisions. Moreover, perturbative calculations of the dilepton rate seem not to converge even in small coupling (g) limit. Nevertheless, the lowest order perturbative $q\bar{q}$ annihilation is the only dilepton rate from the QGP phase that is extensively used in the literatures. However, at large invariant mass this contribution should be dominant but not at low invariant mass, where nonperturbative effects should play an important role. Unfortunately, the lattice data [217] due to its limitations also could not shed any light on the low mass dileptons. However, the lattice calculations [7, 109–112, 218, 219] provide evidence for the existence of nonperturbative effects associated with the bulk properties of the deconfined phase, in and around the deconfined temperature, T_c . Also, indications have been found that the QGP at RHIC energies behaves more as a strongly coupled liquid than a weakly coupled gas [220]. Thus, a nonperturbative analysis of the dilepton rate from the deconfined phase is essential.

The dilepton emission at low invariant mass from the deconfined phase is still an unsettled issue in heavy-ion collisions at SPS and RHIC energies and, in particular, would be an important question for LHC energies and for compact baryonic matter formation in future FAIR energies, and also for the quark-hadron duality [194, 195, 221] that entails a reminiscence to a simple perturbative lowest order quark-antiquark annihilation rate [222]. In this chapter we reconsider the dilepton production rates within the perturbative QCD, and non-perturbative models based on lattice inputs and phenomenological $\rho - q$ interaction in the deconfined phase. The analysis suggests that the nonperturbative dilepton rates are indeed important at the low invariant mass regime.

This chapter is organised in following way. In section (6.2) we discuss the dilepton production rate from the deconfined phase based on both perturbative and non-perturbative models. In section (6.3) we compare the momentum integrated rates from both QGP and Hadron gas (HG). We discuss the quark-hadron duality in section (6.4), and conclude in section (6.5).

6.2 Dilepton Rate From Deconfined Phase

The dilepton production rate is related with the imaginary part of the photon self-energy [21, 321] as

$$\frac{dR}{d^4x d^4P} = -\frac{\alpha_{\text{em}}}{12\pi^4} \frac{1}{e^{E/T} - 1} \frac{\text{Im}\Pi_\mu^\mu(P)}{M^2}, \quad (6.1)$$

where $\alpha_{\text{em}} = e^2/4\pi$ is fine structure constant and P is four momentum of the virtual photon, E is its energy, and we use the notation $P \equiv (p_0 = E, \vec{\mathbf{p}})$ and $p = |\vec{\mathbf{p}}|$. The square of the invariant mass of dilepton pair is $M^2 = p_0^2 - p^2$.

6.2.1 Born Rate

To the lowest order the dilepton rate follows from one-loop photon self energy containing bare quark propagators. This rate corresponds to a dilepton production by the annihilation of bare quarks and antiquarks of the QGP. Alternatively, this so-called Born-rate can also be obtained from the matrix element of the basic annihilation process folded with the thermal distribution functions of quarks. In the case of massless lepton pairs in a QGP with two massless quark flavors with chemical potential one finds [222]

$$\frac{dR}{d^4x d^4P} = \frac{5\alpha_{\text{em}}^2 T}{36\pi^4} \frac{1}{p} \frac{1}{e^{\beta E} - 1} \ln \frac{(x_2 + \exp[-\beta(E + \mu)])(x_1 + \exp[-\beta\mu])}{(x_1 + \exp[-\beta(E + \mu)])(x_2 + \exp[-\beta\mu])}, \quad (6.2)$$

where $\beta = 1/T$, $x_1 = \exp[-\beta(E + p)/2]$ and $x_2 = \exp[-\beta(E - p)/2]$. A finite quark mass can easily be included.

For $\mu = 0$ the dilepton rate becomes

$$\frac{dR}{d^4x d^4P} = \frac{5\alpha_{\text{em}}^2 T}{18\pi^4} \frac{1}{p} \frac{1}{e^{E/T} - 1} \ln \left(\frac{\cosh \frac{E+p}{4T}}{\cosh \frac{E-p}{4T}} \right), \quad (6.3)$$

whereas that for total three momentum $\vec{p} = 0$ is given as

$$\frac{dR}{d^4x d^4P} = \frac{5\alpha_{\text{em}}^2}{36\pi^4} n(E/2 - \mu) n(E/2 + \mu), \quad (6.4)$$

with $n(y) = (\exp(\beta y) + 1)^{-1}$, the Fermi-Dirac distribution function.

6.2.2 Rate using Hard Thermal Loop perturbation theory

In order to judge the reliability of the lowest order result, one should consider higher order corrections. These corrections involve quarks and gluons in the photon self energy beyond the one-loop approximation. Using bare propagators at finite temper-

ature, however, one encounters infrared singularities and gauge dependent results. These problems can be resolved, at least partially, by adopting the Hard-Thermal Loop (HTL) resummation scheme [150, 156]. The key point of this method is the distinction between the soft momentum scale ($\sim gT$) and the hard one ($\sim T$), which is possible in the weak coupling limit ($g \ll 1$). Resumming one-loop self energies, in which the loop momenta are hard (HTL approximation), effective propagators and vertices are constructed, which are as important as bare propagators if the momentum of the quark or gluon is soft. In HTLpt the bare N -point functions (propagator and vertices) are replaced by those effective N -point HTL functions which describe medium effects in the QGP such as the thermal masses for quarks and gluons and Landau damping.

The importance of the medium and other higher order effects on the dilepton rate depends crucially on the invariant mass and the momenta of the virtual photon. Therefore, we will discuss now the different kinematical regimes:

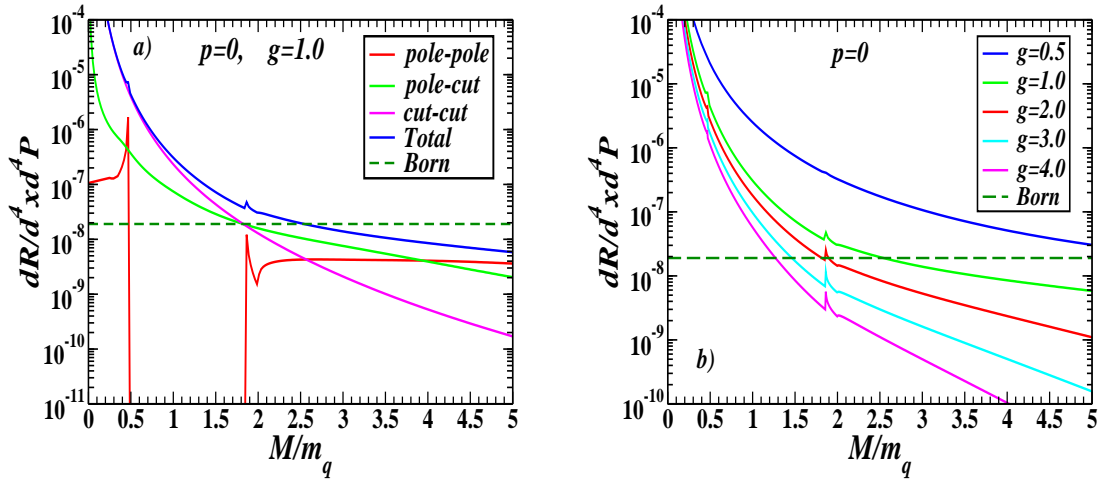


Figure 6.1: Left panel (a): 1-loop dilepton rate for small invariant masses $M \sim gT$ at zero momentum and Born-rate (dashed line) versus the scaled invariant photon mass M/m_q for $g = 1$. The van Hove peaks and energy gap are evident in the 1-loop rate. Right panel (b): Total 1-loop rate for various g values.

Soft Rate ($M \sim gT$ and $p \sim gT$)

For soft invariant masses¹ and momenta of order gT one has to use HTL quark propagators and vertices in the one-loop photon self energy. These corrections are of same order as the Born-term [250]. Physically these corrections correspond to two different processes. First the poles of the HTL resummed quark propagators describe quasiparticles in the QGP with an effective thermal quark mass of the order of gT . Hence dileptons are generated by the annihilation of collective quark modes instead of bare quarks. In particular the HTL quark dispersion contains a so called plasmino branch which exhibits a minimum at finite momentum. This nontrivial dispersion leads to sharp structures (van Hove singularities and energy gap) in the dilepton production rate² in contrast to smooth Born-rate. Secondly, the imaginary part of the HTL quark self energy containing effective HTL N -point (propagators and quark-photon vertex) functions corresponds to processes involving the absorption or emission of thermal gluons.

The 1-loop dilepton rate in HTL approximation for zero momentum can be given from [250] as

$$\begin{aligned}
 \frac{dR}{d^4x d^4P} &= \frac{10\alpha_{\text{em}}^2}{9\pi^4 E^2} \int_0^\infty k^2 dk \int_{-\infty}^\infty \frac{dk_0}{2\pi} \int_{-\infty}^\infty \frac{dk'_0}{2\pi} n(k_0)n(k'_0) \\
 &\times \delta(E - k_0 - k'_0) \left[4 \left(1 - \frac{k_0^2 - k'^2_0}{2kE} \right)^2 \rho_+(k_0, k) \rho_-(k'_0, k) \right. \\
 &+ \left(1 + \frac{k_0^2 + k'^2_0 - 2k^2 - 2m_q^2}{2kE} \right)^2 \rho_+(k_0, k) \rho_+(k'_0, k) \\
 &+ \left. \left(1 - \frac{k_0^2 + k'^2_0 - 2k^2 - 2m_q^2}{2kE} \right)^2 \rho_-(k_0, k) \rho_-(k'_0, k) \right]
 \end{aligned}$$

¹Note that for ultrasoft $M \sim g^2T$ and arbitrary momentum the rate is non-perturbative and cannot be calculated even within the HTL improved perturbation theory. This observation holds in particular for real hard photon [322].

²For a discussion of van Hove singularities in the QGP at $\vec{p} = 0$ see Refs. [250, 290, 323, 324] and also Ref. [325] for $\vec{p} \neq 0$.

$$\begin{aligned}
 & + \Theta(k^2 - k_0^2) \frac{m_q^2}{4kE^2} \left(1 - \frac{k_0^2}{k^2}\right) \left[\left(1 + \frac{k_0}{k}\right) \rho_+(k'_0, k) \right. \\
 & \left. + \left(1 - \frac{k_0}{k}\right) \rho_-(k'_0, k) \right] \Bigg] \tag{6.5}
 \end{aligned}$$

where $\rho_{\pm}(k'_0, k)$ is spectral functions of quark propagator $D_{\pm}((k'_0, k))$ which is defined in Eqn. (2.79) of chapter (2).

In Fig. (6.1) the 1-loop dilepton rate for zero momentum, containing such processes using Eq. (6.5), is displayed as a function of the scaled invariant mass with the thermal quark mass and is also compared with the Born-rate. In the left panel of Fig. (6.1a) the van Hove singularities due to the nontrivial dispersion of quarks in a medium are evident in pole-pole contributions whereas the pole-cut and cut-cut contributions³ are smooth representing absorption and emission of gluons in the medium. The right panel of Fig. (6.1b) displays the total one-loop contribution for a set of values of g , where the energy gaps are smoothed due to the pole-cut and cut-cut contributions. Also the structures due to the van Hove singularities become also less prominent in the total contributions. The HTL rate, in particular, due to the cut contributions is also singular at $M \rightarrow 0$ because the HTL quark-photon vertex is inversely proportional to photon energy.

However, these corrections are not sufficient and two-loop diagrams within HTL perturbation scheme contribute to the same order and are even larger than the one-loop results [216]. The total one- and two-loop rate at $\vec{\mathbf{p}} = 0$ and $M \ll T$ in the leading logarithm, *i.e.*, $\ln(1/g)$ approximation reads [216, 326]

$$\begin{aligned}
 \frac{dR}{d^4x d^4P} = & \frac{5\alpha_{\text{em}}^2 m_q^2}{9\pi^6 M^2} \left[\frac{\pi^2 m_q^2}{4M^2} \ln \frac{T^2}{m_q^2} + \frac{3m_q^2}{M^2} \ln \frac{T^2}{m_g^2} + \frac{\pi^2}{4} \ln \left(\frac{MT}{M^2 + m_q^2} \right) \right. \\
 & \left. + 2 \ln \left(\frac{MT}{M^2 + m_g^2} \right) \right], \tag{6.6}
 \end{aligned}$$

³These are due to the space-like ($k^2 > k_0^2$) part of the N -point HTL functions (k^2) that acquire a cut contribution from below the light cone.

where the thermal gluon mass is given by $m_g^2 = 8m_q^2/3$ with $m_q = gT/\sqrt{6}$. It is worth to mention here that the two-loop rate in 6.6 is not complete, they have consider only gluon in two-loop photon self energy diagram as soft but other fermions as hard. To compute complete two-loop dilepton rate in HTL perturbation theory, one need to consider all the loop momenta as effective. Note that this expression is of the same order in g as the Born-term for soft $M \sim gT$. Now the Born-term for $\vec{p} = 0$ and $M \ll T$ is simply given by

$$\frac{dR}{d^4x d^4P} = \frac{5\alpha_{\text{em}}^2}{144\pi^4} = 1.90 \times 10^{-8} . \quad (6.7)$$

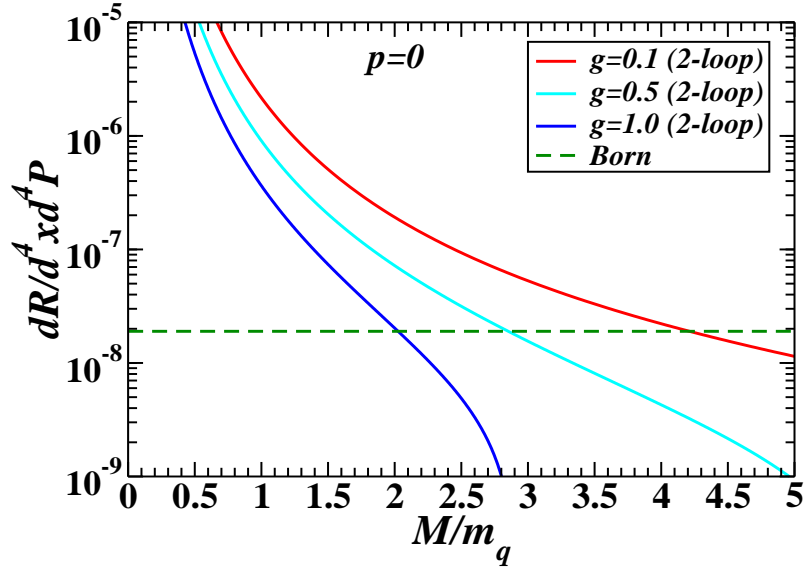


Figure 6.2: Complete 2-loop dilepton rate for small invariant masses $M \sim gT$ at zero momentum and Born-rate (dashed line) versus the scaled invariant photon mass M/m_q with the thermal quark mass m_q .

In Fig. (6.2) the Born-rate and the complete two-loop rate for a set of values of g are compared. It is evident from Fig. (6.2) that the 2-loop rate dominates in the perturbative regime ($g \leq 1$) over the Born-term for low mass domain, $M/m_q \leq 2$. However, the van Hove singularities contained in one-loop do not appear as they are washed out due to the leading logarithm approximation within the two-loop HTL perturbation theory.

Semi-hard Rate ($M \sim T$ and $p \gg T$)

For M of the order of T and hard momenta ($p \gg T$), the α_s -correction to the Born-rate has been calculated [327] within the HTLpt method as

$$\frac{dR}{d^4x d^4P} = \frac{5\alpha_{\text{em}}^2 \alpha_s T^2}{27\pi^3 M^2} e^{-E/T} \left(\ln \frac{T(m_q + k^*)}{m_q^2} + C \right), \quad (6.8)$$

where $k^* \approx |Em_q^2/M^2 - m_q^2/(4E)| < (E + p)/2$ and $C \approx -0.5$ depends weakly on M . In Ref. [296, 328, 329] it has been shown that further corrections to the rate (6.8) are necessary. However, numerical results showed only a slight modification.

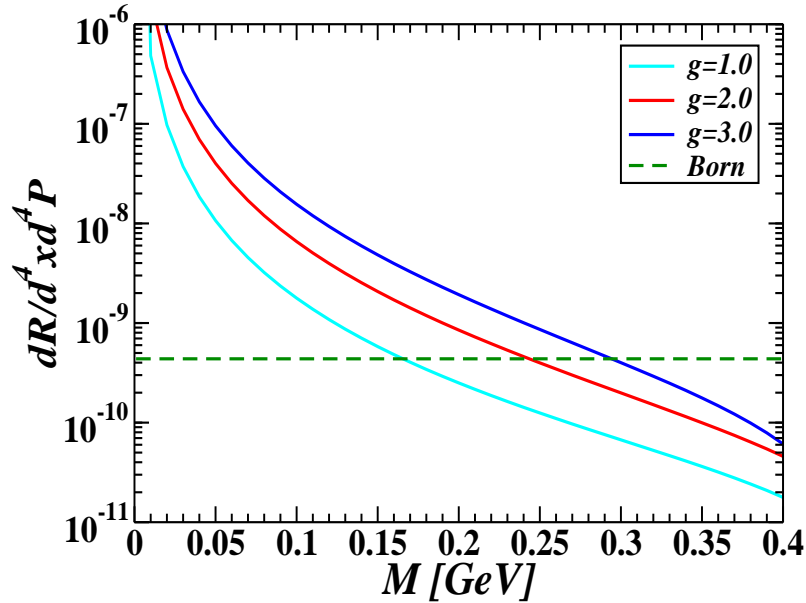


Figure 6.3: α_s -correction to the dilepton rate and Born-rate (dashed line) versus the invariant photon mass M scaled with the thermal quark mass for $T = 200$ MeV and $E = 1$ GeV.

Assuming typical values of the strong coupling constant and temperature, $T = 200$ MeV, these corrections dominate over the Born term for invariant masses below 300 MeV as shown in Fig. (6.3). Similar results have been obtained using bare quark propagators [330]. However, the calculation within naive perturbation theory [331,

[332] resulted in α_s -corrections which are of similar size as the Born-rate in the regime M and p of the order of T .

Hard Rate ($M \gg T$)

For $M \gg T$ naive perturbation theory using bare propagators and vertices is sufficient. This is in contrast to the production of real photons, where one encounters an infrared singularity from bare quark propagator [333, 334]. For finite M , however, this singularity cancels [335]. Bare two-loop calculations [331, 332, 335] showed that the α_s -corrections are negligible in this regime. However, a recent calculation of the α_s -corrections [336] for large invariant mass $M \gg T$ and small momenta $p \ll T$ yielded important corrections to the Born-rate for invariant masses below $(2 - 3)T$. However, this work has also been criticized [337].

The main problem in applying perturbative results discussed above to realistic situations is the fact that g is not small but rather we have $g \sim 1.5 - 2.5$. Close to the critical temperature, T_c , even g could be as high as 6 [60, 61, 338]. Hence the different momentum scales are not distinctly separated in the real sense and, even if one still believes in perturbative results (see Fig. (6.1), 6.2 and 6.3) at least qualitatively, it is not clear which of the above rates applies to heavy-ion collisions. However, in all cases there are substantial corrections to the Born-rate. The perturbative rates within their uncertainties in various regime probably suggest that the Born-rate may not be sufficient for describing the low mass dilepton spectrum.

6.2.3 Rate using Gluon Condensate within the Green Function

An important issue towards the understanding the phase structure of QCD is to understand the various condensates, which serve as order parameters of the broken

symmetry phase. These condensates are non-perturbative in nature and lattice provides a connection with bulk properties of QCD matter. However, the quark condensate has a rather small impact on the bulk properties, *e.g.*, on the equation of state of QCD matter, compared to the gluon condensate [7]. The relation of the gluon condensate to the bulk properties such as equation of states, in principle, can be tested through hydrodynamic or transport properties sensitive to the equation of states, but is a non-trivial task.

A semi-empirical way to consider nonperturbative aspects, *e.g.*, gluon condensate has been suggested by combining lattice results with Green function in momentum space [339, 340]. In this approach the effective N -point functions [339, 340] have been constructed which contain the gluon condensate in the deconfined phase, measured in lattice QCD [7]. The resulting quark dispersion relation with a mass $m_q \sim 1.15T_c$ [339] in the medium shows qualitatively the same behavior as the HTL dispersion, leading again to sharp structures (van Hove singularities, energy gap) in the dilepton production rates [341, 342], indicating that this features are universal in relativistic plasmas independent of the approximation used [323, 324]. In Fig. (6.4) the dilepton production rate using gluon condensate is displayed for various values of momentum at $T = 2T_c$ and also compared with the Born-rate. At very low invariant mass ($M/T_c \leq 2$; for $T_c \sim 165$ MeV, $M \leq 330$ MeV) with realistic momentum the dilepton rate with gluon condensate dominates over the Born-rate. This rate will be important at very low invariant mass as it has non-perturbative input from lattice QCD that describes the bulk properties of the deconfined phase, and is of course free from any uncertainty related to the strong coupling g associated with the perturbative rates discussed in Sec. 6.2.2.

We, however, also note that the rate deviates from the Born-rate at high M/T_c (≥ 4). The difference at high M/T_c has the origin in the asymptotic limit (large momentum k) of the quark dispersion relation with gluon condensates. In this limit

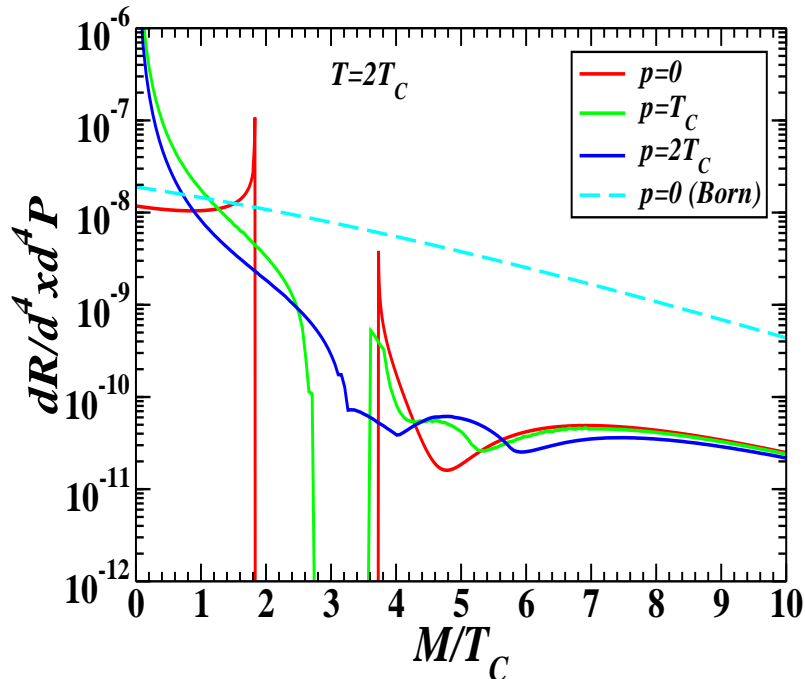


Figure 6.4: Van Hove singularities in the dilepton rate in the presence of gluon condensate as a function of invariant mass scaled with T_c for a set of momenta at $T = 2T_c$. The dashed curve is for Born-rate at zero momentum.

it is found that the normal quark mode behaves like $w_+ = k + c$, where c contains still the non-zero contribution from the condensates. The reason for which is the use of the momentum independent condensate values. This fact has crept in the dilepton rate at high M/T_c . One way out could be to use an *ad hoc* separation scale ($M/T_c \sim 2 - 3$) up to which one may employ the non-perturbative quark dispersion associated with the gluon condensate and beyond which a free dispersion is adopted. Alternatively, one could use a momentum dependent condensate, which is again beyond the scope of our calculation and has to be provided by the lattice analysis. To date we are not aware of such analysis. Nonetheless, we note that the nonperturbative contribution is important only at low invariant mass as we would see later in Sec. 6.3.

6.2.4 Rate from quark and ρ^0 -meson Interaction (ρ -meson in QGP)

We assume that ρ -meson like states ($q\bar{q}$ correlator in the ρ -meson channel) can exist in a deconfined phase like QGP. Then there will also be a contribution from ρ -meson channel to the dilepton pairs (l^+l^-) in addition to the perturbative production. In order to consider such a channel phenomenologically an interaction of $\rho - q$ coupling is introduced through the Lagrangian [343]

$$\mathcal{L} = -\frac{1}{4}\rho_{\mu\nu}^a\rho_a^{\mu\nu} + \frac{1}{2}m_\rho^2\rho_\mu^a\rho_a^\mu + \bar{q}\left(i\gamma_\mu\partial^\mu - m_q + G_\rho\gamma^\mu\frac{\tau_a}{2}\rho_\mu^a\right)q, \quad (6.9)$$

where q is the quark field, m_q is the quark mass, a is the isospin or flavor index, and τ_a is the corresponding isospin matrix. The $\rho - q$ coupling, G_ρ , can be obtained in the same spirit as the 4-point interaction, $G_2(\bar{q}\gamma_\mu\tau_a q)^2$, in NJL-model. This suggests $G_\rho = \sqrt{8m_\rho^2 G_2} \sim 6$, by taking G_2 from the literature. The similar value for G_ρ can be obtained by simply assuming that the ρ -meson couples in a universal way to nucleons, pions and quarks [343].

Now using the Vector Meson Dominance (VMD) [321] the photon self-energy is related to the ρ^0 meson propagator, $D_{\mu\nu}(P)$, by

$$\text{Im}\Pi_\mu^\mu(P) = \frac{e^2}{G_\rho^2}m_\rho^4 \text{Im}D_\mu^\mu(P) . \quad (6.10)$$

Then the thermal dilepton production rate from the ρ -meson can be written as

$$\frac{dR}{d^4x d^4P} = -\frac{1}{3\pi^3} \frac{\alpha_{\text{em}}^2}{G_\rho^2} \frac{m_\rho^4}{M^2} \frac{1}{e^{E_p/T} - 1} (\mathcal{A}_\rho^L + 2\mathcal{A}_\rho^T) , \quad (6.11)$$

and the spectral functions for ρ -meson can be obtained from the self-energy of

ρ -meson as

$$\mathcal{A}_\rho^L(P) = \frac{\text{Im}\mathcal{F}}{(M^2 - m_\rho^2 - \text{Re}\mathcal{F})^2 + (\text{Im}\mathcal{F})^2}, \quad (6.12)$$

$$\mathcal{A}_\rho^T(P) = \frac{\text{Im}\mathcal{G}}{(M^2 - m_\rho^2 - \text{Re}\mathcal{G})^2 + (\text{Im}\mathcal{G})^2}, \quad (6.13)$$

where $\mathcal{F} = -\frac{P^2}{p^2}\Pi^{00}(P)$ and $\mathcal{G} = \Pi_T(P)$ with L and T stand for longitudinal and transverse modes, respectively.

Going beyond the HTL approximation, the integral expression for the matter part of the one-loop photon self energy for assymmetric charges in the deconfined phase (*viz.*, with non-zero chemical potential, μ , which would be appropriate for FAIR energies can be obtained easily by extending the results of Ref. [343] to finite chemical potential as,

$$\begin{aligned} \text{Re } \mathcal{F} = \frac{3G^2}{4\pi^2} \frac{M^2}{p^2} \int_0^\infty dk k \left[\frac{M^2 + 4\omega_k^2}{4p\omega_k} \ln |a| + \frac{p_0}{p} \ln |b| - \frac{2k}{\omega_k} \right] \\ \times [n(\omega_k - \mu) + n(\omega_k + \mu)], \end{aligned}$$

$$\begin{aligned} \text{Im } \mathcal{F} = \frac{3G^2}{4\pi} \frac{M^2}{p^3} \int_{k_-}^{k_+} dk k \left[p_0 - \omega_k - \frac{M^2}{4\omega_k} \right] \\ \times [n(\omega_k - \mu) + n(\omega_k + \mu)], \end{aligned}$$

$$\begin{aligned} \text{Re } \mathcal{G} = \frac{3G^2}{4\pi^2} \int_0^\infty dk \frac{k^2}{\omega_k} \left[- \left(\frac{\omega_k^2 M^2}{2p^3 k} + \frac{M^2}{4pk} + \frac{M^4}{8p^3 k} + \frac{m_q^2}{2pk} \right) \ln |a| \right. \\ \left. + 2 + \frac{M^2}{p^2} - \frac{p_0 M^2 \omega_k}{2p^3 k} \ln |b| \right] [n(\omega_k - \mu) + n(\omega_k + \mu)], \end{aligned}$$

$$\begin{aligned} \text{Im } \mathcal{G} = \frac{3G^2}{8\pi p} \int_{k_-}^{k_+} dk k \left[-\omega_k + \frac{m_q^2}{\omega_k} + \frac{p_0^2}{p^2} \omega_k + \frac{M^2}{2\omega_k} + \frac{M^4}{4\omega_k p^2} - \frac{p_0 M^2}{p^2} \right] \\ \times [n(\omega_k - \mu) + n(\omega_k + \mu)], \quad (6.14) \end{aligned}$$

along with

$$a = \frac{(M^2 + 2pk)^2 - 4p_0^2\omega_k^2}{(M^2 - 2pk)^2 - 4p_0^2\omega_k^2}, \quad b = \frac{M^4 - 4(pk + p_0\omega_k)^2}{M^4 - 4(pk - p_0\omega_k)^2},$$

$$k_- = \frac{1}{2} \left| p_0 \sqrt{1 - \frac{4m_q^2}{M^2}} - p \right|, \quad k_+ = \frac{1}{2} \left(p_0 \sqrt{1 - \frac{4m_q^2}{M^2}} + p \right),$$

where $\omega_k = \sqrt{k^2 + m_q^2}$.

In Fig. (6.5) the ρ -meson spectral function related to the imaginary part of the ρ -meson propagator (left panel) in (6.10) and the dilepton rate (right panel) are displayed for various temperature with $\mu = 0$ and $p = 200$ MeV. As the temperature increases the peak in the imaginary part of the ρ -meson propagator D becomes broader and is also reflected in the dilepton rate. When the invariant mass is low (≤ 1 GeV), the rate is comparable with the Born-rate.

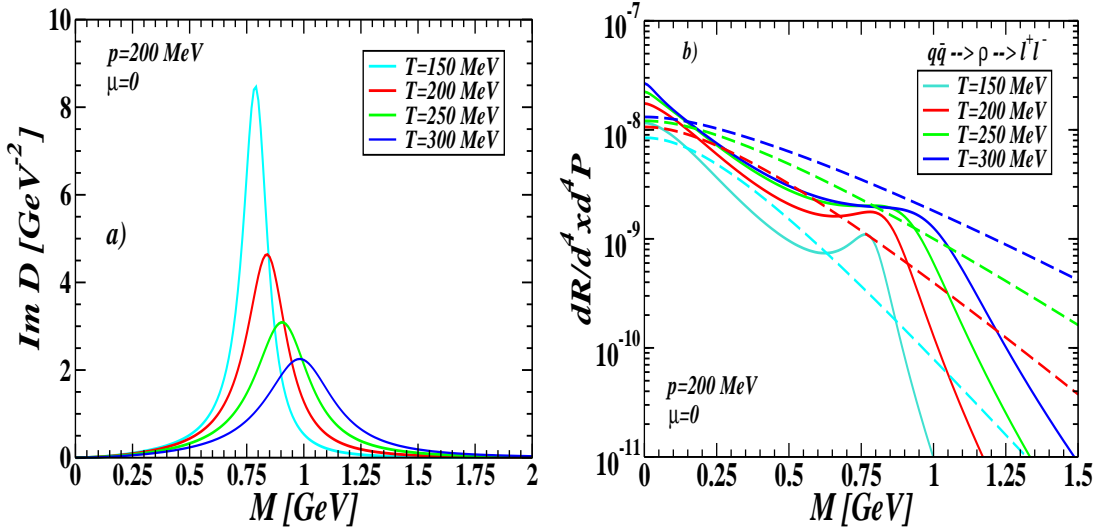


Figure 6.5: *Left panel:* Imaginary part of ρ -meson propagator (spectral function) as a function of the invariant mass M for a set of values T . *Right panel:* The dilepton rate from ρ -meson in a QGP as a function of M . The dashed lines are corresponding Born-rates. We have used $G_\rho = 6$.

In Fig. (6.6) the ρ -meson spectral function (left panel) and the dilepton rate (right panel) are displayed for various μ at $T = 160$ MeV and $p = 200$ MeV, which could

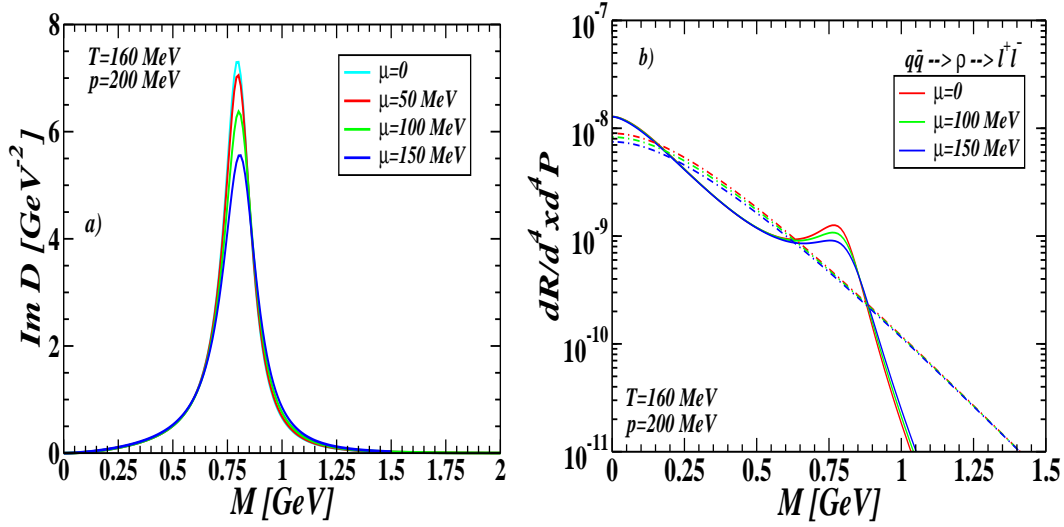


Figure 6.6: *Left panel:* Imaginary part of ρ -meson propagator (spectral function) as a function of M for a set of values of μ . *Right panel:* The dilepton rate from ρ -meson in a QGP as a function of M . We chose $G_\rho = 6$. The dash-dotted lines are corresponding Born-rates.

be appropriate in the perspective of FAIR energies. The effect of broadening of the ρ -meson is far less pronounced with increasing μ than increasing T , indicating that the ρ -meson is not completely melted in the case of a system with finite baryon density such as expected at FAIR energies even above the phase transition. However, dilepton rates from ρ -meson as shown in Figs. (6.5) and (6.6) are comparable with the Born-rate in QGP in the low mass region ($M \leq 1$ GeV), may be an indication for chiral restoration [194, 195, 343]. In addition this rate would be important for invariant masses below 1 GeV.

We also note that if one includes higher mass vector mesons such as ϕ -meson within VMD, then there will be a peak corresponding to an invariant mass of the order of ϕ -meson mass but in low mass region ($M \leq 1$ GeV) there should be a very little change (less than 5%) in the dilepton rate. Since we are interested in the low mass region, we have not discussed ϕ -meson here.

6.2.5 Rate from Lattice Gauge Theory

The thermal dilepton rate describing the production of lepton pairs with energy ω and momentum $\vec{\mathbf{p}}$ is related to the Euclidian correlation function [290] of the vector current, $J_V^\mu = \bar{\psi}(\tau, \vec{\mathbf{x}})\gamma^\mu\psi(\tau, \vec{\mathbf{x}})$, which can be calculated numerically in the framework of lattice gauge theory. The thermal two-point vector correlation function in coordinate space, $\mathcal{G}_V(\tau, \vec{\mathbf{x}})$, is defined as

$$\mathcal{G}_V(\tau, \vec{\mathbf{x}}) = \langle J_V(\tau, \vec{\mathbf{x}}) J_V^\dagger(\tau, \vec{\mathbf{x}}) \rangle = T \sum_{n=-\infty}^{\infty} \int \frac{d^3p}{(2\pi)^3} e^{-i(w_n\tau - \vec{\mathbf{p}} \cdot \vec{\mathbf{x}})} \chi_V(w_n, \vec{\mathbf{p}}), \quad (6.15)$$

where the Euclidian time τ is restricted to the interval $[0, \beta = 1/T]$, and the Fourier transformed correlation function χ_V is given at the discrete Matsubara modes, $w_n = 2\pi nT$. The imaginary part of the momentum space correlator gives the spectral function $\sigma_V(\omega, \vec{\mathbf{p}})$, as

$$\chi_V(w_n, \vec{\mathbf{p}}) = - \int_{-\infty}^{\infty} d\omega \frac{\sigma_V(\omega, \vec{\mathbf{p}})}{i w_n - \omega} \Rightarrow \sigma_V(\omega, \vec{\mathbf{p}}) = \frac{1}{\pi} \text{Im} \chi_V(\omega, \vec{\mathbf{p}}). \quad (6.16)$$

In coordinate space, the spectral representation of the thermal correlation functions at fixed momentum can be obtained using (6.15) and (6.16) as

$$\mathcal{G}(\tau, \vec{\mathbf{p}}) = \int_0^{\infty} d\omega \sigma_V(\omega, \vec{\mathbf{p}}) \frac{\cosh[\omega(\tau - \beta/2)]}{\sinh[\omega\beta/2]}. \quad (6.17)$$

The vector spectral function, σ_V , is related to the differential dilepton production rate [290]⁴ as

$$\sigma_V(\omega, \vec{\mathbf{p}}) = \frac{18\pi^2 N_c}{5\alpha_{\text{em}}^2} \omega^2 (e^{\omega/T} - 1) \frac{dR}{d^4x d^4P}, \quad (6.18)$$

where N_c is the number of color degree of freedom.

⁴A factor of 2 differs from that of Ref. [217]

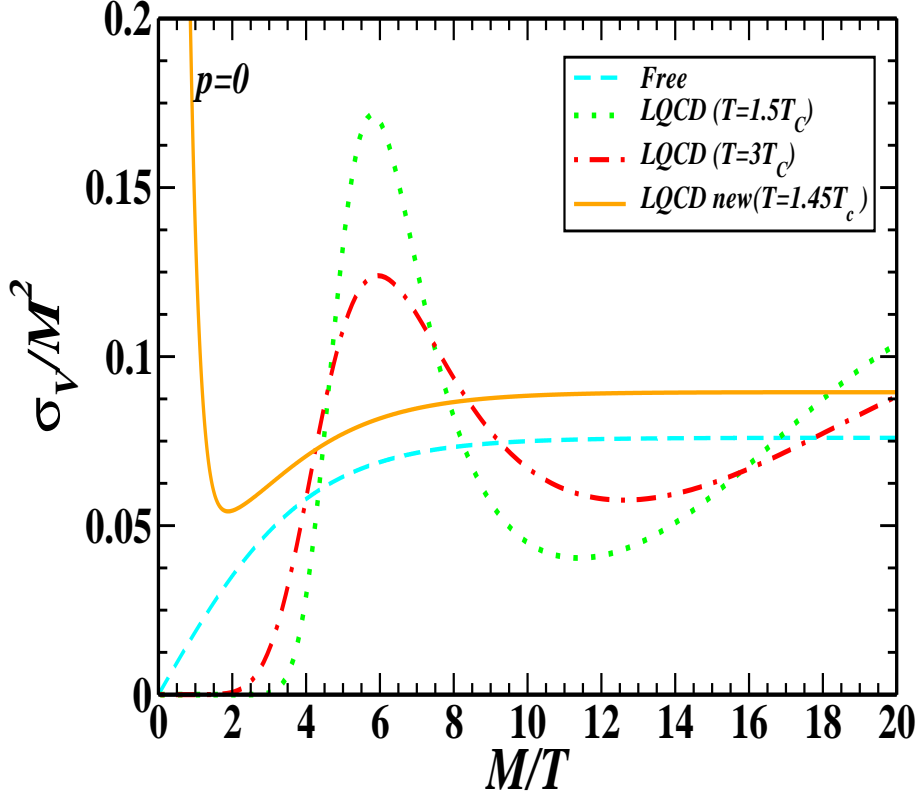


Figure 6.7: The zero momentum ($\vec{\mathbf{p}} = 0$) vector spectral function, reconstructed from the correlation function [217, 305] within lattice gauge theory in quenched QCD using MEM, scaled with M^2 as a function of M/T compared with that of the free one above the deconfinement temperature T_c . Lattice data labeled as LQCD($T=1.5T_c$) and LQCD($T=3T_c$) come from [217] whereas LQCD new($T=1.45T_c$) come from Ref. [305].

A finite temperature lattice gauge theory calculation can not calculate spectral function $\sigma_H(\omega, \vec{\mathbf{p}})$ directly from Eq. (6.16), instead it uses Eq. (6.17) to extract spectral function as discussed in Chapter 3. In Fig. (6.7) such a extracted spectral function [217, 305] scaled with M^2 (equivalently ω^2 for $\vec{\mathbf{p}} = 0$) is displayed as a function of M/T . The vector spectral functions above the deconfinement temperature (*viz.*, $T = 1.5T_c$ and $3T_c$) show an oscillatory behavior compared to the free one. The spectral functions are also found to be vanishingly small for $M/T \leq 4$ due to the sharp cut-off used in the reconstruction.

A direct calculation of the differential dilepton rate using Eq. (6.18) above the

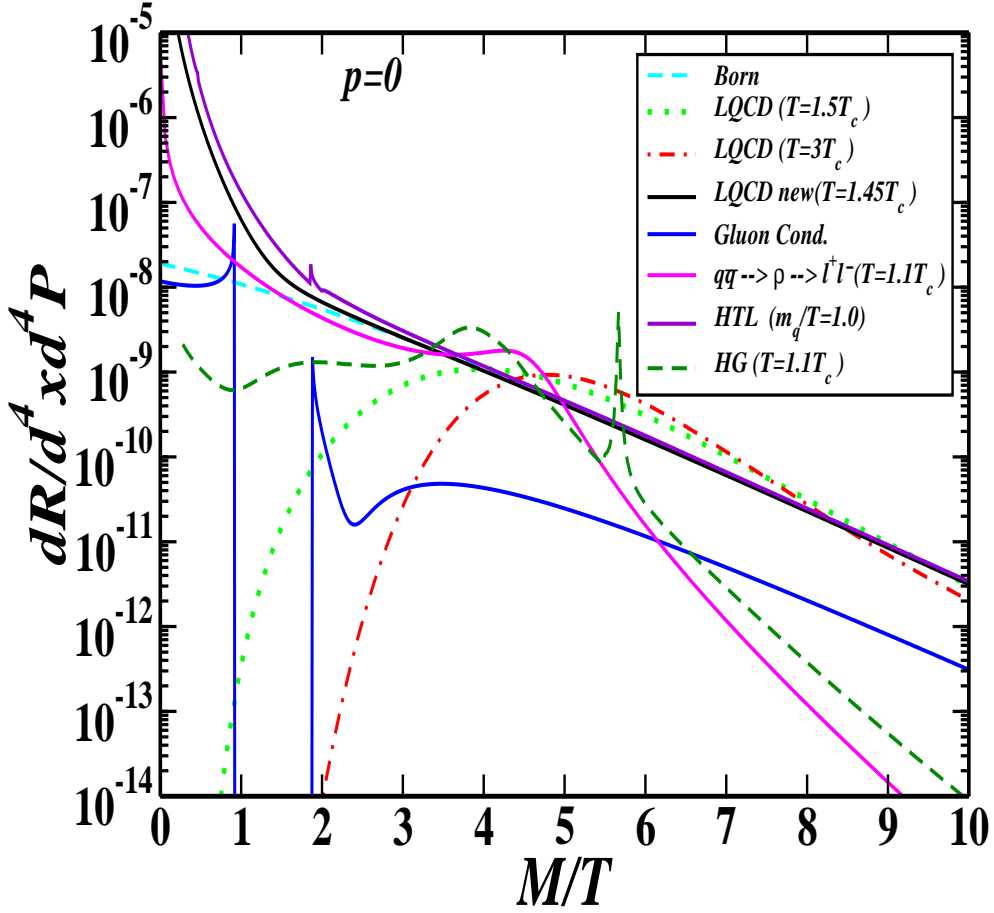


Figure 6.8: Comparison of various dilepton rates in a QGP and in a hadron gas (HG) as a function of M/T for momentum $\vec{p} = 0$. The critical temperature is 165 MeV [112, 219] and the value of G_ρ is chosen as 6. The in-medium HG rate is from the recent calculations of Ref. [344].

deconfined temperature (T_c) at $\vec{p} = 0$ was first time done in Ref. [217] within the lattice gauge theory in quenched QCD using the MEM. Later this calculation was improved in Ref. [305] by choosing different ansatz for the vector spectral function. In Fig. (6.8) the lattice dilepton rates at $\vec{p} = 0$ from [217] for two temperatures ($T = 1.5T_c$ and $3T_c$) and also from [305] for temperature $T = 1.45T_c$ are displayed as a function of the scaled invariant mass with temperature and $M/T = \omega/T$, the energy of the dileptons. We have also compared the perturbative, non-perturbative and in-medium hadrons rates within the same normalization as shown in the plot.

We note that the rate with gluon condensate perfectly scales with the temperature whereas that of HTL one depends on the choice of the effective coupling, $m_q/T \sim g/\sqrt{6}$. The lattice results are comparable within a factor of 2 with the Born-rate as well as that of HTLpt at high invariant mass $M/T \geq 4$. The absence of peak structures around the ρ -mass and also at higher M in the lattice dilepton rate probably constrain the broad resonance structures in the dilepton rates. However, for invariant mass below $M/T \leq 4$ the lattice dilepton rate falls off very fast. This is due to the fact that the sharp cut-off is used to reconstruct the spectral function from the correlation function and the finite volume restriction in the lattice analysis. The lattice analysis is also based on rather small statistics. These lattice artefacts are related to the smaller invariant masses which in turn indicate that it is not yet very clear whether there will be any low mass thermal dileptons from the deconfined phase within the lattice gauge theory calculation. Future analysis could improve the situation in this low mass regime. One cannot rule out [217] the existence of van Hove singularities and energy gap, which are general features of massless fermions in a relativistic plasma [323, 324], in the low mass dileptons. This calls for a further investigations on the lattice gauge theory side by improving and refining the lattice ingredients and constraints.

On the other hand, in HTLpt, apart from the uncertainty in the choice of g , the low mass ($M \rightarrow 0$, vanishing photon energy) one-loop dilepton rate obtained from vector meson spectral function analysis [290] diverges because the quark-photon vertex is inversely proportional to the photon energy. This also requires a further improvement of the HTLpt. However, we assume that the perturbative rate could also be reliable for $M \geq 200$ MeV with $T \geq 200$ MeV and $g \geq 2$. The other two phenomenological models, *viz.*, gluon condensate measured in lattice [7] and $\rho - q$ interaction in the deconfined phase as discussed respectively above in subsec. 6.2.3 and 6.2.4, for non-perturbative dilepton production at low mass regime are at least cleaner than the perturbative rates which depend weakly on the choice of the strong

coupling constant. The rate with gluon condensate is free from strong coupling whereas that from $\rho - q$ interaction does not depend strongly on the choice of the coupling (see below in Fig. (6.9)). In addition to the perturbative rate these two together could also provide a realistic part of the dilepton rate at low mass regime (≤ 1 GeV) from the deconfined phase, as also can be seen in the next section. As a comparison, we have also shown the recent rate from in-medium hadrons of Ref. [344], where the analytic structure of ρ -meson propagator has been used due to its interaction with thermal mesons.

6.3 Momentum Integrated Rate

The momentum integrated dilepton rate can be obtained as

$$\frac{dR}{d^4x dM^2} = \int \frac{d^3p}{2p_0} \frac{dR}{d^4x d^4P}. \quad (6.19)$$

In Fig. (6.9) the momentum integrated dilepton rates from QGP and in-medium hadrons are displayed as a function of invariant mass. As can be seen that at very low invariant mass ($M \leq 200$ MeV) the non-perturbative contribution using gluon condensate becomes important as this domain is beyond reach of any reliable perturbative calculations. The non-perturbative rate is indeed important with input from the first principle calculations [7] that describe the bulk properties of the deconfined phase. The rate from $\rho - q$ interaction is almost of the same order as that of the Born-rate as well as the in-medium hadrons for $M \leq 600$ MeV whereas it is higher than the perturbative one in the domain $600 \leq M(\text{MeV}) \leq 800$ due to the broadening of the ρ peak in the medium. We also note that this rate has a weak dependence on the realistic range of values of the $\rho - q$ coupling (2 – 6). In addition the higher order perturbative rate from HTL, as discussed above, becomes reliable for $M \geq 200$ MeV and also becomes of the order of Born-rate for $M \geq 500$

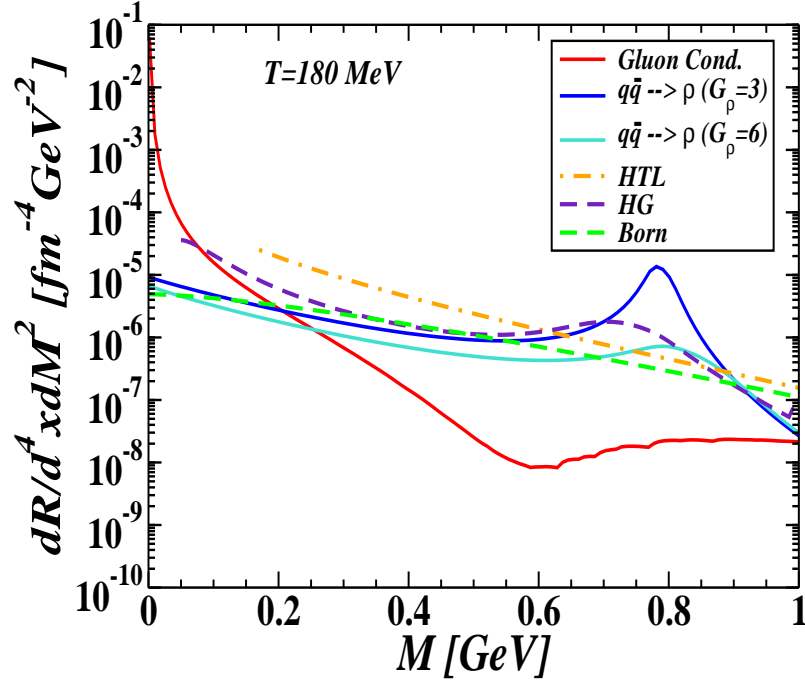


Figure 6.9: Momentum integrated dilepton rate as a function of the invariant mass M . We have used $T_c = 165$ MeV for the nonperturbative rate with gluon condensate. The in-medium hadronic rate (HG) is from Ref. [344].

MeV. We also note that the momentum integrated HTL rate used here has been obtained recently by Rapp et al. [195] through a parametrization of the prefactor of the zero momentum 1-loop HTL rate [250] with a temperature dependent g , which is claimed to reproduce the Born-rate in (6.2) within the appropriate limit. Now for a comparison, we have also shown the recent rate from the in-medium hadrons of Ref. [344]. It is now clear that for low invariant mass (≤ 1 GeV) only the Born-rate from the QGP is not realistic as well as insufficient for describing the dilepton rate. Instead we suggest that the non-perturbative rate with gluon condensate should be important for $M \leq 200$ MeV whereas the rates from ρ - q interaction and HTLpt are important for $M \geq 200$ MeV. Below we discuss some aspects of the quark-hadron duality hypothesis [221].

6.4 Thoughts on the Quark-Hadron Duality Hypothesis

It is advocated [194, 221] that due to the potential broadening of the ρ -meson resonance suffering in a dense hadronic environment the overall (momentum integrated) dilepton rate out of the hadronic gas becomes equivalent to that from deconfined phase as

$$\frac{dR_H}{d^4x dM^2} \approx \frac{dR_Q}{d^4x dM^2} \quad , \quad (6.20)$$

which entails a reminiscence to a simple perturbative $q\bar{q}$ annihilation in the vicinity of the expected QGP phase transition. This hypothesis of 'extended' quark-hadron duality for the thermal source of low mass dileptons has been claimed as an indication for chiral symmetry restoration [194, 195, 221] in the deconfined phase. However, we would like to note that in this hypothesis the volume of QGP and hadronic gas was assumed to be same in a given instant of time and therefore, the dileptons shine equally bright from both phases at a given instant of time per unit volume. This denotion of quark-hadron duality should be carefully re-addressed on its general validity, as the suggestive conclusion is indeed far-reaching. A more realistic way to look into it is envisaged below.

The momentum integrated rate in (6.19) shall be gauged to the adequate degrees of freedom in a particular phase. A certain measure is given by the corresponding entropy density. Hence we suggest that for duality to hold one approximately should have

$$\frac{1}{s_H} \frac{dR_H}{d^4x dM^2} \approx \frac{1}{s_Q} \frac{dR_Q}{d^4x dM^2} \quad , \quad (6.21)$$

where s_i ($i = H, Q$) is the entropy density of the respective phase. For an isoentropic crossing over the phase transition, one has $s_H dV_H \approx s_Q dV_Q$. Hence if one takes into account the respective volume of both phases at a given instant of time, then instead

of (6.20) one should ask for

$$dV_H \frac{dR_H}{d^4x dM^2} \approx dV_Q \frac{dR_H}{d^4x dM^2} \quad , \quad (6.22)$$

where dV_i ($i = Q, H$) is the volume of the respective phase. Now, at a given instant of time this can lead to

$$\frac{dR_H}{dt dM} \approx \frac{dR_Q}{dt dM} \quad , \quad (6.23)$$

where $dR_i/dt dM$ is the total yield per time from total phase i in the system at any instant of time. Therefore, equation (6.23) means that the fireball emits the same number of dileptons per unit time either if described by a hadronic or by a deconfined partonic description. This could likely be a more realistic way to look into the quark-hadron duality. Now, even if the momentum integrated rates in (6.19) from both phases are same in some kinematic domain (*e.g.*, see Fig. (6.9)) may not necessarily imply a quark-hadron duality as given by (6.23) because hadronic volume is expected to be larger than that of QGP by at least a factor of 4 to 5. Furthermore, we also note that the quark-hadron duality should also be true for any momentum at a given instant of time.

6.5 Conclusion

We have discussed the low mass dilepton production rate from the deconfined phase within various models, *viz.*, perturbative and non-perturbative, and compared with that of first principle calculations based on lattice gauge theory and in-medium hadrons. We also have discussed in details the limitations and uncertainties of all those models at various domains of the invariant mass. It turns out that at very low invariant mass (≤ 200 MeV) the non-perturbative rate using gluon condensate measured in lattice becomes important as this domain is beyond reach of any reliable perturbative calculations. The other non-perturbative contribution from $\rho - q$

interaction also becomes important below 1 GeV as it is almost of same order as those of the Born and in-medium hadrons. We also note that these two rates are at least cleaner than the perturbative rates, in the sense that the gluon condensate rate has non-perturbative input from lattice equation of states and is thus free from any coupling uncertainties whereas the $\rho-q$ interaction rate does not depend strongly on the choice of its coupling. We also discussed the $\rho-q$ interaction in the perspective of FAIR scenario.

On the other hand the perturbative contribution, within its various uncertainties, becomes steady and reliable beyond $M > 200$ MeV and also becomes comparable with the Born-rate and the LQCD rate for $M \geq 500$ MeV. The LQCD rate also constrains the broad resonance structure at large invariant mass. More specifically, the rate with gluon condensate is important for $M \leq 200$ MeV whereas those from the $\rho-q$ interaction and HTLpt would be important for $M \geq 200$ MeV for the deconfined phase in heavy-ion collisions. Instead of considering only the Born-rate the various nonperturbative and perturbative rates from appropriate domains of the invariant mass below 1 GeV would comprise a more realistic rate for low mass dileptons from the deconfined phase created in heavy-ion collisions. We hope that more elaborate future lattice gauge theory studies on dileptons above the deconfined temperature can provide a more insight than present LQCD calculations on the low mass region, which could then verify the various model calculations on low mass dileptons above the deconfined temperatures. Finally, we also have discussed a more realistic way to look into the quark-hadron duality hypothesis than it is advocated in the literature.

CHAPTER 7

Summary and Outlook

This thesis is mainly devoted to study the thermodynamics of hot and dense nuclear matter at finite temperature and finite chemical potential. To study the thermodynamical quantities of hot and dense matter produced in heavy ion collision, one would prefer first principle numerical lattice QCD method. But due to sign problem, lattice QCD can be applied to arbitrary temperature but at zero chemical potential. Finite temperature lattice QCD can be extended to calculate thermodynamic potential at small chemical potential by expanding in Taylor series and by calculating coefficients of Taylor series up to some finite order. This expansion up to finite order term is valid for small chemical potential. So the thermodynamic calculations at any chemical potential or at least at any chemical potential which is same order of temperature was essential. To perform these calculations at finite chemical potential one was left with usual perturbation theory. But the poor convergence of conventional perturbation theory at finite temperature/chemical potential has been the main obstacle in the practical application of thermal QCD for decades. To improve the results of usual perturbation theory, a considerable effort has been put into reorganizing the perturbative series at phenomenologically relevant temperatures. The application of HTL perturbation theory to the problem carried out in this thesis leads to laudable results for non-Abelian theories at finite temperature

and at finite chemical potential. Till date thermodynamical quantities using hard thermal loop perturbation theory was available only at finite temperature and zero chemical potential. In this thesis I have systematically calculated most of the relevant thermodynamical quantities in all loop order at finite temperature and finite chemical potential. This was essential to study the hot and dense nuclear medium produced in RHIC BNL and also expected to produce in future experiment in FAIR GSI. Finite temperature and finite chemical thermodynamical calculations were also essential to study various order conserved density fluctuations.

In Chapter 3 we have discussed about leading order thermodynamical quantities *viz.* number density, entropy density, pressure and hence quark number susceptibility and temporal correlation function in hard thermal loop perturbation theory. In Chapter 4 we have discussed about next-to-leading order pressure in HTL perturbation theory. We have also discussed about NLO second and fourth order susceptibilities using NLO pressure in HTL perturbation theory in Chapter 4.

In Chapter 5 we have extended the NLO calculations as discussed in Chapter 4 to NNLO at finite temperature and finite chemical potential. In this chapter we have presented the NNLO pressure, energy density, entropy density, trace anomaly, speed of sound at finite temperature and chemical potential and compared those results with available lattice QCD data. We have also presented the NNLO results of various order conserved charged fluctuations *viz.* diagonal and off-diagonal second-, fourth- and sixth order quark number susceptibilities. In all cases we found very good agreement between the results obtained using the central values of the renormalization scales and available lattice data.

Along-with the computation of thermodynamic quantities of hot and dense matter, we have also discussed in Chapter 6 about low mass dilepton rate from hot and dense medium within various models, *viz.*, perturbative and non-perturbative, and compared with that of first principle calculations based on lattice gauge theory and

in-medium hadrons gas. It turns out that at very low invariant mass (≤ 200 MeV) the non-perturbative rate using gluon condensate measured in lattice becomes important as this domain is beyond reach of any reliable perturbative calculations. The other non-perturbative contribution from $\rho - q$ interaction also becomes important below 1 GeV as it is almost of same order as those of the Born and in-medium hadrons. On the other hand the perturbative contribution from HTL perturbation theory, within its various uncertainties, becomes steady and reliable beyond $M > 200$ MeV and also becomes comparable with the Born-rate and the LQCD rate for $M \geq 500$ MeV. The LQCD rate also constrains the broad resonance structure at large invariant mass.

The HTL perturbation theory is a gauge invariant reorganization of usual perturbation theory and it shifts the expansion from usual perturbation theory around an ideal gas of massless particles to that of massive quasiparticles. The HTL Feynman rules as discussed in this thesis for scalar as well as for gauge theory show clearly that the propagators and vertices become dressed systematically by the thermal medium, as a result the interactions also get screened in the medium which can be seen that the coupling strength gets screened by the thermal mass term explicitly. Therefore the expansion in terms of the HTL Feynman rules are self-consistently around non-interacting quark gluon gas. The fact that the mass parameters are not arbitrary but a function of coupling constant g , temperature T , and chemical potential μ and determined variationally or perturbatively also indicates that HTLpt doesn't modify the original gauge theory but just reorganizes the usual perturbation series. Although the renormalizability of HTL perturbation is not yet proven, the fact that it can be renormalized at every order using only known counterterms *viz.* vacuum energy, debye and thermal quark mass and running coupling counterterm shows promising results till now.

So far, thermodynamics for hot and dense nuclear medium has been studied in-

tensively, both in leading or in higher order perturbation theory or numerically on the lattice, however real-time dynamics is still in its very early stage of development. Transport coefficients such as coefficients of viscosity, conductivity, diffusion rate etc. are of great interest since they are theoretically clean and well defined non-equilibrium dynamical quantities. A considerable efforts have been devoted to calculate transport coefficients at leading order in perturbation theory [268, 269, 293, 294, 345–351]. However the only known transport coefficients in next-to-leading order are shear viscosity in scalar ϕ^4 theory [352], heavy quark diffusion rate in QCD and $\mathcal{N} = 4$ supersymmetric Yang-Mills theory [353, 354], and transverse diffusion rate \hat{q} in QCD [355], and all of them exhibit poor convergence as bad as pressure in bare perturbation theory. Since dynamical quantities are still not well described by lattice gauge theory, the computation transport coefficients using HTL perturbation theory would interesting in order to achieve a better understanding of that quantities.

Further this thesis was focused to calculate various quantities with vanishing quark mass and $\mu \lesssim 2\pi T$, it would be very interesting to include the quark mass effect in higher order calculation using HTL perturbation theory. This would be required to investigate various order conserved density fluctuations for massive quark along-with massless quarks and also to investigate chiral susceptibility. Also it would be very interesting to extend the thermodynamic calculation at $\mu > 2\pi T$ and eventually at zero temperature to study the EoS of Neutron star and other astrophysical objects.

APPENDIX A

Properties of the \aleph functions

For some frequently occurring combinations of special functions in Chapter 5 we will apply the following abbreviations

$$\zeta'(x, y) \equiv \partial_x \zeta(x, y), \quad (\text{A.1})$$

$$\aleph(n, z) \equiv \zeta'(-n, z) + (-1)^{n+1} \zeta'(-n, z^*), \quad (\text{A.2})$$

$$\aleph(z) \equiv \Psi(z) + \Psi(z^*), \quad (\text{A.3})$$

where n is assumed to be a non-negative integer and z is a general complex number given here by $z = 1/2 - i\hat{\mu}$. Above ζ denotes the Riemann zeta function, and Ψ is the digamma function

$$\Psi(z) \equiv \frac{\Gamma'(z)}{\Gamma(z)}. \quad (\text{A.4})$$

Below we list Taylor expansions of the function \aleph and $\aleph(n, z)$ for values of n necessary for calculation of the susceptibilities presented in the main text. For general application we evaluate the \aleph functions exactly using *Mathematica*.

$$\aleph(z) = -2\gamma_E - 4 \ln 2 + 14\zeta(3)\hat{\mu}^2 - 62\zeta(5)\hat{\mu}^4 + 254\zeta(7)\hat{\mu}^6 + \mathcal{O}(\hat{\mu}^8), \quad (\text{A.5})$$

$$\aleph(0, z) = 2(2 \ln 2 + \gamma_E) i \hat{\mu} - \frac{14}{3} \zeta(3) i \hat{\mu}^3 + \frac{62}{5} \zeta(5) i \hat{\mu}^5 + \mathcal{O}(\hat{\mu}^7), \quad (\text{A.6})$$

$$\begin{aligned} \aleph(1, z) &= -\frac{1}{12} \left(\ln 2 - \frac{\zeta'(-1)}{\zeta(-1)} \right) - (1 - 2 \ln 2 - \gamma_E) \hat{\mu}^2 - \frac{7}{6} \zeta(3) \hat{\mu}^4 \\ &+ \frac{31}{15} \zeta(5) \hat{\mu}^6 + \mathcal{O}(\hat{\mu}^8), \end{aligned} \quad (\text{A.7})$$

$$\begin{aligned} \aleph(1, z + z') &= -\frac{1}{6} \frac{\zeta'(-1)}{\zeta(-1)} - (1 - \gamma_E) (\hat{\mu} + \hat{\mu}')^2 - \frac{\zeta(3)}{6} (\hat{\mu} + \hat{\mu}')^4 \\ &+ \frac{\zeta(5)}{15} (\hat{\mu} + \hat{\mu}')^6 + \mathcal{O}(\hat{\mu}^8, \hat{\mu}'^8), \end{aligned} \quad (\text{A.8})$$

$$\begin{aligned} \aleph(2, z) &= \frac{1}{12} \left(1 + 2 \ln 2 - 2 \frac{\zeta'(-1)}{\zeta(-1)} \right) i \hat{\mu} + \frac{1}{3} (3 - 2\gamma_E - 4 \ln 2) i \hat{\mu}^3 \\ &+ \frac{7}{15} \zeta(3) i \hat{\mu}^5 + \mathcal{O}(\hat{\mu}^7), \end{aligned} \quad (\text{A.9})$$

$$\begin{aligned} \aleph(2, z + z') &= -\frac{1}{6} \left(1 - 2 \frac{\zeta'(-1)}{\zeta(-1)} \right) i (\hat{\mu} + \hat{\mu}') + \frac{1}{3} (3 - 2\gamma_E) i (\hat{\mu} + \hat{\mu}')^3 \\ &+ \frac{\zeta(3)}{15} i (\hat{\mu} + \hat{\mu}')^5 + \mathcal{O}(\hat{\mu}^7, \hat{\mu}'^7), \end{aligned} \quad (\text{A.10})$$

$$\begin{aligned} \aleph(3, z) &= \frac{1}{480} \left(\ln 2 - 7 \frac{\zeta'(-3)}{\zeta(-3)} \right) + \frac{1}{24} \left(5 + 6 \ln 2 - 6 \frac{\zeta'(-1)}{\zeta(-1)} \right) \hat{\mu}^2 \\ &+ \frac{1}{12} (11 - 6\gamma_E - 12 \ln 2) \hat{\mu}^4 + \frac{7}{30} \zeta(3) \hat{\mu}^6 + \mathcal{O}(\hat{\mu}^8), \end{aligned} \quad (\text{A.11})$$

$$\begin{aligned} \aleph(3, z + z') &= \frac{1}{60} \frac{\zeta'(-3)}{\zeta(-3)} - \frac{1}{12} \left(5 - 6 \frac{\zeta'(-1)}{\zeta(-1)} \right) (\hat{\mu} + \hat{\mu}')^2 \\ &+ \frac{1}{12} (11 - 6\gamma_E) (\hat{\mu} + \hat{\mu}')^4 + \frac{\zeta(3)}{30} (\hat{\mu} + \hat{\mu}')^6 + \mathcal{O}(\hat{\mu}^8, \hat{\mu}'^8). \end{aligned} \quad (\text{A.12})$$

where γ_E =Euler gamma.

Bibliography

- [1] BRAHMS Collaboration, I. Arsene *et al.*, Nucl. Phys. **A757**, 1 (2005).
- [2] PHENIX Collaboration, K. Adcox *et al.*, Nucl. Phys. **A757**, 184 (2005).
- [3] B. Back *et al.*, Nucl. Phys. **A757**, 28 (2005), arXiv:nucl-ex/0410022.
- [4] STAR Collaboration, J. Adams *et al.*, Nucl. Phys. **A757**, 102 (2005).
- [5] Z. Fodor and S. Katz, JHEP **0404**, 050 (2004), arXiv:hep-lat/0402006.
- [6] S. Gupta, X. Luo, B. Mohanty, H. G. Ritter, and N. Xu, Science **332**, 1525 (2011), arXiv:1105.3934.
- [7] G. Boyd *et al.*, Nucl. Phys. **B469**, 419 (1996), arXiv:hep-lat/9602007.
- [8] S. Borsanyi *et al.*, JHEP **1011**, 077 (2010), arXiv:1007.2580.
- [9] S. Borsanyi *et al.*, JHEP **1208**, 126 (2012), arXiv:1205.0440.
- [10] S. Borsanyi *et al.*, JHEP **1208**, 053 (2012), arXiv:1204.6710.
- [11] S. Borsanyi *et al.*, JHEP **1201**, 138 (2012), arXiv:1112.4416.
- [12] K. Kajantie, M. Laine, K. Rummukainen, and Y. Schroder, Phys. Rev. **D67**, 105008 (2003), arXiv:hep-ph/0211321.
- [13] A. Vuorinen, Phys. Rev. **D68**, 054017 (2003), arXiv:hep-ph/0305183.
- [14] N. Haque and M. G. Mustafa, (2010), arXiv:1007.2076.
- [15] N. Haque, M. G. Mustafa, and M. Strickland, Phys. Rev. **D87**, 105007 (2013), arXiv:1212.1797.
- [16] N. Haque, J. O. Andersen, M. G. Mustafa, M. Strickland, and N. Su, Phys. Rev. **D89**, 061701 (2014), arXiv:1309.3968.

- [17] N. Haque *et al.*, JHEP **1405**, 027 (2014), arXiv:1402.6907.
- [18] N. Haque, M. G. Mustafa, and M. H. Thoma, Phys. Rev. **D84**, 054009 (2011), arXiv:1103.3394.
- [19] N. Haque and M. G. Mustafa, Nucl. Phys. **A862-863**, 271 (2011), arXiv:1109.0799.
- [20] N. Haque, M. G. Mustafa, and M. Strickland, JHEP **1307**, 184 (2013), arXiv:1302.3228.
- [21] L. D. McLerran and T. Toimela, Phys. Rev. **D31**, 545 (1985).
- [22] C. Greiner, N. Haque, M. G. Mustafa, and M. H. Thoma, Phys. Rev. **C83**, 014908 (2011), arXiv:1010.2169.
- [23] D. J. Gross and F. Wilczek, Phys. Rev. Lett. **30**, 1343 (1973).
- [24] ALICE Collaboration, F. Carminati *et al.*, J. Phys. **G30**, 1517 (2004).
- [25] ALICE Collaboration, B. Alessandro *et al.*, J. Phys. **G32**, 1295 (2006).
- [26] B. Friman *et al.*, Lect. Notes Phys. **814**, 1 (2011).
- [27] U. W. Heinz and M. Jacob, (2000), arXiv:nucl-th/0002042.
- [28] PHENIX Collaboration, A. Adare *et al.*, Phys. Rev. **C81**, 034911 (2010), arXiv:0912.0244.
- [29] PHENIX Collaboration, S. Adler *et al.*, Phys. Rev. Lett. **98**, 012002 (2007), arXiv:hep-ex/0609031.
- [30] PHENIX Collaboration, A. Adare *et al.*, Phys. Rev. Lett. **98**, 162301 (2007), arXiv:nucl-ex/0608033.
- [31] PHENIX Collaboration, K. Adcox *et al.*, Phys. Rev. Lett. **89**, 092302 (2002), arXiv:nucl-ex/0204007.
- [32] PHENIX Collaboration, T. Chujo, Nucl. Phys. **A715**, 151 (2003), arXiv:nucl-ex/0209027.
- [33] ALICE Collaboration, K. Aamodt *et al.*, Phys. Rev. Lett. **105**, 252302 (2010), arXiv:1011.3914.
- [34] ALICE Collaboration, K. Aamodt *et al.*, Phys. Lett. **B696**, 30 (2011), arXiv:1012.1004.

- [35] CMS Collaboration, S. Chatrchyan *et al.*, Phys. Rev. **C84**, 024906 (2011), arXiv:1102.1957.
- [36] ALICE Collaboration, K. Aamodt *et al.*, Phys. Rev. Lett. **106**, 032301 (2011), arXiv:1012.1657.
- [37] ALICE Collaboration, K. Aamodt *et al.*, Phys. Rev. Lett. **105**, 252301 (2010), arXiv:1011.3916.
- [38] ALICE Collaboration, K. Aamodt *et al.*, Phys. Rev. Lett. **107**, 032301 (2011), arXiv:1105.3865.
- [39] T. Hatsuda and T. Kunihiro, Phys. Rept. **247**, 221 (1994), arXiv:hep-ph/9401310.
- [40] T. Kunihiro, Phys. Lett. **B271**, 395 (1991).
- [41] Y. Hatta and T. Ikeda, Phys. Rev. **D67**, 014028 (2003), arXiv:hep-ph/0210284.
- [42] C. Sasaki, B. Friman, and K. Redlich, Phys. Rev. **D75**, 054026 (2007), arXiv:hep-ph/0611143.
- [43] K. Fukushima, Phys. Rev. **D68**, 045004 (2003), arXiv:hep-ph/0303225.
- [44] K. Fukushima, Phys. Lett. **B591**, 277 (2004), arXiv:hep-ph/0310121.
- [45] C. Ratti, M. A. Thaler, and W. Weise, Phys. Rev. **D73**, 014019 (2006), arXiv:hep-ph/0506234.
- [46] S. K. Ghosh, T. K. Mukherjee, M. G. Mustafa, and R. Ray, Phys. Rev. **D73**, 114007 (2006), arXiv:hep-ph/0603050.
- [47] S. K. Ghosh, T. K. Mukherjee, M. G. Mustafa, and R. Ray, Phys. Rev. **D77**, 094024 (2008), arXiv:0710.2790.
- [48] S. Mukherjee, M. G. Mustafa, and R. Ray, Phys. Rev. **D75**, 094015 (2007), arXiv:hep-ph/0609249.
- [49] S. Roessner, C. Ratti, and W. Weise, Phys. Rev. **D75**, 034007 (2007), arXiv:hep-ph/0609281.
- [50] C. Sasaki, B. Friman, and K. Redlich, Phys. Rev. **D75**, 074013 (2007), arXiv:hep-ph/0611147.

- [51] A. Bhattacharyya, P. Deb, S. K. Ghosh, and R. Ray, Phys. Rev. **D82**, 014021 (2010), arXiv:1003.3337.
- [52] A. Bhattacharyya, P. Deb, A. Lahiri, and R. Ray, Phys. Rev. **D82**, 114028 (2010), arXiv:1008.0768.
- [53] A. Bhattacharyya, P. Deb, A. Lahiri, and R. Ray, Phys. Rev. **D83**, 014011 (2011), arXiv:1010.2394.
- [54] A. Bhattacharyya, S. K. Ghosh, S. Majumder, and R. Ray, Phys. Rev. **D86**, 096006 (2012), arXiv:1107.5941.
- [55] A. Bhattacharyya *et al.*, Phys. Rev. **C89**, 064905 (2014), arXiv:1212.6134.
- [56] J. Steinheimer and S. Schramm, (2014), arXiv:1401.4051.
- [57] C. Ratti, S. Roessner, and W. Weise, Phys. Lett. **B649**, 57 (2007), arXiv:hep-ph/0701091.
- [58] B.-J. Schaefer and J. Wambach, Phys. Rev. **D75**, 085015 (2007), arXiv:hep-ph/0603256.
- [59] B.-J. Schaefer, M. Wagner, and J. Wambach, Phys. Rev. **D81**, 074013 (2010), arXiv:0910.5628.
- [60] A. Peshier, B. Kampfer, O. Pavlenko, and G. Soff, Phys. Lett. **B337**, 235 (1994).
- [61] A. Peshier, B. Kampfer, O. Pavlenko, and G. Soff, Phys. Rev. **D54**, 2399 (1996).
- [62] A. Peshier, B. Kampfer, and G. Soff, Phys. Rev. **C61**, 045203 (2000), arXiv:hep-ph/9911474.
- [63] A. Peshier, B. Kampfer, and G. Soff, Phys. Rev. **D66**, 094003 (2002), arXiv:hep-ph/0206229.
- [64] M. Bluhm, B. Kampfer, R. Schulze, D. Seipt, and U. Heinz, Phys. Rev. **C76**, 034901 (2007), arXiv:0705.0397.
- [65] M. Bluhm and B. Kampfer, Phys. Rev. **D77**, 034004 (2008), arXiv:0711.0590.
- [66] V. M. Bannur, JHEP **0709**, 046 (2007), arXiv:hep-ph/0604158.
- [67] V. M. Bannur, Phys. Rev. **C78**, 045206 (2008), arXiv:0712.2886.

- [68] F. Gardim and F. Steffens, Nucl.Phys. **A825**, 222 (2009), arXiv:0905.0667.
- [69] V. Skokov, B. Friman, and K. Redlich, Phys. Rev. **C83**, 054904 (2011), arXiv:1008.4570.
- [70] T. K. Herbst, J. M. Pawłowski, and B.-J. Schaefer, Phys. Rev. **D88**, 014007 (2013), arXiv:1302.1426.
- [71] T. K. Herbst, M. Mitter, J. M. Pawłowski, B.-J. Schaefer, and R. Stiele, Phys. Lett. **B731**, 248 (2014), arXiv:1308.3621.
- [72] K. Jo, Y. Kim, H. K. Lee, and S.-J. Sin, JHEP **0811**, 040 (2008), arXiv:0810.0063.
- [73] K.-i. Kim, Y. Kim, S. Takeuchi, and T. Tsukioka, Prog. Theor. Phys. **126**, 735 (2011), arXiv:1012.2667.
- [74] Y. Kim, Y. Matsuo, W. Sim, S. Takeuchi, and T. Tsukioka, JHEP **1005**, 038 (2010), arXiv:1001.5343.
- [75] L.-X. Cui, S. Takeuchi, and Y.-L. Wu, Phys. Rev. **D84**, 076004 (2011), arXiv:1107.2738.
- [76] T. DeGrand and C. DeTar, *Lattice Methods for Quantum Chromodynamics* (World Scientific, 2006).
- [77] M. Creutz, *Quarks, gluons and lattices* (Cambridge University Press, Cambridge, 1985).
- [78] J. Berges, S. Borsanyi, U. Reinosa, and J. Serreau, Phys. Rev. **D71**, 105004 (2005), arXiv:hep-ph/0409123.
- [79] S. Borsanyi, G. Endrodi, Z. Fodor, S. Katz, and K. Szabo, JHEP **1207**, 056 (2012), arXiv:1204.6184.
- [80] S. Borsanyi *et al.*, Phys. Lett. **B730**, 99 (2014), arXiv:1309.5258.
- [81] S. Borsanyi *et al.*, Phys. Lett. **B713**, 342 (2012), arXiv:1204.4089.
- [82] S. Borsanyi, Nucl. Phys. **A904-905**, 270c (2013), arXiv:1210.6901.
- [83] Wuppertal-Budapest Collaboration, C. Ratti *et al.*, Nucl. Phys. **A855**, 253 (2011), arXiv:1012.5215.
- [84] S. Borsanyi and U. Reinosa, Phys. Lett. **B661**, 88 (2008), arXiv:0709.2316.

- [85] Wuppertal-Budapest Collaboration, S. Borsanyi *et al.*, J. Phys. **G38**, 124060 (2011), arXiv:1109.5030.
- [86] S. Borsanyi *et al.*, PoS **LATTICE2011**, 209 (2011), arXiv:1111.3500.
- [87] S. Borsanyi *et al.*, (2010), arXiv:1011.4229.
- [88] Y. Aoki, G. Endrodi, Z. Fodor, S. D. Katz and K. K. Szabo, Nature **443**, 675 (2006) [hep-lat/0611014].
- [89] S. Borsanyi *et al.*, J. Phys. **G38**, 124101 (2011).
- [90] S. Borsanyi *et al.* [Wuppertal-Budapest Collaboration], JHEP **1009**, 073 (2010) [arXiv:1005.3508 [hep-lat]].
- [91] Y. Aoki, Z. Fodor, S. D. Katz and K. K. Szabo, Phys. Lett. B **643**, 46 (2006) [hep-lat/0609068].
- [92] Y. Aoki, S. Borsanyi, S. Durr, Z. Fodor, S. D. Katz, S. Krieg and K. K. Szabo, JHEP **0906**, 088 (2009) [arXiv:0903.4155 [hep-lat]].
- [93] S. Borsanyi *et al.*, PoS **LATTICE2013**, 155 (2013), arXiv:1312.2193.
- [94] S. Datta and S. Gupta, Phys. Rev. **D82**, 114505 (2010), arXiv:1006.0938.
- [95] S. Gupta, N. Karthik, and P. Majumdar, (2014), arXiv:1405.2206.
- [96] R. Gavai and S. Gupta, Phys. Rev. **D78**, 114503 (2008), arXiv:0806.2233.
- [97] S. Datta and S. Gupta, Nucl. Phys. **A830**, 749C (2009), arXiv:0906.3929.
- [98] R. V. Gavai, S. Gupta, and S. Mukherjee, Pramana **71**, 487 (2008), arXiv:hep-lat/0506015.
- [99] R. V. Gavai, S. Gupta, and S. Mukherjee, Phys. Rev. **D71**, 074013 (2005), arXiv:hep-lat/0412036.
- [100] R. Gavai, S. Gupta, and R. Ray, Prog. Theor. Phys. Suppl. **153**, 270 (2004), arXiv:nucl-th/0312010.
- [101] R. V. Gavai and S. Gupta, Phys. Rev. **D68**, 034506 (2003), arXiv:hep-lat/0303013.
- [102] R. V. Gavai and S. Gupta, Phys. Rev. **D65**, 094515 (2002), arXiv:hep-lat/0202006.

- [103] R. V. Gai, S. Gupta, and P. Majumdar, Phys. Rev. **D65**, 054506 (2002), arXiv:hep-lat/0110032.
- [104] R. V. Gai and S. Gupta, Phys. Rev. **D64**, 074506 (2001), arXiv:hep-lat/0103013.
- [105] R. V. Gai and S. Sharma, (2014), arXiv:1406.0474.
- [106] R. Gai and S. Sharma, Phys. Rev. **D85**, 054508 (2012), arXiv:1112.5428.
- [107] D. Banerjee, R. Gai, and S. Sharma, Phys. Rev. **D78**, 014506 (2008), arXiv:0803.3925.
- [108] R. Gai and S. Sharma, Phys. Rev. **D79**, 074502 (2009), arXiv:0811.3026.
- [109] C. Allton *et al.*, Phys. Rev. **D71**, 054508 (2005), arXiv:hep-lat/0501030.
- [110] A. Bazavov *et al.*, Phys. Rev. **D80**, 014504 (2009), arXiv:0903.4379.
- [111] MILC Collaboration, C. Bernard *et al.*, Phys. Rev. **D71**, 034504 (2005), arXiv:hep-lat/0405029.
- [112] P. Petreczky, Nucl. Phys. **A830**, 11C (2009), arXiv:0908.1917.
- [113] S. A. Gottlieb, W. Liu, D. Toussaint, R. Renken, and R. Sugar, Phys. Rev. Lett. **59**, 2247 (1987).
- [114] S. A. Gottlieb, W. Liu, D. Toussaint, R. Renken, and R. Sugar, Phys. Rev. **D38**, 2888 (1988).
- [115] R. Gai, J. Potvin, and S. Sanielevici, Phys. Rev. **D40**, 2743 (1989).
- [116] RBC-Bielefeld Collaboration, P. Petreczky, P. Hegde, and A. Velytsky, PoS **LAT2009**, 159 (2009), arXiv:0911.0196.
- [117] M. Cheng *et al.*, Phys. Rev. **D81**, 054504 (2010), arXiv:0911.2215.
- [118] P. Petreczky, J.Phys. **G39**, 093002 (2012), arXiv:1203.5320.
- [119] S. Borsanyi *et al.*, Phys. Rev. Lett. **111**, 062005 (2013), arXiv:1305.5161.
- [120] S. Sharma, Adv. High Energy Phys. **2013**, 452978 (2013), arXiv:1403.2102.
- [121] F. Karsch, E. Laermann, and A. Peikert, Phys. Lett. **B478**, 447 (2000), arXiv:hep-lat/0002003.

BIBLIOGRAPHY

- [122] A. Bazavov *et al.*, Phys. Rev. Lett. 111, **082301**, 082301 (2013), arXiv:1304.7220.
- [123] A. Bazavov *et al.*, Phys. Rev. **D88**, 094021 (2013), arXiv:1309.2317.
- [124] A. Bazavov *et al.*, Phys. Rev. Lett. **109**, 192302 (2012), arXiv:1208.1220.
- [125] HotQCD Collaboration, A. Bazavov *et al.*, Phys. Rev. **D86**, 034509 (2012), arXiv:1203.0784.
- [126] M. Cheng *et al.*, Phys. Rev. **D79**, 074505 (2009), arXiv:0811.1006.
- [127] N. Brambilla *et al.*, (2014), arXiv:1404.3723.
- [128] B. A. Freedman and L. D. McLerran, Phys. Rev. **D16**, 1147 (1977).
- [129] B. A. Freedman and L. D. McLerran, Phys. Rev. **D16**, 1169 (1977).
- [130] E. V. Shuryak, Sov. Phys. JETP **47**, 212 (1978).
- [131] S. Chin, Phys. Lett. **B78**, 552 (1978).
- [132] J. I. Kapusta, Nucl. Phys. **B148**, 461 (1979).
- [133] T. Toimela, Phys. Lett. **B124**, 407 (1983).
- [134] J. Frenkel, A. Saa, and J. Taylor, Phys. Rev. **D46**, 3670 (1992).
- [135] P. B. Arnold and C.-X. Zhai, Phys. Rev. **D50**, 7603 (1994), arXiv:hep-ph/9408276.
- [136] P. B. Arnold and C.-x. Zhai, Phys. Rev. **D51**, 1906 (1995), arXiv:hep-ph/9410360.
- [137] R. R. Parwani and C. Coriano, Nucl.Phys. **B434**, 56 (1995), arXiv:hep-ph/9409269.
- [138] R. Parwani and H. Singh, Phys. Rev. **D51**, 4518 (1995), arXiv:hep-th/9411065.
- [139] E. Braaten and A. Nieto, Phys. Rev. **D51**, 6990 (1995), arXiv:hep-ph/9501375.
- [140] R. R. Parwani, Phys. Lett. **B334**, 420 (1994), arXiv:hep-ph/9406318.
- [141] J. O. Andersen, Phys. Rev. **D53**, 7286 (1996), arXiv:hep-ph/9509409.

- [142] C.-x. Zhai and B. M. Kastening, *Phys. Rev.* **D52**, 7232 (1995), arXiv:hep-ph/9507380.
- [143] E. Braaten and A. Nieto, *Phys. Rev. Lett.* **76**, 1417 (1996), arXiv:hep-ph/9508406.
- [144] E. Braaten and A. Nieto, *Phys. Rev.* **D53**, 3421 (1996), arXiv:hep-ph/9510408.
- [145] A. Ipp, K. Kajantie, A. Rebhan, and A. Vuorinen, *Phys. Rev.* **D74**, 045016 (2006), arXiv:hep-ph/0604060.
- [146] A. Vuorinen, *Phys. Rev.* **D67**, 074032 (2003), arXiv:hep-ph/0212283.
- [147] A. Gynther, M. Laine, Y. Schroder, C. Torrero, and A. Vuorinen, *JHEP* **0704**, 094 (2007), arXiv:hep-ph/0703307.
- [148] J. O. Andersen, L. Kyllingstad, and L. E. Leganger, *JHEP* **0908**, 066 (2009), arXiv:0903.4596.
- [149] A. D. Linde, *Phys. Lett.* **B96**, 289 (1980).
- [150] E. Braaten and R. D. Pisarski, *Nucl. Phys.* **B337**, 569 (1990).
- [151] J.-P. Blaizot, E. Iancu, and A. Rebhan, (2003), arXiv:hep-ph/0303185.
- [152] U. Kraemmer and A. Rebhan, *Rept. Prog. Phys.* **67**, 351 (2004), arXiv:hep-ph/0310337.
- [153] J. O. Andersen and M. Strickland, *Annals Phys.* **317**, 281 (2005), arXiv:hep-ph/0404164.
- [154] S. Chiku and T. Hatsuda, *Phys. Rev.* **D58**, 076001 (1998), arXiv:hep-ph/9803226.
- [155] E. Braaten and R. D. Pisarski, *Phys. Rev.* **D45**, 1827 (1992).
- [156] E. Braaten and R. D. Pisarski, *Phys. Rev. Lett.* **64**, 1338 (1990).
- [157] J. Blaizot, E. Iancu, and A. Rebhan, *Phys. Lett.* **B523**, 143 (2001), arXiv:hep-ph/0110369.
- [158] Y. Jiang, H.-x. Zhu, W.-m. Sun, and H.-s. Zong, *J. Phys.* **G37**, 055001 (2010), arXiv:1003.5031.

- [159] J. Blaizot, E. Iancu, and A. Rebhan, Phys. Lett. **B470**, 181 (1999), arXiv:hep-ph/9910309.
- [160] J. Blaizot, E. Iancu, and A. Rebhan, Phys. Rev. **D63**, 065003 (2001), arXiv:hep-ph/0005003.
- [161] J. O. Andersen and M. Strickland, Phys. Rev. **D66**, 105001 (2002), arXiv:hep-ph/0206196.
- [162] J. Blaizot, E. Iancu, and A. Rebhan, Phys. Rev. Lett. **83**, 2906 (1999), arXiv:hep-ph/9906340.
- [163] J. O. Andersen, E. Braaten, and M. Strickland, Phys. Rev. Lett. **83**, 2139 (1999), arXiv:hep-ph/9902327.
- [164] J. O. Andersen, E. Braaten, and M. Strickland, Phys. Rev. **D61**, 014017 (2000), arXiv:hep-ph/9905337.
- [165] J. O. Andersen, E. Braaten, and M. Strickland, Phys. Rev. **D61**, 074016 (2000), arXiv:hep-ph/9908323.
- [166] P. Chakraborty, M. G. Mustafa, and M. H. Thoma, Eur. Phys. J. **C23**, 591 (2002), arXiv:hep-ph/0111022.
- [167] P. Chakraborty, M. G. Mustafa, and M. H. Thoma, Phys. Rev. **D67**, 114004 (2003), arXiv:hep-ph/0210159.
- [168] P. Chakraborty, M. G. Mustafa, and M. H. Thoma, Phys. Rev. **D68**, 085012 (2003), arXiv:hep-ph/0303009.
- [169] J. Blaizot, E. Iancu, and A. Rebhan, Eur. Phys. J. **C27**, 433 (2003), arXiv:hep-ph/0206280.
- [170] J. O. Andersen, S. Mogliacci, N. Su, and A. Vuorinen, Phys. Rev. **D87**, 074003 (2013), arXiv:1210.0912.
- [171] N. Su, Commun. Theor. Phys. **57**, 409 (2012), arXiv:1204.0260.
- [172] J. O. Andersen, E. Braaten, E. Petitgirard, and M. Strickland, Phys. Rev. **D66**, 085016 (2002), arXiv:hep-ph/0205085.
- [173] J. O. Andersen, E. Petitgirard, and M. Strickland, Phys. Rev. **D70**, 045001 (2004), arXiv:hep-ph/0302069.

BIBLIOGRAPHY

- [174] J. O. Andersen, M. Strickland, and N. Su, Phys. Rev. Lett. **104**, 122003 (2010), arXiv:0911.0676.
- [175] J. O. Andersen, M. Strickland, and N. Su, JHEP **1008**, 113 (2010), arXiv:1005.1603.
- [176] J. O. Andersen, M. Strickland, and N. Su, Phys. Rev. **D80**, 085015 (2009), arXiv:0906.2936.
- [177] J. O. Andersen, L. E. Leganger, M. Strickland, and N. Su, Phys. Lett. **B696**, 468 (2011), arXiv:1009.4644.
- [178] J. O. Andersen, L. E. Leganger, M. Strickland, and N. Su, JHEP **1108**, 053 (2011), arXiv:1103.2528.
- [179] J. O. Andersen, L. E. Leganger, M. Strickland, and N. Su, Phys. Rev. **D84**, 087703 (2011), arXiv:1106.0514.
- [180] V. Yukalov, Teor. Mat. Fiz. **26**, 403 (1976).
- [181] P. M. Stevenson, Phys. Rev. **D23**, 2916 (1981).
- [182] A. Duncan and M. Moshe, Phys. Lett. **B215**, 352 (1988).
- [183] A. Duncan and H. Jones, Phys. Rev. **D47**, 2560 (1993).
- [184] A. Sisakian, I. Solovtsov, and O. Shevchenko, Int.J.Mod.Phys. **A9**, 1929 (1994).
- [185] W. Janke and H. Kleinert, Phys. Rev. Lett. **75**, 2787 (1995).
- [186] F. Karsch, A. Patkos, and P. Petreczky, Phys. Lett. **B401**, 69 (1997), arXiv:hep-ph/9702376.
- [187] J. O. Andersen, E. Braaten, and M. Strickland, Phys. Rev. **D63**, 105008 (2001), arXiv:hep-ph/0007159.
- [188] J. Andersen and M. Strickland, Phys.Rev. **D64**, 105012 (2001), arXiv:hep-ph/0105214.
- [189] J. O. Andersen and L. Kyllingstad, Phys. Rev. **D78**, 076008 (2008), arXiv:0805.4478.
- [190] CERES Collaboration, G. Agakichiev *et al.*, Phys. Rev. Lett. **75**, 1272 (1995).

- [191] CERES/NA45 Collaboration, G. Agakishiev *et al.*, Phys. Lett. **B422**, 405 (1998), arXiv:nucl-ex/9712008.
- [192] HELIOS Collaboration, M. Maserà, Nucl. Phys. **A590**, 93C (1995).
- [193] A. Drees, Nucl. Phys. **A630**, 449C (1998).
- [194] R. Rapp and J. Wambach, Adv. Nucl. Phys. **25**, 1 (2000), arXiv:hep-ph/9909229.
- [195] R. Rapp, J. Wambach, and H. van Hees, (2009), arXiv:0901.3289.
- [196] W. Cassing and E. Bratkovskaya, Phys. Rept. **308**, 65 (1999).
- [197] G. Brown and M. Rho, Phys. Rev. Lett. **66**, 2720 (1991).
- [198] B. Friman and H. Pirner, Nucl. Phys. **A617**, 496 (1997), arXiv:nucl-th/9701016.
- [199] R. Rapp, G. Chanfray, and J. Wambach, Nucl. Phys. **A617**, 472 (1997), arXiv:hep-ph/9702210.
- [200] R. Rapp, G. Chanfray, and J. Wambach, Phys. Rev. Lett. **76**, 368 (1996), arXiv:hep-ph/9508353.
- [201] C. Gale and P. Lichard, Phys. Rev. **D49**, 3338 (1994), arXiv:hep-ph/9307363.
- [202] R. Rapp and C. Gale, Phys. Rev. **C60**, 024903 (1999), arXiv:hep-ph/9902268.
- [203] F. Klingl, N. Kaiser, and W. Weise, Nucl. Phys. **A624**, 527 (1997), arXiv:hep-ph/9704398.
- [204] W. Peters, M. Post, H. Lenske, S. Leupold, and U. Mosel, Nucl. Phys. **A632**, 109 (1998), arXiv:nucl-th/9708004.
- [205] W. Cassing, E. Bratkovskaya, R. Rapp, and J. Wambach, Phys. Rev. **C57**, 916 (1998), arXiv:nucl-th/9708020.
- [206] M. Post, S. Leupold, and U. Mosel, Nucl. Phys. **A689**, 753 (2001), arXiv:nucl-th/0008027.
- [207] D. Srivastava, B. Sinha, and C. Gale, Phys. Rev. **C53**, 567 (1996).
- [208] D. Pal, D. Srivastava, and K. Haglin, Phys. Rev. **C54**, 1366 (1996).

BIBLIOGRAPHY

- [209] D. Srivastava, B. Sinha, D. Pal, C. Gale, and K. Haglin, Nucl. Phys. **A610**, 350C (1996).
- [210] D. Pal and M. G. Mustafa, Phys. Rev. **C60**, 034905 (1999), arXiv:nucl-th/9808049.
- [211] D. K. Srivastava, M. G. Mustafa, and B. Muller, Phys.Rev. **C56**, 1064 (1997), arXiv:nucl-th/9611041.
- [212] J. Alam, S. Sarkar, P. Roy, T. Hatsuda, and B. Sinha, Annals Phys. **286**, 159 (2001), arXiv:hep-ph/9909267.
- [213] J.-e. Alam, P. Roy, S. Sarkar, and B. Sinha, Phys. Rev. **C67**, 054901 (2003), arXiv:nucl-th/0106038.
- [214] K. Dusling and I. Zahed, Nucl. Phys. **A825**, 212 (2009), arXiv:0712.1982.
- [215] E. Bratkovskaya, W. Cassing, and O. Linnyk, Phys. Lett. **B670**, 428 (2009), arXiv:0805.3177.
- [216] P. Aurenche, F. Gelis, R. Kobes, and H. Zaraket, Phys. Rev. **D58**, 085003 (1998), arXiv:hep-ph/9804224.
- [217] F. Karsch, E. Laermann, P. Petreczky, S. Stickan, and I. Wetzorke, Phys. Lett. **B530**, 147 (2002), arXiv:hep-lat/0110208.
- [218] C. Allton *et al.*, Phys. Rev. **D68**, 014507 (2003), arXiv:hep-lat/0305007.
- [219] P. Petreczky, Mod. Phys. Lett. **A25**, 3081 (2010), arXiv:1009.5935.
- [220] M. H. Thoma, J. Phys. **G31**, L7 (2005), arXiv:hep-ph/0503154.
- [221] R. Rapp and J. Wambach, Eur. Phys. J. **A6**, 415 (1999), arXiv:hep-ph/9907502.
- [222] J. Cleymans, J. Fingberg, and K. Redlich, Phys. Rev. **D35**, 2153 (1987).
- [223] J. Blaizot, E. Iancu, and A. Rebhan, Phys. Rev. **D68**, 025011 (2003), arXiv:hep-ph/0303045.
- [224] A. Vuorinen, (2004), arXiv:hep-ph/0402242.
- [225] M. Laine and Y. Schroder, Phys. Rev. **D73**, 085009 (2006), arXiv:hep-ph/0603048.

- [226] A. Rebhan and P. Romatschke, Phys. Rev. **D68**, 025022 (2003), arXiv:hep-ph/0304294.
- [227] W. Cassing, Nucl. Phys. **A795**, 70 (2007), arXiv:0707.3033.
- [228] A. Kurkela, P. Romatschke, and A. Vuorinen, Phys. Rev. **D81**, 105021 (2010), arXiv:0912.1856.
- [229] A. Bazavov *et al.*, Phys. Rev. **D86**, 114031 (2012), arXiv:1205.6155.
- [230] Particle Data Group Collaboration, J. Beringer *et al.*, Phys. Rev. **D86**, 010001 (2012).
- [231] T. van Ritbergen, J. Vermaseren, and S. Larin, Phys. Lett. **B400**, 379 (1997), arXiv:hep-ph/9701390.
- [232] H. D. Politzer, Phys. Rev. Lett. **30**, 1346 (1973).
- [233] S. Bethke, Prog.Part.Nucl.Phys. **58**, 351 (2007), arXiv:hep-ex/0606035.
- [234] J. I. Kapusta and C. Gale, *Finite Temperature Field Theory Principle and Applications*, 2nd ed. (Cambridge University Press, Cambridge, 1996).
- [235] M. LeBellac, *Thermal Field Theory*, 1st ed. (Cambridge University Press, Cambridge, England, 1996).
- [236] R. D. Pisarski, Nucl. Phys. **A525**, 175 (1991).
- [237] J. Frenkel and J. Taylor, Nucl. Phys. **B334**, 199 (1990).
- [238] E. Braaten and R. D. Pisarski, Nucl. Phys. **B339**, 310 (1990).
- [239] J. Taylor and S. Wong, Nucl. Phys. **B346**, 115 (1990).
- [240] R. Kobes, G. Kunstatter, and A. Rebhan, Nucl. Phys. **B355**, 1 (1991).
- [241] V. Silin, Sov.Phys. JETP **11**, 1136 (1960).
- [242] N. Su, (2011), arXiv:1104.3450.
- [243] V. Klimov, Sov. J. Nucl. Phys. **33**, 934 (1981).
- [244] V. Klimov, Sov. Phys. JETP **55**, 199 (1982).
- [245] H. A. Weldon, Phys. Rev. **D26**, 1394 (1982).

- [246] S. Mogliacci, J. O. Andersen, M. Strickland, N. Su, and A. Vuorinen, *JHEP* **1312**, 055 (2013), arXiv:1307.8098.
- [247] S. Mogliacci and N. Su, *EPJ Web Conf.* **70**, 00031 (2014).
- [248] N. Su, *PoS ConfinementX*, 189 (2012).
- [249] S. Mogliacci, *J. Phys. Conf. Ser.* **503**, 012005 (2014), arXiv:1311.2101.
- [250] E. Braaten, R. D. Pisarski, and T.-C. Yuan, *Phys. Rev. Lett.* **64**, 2242 (1990).
- [251] R. Baier, S. Peigne, and D. Schiff, *Z. Phys.* **C62**, 337 (1994), arXiv:hep-ph/9311329.
- [252] M. G. Mustafa, M. H. Thoma, and P. Chakraborty, *Phys. Rev.* **C71**, 017901 (2005), arXiv:hep-ph/0403279.
- [253] M. G. Mustafa, P. Chakraborty, and M. H. Thoma, *J. Phys. Conf. Ser.* **50**, 438 (2006), arXiv:hep-ph/0504174.
- [254] P. Chakraborty, M. G. Mustafa, and M. H. Thoma, *Phys. Rev.* **D74**, 094002 (2006), arXiv:hep-ph/0606316.
- [255] P. Chakraborty, M. G. Mustafa, R. Ray, and M. H. Thoma, *J. Phys.* **G34**, 2141 (2007), arXiv:0705.1447.
- [256] M. Laine, O. Philipsen, P. Romatschke, and M. Tassler, *JHEP* **0703**, 054 (2007), arXiv:hep-ph/0611300.
- [257] A. Dumitru, Y. Guo, and M. Strickland, *Phys. Lett.* **B662**, 37 (2008), arXiv:0711.4722.
- [258] A. Dumitru, Y. Guo, A. Mocsy, and M. Strickland, *Phys. Rev.* **D79**, 054019 (2009), arXiv:0901.1998.
- [259] A. Dumitru, Y. Guo, and M. Strickland, *Phys. Rev.* **D79**, 114003 (2009), arXiv:0903.4703.
- [260] L. Thakur, N. Haque, U. Kakade, and B. K. Patra, *Phys. Rev.* **D88**, 054022 (2013), arXiv:1212.2803.
- [261] L. Thakur, U. Kakade, and B. K. Patra, (2013), arXiv:1401.0172.
- [262] R. Pisarski, *Phys. Rev.* **D47**, 5589 (1993).

BIBLIOGRAPHY

- [263] S. Peigne, E. Pilon, and D. Schiff, *Z. Phys.* **C60**, 455 (1993), arXiv:hep-ph/9306219.
- [264] S. Sarkar and A. K. Dutt-Mazumder, *Phys. Rev.* **D88**, 054006 (2013), arXiv:1205.4895.
- [265] A. Abada and N. Daira-Aifa, *JHEP* **1204**, 071 (2012), arXiv:1112.6065.
- [266] E. Braaten and R. D. Pisarski, *Phys. Rev.* **D42**, 2156 (1990).
- [267] E. Braaten and M. H. Thoma, *Phys. Rev.* **D44**, 1298 (1991).
- [268] E. Braaten and M. H. Thoma, *Phys. Rev.* **D44**, 2625 (1991).
- [269] M. H. Thoma and M. Gyulassy, *Nucl. Phys.* **B351**, 491 (1991).
- [270] P. Romatschke and M. Strickland, *Phys. Rev.* **D69**, 065005 (2004), arXiv:hep-ph/0309093.
- [271] P. Romatschke and M. Strickland, *Phys. Rev.* **D71**, 125008 (2005), arXiv:hep-ph/0408275.
- [272] M. G. Mustafa, *Phys. Rev.* **C72**, 014905 (2005), arXiv:hep-ph/0412402.
- [273] M. G. Mustafa and M. H. Thoma, *Acta Phys. Hung.* **A22**, 93 (2005), arXiv:hep-ph/0311168.
- [274] M. Djordjevic, *Phys. Rev.* **C74**, 064907 (2006), arXiv:nucl-th/0603066.
- [275] P. Chakraborty, M. G. Mustafa, and M. H. Thoma, *Phys. Rev.* **C75**, 064908 (2007), arXiv:hep-ph/0611355.
- [276] G.-Y. Qin *et al.*, *Phys. Rev. Lett.* **100**, 072301 (2008), arXiv:0710.0605.
- [277] G.-Y. Qin, A. Majumder, H. Song, and U. Heinz, *Phys. Rev. Lett.* **103**, 152303 (2009), arXiv:0903.2255.
- [278] G.-Y. Qin and A. Majumder, *Phys. Rev. Lett.* **105**, 262301 (2010), arXiv:0910.3016.
- [279] S. Mrowczynski and M. H. Thoma, *Phys. Rev.* **D62**, 036011 (2000), arXiv:hep-ph/0001164.
- [280] P. Romatschke and M. Strickland, *Phys. Rev.* **D68**, 036004 (2003), arXiv:hep-ph/0304092.

- [281] P. Romatschke and M. Strickland, *Phys. Rev.* **D70**, 116006 (2004), arXiv:hep-ph/0406188.
- [282] A. Rebhan, P. Romatschke, and M. Strickland, *Phys. Rev. Lett.* **94**, 102303 (2005), arXiv:hep-ph/0412016.
- [283] B. Schenke and M. Strickland, *Phys. Rev.* **D74**, 065004 (2006), arXiv:hep-ph/0606160.
- [284] A. Rebhan, M. Strickland, and M. Attems, *Phys. Rev.* **D78**, 045023 (2008), arXiv:0802.1714.
- [285] M. Attems, A. Rebhan, and M. Strickland, *Phys. Rev.* **D87**, 025010 (2013), arXiv:1207.5795.
- [286] C. Kiessig and M. Plumacher, *JCAP* **1209**, 012 (2012), arXiv:1111.1235.
- [287] C. Kiessig and M. Plumacher, *JCAP* **1207**, 014 (2012), arXiv:1111.1231.
- [288] T. Hashimoto, A. Nakamura, and I. Stamatescu, *Nucl. Phys.* **B400**, 267 (1993).
- [289] G. Boyd, S. Gupta, F. Karsch, and E. Laermann, *Z. Phys.* **C64**, 331 (1994), arXiv:hep-lat/9405006.
- [290] F. Karsch, M. Mustafa, and M. Thoma, *Phys. Lett.* **B497**, 249 (2001), arXiv:hep-ph/0007093.
- [291] W. Alberico, A. Beraudo, P. Czerski, and A. Molinari, *Nucl. Phys.* **A775**, 188 (2006), arXiv:hep-ph/0605060.
- [292] P. Czerski, *Nucl. Phys.* **A807**, 11 (2008).
- [293] P. B. Arnold, G. D. Moore, and L. G. Yaffe, *JHEP* **0011**, 001 (2000), arXiv:hep-ph/0010177.
- [294] P. B. Arnold, G. D. Moore, and L. G. Yaffe, *JHEP* **0112**, 009 (2001), arXiv:hep-ph/0111107.
- [295] P. B. Arnold, G. D. Moore, and L. G. Yaffe, *JHEP* **0305**, 051 (2003), arXiv:hep-ph/0302165.
- [296] P. Aurenche, F. Gelis, G. Moore, and H. Zaraket, *JHEP* **0212**, 006 (2002), arXiv:hep-ph/0211036.

BIBLIOGRAPHY

- [297] NA49 Collaboration, H. Appelshauser *et al.*, Nucl. Phys. **A638**, 91 (1998).
- [298] NA49 Collaboration, H. Appelshauser *et al.*, Phys. Lett. **B459**, 679 (1999), arXiv:hep-ex/9904014.
- [299] NA49 Collaboration, J. Reid, Nucl. Phys. **A661**, 407 (1999).
- [300] M. A. Stephanov, K. Rajagopal, and E. V. Shuryak, Phys. Rev. Lett. **81**, 4816 (1998), arXiv:hep-ph/9806219.
- [301] M. A. Stephanov, K. Rajagopal, and E. V. Shuryak, Phys. Rev. **D60**, 114028 (1999), arXiv:hep-ph/9903292.
- [302] D. Forster, *Hydrodynamics Fluctuation, Broken Symmetry and Correlation Function* (Benjamin/Cummings, Menlo Park, CA, 1975).
- [303] H. B. Callen and T. A. Welton, Phys. Rev. **83**, 34 (1951).
- [304] R. Kubo, J. Phys. Soc. Jap. **12**, 570 (1957).
- [305] H.-T. Ding *et al.*, Phys. Rev. **D83**, 034504 (2011), arXiv:1012.4963.
- [306] B. Sheikholeslami and R. Wohlert, Nucl. Phys. **B259**, 572 (1985).
- [307] M. Luscher, S. Sint, R. Sommer, and H. Wittig, Nucl. Phys. **B491**, 344 (1997), arXiv:hep-lat/9611015.
- [308] Y. Nakahara, M. Asakawa, and T. Hatsuda, Phys. Rev. **D60**, 091503 (1999), arXiv:hep-lat/9905034.
- [309] M. Asakawa, T. Hatsuda, and Y. Nakahara, Prog. Part. Nucl. Phys. **46**, 459 (2001), arXiv:hep-lat/0011040.
- [310] I. Wetzorke and F. Karsch, p. 193 (2000), hep-lat/0008008.
- [311] F. Karsch, private communication.
- [312] P. Huovinen and P. Petreczky, Nucl. Phys. **A837**, 26 (2010), arXiv:0912.2541.
- [313] C. Korthals-Altes, A. Kovner, and M. A. Stephanov, Phys. Lett. **B469**, 205 (1999), arXiv:hep-ph/9909516.
- [314] R. D. Pisarski, Phys. Rev. **D62**, 111501 (2000), arXiv:hep-ph/0006205.
- [315] C. Korthals-Altes and A. Kovner, Phys. Rev. **D62**, 096008 (2000), arXiv:hep-ph/0004052.

- [316] D. Zwanziger, Phys. Rev. Lett. **94**, 182301 (2005), arXiv:hep-ph/0407103.
- [317] A. Vuorinen and L. G. Yaffe, Phys. Rev. **D74**, 025011 (2006), arXiv:hep-ph/0604100.
- [318] P. de Forcrand, A. Kurkela, and A. Vuorinen, Phys. Rev. **D77**, 125014 (2008), arXiv:0801.1566.
- [319] K. Fukushima and N. Su, Phys. Rev. **D88**, 076008 (2013), arXiv:1304.8004.
- [320] S. Datta, R. Gavai, and S. Gupta, PoS **LATTICE2013**, 202 (2014).
- [321] C. Gale and J. I. Kapusta, Nucl. Phys. **B357**, 65 (1991).
- [322] P. Aurenche, F. Gelis, and H. Zaraket, Phys. Rev. **D61**, 116001 (2000), arXiv:hep-ph/9911367.
- [323] M. G. Mustafa and M. H. Thoma, Pramana **60**, 711 (2003), arXiv:hep-ph/0201060.
- [324] A. Peshier and M. H. Thoma, Phys. Rev. Lett. **84**, 841 (2000), arXiv:hep-ph/9907268.
- [325] S. Wong, Z. Phys. **C53**, 465 (1992).
- [326] P. Aurenche, F. Gelis, R. Kobes, and H. Zaraket, Phys. Rev. **D60**, 076002 (1999).
- [327] M. H. Thoma and C. T. Traxler, Phys. Rev. **D56**, 198 (1997), arXiv:hep-ph/9701354.
- [328] M. Carrington, A. Gynther, and P. Aurenche, Phys. Rev. **D77**, 045035 (2008).
- [329] P. Aurenche, F. Gelis, and H. Zaraket, JHEP **0207**, 063 (2002).
- [330] T. Altherr and P. Ruuskanen, Nucl. Phys. **B380**, 377 (1992).
- [331] J. Cleymans and I. Dadic, Phys. Rev. **D47**, 160 (1993).
- [332] J. Cleymans, I. Dadic, and J. Joubert, Phys. Rev. **D49**, 230 (1994).
- [333] J. I. Kapusta, P. Lichard, and D. Seibert, Phys. Rev. **D44**, 2774 (1991).
- [334] R. Baier, H. Nakkagawa, A. Niegawa, and K. Redlich, Z. Phys. **C53**, 433 (1992).

- [335] T. Altherr and P. Aurenche, *Z. Phys.* **C45**, 99 (1989).
- [336] J. I. Kapusta and S. Wong, *Phys. Rev.* **C62**, 027901 (2000), arXiv:hep-ph/0003196.
- [337] P. Aurenche *et al.*, *Phys. Rev.* **D65**, 038501 (2002), arXiv:hep-ph/0009074.
- [338] P. Levai and U. W. Heinz, *Phys. Rev.* **C57**, 1879 (1998).
- [339] A. Schaefer and M. H. Thoma, *Phys. Lett.* **B451**, 195 (1999).
- [340] M. G. Mustafa, A. Schaefer, and M. H. Thoma, *Phys. Lett.* **B472**, 402 (2000), arXiv:hep-ph/9911398.
- [341] M. Mustafa, A. Schafer, and M. Thoma, *Nucl. Phys.* **A661**, 653 (1999), arXiv:hep-ph/9906391.
- [342] M. G. Mustafa, A. Schafer, and M. H. Thoma, *Phys. Rev.* **C61**, 024902 (2000), arXiv:hep-ph/9908461.
- [343] M. H. Thoma, S. Leupold, and U. Mosel, *Eur. Phys. J.* **A7**, 219 (2000), arXiv:nucl-th/9905016.
- [344] S. Ghosh, S. Sarkar, and J.-e. Alam, *Eur. Phys. J.* **C71**, 1760 (2011).
- [345] A. Hosoya, M.-a. Sakagami, and M. Takao, *Annals Phys.* **154**, 229 (1984).
- [346] A. Hosoya and K. Kajantie, *Nucl. Phys.* **B250**, 666 (1985).
- [347] B. Svetitsky, *Phys. Rev.* **D37**, 2484 (1988).
- [348] G. Baym, H. Monien, C. Pethick, and D. Ravenhall, *Phys. Rev. Lett.* **64**, 1867 (1990).
- [349] S. Jeon, *Phys. Rev.* **D52**, 3591 (1995), arXiv:hep-ph/9409250.
- [350] S. Jeon and L. G. Yaffe, *Phys. Rev.* **D53**, 5799 (1996).
- [351] P. B. Arnold, G. D. Moore, and L. G. Yaffe, *JHEP* **0206**, 030 (2002).
- [352] G. D. Moore, *Phys. Rev.* **D76**, 107702 (2007).
- [353] S. Caron-Huot and G. D. Moore, *Phys. Rev. Lett.* **100**, 052301 (2008).
- [354] S. Caron-Huot and G. D. Moore, *JHEP* **0802**, 081 (2008).
- [355] S. Caron-Huot, *Phys. Rev.* **D79**, 065039 (2009).